

ABSTRACT

MORRISON, MACHEL LEIGH. Innovative Seismic Performance Enhancement Techniques for Steel Building Moment Resisting Connections. (Under the direction of Dr. Tasnim Hassan).

Seismic performance enhancement techniques for steel building moment connections intended for use in special moment frames are studied experimentally and through rigorous simulation modeling. The first performance enhancement technique involves reducing the strength of steel over specified regions of the beam flanges by exposing the regions to high temperatures followed by slow cooling. This technique promotes development of the beam plastic hinge away from the welded joint. The second technique involves relocation of the bolts of an 8-bolt extended end plate connection to distribute bolt forces uniformly, and thereby avoid bolt and end plate failures. The third technique involves a new shear tab design and bolt arrangement of welded unreinforced flange bolted-web (WUF-B) connections to more effectively transfer stress from the beam web to the column flange. Finally, the fourth performance enhancement technique involves stiffening the beam web within the plastic hinge region to delay the onset of local web and flange buckling resulting in the delay of strength degradation. Experimental validations of these seismic performance enhancement techniques are presented. Rigorous simulation models of the connections were developed based on an advanced non-linear kinematic hardening rule constitutive model in ANSYS Finite Element Software. The simulation results were instrumental in developing the novel ideas for enhancing seismic performance of steel building moment connections.

© Copyright 2015 Machel Leigh Morrison

All Rights Reserved

Innovative Seismic Performance Enhancement Techniques for Steel Building Moment
Resisting Connections

by
Machel Leigh Morrison

A dissertation submitted to the Graduate Faculty of
North Carolina State University
in partial fulfillment of the
requirements for the degree of
Doctor of Philosophy

Civil Engineering

Raleigh, North Carolina

2015

APPROVED BY:

Dr. Tasnim Hassan
Committee Chair

Dr. Jim Nau

Dr. Mervyn Kowalsky

Dr. Korukonda Murty

DEDICATION

To my parents Dennis Morrison and Rose Morrison

In loving memory of my grandfather Kelvin Allwood

BIOGRAPHY

Machel Morrison was born in Kingston, Jamaica on May 6, 1982. He received a B.A. degree in Engineering from Lafayette College in 2004 and a Master of Engineering Management degree from Duke University in 2005. After graduating from Duke University, he joined Skanska USA Building Inc. in Durham, NC as a project engineer. As a project engineer he assisted with on-site problem solving in the construction of commercial building projects in the Raleigh-Durham area. This field experience sparked his interest in the theory, behavior and design of structures. In 2010 he started his PhD studies at North Carolina State University, Raleigh, NC where he conducted research under the supervision of Dr. Tasnim Hassan on the development of seismic performance enhancement techniques for welded steel moment connections.

ACKNOWLEDGMENTS

Funding for this research was provided by the National Science Foundation under the Network for Earthquake Engineering Simulation (NSF Grant no. 0936547).

This enlightening and fulfilling journey would not have been possible without the kind assistance and support of many people. I wish to express my sincere gratitude to my advisor Dr. Tasnim Hassan for his enthusiasm, and patience, for allowing me the freedom to pursue areas of research that interests me, and especially for his unrelenting encouragement and support in all my academic endeavors. A special thank you is extended to the other members of my dissertation committee in particular Dr. Jim Nau for his warm support throughout the pursuit of my degree.

I am indebted to my research partners Doug Schweizer, and Shahriar Quayyum for their hard work and numerous contributions towards the success of the research program. In addition the help provided by Boopathy Kombaiah in performing optical microscopy and hardness testing of steel samples is greatly appreciated. I also thank my other colleagues Raashed Ahmed, Paul Barrett, Graham Pritchard, Nazrul Islam, Matthew Fenton and Farhan Rahman with whom I enjoyed several interesting and vibrant conversations and debates.

I am grateful for the support of the many industry partners who played an integral role in the success of this research program. These partners include Lejune Steel Inc., Danny's Construction Co., Ameritherm Inc., Furmanite Inc., Steel Fab Inc., and Flores Welding Inc. The efforts and assistance provided by staff of the Constructed Facilities laboratory at NC State, the MAST laboratory at the University of Minnesota, and the Analytical

Instrumentation Facility at NC State are also gratefully acknowledged. In-kind support provided by Skanska USA building, GWY Inc., and CMC South Carolina Steel is gratefully acknowledged.

Last but not least, I would like to thank my family members Dennis Morrison, Rose Morrison and Shonel Morrison for their unconditional love and support.

TABLE OF CONTENTS

LIST OF TABLES	xi
LIST OF FIGURES	xii
CHAPTER 1: Introduction.....	1
1.1 Background- Damage during 1994 Northridge Earthquake	1
1.2 Causes for Failures and Improvements to Connection Design.....	3
1.2.1 Problems and solutions related to weld details, weld flaws and weld metal	5
1.2.2 Problems and solutions related to flange overstress.....	8
1.3 Introduction to current study	13
2. Scope and Organization	16
3. References	17
CHAPTER 2: An Innovative Seismic Performance Enhancement Technique for Steel Building Moment Resisting Connections Part I.....	20
1. Introduction.....	21
2. Heat-treatment	25
2.1 Application of Heat-treatment to Wide Flange Beams	27
3. Experimental Setup and Connection Design	28
4. Results	32
4.1 HBS specimens	34
4.2 HBS 3 Welding Error	35
4.3 WUF-W Test Results	35
4.4 Evaluation of HBS performance	38
5. Post-experiment microstructure analysis of Heat-treated A992 steel.....	44
6. Posttest FE Analysis.....	45
6.1 Effect of HBS material properties	50
6.2 Effect of welded shear tab	51
8. References	55
CHAPTER 3: An Innovative Seismic Performance Enhancement Technique for Steel Building Moment Resisting Connections Part II	58

1. Overview of Steel Moment Connection advances since Northridge Earthquake	59
2. Introduction to the Novel Connection Concept.....	66
3. Heat-treatment thermal process	68
4. HBS Connection Design Development.....	72
5. Heat-treatment method for full scale beams	76
6. Connection Design and Experimental Setup	78
7. Instrumentation.....	81
8. Test Results.....	82
8.1. Global response of HBS connections	82
8.2 Plastic hinge formation in HBS Connection.....	85
8.3 Failure Mechanism of HBS connections.....	88
8.4 Comments on a possible design method of HBS connections	92
9. Conclusion	93
10. References	95
CHAPTER 4: Seismic Enhancement of Eight Bolt Extended End Plate Moment Connections Part I: Numerical Modeling and Design Development	99
1. Introduction.....	100
2. Finite Element Modeling and Analysis of Extended End plate Connections	106
2.1 Finite element modeling details	107
2.2 Material models	109
2.3 Loads and Boundary Conditions.....	112
3. Validation of Finite Element Model	114
4. Finite Element Analysis of Extended End plate Connections.....	117
4.1 Eight Bolt Stiffened Extended End plate Connection (8ES)	119
4.2 Eight Bolt 4 Wide Unstiffened Extended End plate Connection (8E-4W).....	124
4.3 Eight Bolt Unstiffened Extended End plate Connection (8E)	129
4.4 Eight Bolt Unstiffened Modified Extended End plate Connection (8EUH)....	131
4.5 Comparison of 8ES, 8E-4W and 8EUH Connections.....	135

4.6 Further Development of the Modified Eight Bolt Unstiffened Extended End plate Connection (8EM)	137
5. Conclusions.....	151
6. References	152
CHAPTER 5: Seismic Enhancement of Eight Bolt Extended End Plate Moment Connections Part II: Experimental Validation and Addressing Further Development	157
1. Introduction.....	158
2. Review of proposed novel performance enhancing techniques	160
3. Connection Design and Experimental Setup	162
4. Instrumentation.....	166
5. Test Results.....	167
5.1 Global response of modified Extended End plate connection	167
5.2 Plastic hinge formation in the modified BEEP connection.....	170
5.3 Bolt response in the modified Extended End plate connection	173
5.4 Failure Mechanism	175
6. Post-test FEA and discussion	177
7. Future development of Modified Extended End Plate Connections	182
7.1 Future work on web stiffener	184
7.2 Design Development	185
8. Conclusion	185
9. References	186
CHAPTER 6: Seismic Enhancement of Welded Unreinforced Flange Bolted Web Moment Connections	188
1. Introduction.....	189
2. Finite Element Modeling of WUF-B Connections	194
2.1 Finite Element Modelling.....	195
2.1.1 Global Model.....	195
2.1.2 Material and Geometric nonlinearities.....	198
2.1.3 Sub model and Cyclic Void Growth Damage Model.....	200

2.2 Validation of Numerical Modelling.....	204
2.2.1 Simulation of slip in a simple bolted assembly.....	204
2.2.2 Simulation of Post Northridge WUF-B connection	205
3. Monotonic Analysis and comparative study of WUF-B connections	209
4. Seismic Enhancement of WUF-B moment connections	218
4.1 Overview of Connection Design	221
4.2 Finite element analysis of enhanced WUF-B connection.....	225
4.2.1 Global responses of enhanced WUF-B connection.....	225
4.2.2 Local responses of enhanced WUF-B connection.....	227
4.2.3 Cyclic Analysis of enhanced WUF-B connection.....	230
5. Experimental Validation	231
5.1. Connection Design and Experimental Setup.....	231
5.2 Instrumentation	235
5.3. Test Results	236
5.4 Plastic hinge formation in the modified WUF-B connection	239
5.5 Bolt response in the modified WUF-B connection.....	242
6. Future work on modified WUF-B connections	242
7. Conclusion	243
8. References	244
CHAPTER 7: Resilient Welded Steel Moment Connections (WSMC) by Enhanced Beam Buckling Resistance	250
1. Introduction.....	251
2. Buckling of Recently Developed Seismically Resilient WSMC	257
3. Proposed Techniques for enhancing beam buckling resistance of WSMC ..	262
3.1. Finite Element Modeling of Enhanced Connections	264
3.2. Finite Element Analysis Results and Discussion.....	266
4. Experimental Validation	271
4.1. Connection Design and Experimental Setup.....	271
4.2 Instrumentation	274

5. Test Results.....	275
5.1. Global response of HBS 8	275
5.2. Comparative Analysis of HBS 8	277
5.2.1 Global Response.....	277
5.2.2 Plastic Hinge Formation	278
5.2.3 Local buckling.....	281
5.2.4 HBS 8 Web stiffener fillet weld failure.....	283
6. Future Work on web stiffener	284
7. Conclusion	285
8. References	286
CHAPTER 8: Conclusions and Recommendations	289
1. Conclusions.....	289
2. Recommendations	292
2.1 Heat-treatment method and Thermal cycle	292
2.2 All welded HBS connections	293
2.3 Modified 8 bolt unreinforced extended end plate connection	293
2.4 Modified post Northridge WUF-B connection.....	293
2.5 Web stiffener	294

LIST OF TABLES

CHAPTER 2: An Innovative Seismic Performance Enhancement Technique for Steel Building Moment Resisting Connections Part I

Table 1 Summary of test specimens.....	32
Table 2 Summary of test results.....	40

CHAPTER 3: An Innovative Seismic Performance Enhancement Technique for Steel Building Moment Resisting Connections Part II

Table 1 Summary of material properties of A992 before and after heat-treatment	71
Table 2 Bending moments developed in HBS test specimens	93

CHAPTER 4: Seismic Enhancement of Eight Bolt Extended End Plate Moment Connections Part I: Numerical Modeling and Design Development

Table 1 Nonlinear kinematic hardening parameters for different steels	111
--	-----

CHAPTER 6: Seismic Enhancement of Welded Unreinforced Flange Bolted Web Moment Connections

Table 1 Nonlinear Kinematic hardening model material parameters	199
--	-----

LIST OF FIGURES

CHAPTER 1: Introduction

Fig. 1. Sketch showing beam-column connection and common mode of fracture during 1994 Northridge earthquake [3]	2
Fig. 2. Photographs showing beam to column connection fractures during the 1994 Northridge Earthquake (a) Fusion zone fracture, (b) column flange ‘divot’ fracture, (c) fracture progression through column flange and, (d) fracture progression through column flange and column web [3]	3
Fig. 3. W1 indication (a) Polished and etched sample with W1 (b) Sketch of beam bottom flange to column flange weld showing W1 [2].....	6
Fig. 4. Tests of pull plate ‘T’ assemblies (a) Welded with Pre-Northridge E70T-4 electrode and weld details, (b) Welded with Pre-Northridge E70T-4 electrode but with backing bar removed, (c) Welded with E7018 electrode and backing bar removed (d) Force-displacement curves showing from left to right the results of the 3 pull plate tests. [10]	7
Fig. 5. Fractures in beam flange base metal in Post Northridge WUF-B connections. [11-13].....	9
Fig. 6. Examples of modified connections (a) cover plate (b) upstanding rib (c) haunch (d) dog bone [14]	11
Fig. 7. Photographs during simulated seismic testing of connections with overstress mitigation strategies (a) Haunch connection (with concrete slab) [19] (b) RBS connection [23]	12
Fig. 8. (a) Heat-treated Beam Section (HBS) (b) Engineering Stress-Strain response of A992 and heat-treated A992 steel.....	15

CHAPTER 2: An Innovative Seismic Performance Enhancement Technique for Steel Building Moment Resisting Connections Part I

Fig. 1. Reinforced steel moment connections (a) Stiffened extended end plate (b) bolted flange plate (BFP) (c) Kaiser bolted bracket (KBB) and (d) Welded unreinforced flange-welded web (WUF-W) (figures from [11])	22
Fig. 2. (a) Reduced Beam Section (RBS) (b) Heat-treated Beam Section (HBS) (c) Temperature history of A992 heat-treatment (d) Engineering Stress-Strain response of A992 and heat-treated A992 steel.....	24
Fig. 3. Uniaxial Stress Strain response of Heat-treated A992 Steel a) Effect of peak temperature b) Effect of cooling rate	27
Fig. 4. Induction heating of wide flange beam, (a) schematic showing heat-treatment setup (b) photograph showing induction heating of beam flange	28
Fig. 5. Test setup and connection details a) sketch of the test setup, b) sketch of the connection details, c) photograph showing test setup and, d) photograph of control 1 connection prior to testing	30
Fig. 6. Moment-rotation responses of test specimens a) HBS 1 b) HBS 2 c) HBS 3 and, d) Control 1	33
Fig. 7. Plastic hinging and local buckling of a) HBS 1 and, b) Control 1	35
Fig. 8. Progression of yielding of Control 1 a) Initiation of yield at beam bottom flange weld toe at 1% drift b) Yielding in beam web around welded shear tab at 1.5% drift c)progression of yielding away from connection at 2% drift d) further progression of yielding away from connection at 3% drift.....	37
Fig. 9. Comparison of beam yielding for HBS 3 and Control 1, (a) Photograph of HBS 3 at 3% drift (b) Photograph of Control 1 at 3% drift (c) Recorded longitudinal strains along the side of the beam top flange 178 mm (7") from the column face for Control 1 and HBS 3 (d) Recorded longitudinal strains along the side of the beam top flange 13mm (0.5") from the column face for Control 1 and HBS 3	39
Fig. 10. Comparison of Uniaxial Stress Strain response of Heat-treated A992 Steel	42
Fig. 11. Comparison of hysteresis loops from 1% to 4% story drift for HBS 2 and Control 1	43

Fig. 12. Optical micro graphs and Vickers Hardness numbers of A992 Steel (a) Before heat-treatment (b) After furnace heat-treatment (c) After induction heat-treatment	45
Fig. 13. (a) Finite element mesh and boundary conditions (b) Chaboche model simlation of A992 1% strain amplitude hysteresis curve.....	46
Fig. 14. Comparison of experimental and FE predicted moment rotation response for (a) HBS 3 and (b) Control 1	47
Fig. 15. Comparison of experimental and FE predicted longitudinal strain responses 127mm (5") from the column face for control 1.....	48
Fig. 16. Photograph of control 1 during loading cycles at 4% drift showing local flange buckling b) FEA prediction of deformation of control 1 top flange buckling at 4% drift c) Photograph showing plastic hinge formation of control 1 during loading cycles at 4% d) accumulated equivalent plastic strain solution for control 1	49
Fig. 17. FE analysis prediction of longitudinal strains along the width of the beam top flange 50mm (2in) away from the column flange for HBS specimens	51
Fig. 18. Finite element simulation of the effect of the welded shear tab (a) accumulated equivalent plastic strain solution for WUF-W at 4% drift (b) accumulated equivalent plastic strain solution for WUF-W without welded shear tab at 4% drift (c) FE analysis prediction of longitudinal strains along the width of the beam top flange at the weld toe for WUF-W (d) FE analysis prediction of longitudinal strains along the width of the beam top flange at the weld toe for WUF-W without welded shear tab	53
CHAPTER 3: An Innovative Seismic Performance Enhancement Technique for Steel Building Moment Resisting Connections Part II	
Fig. 1. Moment-rotation experimental backbone curves (in positive bending) of stiffened connections.	61
Fig. 2. Sketch of (a) Reduced Beam Section (RBS) and (b) Heat-treated Beam Section (HBS).	64

Fig. 3. Moment-rotation experimental backbone curves (in positive bending) of welded unreinforced connections	66
Fig. 4. (a) Temperature history of A992 heat-treatment (b) Engineering Stress-Strain response of A992 and heat-treated A992 steel	67
Fig. 5. Optical micro graphs of A992 Steel (a) Before heat-treatment (b) After heat-treatment at 1050°C cooled at 20°C/hr to 500°C followed by air cooling. Nital etch. Original Magnification: 100x.....	69
Fig. 6. Uniaxial stress strain responses of heat-treated A992 Steel, (a) effect of peak temperature, (b) effect of cooling rate	70
Fig. 7. Finite element analysis of RBS and HBS connections, (a) comparison of experimental and analytical results for specimen DB 3 Engelhardt et al. [22] (b) comparison of M-θ envelop (Moments are normalized to the plastic moment capacity of the beam at the face of the column), (c) equivalent plastic strain solution of RBS @ 4.5% story drift (d) equivalent plastic strain solution of HBS @ 4.5% story drift, (e) longitudinal stress and strain at the center of the RBS @ 2% story drift (f) longitudinal stress and strain at the center of the HBS @ 2% story drift.....	75
Fig. 8. Heat-treatment setup (a) photograph showing electric surface heating pads during installation on a beam flange, (b) photograph showing insulation of beam flange for well controlled heating and cooling, (c) schematic showing section view of heat-treatment setup, and (d) contour plot from thermal finite element analysis [36] of temperature (absolute scale) distribution during heating of the beam.....	78
Fig. 9. HBS test setup and connection details a) sketch of the test setup, b) sketch of the connection details, c) photograph showing test setup and, d) photograph of HBS 5 connection prior to testing	79
Fig. 10. Instrumentation of HBS 5, a) LED markers placed on beam web and the sides of beam top and bottom flanges, and b) LED markers placed on beam top flange	80
Fig. 11. Moment-rotation responses of HBS connections, a) HBS 5 and, b) HBS 7	83

Fig. 12. Plastic rotation contributions by components of HBS 7, (a) total connection plastic rotation, (b) panel zone shear plastic rotation (c) column flexural plastic rotation and, (d) beam plastic rotation	84
Fig. 13. Total rotation contributions of HBS connections, (a) HBS 5 and, (b) HBS 7	85
Fig. 14. Recorded longitudinal strains along the center of top flange of the beam from HBS 5.....	87
Fig. 15. Yielding and plastic hinge formation of HBS 7, (a) view of beam bottom flange at 1 % Drift, (b) Connection at 3% drift, (c) Connection at 4% drift and, (d) Connection at 6% drift.....	88
Fig. 16. HBS 5 progression of beam web and flange buckling recorded 406mm away from the column flange at interstory drifts of (a) 2%, (b) 3%, (c) 4% and, (d) 5% (Beam is in positive bending i.e. top flange in compression).	89
Fig. 17. HBS 5 progression of beam web and flange buckling recorded 106mm away from the column flange of HBS 5 at interstory drifts of (a) 3%, (b) 4% and, (c) 5% (Beam is in positive bending i.e. top flange in compression).	90
Fig. 18. Photograph showing post-test local flange buckling amplitude of HBS 7 (after 1 cycle of 6% drift).	92
CHAPTER 4: Seismic Enhancement of Eight Bolt Extended End Plate Moment Connections Part I: Numerical Modeling and Design Development	
Fig. 1. ANSI/AISC 358 Prequalified Extended End Plate Connections (a) Four bolt unstiffened (4E), (b) four bolt stiffened (4ES), (c) eight-bolt stiffened (8ES) [9].....	102
Fig. 2. (a) Finite element mesh of an eight bolt stiffened (8ES) extended end plate connection (b) Close up view of finite element mesh.....	108
Fig. 3. Experimental and simulated response of strain controlled hysteresis loop with Chaboche model parameters. (a) ASTM A572 Gr.50 steel, (b) ASTM A36 steel, (c) ASTM A992 steel.	112

Fig. 4. (a) Experimental monotonic stress-strain response and simulated response for ASTM A490 bolt with Chaboche model parameters, (b) Experimental monotonic stress-strain response [40] and simulated response for ASTM A325 bolt with Chaboche model parameters, (c) bilinear model for E70 weld obtained from the reported yield and tensile strength data [14].	113
Fig. 5. (a) Boundary conditions adopted in the seismic analysis of extended end plate connection, (b) SAC loading protocol [41].....	114
Fig. 6. Comparison between experimental and simulated moment-rotation response of (a) eight bolt stiffened (8ES), and (b) four bolt unstiffened (4E) extended end plate connections tested by Sumner <i>et al.</i> [7].....	115
Fig. 7. Comparison of experimental and simulated deformed shape for 8ES specimen tested by Sumner <i>et al.</i> [7] a) Post-test photograph of specimen 8E-1.25-1.75-30 b) Accumulated equivalent plastic strain FE prediction showing plastic hinge formation at the base of the endplate stiffener.....	116
Fig. 8. Comparison of experimental and simulated deformed shape for 8ES specimen tested by Sumner <i>et al.</i> [7] a) Post-test photograph of specimen 4E-1.25-1.5-24 b) Accumulated equivalent plastic strain FE	116
Fig. 9. Comparison of experimental and simulated bolt strains for 8ES specimen tested by Sumner et al. [7]. (a) Experimental response, (b) simulated response.	117
Fig. 10. Eight bolt stiffened extended end plate connection (8ES). (a) FE mesh, (b) accumulated equivalent plastic strain contour showing formation of plastic hinge after cyclic loading up to 6% interstory drift.....	119
Fig. 11. Cyclic response of 8ES connection. (a) Moment-rotation hysteresis response, (b) rotation contribution of connection components.	120
Fig. 12. Bolt strains for 8ES configuration during loading cycles at the top flange of the beam.....	121
Fig. 13. Axial strain profile along the width of beam bottom flange at the weld toe for 8ES connection	123

Fig. 14. (a) Von-Mises stress distribution along the beam centerline (b) Von-Mises (Equivalent) plastic strain distribution along the beam centerline.....	124
Fig. 15. FE Simulation of Eight bolt 4 wide unstiffened extended end plate connection (8E-4W-30x99). (a) FE mesh, (b) accumulated equivalent plastic strain contour showing at 3% interstory drift angle.....	126
Fig. 16. Axial strain profile along the width of beam flange at the weld toe for 8E-4W-W30x99 connection.	127
Fig. 17. Simulated bolt strains for 8E-4W under SAC loading cycles at the top flange of the beam.....	128
Fig. 18. FE Simulation of 8E-4W-W30×99 (a) Accumulated equivalent plastic strain contour of end plate at the end of 3% interstory drift angle, (b) moment-rotation hysteresis response of 8E-4W connection.	129
Fig. 19. FE Simulation of Eight bolt unstiffened extended end plate connection (8E-W30×99). (a) FE mesh, (b) accumulated equivalent plastic strain contour showing formation of plastic hinge after cyclic loading up to 6% interstory drift.	130
Fig. 20. Axial strain profile along the width of beam bottom flange at the weld toe for 8E-W30x99 connection.	131
Fig. 21. Simulated bolt strains for 8E configuration under SAC loading cycles at the top flange of the beam.....	131
Fig. 22. (a) Proposed bolt rearrangement in a hexagonal pattern, (b) FE mesh with the modified bolt arrangement for 8EUH configuration of the connection, (c) accumulated equivalent plastic strain contour of 8EUH connection at 5% drift	132
Fig. 23. Cyclic response of 8EUH configuration of connection. (a) Moment-rotation hysteresis response for cyclic loading up to 6% interstory drift, (b) rotation contribution of connection components.....	134
Fig. 24. Bolt strains for 8EUH-W30x99 during loading cycles at the top flange of the beam.....	135

Fig. 25. (a) Axial strain profile along the width of beam bottom flange at the weld toe for 8EUH configuration of the connection, (b) moment-rotation envelopes of the extended end plate connections for different bolt arrangements.	136
Fig. 26. FE simulation of 8EM connection. (a) Equivalent plastic strain contour for 8EM-W30x148 (b) Axial strain profile along the width of the beam flange for 8EM-W30x148 (c) Equivalent plastic strain contour for 8EMH-W36x170 (d) Axial strain profile along the width of the beam flange for 8EM-W36x170.....	139
Fig. 27. Bolt strains for 8EM-W36x170 connection during loading cycles at the top flange of the beam.....	141
Fig. 28. HBS applied to modified extended end plate connection for seismic performance enhancement. (a) FE mesh for 8EMH connection (b) Temperature-Time history applied to HBS.....	141
Fig. 29. (a) Monotonic stress-strain response of A992 and heat-treated A992 steel (b) Experimental and simulated response of strain controlled hysteresis loop with Chaboche parameters for heat-treated ASTM A992 steel.	142
Fig. 30. Cyclic response of 8EMH connection. (a) Equivalent plastic strain contour for 8EMH-W30x148 (b) Equivalent plastic strain contour for 8EMH-W36x170 (c) Moment-rotation response up to 6% interstory drift angle for 8EMH-W30x148 (d) Moment-rotation response up to 6% interstory drift angle for 8EMH-W36x170.....	144
Fig. 31. Axial strain profile along beam flange-to-end plate CJP weld toe (a) 8EMH-W30x148 (b) 8EMH-W36x170	145
Fig. 32. Bolt strains for 8EMH -W36×170 connection.	145
Fig. 33. Bolt strains for 8EMH -W30×148 connection.	146
Fig. 34. Local buckling of beam web and flanges at different loading cycles for 8EMH-W30x148 connection.	147
Fig. 35. (a) FE mesh of modified extended end plate connection (8EMH-W) with heat-treatment and web stiffener (b) Equivalent plastic strain contour plot showing formation of	

plastic hinge in the heat-treated region of the beam flanges of 8EMH-W connection at 5% drift..... 148

Fig. 36. Cyclic response of 8EMH-W-W30-148 connection up to 6% interstory drift (a) Moment-rotation hysteresis response; (b) Axial strain profile along beam flange at the weld toe..... 149

Fig. 37. Bolt strains for 8EMH-W-W30x148 connection. 150

Fig. 38. Moment-rotation envelopes of different configurations of the extended end plate connections. (a) W30×148 beam section (b) W30×99 beam section. 151

CHAPTER 5: Seismic Enhancement of Eight Bolt Extended End Plate Moment Connections Part II: Experimental Validation and Addressing Further Development

Fig. 1. Sketch of Modified BEEP Connection..... 161

Fig. 2. Engineering stress-strain response of A992 and heat-treated A992 steel 161

Fig. 3. HBS 4 Test setup a) sketch of test setup, b) photograph showing test setup 163

Fig. 4. HBS 4 connection details a) elevation of connection, b) photograph of HBS 4 connection prior to testing, c) section A-A showing connection of beam web and web stiffeners to endplate, d)elevation of end plate showing modified bolt arrangement 164

Fig. 5. Heat-treatment setup (a) photograph showing electric surface heating pads during installation on a beam flange, (b) photograph showing insulation of beam flange for well controlled heating and cooling..... 165

Fig. 6. Instrumentation of HBS 4, a) LED markers placed on beam top flange, beam web and web stiffeners, b) LED markers placed on the sides of beam top and bottom flange, beam web and webstiffners..... 167

Fig. 7. a) Moment Rotation Response b) Total Rotation Contributions..... 168

Fig. 8. Plastic rotation contributions by components of HBS 4, (a) total connection plastic rotation, (b) panel zone shear plastic rotation (c) column flexural plastic rotation and, (d) beam plastic rotation	169
Fig. 9. Recorded longitudinal strains along the center of top flange of the beam from HBS 4.....	170
Fig. 10. Progression of yielding and plastic hinge formation in HBS 4 a) 1% drift b) 2% drift c) 3% drift and d) 4% drift	171
Fig. 11. Measured flexural strains from strain gages placed on the bottom flange of HBS 4. Strains are shown from the beginning of test to the second cycle of 3% drift.	172
Fig. 12. Recorded axial bolt strain vs column centerline moment	175
Fig. 13. Local buckling failure of HBS 4: a) Post test photograph showing flange and web local buckling b) Photograph showing fracture of beam flange in the crest of flange buckle	176
Fig. 14. Validation of post-test FEA of HBS 4 a) FEA discretization including initial distortion of web stiffener plates b) Comparison between FEA prediction and the recorded moment-rotation response c) Photograph of HBS 4 during loading cycles at 6% d) FEA prediction of deformation at 6% drift e) Comparison between FEA predictions and recorded top flange vertical displacements during various stages of loading history f) Photograph of HBS 4 top flange during loading at 4% drift	180
Fig. 15. Post-test FEA Simulation results showing the effect of initial web stiffener plate distortion: a) moment rotation envelop b) Accumulated equivalent plastic strain prediction at 5% drift for HBS 4 (post-test simulation with initial web stiffener distortion) c) Accumulated equivalent plastic strain prediction at 5% drift for HBS 4 (pre-test simulation without initial web stiffener distortion)	181
CHAPTER 6: Seismic Enhancement of Welded Unreinforced Flange Bolted Web Moment Connections	
Fig. 1. Post Northridge WUF-B (specimen 6.1 [14]) (a) Connection details (b) Sketch of ductile fracture failure of specimen 6.1[14].....	192

Fig. 2. Finite element mesh (a) Specimen 6.1 [12] mesh and boundary conditions (b) Close up view of specimen 6.1[12] mesh (c) fitted ASTM A572 gr 50 hysteresis curve for determing Chaboche model parameters (Experimental data from [32]), and (d) FE submodel mesh	196
Fig. 3. Finite element anlysis of a bolted plate assembly, (a) FE mesh of plate (b) Load-displacement response	205
Fig. 4. Finite element analysis of WUF-B connection specimen 6.1 [12] (a) load history (b) comparison of experimental and analytical results for specimen 6.1 [12] (c) comparison of experimental and analytical results for specimen 6.1 with modelling simplication of web connection (d) comparison of experimental and analytical results for specimen 6.1 with multiliear constitutive model calibrated from monotonic tensile test data (e) Void growth indices for CVGM failure prediction (f) Sketch showing location of CVGM failure prediction	207
Fig. 5. Comparison of finite element monotonic response prediction for WUF-B and all welded moment connection (a) moment-rotation responses (b) Horizontal nodal displacements on the vertical edge of the beam web adjacent to the column flange (along line A-A) and horizontal displacements of the adjacent nodes on the shear tab for WUF-B connection	210
Fig. 6. Finite element analysis of WUF-B connection (a) contour plot of longitudinal stress distribution in beam (b) longitudinal stress along beam depth at section 1-1 (c) longitudinal stress along beam depth at section 2-2 (d) longitudinal stress along beam depth at section 3-3 (e) vertical shear stress along beam depth at section 1-1 (f) vertical shear stress along beam depth at section 2-2 (g) vertical shear stress along beam depth at section 3-3	213
Fig. 7. Finite element monotonic response of WUF-B connection at yield moment (M_y) (a) contour plot of longitudinal stress distribution in beam, (b) longitudinal stress along beam depth at section 1-1, (c) longitudinal stress along beam depth at section 2-2, (d) longitudinal stress along beam depth at section 3-3, (e) vertical shear stress along beam depth at section 1-1, (f) vertical shear stress along beam depth at section 2-2, and (g) vertical shear stress along beam depth at section 3-3.....	215
Fig. 8. (a) Principle stress vector plot around access hole (b) Vertical shear stress along beam depth at section II-II at 0.02 rad story drift	216

Fig. 9. (a) WUF-B connection with proposed modifications including modified bolt design and HBS, and (b) Free body diagram of shear tab (only one bolt force vector is shown for clarity)	220
Fig. 10. (a) Temperature history of A992 steel heat-treatment (b) Engineering stress-strain response of A992 and heat-treated A992 steel	220
Fig. 11. Seismic moment distribution for design force determination	221
Fig. 12. Comparison of finite element monotonic response prediction for HBS-W, HBS-B and WUF-B w/HBS (a) moment-rotation responses (b) Horizontal nodal displacements on the vertical edge of the beam web adjacent to the column flange (along line A-A) and horizontal displacements of the adjacent nodes on the shear tab for WUF-B connection ..	226
Fig. 13. Stress and strain acting on beam flange at the access hole location under monotonic loading (a) longitudinal stress acting on beam flange at access hole location. Beam tip forces applied to produce a bending moment equal to half M_y at the column face (b) Longitudinal strains across beam flange at 0.03 radians story drift	228
Fig. 14. Finite element analysis of WUF-B and HBS-B connections a) equivalent plastic strain solution of WUF-B at 0.04 radians story drift b) equivalent plastic strain solution of HBS-B at 0.04 radians story drift	230
Fig. 15. Cyclic FE analysis of HBS-B (a) Moment rotation response prediction (b) Void growth indices for CVGM failure prediction.....	231
Fig. 16. Heat-treatment setup (a) photograph showing electric surface heating pads during installation on a beam flange, (b) photograph showing insulation of beam flange for well controlled heating and cooling.....	232
Fig. 17. HBS 6 test setup, connection details and instrumentation a) sketch of test setup, b) sketch of connection details, c) LED markers placed on beam web and the sides of beam top and bottom flanges and, d) photograph of HBS 6 connection prior to testing	234
Fig. 18. Moment-rotation response of HBS 6.....	237
Fig. 19. Yielding, plastic hinge formation and fracture of HBS 6, (a) connection at 3 % drift, (b) connection at 4% drift, (c) connection at 5% drift and, (d) west view of connection at 5%	

drift showing beam flange buckling (e) fracture of beam flange at 5% drift and (f) close up view of beam flange at location of fracture 238

Fig. 20. Plastic rotation contributions by components of HBS 6, (a) total connection plastic rotation, (b) panel zone shear plastic rotation (c) column flexural plastic rotation and, (d) beam plastic rotation 239

Fig. 21. Recorded longitudinal strains along the center of top flange of the beam from HBS 6..... 241

Fig. 22. (a) Recorded axial bolt strain vs column centerline moment (b) Sketch showing location of instrumented bolt 241

CHAPTER 7: Resilient Welded Steel Moment Connections (WSMC) by Enhanced Beam Buckling Resistance

Fig. 1. Web and flange buckling in the plastic hinge region, a) RBS w/concrete floor slab [Jones et. al. [7]] b) eight bolted stiffened EEP [8], c) KBB [10]. 252

Fig. 2. Beam buckling of RBS connection, (a) Web local buckling (WLB), lateral torsional buckling (LTB) and flange local buckling (FLB), and strength degradation at 3% interstory drift, (b) buckling damage in the RBS at 0.03 radians plastic rotation [SAC/BD-99/19, Uang and Fan [14]]...... 254

Fig. 3. (a) Sketch of Heat-treated Beam Section (HBS) connection (b) Engineering Stress-Strain response of A992 and heat-treated A992 steel 258

Fig. 4. Test results of HBS 5 connection, (a) moment-rotation experimental response and FE simulation (b) experimental backbone curve and FE simulation (c) photograph showing plastic hinge formation at 5% interstory drift (d) Photograph showing fracture of beam flange in the crest of flange buckle 259

Fig. 5. Progression of buckling in beam web of HBS 5 at various stages of loading history (a) initial position (b) 2.0% drift (c) 3.0% drift (d)4.0% drift (e)5.0% drift (Beam is in positive bending i.e. top flange in compression) 260

Fig. 6. Progression of HBS beam cross-section buckling at interstory drifts, (a) 3%, (b) 4%, and (c) 5%. Cross-section is located 406mm from the column face, FE simulation

predictions are plotted against recorded data from test	261
Fig. 7. Buckling failures in HBS connections (a) 8 bolt unreinforced EEP (HBS 4), (b) welded unreinforced flange bolted web (HBS 6) (c) HBS 7 (Repeat of HBS 5, all welded connection).....	262
Fig. 8. Proposed enhanced Connections (a) HBS with web stiffener (HBS-WS) (b) HBS applied to both flanges and web (HBS-W)	263
Fig. 9. Finite element mesh (a) Beam to column connection mesh and boundary conditions (b) Close up view of mesh showing multi point displacement constraints used to simulate welding attachment of web stiffener to beam web	265
Fig. 10. Moment rotation response for proposed connections (a) HBS-WS (b) HBS-W ...	267
Fig. 11. Moment rotation backbone curves for HBS (experiment and simulation), HBS-WS and HBS-W	268
Fig. 12. Accumulated Equivalent Plastic strain contours at 5% story drift for moment connecitons (a) HBS (isometric) (b) HBS (elevation) (c) HBS-W (isometric) (d) HBS-W (elevation) (e) HBS-WS (isometric) (f) HBS-WS (elevation).....	269
Fig. 13. HBS 8 test setup and connection details a) sketch of the test setup, b) sketch of the connection details, c) photograph showing test setup and, d) photograph of HBS 8 connection prior to testing	272
Fig. 14. Heat-treatment setup (a) photograph showing electric surface heating pads during installation on a beam flange, (b) photograph showing insulation of beam flange for well controlled heating and cooling.....	273
Fig. 15. Moment-rotation response of HBS 8.....	276
Fig. 16. Plastic rotation contributions by components of HBS 6, (a) total connection plastic rotation, (b) panel zone shear plastic rotation (c) column flexural plastic rotation and, (d) beam plastic rotation	277
Fig. 17. Moment rotation backbone curves for HBS 5, HBS 7 and HBS 8	278

Fig. 18. Recorded longitudinal strains along the center of top flange of the beam (a-d) HBS 5 and (e-h) HBS 8	280
Fig. 19. Progression of beam web and flange buckling recorded 406mm away from the column flange (a-c) HBS 5 and (d-f) HBS 8 (Beam is in positive bending i.e. top flange in compression).	282
Fig. 20. Photographs comparing the yielding, plastic hinging and local buckling at various stages of the loading history for (a-c) HBS 5, (d-f) HBS7, and (g-i) HBS8.....	283
Fig. 21. (a) Posttest photograph showing fracture of web stiffener fillet weld and beam web (b) Enlarged photograph at the fracture location (c) Sketch of web stiffener slot fillet weld detail.....	285

CHAPTER 1: Introduction

1.1 Background- Damage during 1994 Northridge Earthquake

Steel moment resisting frames have been popular lateral force resisting systems in many high seismic regions due to their perceived ductility and architectural versatility [1]. The perceived ductility of steel moment frames was challenged during the 1994 Northridge (Los Angeles, U.S.) and the 1995 Hyogo-ken Nanbu (Kobe, Japan) Earthquakes. In both earthquakes widespread damage to welded steel moment connections mostly in the form of fractures at or near the beam flange to column flange welds was observed [1]. In the Northridge earthquake, well over a 1000 weld fractures were found in over 200 surveyed buildings [2]. Most frequently, cracks initiated at the root of the beam bottom flange complete joint penetration (CJP) weld (Fig. 1) and were either confined to the weld metal or propagated to adjacent base metal (Fig. 2) [1,3]. In numerous reports and journal articles these fractures were described as being “brittle” as they occurred with little evidence of widespread yielding in the connecting members [3, 4, 5].

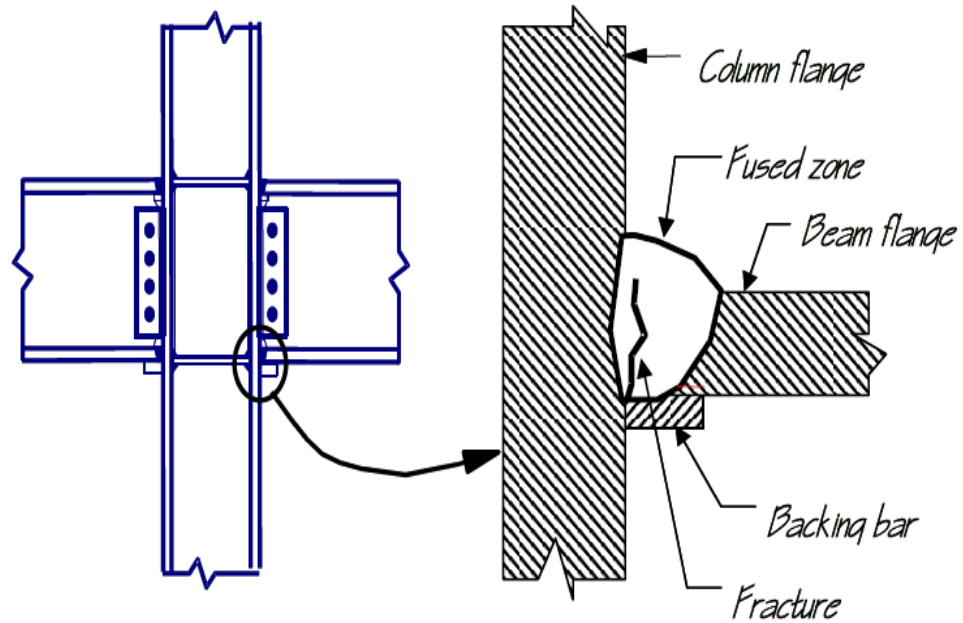


Fig. 1. Sketch showing beam-column connection and common mode of fracture during 1994 Northridge earthquake [3]

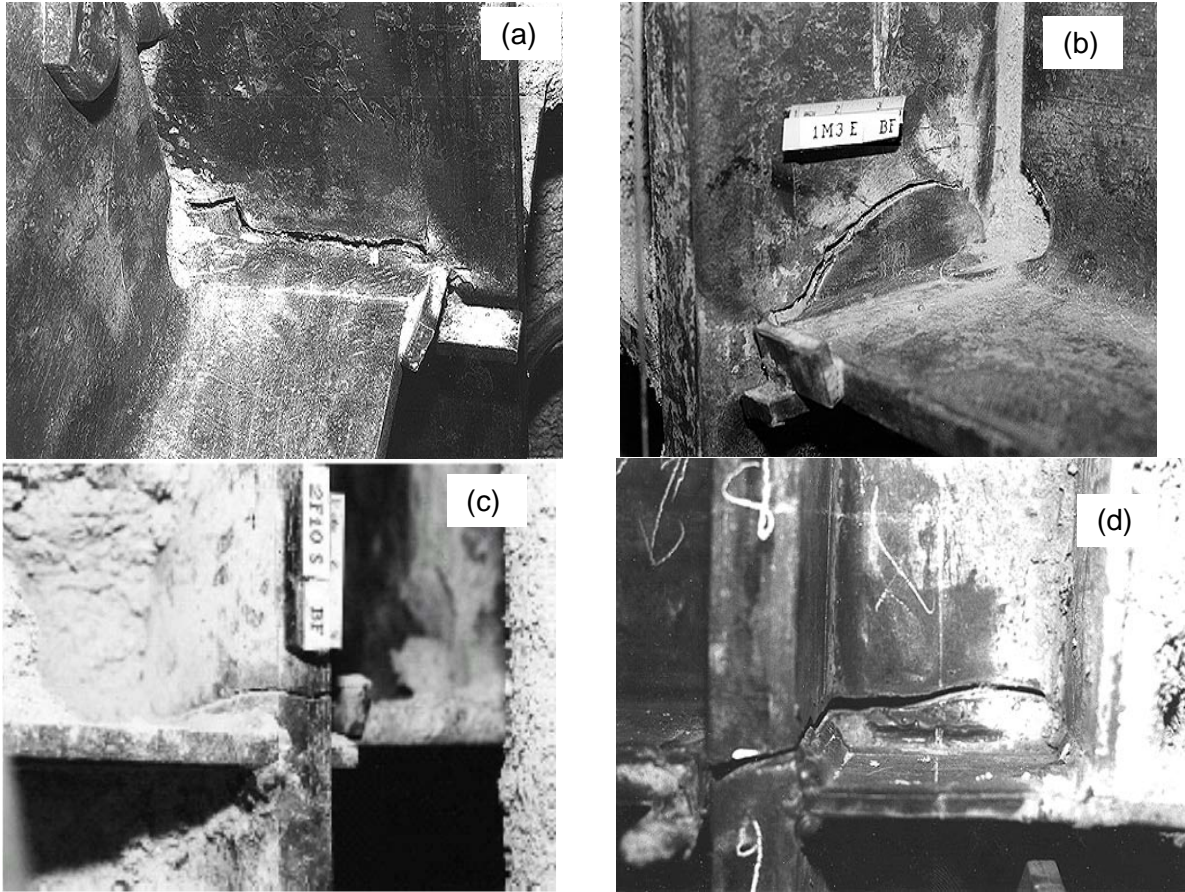


Fig. 2. Photographs showing beam to column connection fractures during the 1994 Northridge Earthquake (a) Fusion zone fracture, (b) column flange ‘divot’ fracture, (c) fracture progression through column flange and, (d) fracture progression through column flange and column web [3]

The poor performance of steel moment frames in the afore-mentioned earthquakes led to intensive research led by the SAC joint venture to uncover the underlying causes to these failures and to improve seismic design and construction practice going forward [6].

1.2 Causes for Failures and Improvements to Connection Design

The vulnerability of steel moment resisting connections to suffer premature fractures under severe seismic loading can be traced to 2 main factors. Firstly, moment resting frames

in their simplest form are rectilinear assemblages of beams and columns with beams rigidly connected to columns at their ends. At these rigid connections, deformations primarily due to shear and bending moments, which are developed to resist lateral forces, are restrained by the adjacent members. In other words, at the beam to column connections, beam deformations are restrained by the column and column deformations are restrained by the beam. These restraints lead to multi-axial stress states, and stress concentrations in the vicinity of the connection (particularly at the beam flange to column flange intersection) which cannot be calculated using classical beam theory.

Secondly, these stress concentrations are in most cases exacerbated by geometric stress risers (e.g. weld flaws, weld access holes etc.), residual stresses (either from manufacturing or welding). In addition to these stresses is the reduced fatigue resilience and ductility of the material in the weld heat affected zone (HAZ). All of these are introduced during the detailing, fabrication, and construction process. Therefore without careful connection design, detailing and high quality craftsmanship, steel moment connections may not deliver high levels of ductility (as intended) in moderate to severe earthquakes.

During the SAC joint venture research program attention was drawn to several of the afore-mentioned vulnerabilities. Strategies were developed to reduce or eliminate them and by so doing, enhance the seismic performance of steel moment resisting connections. A brief summary of some of the key research findings and recommendations is presented in the following.

1.2.1 Problems and solutions related to weld details, weld flaws and weld metal

Survey assessments of steel moment connections in buildings affected by the Northridge earthquake through visual and ultrasonic (UT) methods found that the vast majority of weld fractures emanated from large planar root indications/defects at the beam flange CJP welds[2]. These so called “root cracks” were classified as W1 indications by SAC investigators (Fig. 3) [2]. The single bevel weld detail shown in Fig. 3b is commonly used in field welding of joints as it allows welding in the preferred down hand position. However, this detail is especially vulnerable to undetected root defects due to the difficulty in visually inspecting the root pass and the well-known unreliability of UT inspection in conclusively identifying this weld flaw [7, 8]. The stress concentration at the tip of this crack-like-flaw is exacerbated at the beam bottom flange by local bending of the beam flange which places additional demands at the extreme fibers of the beam top and bottom flanges, and by the presence of the concrete slab which raises the neutral axis placing higher strain demands at bottom flange extreme fibers. Note that a W1 indication occurs at the extreme fibers of the bottom flange but not the extreme fibers of the top flange.

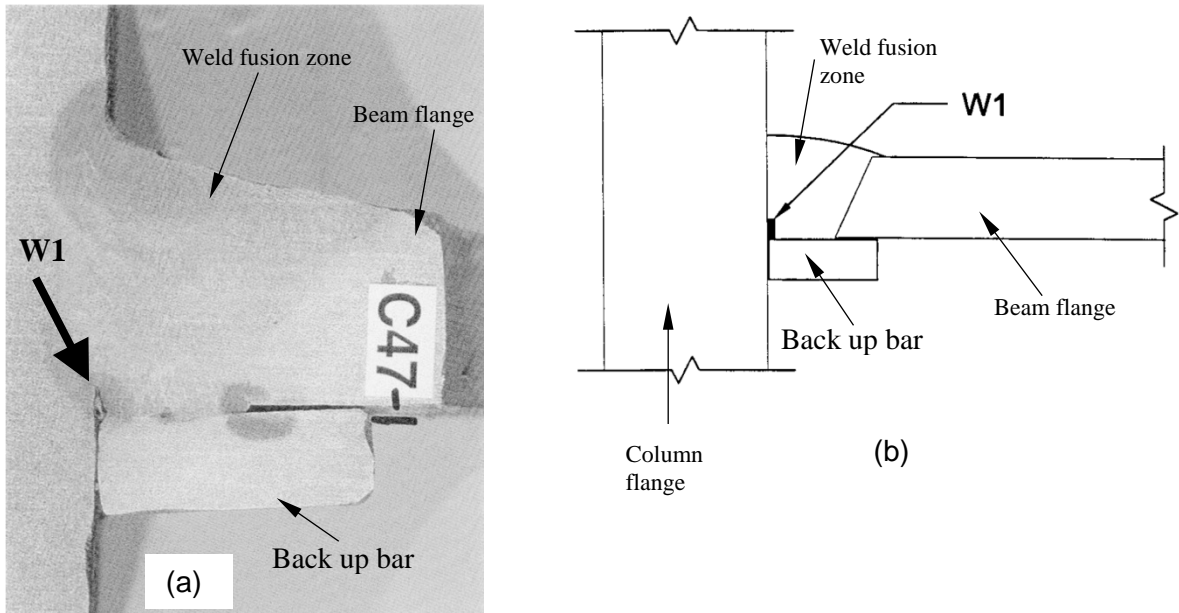


Fig. 3. W1 indication (a) Polished and etched sample with W1 (b) Sketch of beam bottom flange to column flange weld showing W1 [2]

Based on these findings, post Northridge connection details for welded unreinforced flange moment connections emphasized the use of visual inspection to identify this defect at the bottom flange. This involved removal of the bottom flange backing bar and visual inspection and repair (if necessary) of the weld root followed by the installation of a reinforcing fillet weld made in the overhead welding position. At the top flange, the backing bar is left in place but a reinforcing fillet weld is placed between the backing bar and the column flange.

Despite these efforts, studies showed that the inherently low toughness of the weld metal deposited by the commonly used E70T-4 electrode limited the ductility of connections with improved welding details. Studies on both full scale beam to column connections and pull plate test assemblies [9, 10] demonstrated this problem. It was found that use of

electrodes with minimum specified Charpy V notch-toughness (E70T-6, E70-TGK2 or E7018) significantly improved the ductility of pull plate test assemblies with the aforementioned improved welding details [10]. Figure 4 illustrates the observed distinct improvements in the ductility of these pull plate test assemblies when improved weld details and notch tough electrodes are used.

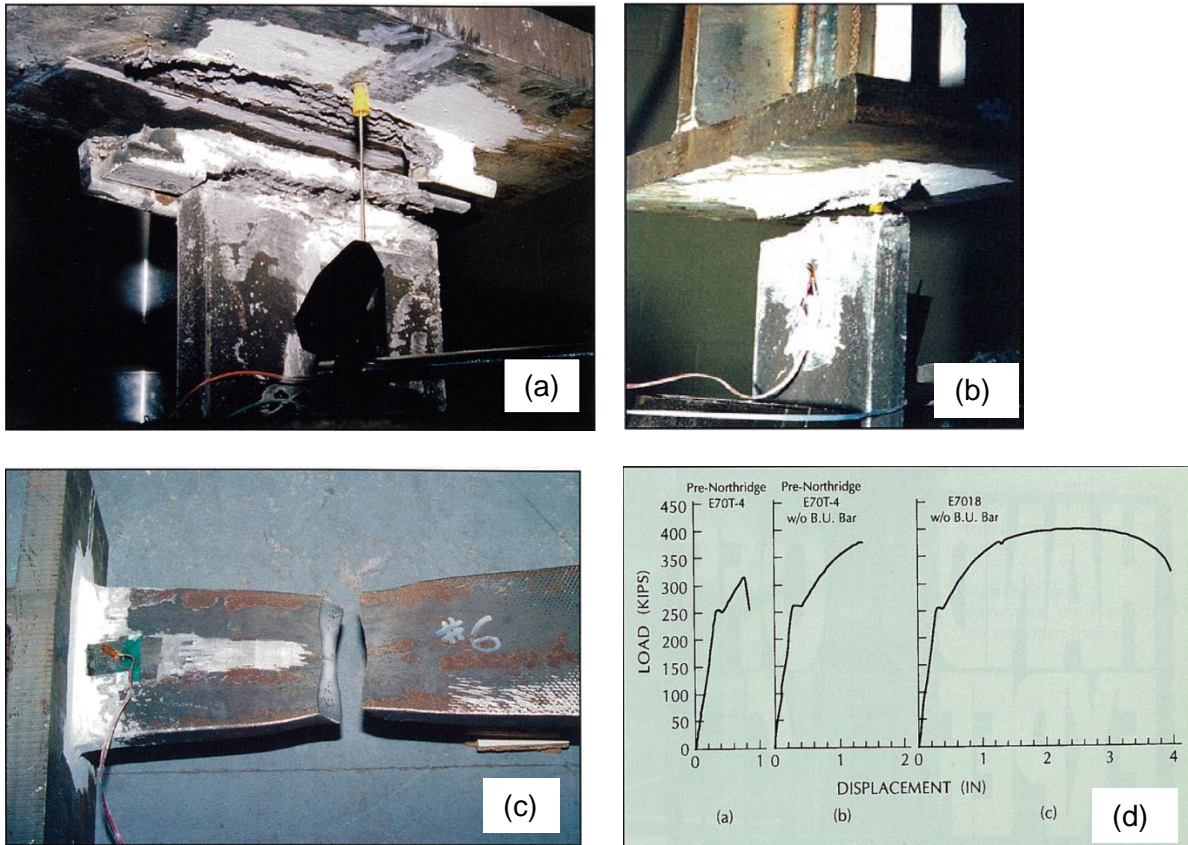


Fig. 4. Tests of pull plate ‘T’ assemblies (a) Welded with Pre-Northridge E70T-4 electrode and weld details, (b) Welded with Pre-Northridge E70T-4 electrode but with backing bar removed, (c) Welded with E7018 electrode and backing bar removed (d) Force-displacement curves showing from left to right the results of the 3 pull plate tests. [10]

1.2.2 Problems and solutions related to flange overstress

Despite the afore-described weld fracture mitigation strategies post-Northridge welded unreinforced flanged bolted web (WUF-B) connections were still found to be incapable of achieving the target 0.03 rads plastic rotation in standard proof tests [11]. In experiments carried out by Stojadinovic et al. 2000 [11], the failure mode change from brittle weld metal fractures (observed in pre-Northridge WUF-B connections) to ductile tearing followed by fast fracture of the base metal nucleating between the edge of the weld fusion zone and the base of the weld access hole. Whereas pre-Northridge WUF-B connections suffered from fractures mostly at the bottom flange welds, post-Northridge WUF-B connection failures showed no bias in either flange[11]. Figure 5 shows some examples of these failures from various studies. This new failure mechanism demonstrated that weld fracture mitigation strategies were effective in preventing weld failures but “overstress mitigation” strategies were also needed to alleviate premature failures [11].

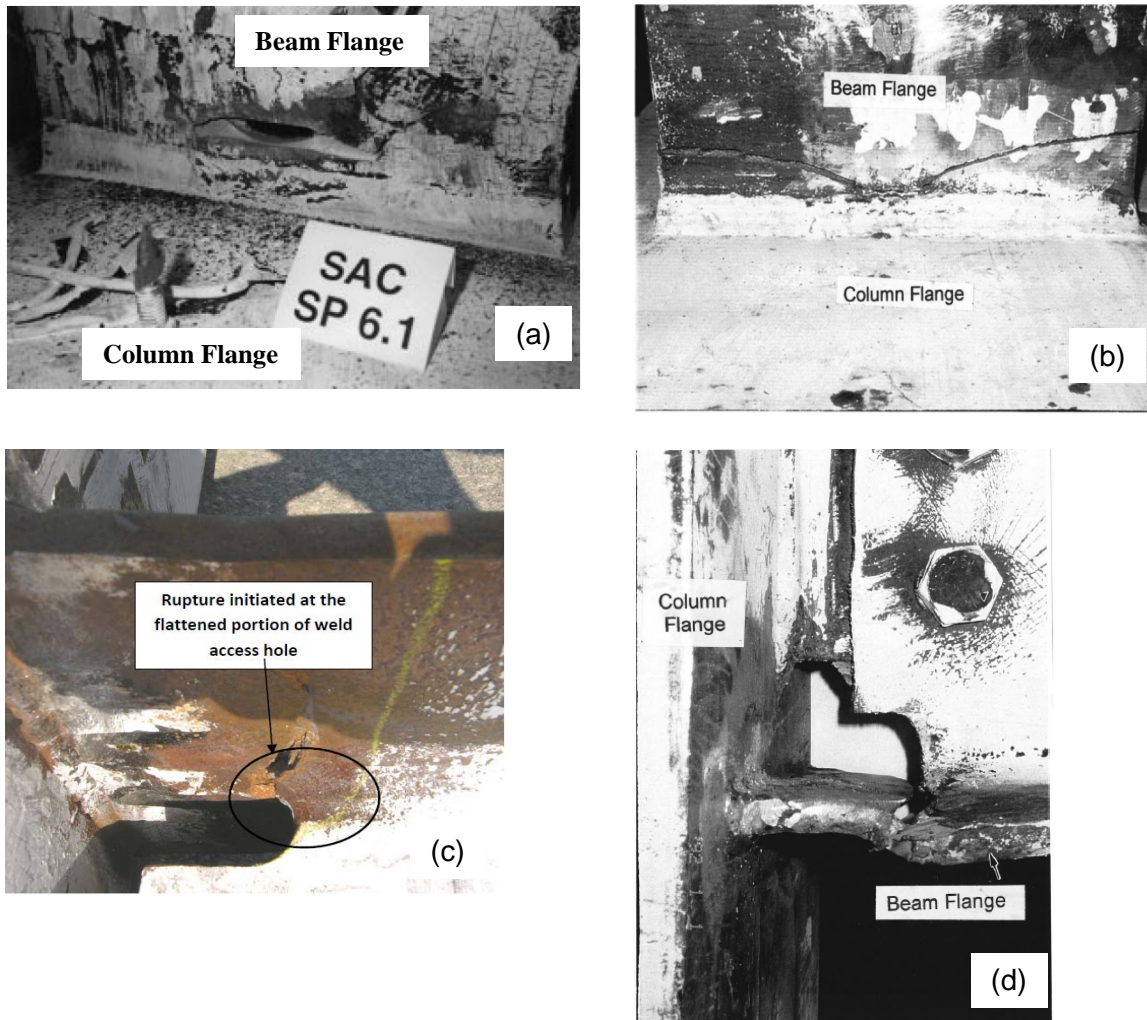


Fig. 5. Fractures in beam flange base metal in Post Northridge WUF-B connections. [11-13]

It was identified that in the post-Northridge WUF-B, beam flange ‘overstress’ occurred due to several factors including the lack of moment resistance provided by the beam web connection bolts [14], the additional stresses and severe stress gradients arising from deformation restraints at the connection [15] and stress concentrations due to the access hole cuts [14]. Based on these observations the SAC recommendations for future welded flange connections were to utilize CJP welded webs instead of their bolted counterparts [16],

improved access hole geometry to reduce stress concentrations [16] and most notably, strategies to shift plastic hinging of the beam away from the connection joint (connection overstress mitigation) [14].

Most of these connection overstress mitigation strategies involve either strengthening the connection or weakening the beam. Figure 6 shows some examples of these strategies from the literature.

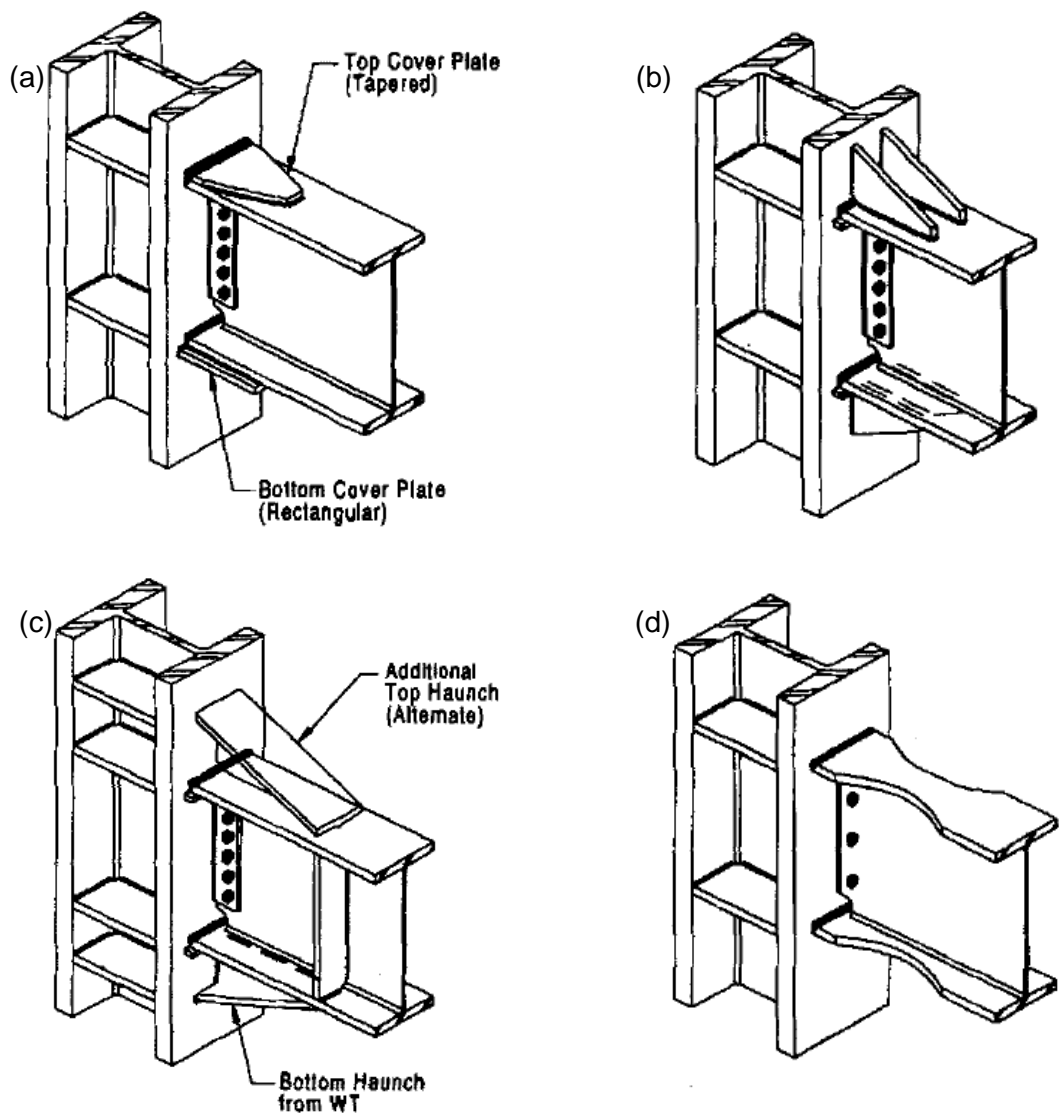


Fig. 6. Examples of modified connections (a) cover plate (b) upstanding rib (c) haunch (d) dog bone [14]

Note from Fig. 6 that the ‘dog bone’ or reduced beam section (RBS) (Fig. 6d) is the only beam weakening strategy, all others strengthen the connection.

Studies which incorporated weld fracture and connection overstress mitigation strategies resulted in significantly improved ductility compared to Post-Northridge and Pre-

Northridge WUF-B connections [17, 18]. Figure 7 shows photographs of the Haunch (Fig. 7a) and the RBS connections (Fig 7b) during laboratory testing. Note that yielding and beam plastic hinging take place away from the connection in both cases.

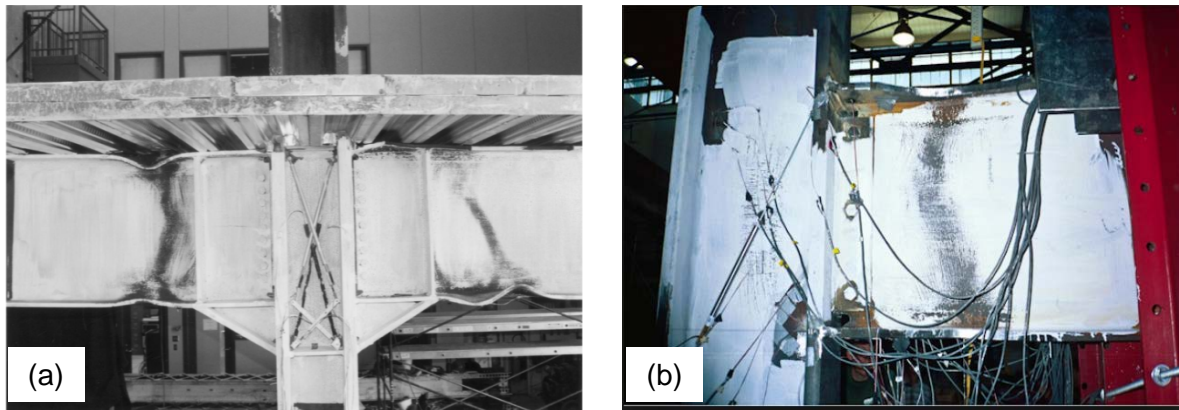


Fig. 7. Photographs during simulated seismic testing of connections with overstress mitigation strategies (a) Haunch connection (with concrete slab) [19] (b) RBS connection [23]

Both connection strengthening and beam weakening have their advantages and disadvantages. Connection strengthening strategies such as the haunch (Fig. 6c) have performed better (compared to the RBS) in enhancing the performance of pre-Northridge WUF-B connections [19]. This has been attributed to redirection of stresses away from the beam to column flange CJP welds by strut action in the haunch. This mechanism transfers much of the shear and bending stresses to the column [20]. However, in general, connection reinforcing strategies such as the haunch and cover plate (Fig. 6a) add significant cost and complexity to the design and construction of moment connections when compared to the RBS. In addition, although reinforcement is effective in shielding the beam flange welds

from large stresses, they create stress concentrations at the end of the strengthened region in the plastic hinge (e.g. at the toe of the haunch or rib and at the end of the cover plate) which may cause premature failure in these regions in the absence of ductile detailing and high quality craftsmanship [21].

The RBS weakens the beam by removing material from the beam flange in the dog bone shaped shown in Fig. 6d. Weakening of the beam promotes yielding and plastic hinging in the reduced section, and lowers demands on the beam flanges near the vicinity of the connection. The RBS does not alter the stress transfer path through the connection and does not prevent yielding of the beam flange CJP welds; as such, the RBS delivers better results when used in combination with the weld fracture mitigation techniques described in section 1.2.1 [19]. However, due to its economy and simplicity in design and construction and its sound performance in laboratory tests [17], the RBS is a popular connection overstress mitigation technique for new building construction in high seismic regions in the USA [22].

As a consequence of flange reductions, the RBS sacrifices elastic stiffness and buckling resistance. These shortcomings of the RBS connection have motivated the development of an alternative connection overstress mitigation strategy through beam weakening, which forms the cornerstone of the seismic performance enhancement techniques studied in this dissertation. These performance enhancement techniques are introduced in the following section.

1.3 Introduction to current study

This study involves the development and validation of performance enhancing techniques for steel building beam to column moment resisting connections. The first and

foremost of which is called the ***heat-treated beam section***. This technique involves selectively reducing the strength of the beam flanges (highlighted red in Fig. 8a) by subjecting them to high temperatures followed by slow cooling. Such a heat-treatment reduces the strength of the material as shown in Fig. 8b. As a consequence, under seismic loading, yielding and plastic hinging of the beam would take place in the heat-treated beam section (HBS). In a similar manner to the RBS, this connection provides overstress mitigation by weakening the beam, however, since the elastic modulus of the heat-treated steel is unaltered (Fig. 8b) the HBS does not sacrifice elastic stiffness as does the RBS. In addition, since the beam section remains intact and the plastic modulus of the heat-treated steel is also unaltered (note the downward shift of the stress-strain curve in Fig. 8b), the buckling resistance of a beam with the HBS is expected to be similar to that of the unmodified beam.

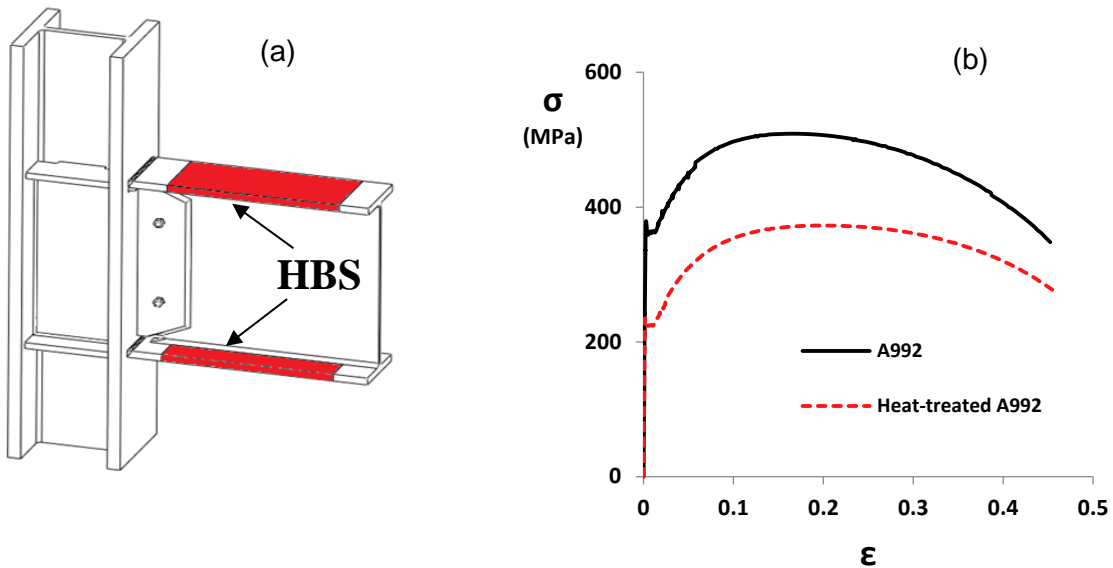


Fig. 8. (a) Heat-treated Beam Section (HBS) (b) Engineering Stress-Strain response of A992 and heat-treated A992 steel

In this study the HBS technique is applied to welded unreinforced flange-welded web (WUF-W), all welded (welded flange welded web), 8 bolt unstiffened extended endplate (EEP), and welded unreinforced flange bolted web (WUF-B) moment resisting connections. In both the EEP and WUF-B connections, modified bolt designs for further reducing the vulnerability of these connections to premature non-ductile failures have also been developed through detailed finite element (FE) analysis. Finally, a technique to improve the beam buckling resistance of HBS beam to column moment connections was developed. This technique called ***web stiffener*** involves attaching a steel plate to the beam web and column flange in the expected plastic hinge region. By so doing, the local buckling of the beam is delayed along with the associated strength degradation. Development of these performance

enhancing techniques through detailed FE analysis and experimental validation through full scale simulated seismic testing are described herein.

2. Scope and Organization

The findings of this study are presented through six chapters (Chapters 2 to 7) written in journal paper format. In addition Chapter 1 is the current introduction chapter and chapter 8 is the conclusions and recommendations for future work.

Chapter 2 describes application of the HBS technique to the WUF-W connection. This portion of the study included the full scale simulated seismic testing of four (4) WUF-W connections three (3) of which were modified with the HBS. Heating of the flanges in the HBS was accomplished with induction heating methods. The results of full scale simulated seismic testing as well as post-test FE analysis are presented in this chapter.

In chapter 3, the HBS is applied to an all welded (welded flange welded web) connection. The full scale test results of two (2) all welded connections modified with the HBS are presented. As a result of the findings in chapter 2, induction heating was replaced with traditional electrical resistance heating methods and improved results were obtained. Detailed discussion of experimental data to validate the HBS technique is presented.

Detailed FE studies of 8 bolt EEP connections are presented in chapter 4. This numerical study was led by Shahriar Quayyum. The chapter presents the use of advanced numerical techniques in the analysis of bolted EEP connections. These analyses were conducted to study the failure mechanisms of 8 bolt EEP connections and in so doing, prescribe and develop seismic enhancement techniques to improve connection performance.

This chapter proposes a modified unreinforced 8 bolt EEP connection which showed improved performance to the currently prequalified 8 bolt stiffened EEP connection in FE simulations.

In chapter 5 the experimental validation of the modified unreinforced 8 bolt EEP connection is discussed. Detailed experimental results to validate the performance enhancement techniques are presented along with post-test FE simulations. Areas for further improving the performance of this connection are identified.

The post-Northridge WUF-B connection is examined in detail in chapter 6. FE analysis is used to study the failure mechanisms which were observed in experiments and discussed in the literature, but had not been accurately captured through numerical or analytical methods. The FE model was then used to study a modified bolt arrangement which when combined with the HBS, significantly enhanced the seismic performance of the WUF-B connection. Finally, experimental validation of this improved WUF-B connection is described in detail.

Based on the observed local buckling failures of the previously mentioned connections, a technique for stiffening the beam web as a means to delay and reduce the rapid strength degradation from local buckling was explored in chapter 7. Finite element development and experimental validation of this web stiffening technique are presented. Detailed analysis of experiment results and comparative studies with control test specimens are discussed.

3. References

- [1] Bruneau, M., Uang, C.M., & Whittaker, A. (1998). *Ductile design of steel structures*. New York: McGraw Hill Companies.
- [2] Paret, T. F. (2000). The W1 issue. I: Extent of weld fracturing during Northridge earthquake. *Journal of structural engineering*, 126(1), 10-18.

- [3] FEMA-350, 2000, *Recommended Seismic Design Criteria for New Steel Moment-FrameBuildings*, prepared by the SAC Joint Venture for the Federal Emergency Management Agency, Washington, DC.
- [4] Tremblay, R., Filiatrault, A., Timler, P., & Bruneau, M. (1995). Performance of steel structures during the 1994 Northridge earthquake. *Canadian Journal of Civil Engineering*, 22(2), 338-360.
- [5] Popov, E.P., Yang, T., & Chang, S., (1998) "Design of steel MRF connections before and after 1994 Northridge earthquake," *Engineering Structures*, 20(12), 1030-1038.
- [6] Kunnath, S.K., & Malley J.O. "Structural Forum." *Journal of Structural Engineering* 126.1 (2000): 4-9.
- [7] Dubina, D., & Stratan, A. (2002). Behaviour of welded connections of moment resisting frames beam-to-column joints. *Engineering structures*, 24(11), 1431-1440.
- [8] FEMA-355B, 2000, *State of the Art Report on Welding and Inspection*, prepared by the SAC Joint Venture for the Federal Emergency Management Agency, Washington, DC
- [9] Sabol, T.A., Engelhardt, M.D., Aboutaha, R.S., Frank, K.H., "Overview of the AISC Northridge Moment Connection Test Program", in Proceeding of the World Conference on Earthquake Engineering (11WCEE), 1996.
- [10] Kaufmann, E.J., Xue, M., Lu, L. and Fisher, J.W., (1996) "Achieving Ductile Behavior of Moment Connections" *Modern Steel Construction June 1996*.
- [11] Stojadinovic, B., Subhash C.G., Lee, K-H, Margarian, A.G., and Choi, J-H (2000), "Parametric Tests on Unreinforced Steel Moment Connections," *Journal of Structural Engineering*, Vol. 126, pp. 40-49.
- [12] Barsom, J. M., & Pellegrino Jr, J. V. (2002). Failure analysis of welded steel moment-resisting frame connections. *Journal of materials in civil engineering*, 14(1), 24-34.
- [13] Syed S. Influence of weld sequence on the seismic failure of welded steel moment connections in building structures. MS Thesis, North Carolina State University, Raleigh, NC, 2009.
- [14] Engelhardt, M. D. and Sabol, T. A. (1997), Seismic-resistant steel moment connections: developments since the 1994 Northridge earthquake. *Prog. Struct. Engng Mater.*, 1: 68–77.
- [15] Richard, R.M., Partridge, J.E., Allen, J., "Finite Element Analyses and Tests of Beam-to-Column Connections", *Modern Steel Construction*, AISC, October 1995.

- [16] SAC Joint Venture (2000) “Development and Evaluation of Improved details for Ductile Welded Unreinforced Flange Connections” *Rep. No. SAC/BD-00/24*.
- [17] Engelhardt, M., Winneberger, T., Zekany, A., & Potyraj, T. (1998). Experimental investigation of dogbone moment connections. *Engineering Journal*, 35(4), 128-139.
- [18] Kim, T., Whittaker, A.S., Bertero, V.V., Gilani, A.S.J., and Takhirov, S.M. “Steel Moment Resisting Connections Reinforced with Cover and Flange Plates, SAC Joint Venture: Report SAC BD-00/27; 2000.
- [19] Uang, C., Yu, Q., Noel, S., and Gross, J. (2000). ”Cyclic Testing of Steel Moment Connections Rehabilitated with RBS or Welded Haunch.” *J. Struct. Eng.*, 126(1), 57–68.
- [20] Yu, Q., Uang, C., and Gross, J. (2000). ”Seismic Rehabilitation Design of Steel Moment Connection with Welded Haunch.” *J. Struct. Eng.*, 126(1), 69–78.
- [21] Chen, C. C., Chen, S. W., Chung, M. D., & Lin, M. C. (2005). Cyclic behaviour of unreinforced and rib-reinforced moment connections. *Journal of Constructional Steel Research*, 61(1), 1-21.
- [22] Ricles, J. M., & Zhang, X. (2006). Seismic Performance of Reduced Beam Section Moment Connections to Deep Columns. In *Structures Congress 2006@ sStructural Engineering and Public Safety* (pp. 1-10). ASCE.
- [23] Adan, S. M., 2011, “Design Parameters for Steel Special Moment Frame Connections,” Proceedings of the 2011 SEAOC Convention, Structural Engineers Association of California.

CHAPTER 2: An Innovative Seismic Performance Enhancement Technique for Steel Building Moment Resisting Connections Part I

Abstract

Results of an experimental study to validate an innovative technique for enhancing the seismic performance of steel beam to column moment connections are presented. The technique involves reducing the strength of specified regions of the beam flanges by exposing them to high temperatures followed by slow cooling. Analogous to the reduced beam section (RBS) connection, yielding and plastic hinge formation is promoted in the heat-treated section (HBS). However, buckling resistance and subsequent strength degradation of the HBS connection is expected to be superior to that of the RBS connection. A total of 4 large scale welded unreinforced flange- welded web (WUF-W) connections were tested in this study, all of which were modified by HBS. The test program showed that while the proposed heat-treatment technique was successful in the promotion of yielding and plastic hinge development in the heat-treated regions, the induction heating method applied to full scale beams needs further development. Finite element simulations of test specimens using an advanced constitutive model were helpful in explaining a connection strengthening detail of the WUF-W connection. Important observations are made for future development of the proposed HBS connection.

Keywords: Steel moment connection; seismic performance enhancement; beam plastic hinge; heat-treated beam section; reduced beam section;

1. Introduction

Extensive damage to welded steel moment resisting connections (WSMC) during the 1994 Northridge Earthquake instigated a comprehensive research effort led by the SAC joint venture intended to develop a broad and fundamental understanding of the seismic performance of moment frame connections [1]. Through this and other research efforts [2, 3, 4], several moment connections have emerged which demonstrate improved performance to that of pre-Northridge connections in laboratory testing. The 2010 ANSI/AISC 358 [5] currently qualifies several of these moment connections (Fig. 1) for use in Special and Intermediate Moment Frames (SMF and IMF).

The fundamental change to the design intent of special moment frame connections is to shift the plastic hinge away from the column face and into the adjacent beam interior. In some prequalified connections, the relocation of the plastic hinge is accomplished through strengthening and stiffening the connection to force the most of the inelastic action to occur in the beam flanges and web outside of the strengthened region. Connections which readily fit this category are the stiffened extended end plate (EEP) shown in Fig. 1a, bolted flange plate (BFP) shown in Fig. 1b, and the Kaiser bolted bracket (KBB) shown in Fig. 1c. Experimental studies [6, 7, 8] have shown that these connections were successful in causing hinging of the beam section beyond the strengthened region and that this led to improved seismic performance when compared to the pre-Northridge connection.

At first glance the welded unreinforced flange welded web (WUF-W) shown in Fig. 1d connection may not appear to employ a strengthening strategy. Previous research studies show good performance of WUF-W connections [9, 10] without clearly demonstrating how

all aspects of the connection detailing improves ductility. In the study reported herein (details provide later), it was found that the detailing of the WUF-W does provide reinforcement of the connection which reduces deformations near the welded joint and as a result, enhances seismic performance of the connection.

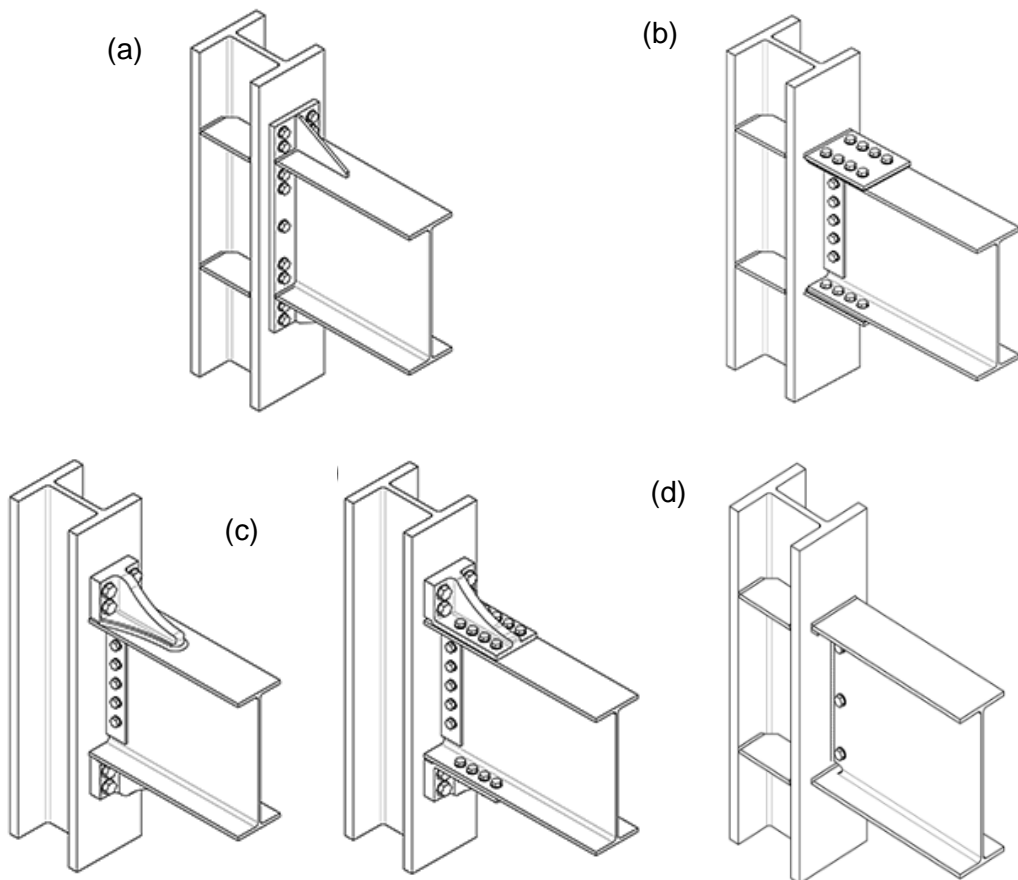


Fig. 1. Reinforced steel moment connections (a) Stiffened extended end plate (b) bolted flange plate (BFP) (c) Kaiser bolted bracket (KBB) and (d) Welded unreinforced flange-welded web (WUF-W) (figures from [11])

Contrary to the strengthened connections (EEP, BFP, KBB and WUF-W), the reduced beam section (RBS) is the only prequalified special moment frame connection in which the beam is intentionally weakened by removing beam flange material adjacent to the connection for relocation of the plastic hinge (Fig. 2a). During simulated seismic loading the RBS successfully develops plastic hinging of the beam in the reduced section and as a result relieves the high inelastic strain demands at the beam flange groove welds, thereby reducing the likelihood of fatigue failures and improving the ductility of the connection [12, 13]. However, the RBS sacrifices elastic stiffness and buckling resistance as a consequence of flange area reductions [14]. Despite these draw backs the RBS has found wide use in special moment frames [SMF's].

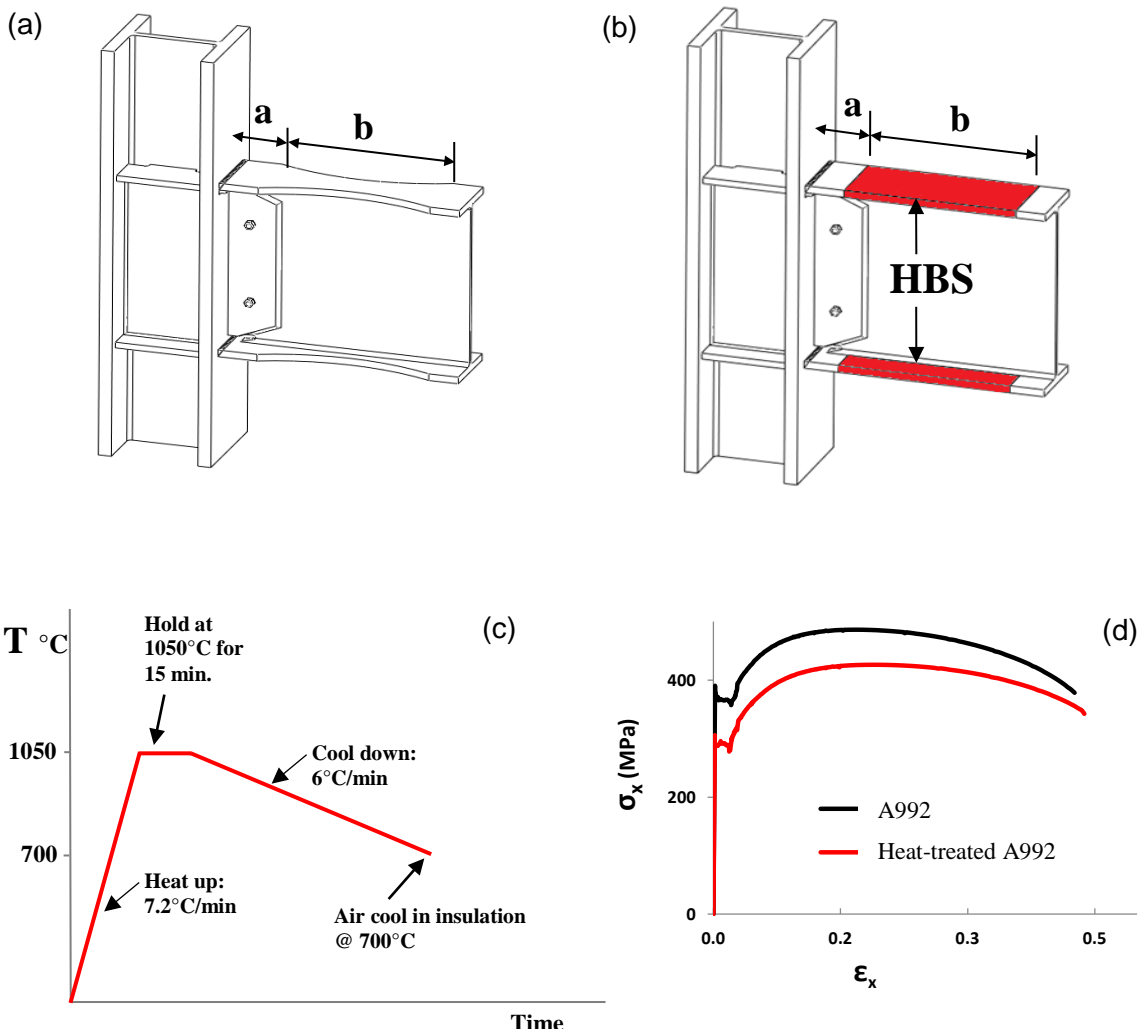


Fig. 2. (a) Reduced Beam Section (RBS) (b) Heat-treated Beam Section (HBS) (c) Temperature history of A992 heat-treatment (d) Engineering Stress-Strain response of A992 and heat-treated A992 steel

This study developed a novel performance enhancing technique through beam weakening. However, weakening is accomplished by heat-treating the beam flanges in the areas highlighted red in Fig. 2b according to the thermal history shown in Fig. 2c. The material strength in the heat-treated region is reduced as shown in Fig. 2d and consequently,

under simulated seismic loading, plastic hinging of the beam takes place in the heat-treated beam section (HBS). In a similar manner to the RBS, this connection provides a ductile seismic fuse through weakening, but because the elastic modulus and beam moment of inertia of the heat-treated section remain unchanged, the HBS does not sacrifice elastic stiffness as does the RBS. Also, since the cross section of the beam is unaltered and the inelastic portion of the stress-strain curve is also not significantly modified (Fig. 2d) the buckling resistance of a beam modified with the HBS is similar to that of an un-weakened beam.

The objective of this study is to experimentally validate the HBS concept. The results of four (4) full scale experiments performed on welded unreinforced flange welded web (WUF-W) connections, three (3) of which were modified with the HBS and one (1) which was unmodified are presented along with details of the heat-treatment method. Insights are drawn about one of the critical heat-treatment parameters and the effect that it has on both the material response and structural response observed in the full scale experiments. Posttest finite element analysis were conducted to more closely examine experimental observations. Results of experiment and finite studies are analyzed and important observations for future development of the proposed seismic enhancement technique are discussed.

2. Heat-treatment

Annealing is a heat-treatment practice which is used in the processing and manufacturing of a wide variety of tools, components and equipment. It usually involves heating the material to a particular temperature followed by a “soak” period and subsequent

cooling at a prescribed rate. The parameters of the annealing cycle are determined primarily based on the chemical, physical and metallographic properties of the material prior to annealing and the desired post anneal properties. In the production of steel alloy machine tools, annealing is usually done as an intermediary step in the manufacturing process to reduce hardness and improve workability and ductility of the material prior to cutting and shaping of the tool [15]. Because of the body centered cubic to face centered cubic phase transformation that steel undergoes above the lower critical temperature, the formation of new crystal grains is possible through phase transformation. In this annealing process the grain structure is recrystallized during heating above and cooling below the lower critical temperature. Careful control of the heating and subsequent cooling leads to a new coarser (larger grain size) grain structure from the annealing process. This coarsening of the grain structure through annealing is primarily responsible for the reduction in hardness of the work piece which is consistent with the well-established Hall-Petch relationship.

In this study annealing is employed in a similar way as is described above, except that the mechanical properties of interest are the uniaxial yield and tensile strength. Figures 4a and 4b show the effect of peak annealing temperature and cooling rate on the tensile properties of A992 steel. This data was obtained by heat-treating A992 steel coupons in a furnace followed by tensile testing. It can be seen from both these figures that with higher peak annealing temperatures and slower cooling rates the tensile behavior is softened (yield strength and tensile strength are lowered), it is also of importance to note, that the elastic modulus is unaltered from the annealing process.

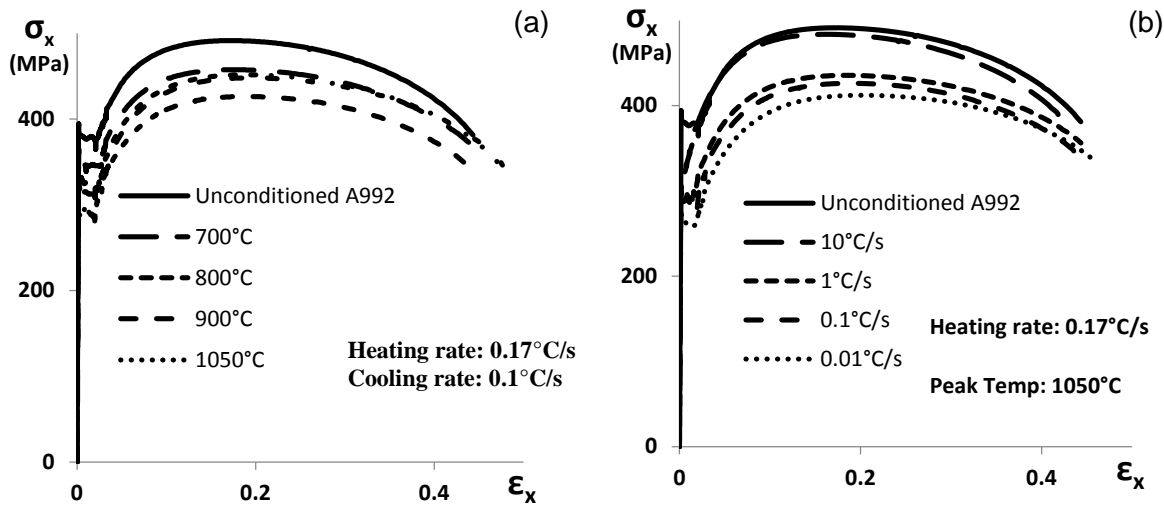


Fig. 3. Uniaxial Stress Strain response of Heat-treated A992 Steel a) Effect of peak temperature b) Effect of cooling rate

2.1 Application of Heat-treatment to Wide Flange Beams

Induction heating which provides a relatively energy efficient (compared to furnace heating methods) non-contact method of heating electrical conducting components was chosen as the method of heating wide flange beams for this study. Induction heating involves passing an alternating current through an electromagnetic coil (fig. 5a) at a high frequency. This generates an alternating magnetic field which induces eddy currents in the nearby located metallic work piece. The electrical resistance of the work piece leads to Joule heating of the metal. Induction heating has the advantage of isolating heat input to selected areas of the work piece through appropriate design of the induction coil. The apparatus shown in Fig 5a and 5b was utilized for induction heat-treatment of the beam flanges. This heat-treatment was carried out after the beams were fabricated but prior to field welding of the beams to the

columns.

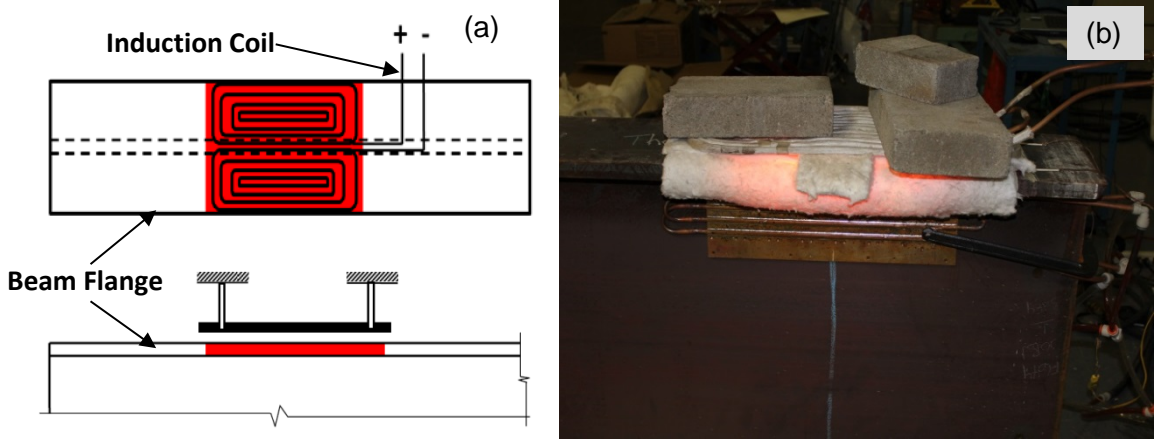


Fig. 4. Induction heating of wide flange beam, (a) schematic showing heat-treatment setup (b) photograph showing induction heating of beam flange

3. Experimental Setup and Connection Design

The experimental investigation consisted of four welded unreinforced flange, welded web (WUF-W) connections, three of which were modified with the HBS. See Figs. 6a and 6c for the test setup. The specimens were tested in the beam vertical, column horizontal position to facilitate ease of testing as shown in Fig. 6c. Two clevis supports were bolted to the lab floor and to the specimen column to simulate points of inflection in prototype frames. Two 978 kN (220 kip) hydraulic actuators were attached to the reaction wall, and connected to bracket beams which were bolted to the specimen beam.

A summary of the test specimens is shown in table 1. The beam and column section sizes and lengths were chosen to be similar to those of specimen DB5 studied by Engelhardt et al. [13]. Connection details are shown in Fig. 6b and were kept the same for all specimens

except the panel zone reinforcement which was increased in proportion to the expected increase in panel zone shear demands from increased bending moments at the column face for the control 1 specimen. All column doubler plates and continuity plates were made with ASTM A572 Gr. 50 steel and the doubler plates were sized to create a balanced panel zone based on the recommendations of Uang et al²³

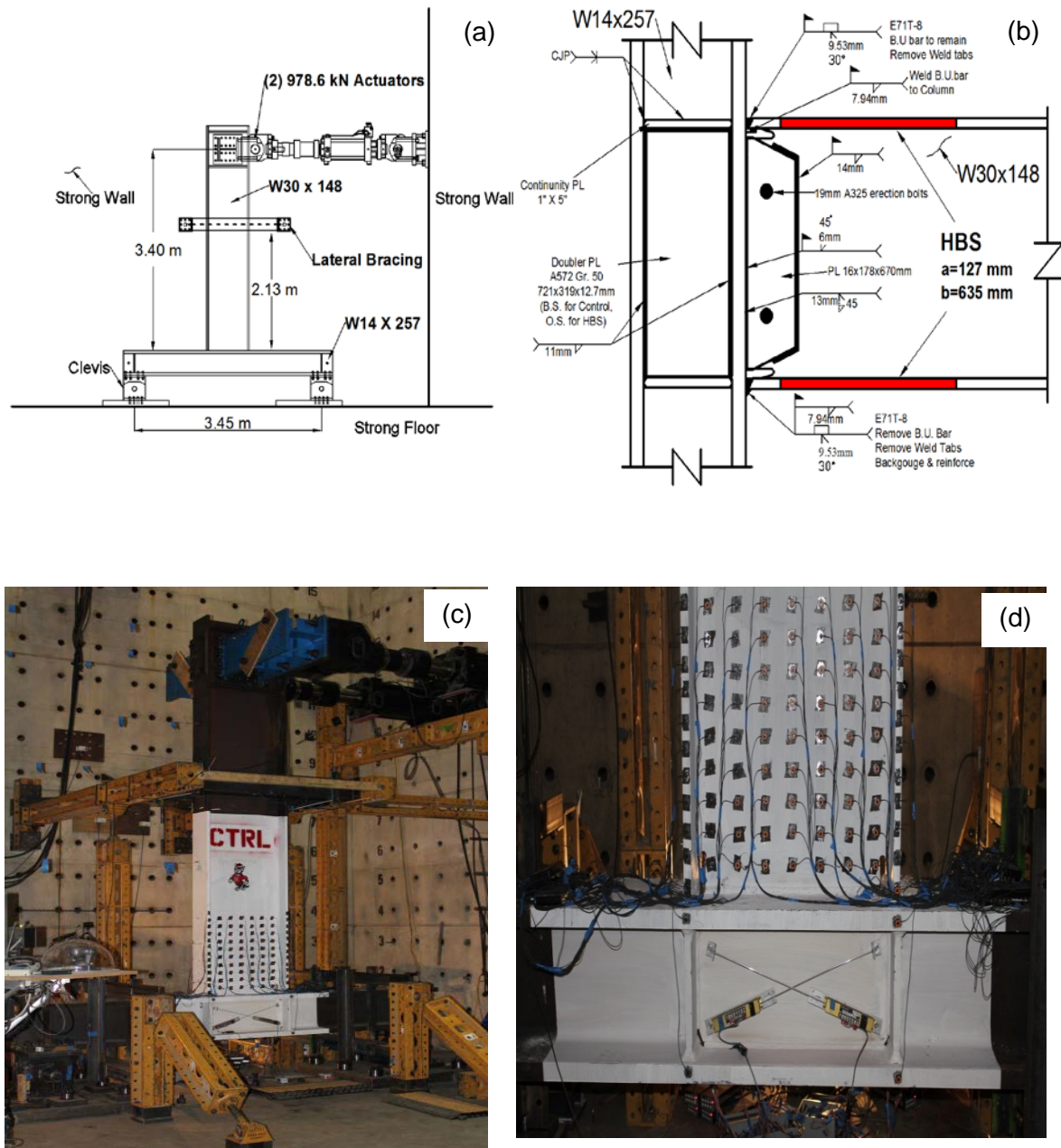


Fig. 5. Test setup and connection details a) sketch of the test setup, b) sketch of the connection details, c) photograph showing test setup and, d) photograph of control 1 connection prior to testing

All field-welding of the specimens were completed in the column vertical beam horizontal orientation. Complete joint penetration (CJP) welds were made with E71T-8 self-shielded flux-cored electrode with 1.8mm (0.072") diameter electrode wire. The E71T-8 electrode wire produces weld metal with high toughness that meets Charpy V-notch (CVN) toughness requirements of 27 J (20 ft.-lbs.) at -28 °C (-20°F). Top and bottom CJP weld passes were alternated for each pass to reduce distortion, also the location of weld starts and terminations for the bottom flange CJP weld were alternated for each pass to avoid the possible accumulation of flaws at one location. Upon completion of beam flange to column flange CJP welds, the beam webs were attached to the column flange by a 6mm (1/4") root CJP vertical weld and a 14 mm (9/16") fillet weld was placed around the perimeter of the shear tab to complete web attachment. Removal of the beam flange to column flange CJP weld runoff tabs were done with air carbon arc gouging and ground smooth to prevent notch effects. The top flange back up bar was left in place and was reinforced with an 8mm (5/16") overhead fillet weld on the column side. The backer bar and root in the bottom flange CJP weld was removed by air carbon arc gouging and was re-welded and reinforced with an 8mm (5/16") overhead fillet weld. All CJP welds were ultrasonically (UT) tested by a certified inspector in conformance with AWS D1.1-10 and AWS D1.8-09.

Table 1 Summary of test specimens

Specimen	Connection Detail	Heat-treated	Doubler Plate thickness (mm)	Continuity plate thickness (mm)
HBS 1	WUF-W	yes	1 @ 12	25
HBS 2	WUF-W	yes	1 @ 12	25
HBS 3	WUF-W	yes	1 @ 12	25
Control 1	WUF-W	no	2 @ 12	25

Each specimen was equipped with strain gauges along the beam flanges to monitor longitudinal flange strains, at various locations including the weld toe and HBS region. Non-contact displacement measurement devices, string potentiometers and linear variable differential transformers (LVDTs) were used to monitor displacements in the column, beam and panel zone. Calibrated load cells in the hydraulic actuators provided readings of force response during the experiment. All specimens were painted with hydrated lime prior to testing to visually indicate regions of yielding.

4. Results

Testing was conducted at the University of Minnesota multi axial sub assemblage (MAST) testing laboratory on an exterior type sub-assemblage (single cantilever). Loads were applied at the beam tip in accordance with the 2010 ANSI/AISC 341 [16] seismic provisions Appendix S loading protocol consisting of quasi-static increasing amplitude displacement cycles. Figure 7 shows the moment-rotation response of the four specimens. All

specimens met or exceeded the AISC Seismic Provisions (ANSI/AISC 341-10) SMF qualifying 4% interstory drift angle without significant strength loss.

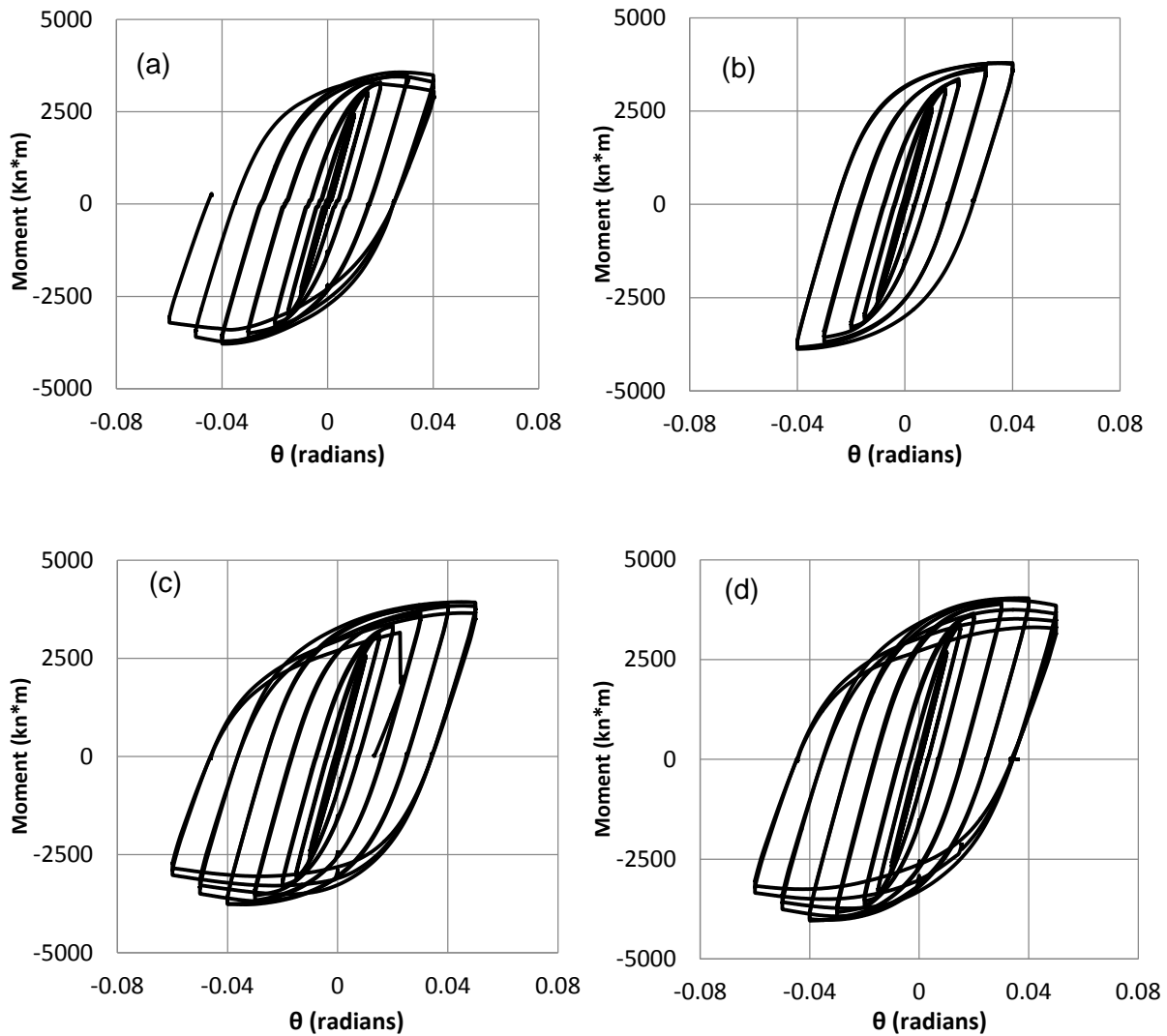


Fig. 6. Moment-rotation responses of test specimens a) HBS 1 b) HBS 2 c) HBS 3 and, d) Control 1

4.1 HBS specimens

Initiation of yielding observed from the flaking of white wash occurred during the first cycle of loading at 1% drift for connections modified with the HBS. Yielding was primarily observed on the beam flanges in the heat-treated regions, the panel zone and to a lesser extent the beam web. As loading progressed to higher drift amplitudes yielding progressed throughout the beam flanges outside of the heat-treated regions though most of the damage remained in the heat-treated regions. Slight lateral beam buckling followed by local flange and local web buckling (in the HBS region) initiated during the first cycle at 4% drift. Local flange and web buckling were followed by lateral torsional buckling which then led to strength degradation. Figure 8a shows plastic hinging and local flange buckling of HBS 1. Loading of HBS 1 and HBS 2 was terminated prior to specimen failure to prevent damage to the experimental setup due to the twisting beam. Damage of the experimental setup occurred at the clevis supports at the column ends which led to rigid body rotation of the column during cycles at drift angles of 4% or higher. The columns of specimens HBS 3 and WUF-W were laterally braced at each clevis support to prevent this damage from reoccurring.

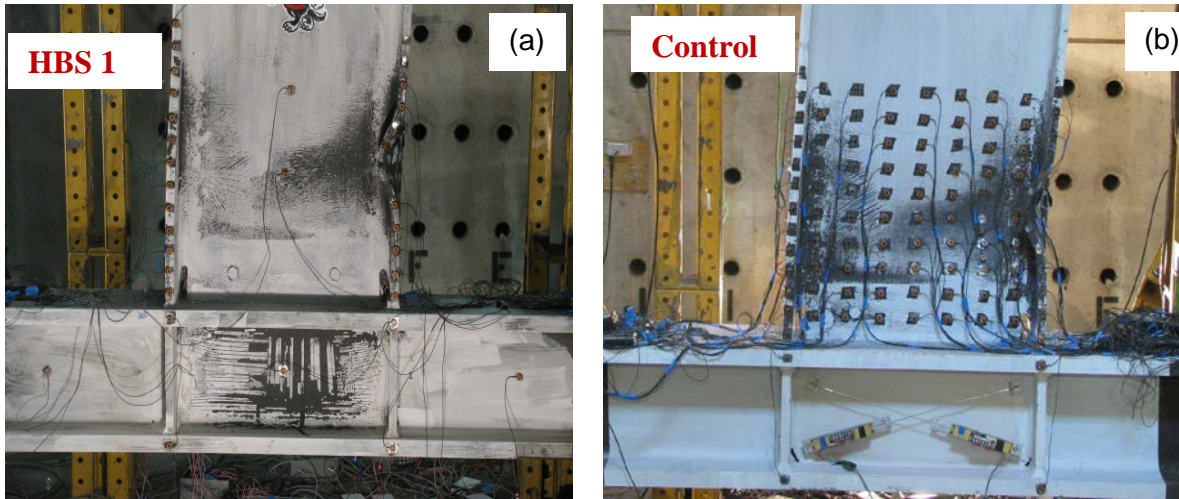


Fig. 7. Plastic hinging and local buckling of a) HBS 1 and, b) Control 1

4.2 HBS 3 Welding Error

An inadvertent error was made during the welding of specimen HBS 3 where a fillet weld was placed between the back-up bar and the beam top flange. An attempt was made to remove this weld by carbon air arc gouging. However, to prevent significant damage to the beam flange from the back gouging process, a small region of fusion remained between the beam flange and backup bar. Due to the added column bracing at the clevis supports loading was continued past 4% drift for HBS 3 and was eventually terminated due to the fracture of the beam top flange initiating in the area of fusion between the beam flange and the backup bar from the afore mentioned welding error.

4.3 WUF-W Test Results

Yielding of the WUF-W specimen was observed to initiate at the toe of the beam flange CJP welds during the first cycle of loading at 1% drift (Fig.9a). This yielding propagated throughout the beam flange and web with only slight yielding observed in the

panel zone. The onset and progression of lateral and local beam buckling led to progressive strength deterioration at loading cycles greater than 4% drift. Loading was eventually discontinued due to damage sustained to the column lateral bracing frame. It was observed that though yielding of the beam flange initiated at the CJP flange weld toe, yielding of the beam web was forced away from the connection region and took place primarily just outside of the welded shear tab. As a result, yielding of the full cross section of the beam took place approximately 8 inches away from the column face. This stiffening of the beam web also appeared to prevent local buckling within the stiffened region. Fig. (8b) shows the plastic hinging and local buckling of the WUF-W. Note the pattern of substantial yielding (indicated by the flaking of the white wash) of the beam web around the shear tab. Note also, that the shear tab is located on the opposite side of the beam web, however the outline of the shear tab is visible in this photograph as the strengthening effect created by the shear tab forces most of the deformation of the beam web to occur away from the connection (just outside of the shear tab).

To better illustrate the stiffening effect of the welded shear tab, the progression of yielding in control 1 is plotted in Fig. 9a-9d. Yielding of the beam flange (weld toe) during cycles at 1% drift is shown in Fig.9a. This is followed by a pronounced yielding of the beam web around the welded shear tab at 1.5% drift shown in Fig. 9b. During subsequent cycles at 2% and 3% drift further yielding of the beam flanges and web are observed to spread away from the connection as show in Fig 9c and 9d.

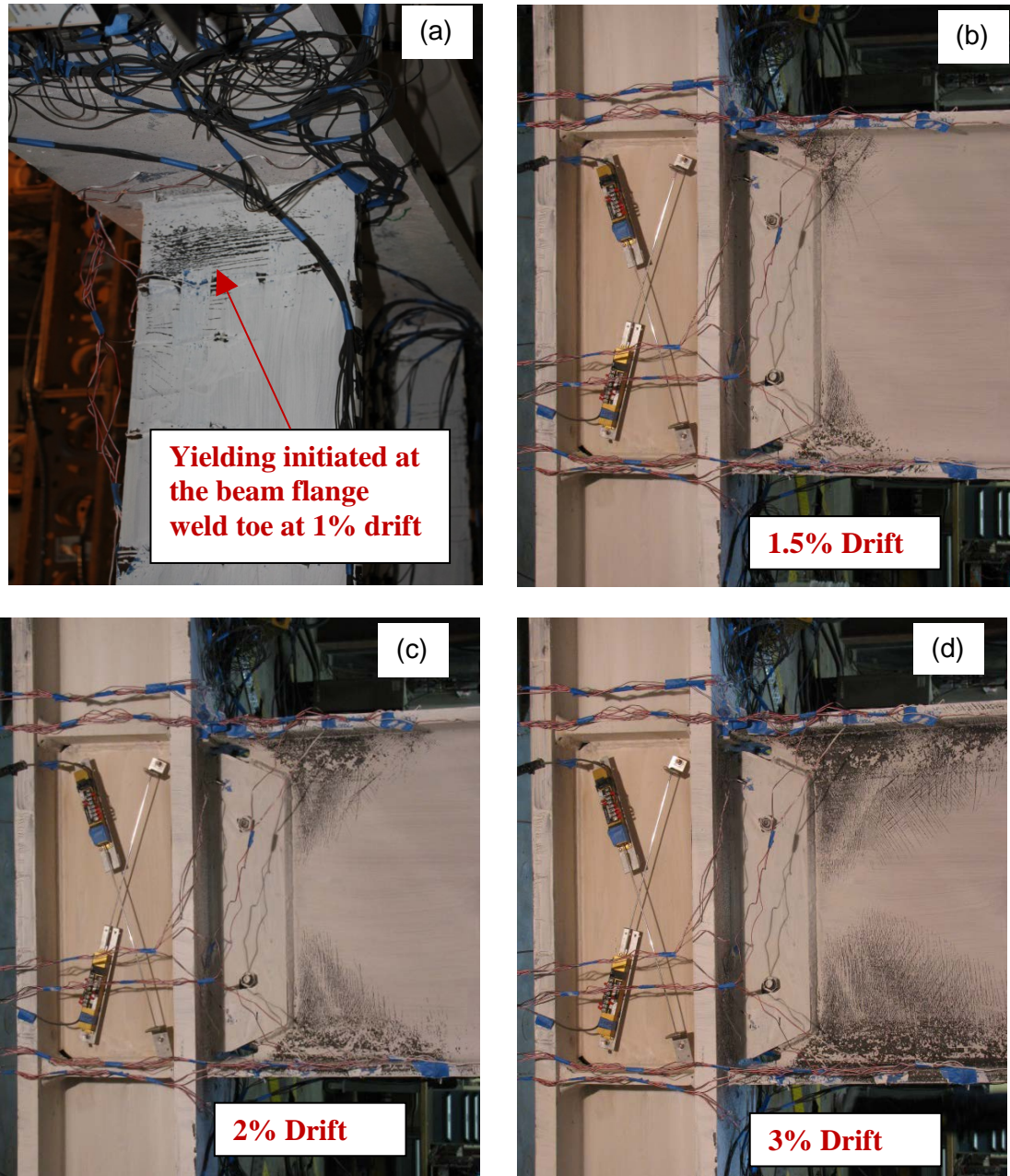


Fig. 8. Progression of yielding of Control 1 a) Initiation of yield at beam bottom flange weld toe at 1% drift b) Yielding in beam web around welded shear tab at 1.5% drift c)progression of yielding away from connection at 2% drift d) further progression of yielding away from connection at 3% drift

4.4 Evaluation of HBS performance

Figures 10c and 10d shows comparisons of average longitudinal strains measured at 2 locations on the beam flanges of specimens HBS 3 and WUF-W. These strains were computed by post processing position time history data obtained from Krypton LED markers which were attached to the beam flanges. Figure 10c shows the comparison of strains measured approximately 178 mm (7") away from the column flange (within the region of heat-treatment in the case of HBS 3) and figure 10d compares strains measured approximately 13mm (0.5") from the toe of the CJP flange weld. The effect of the HBS in reducing strain demands near the beam flange CJP welds is apparent through examination of these graphs. Also, note that reduction in strain demands at the beam flange weld toe recorded in specimen HBS 3 were accompanied by higher strains in the regions of heat-treatment which confirms the relocation of damage and plastic hinge formation observed visually as shown in Fig.10a. Note in Fig. 10a that in the case of the HBS majority of the white wash was flaking takes place in the HBS (region A in Fig. 10a), while in the case of the control specimen yielding is more pronounced closer to the connection region (region B in Fig. 10b).

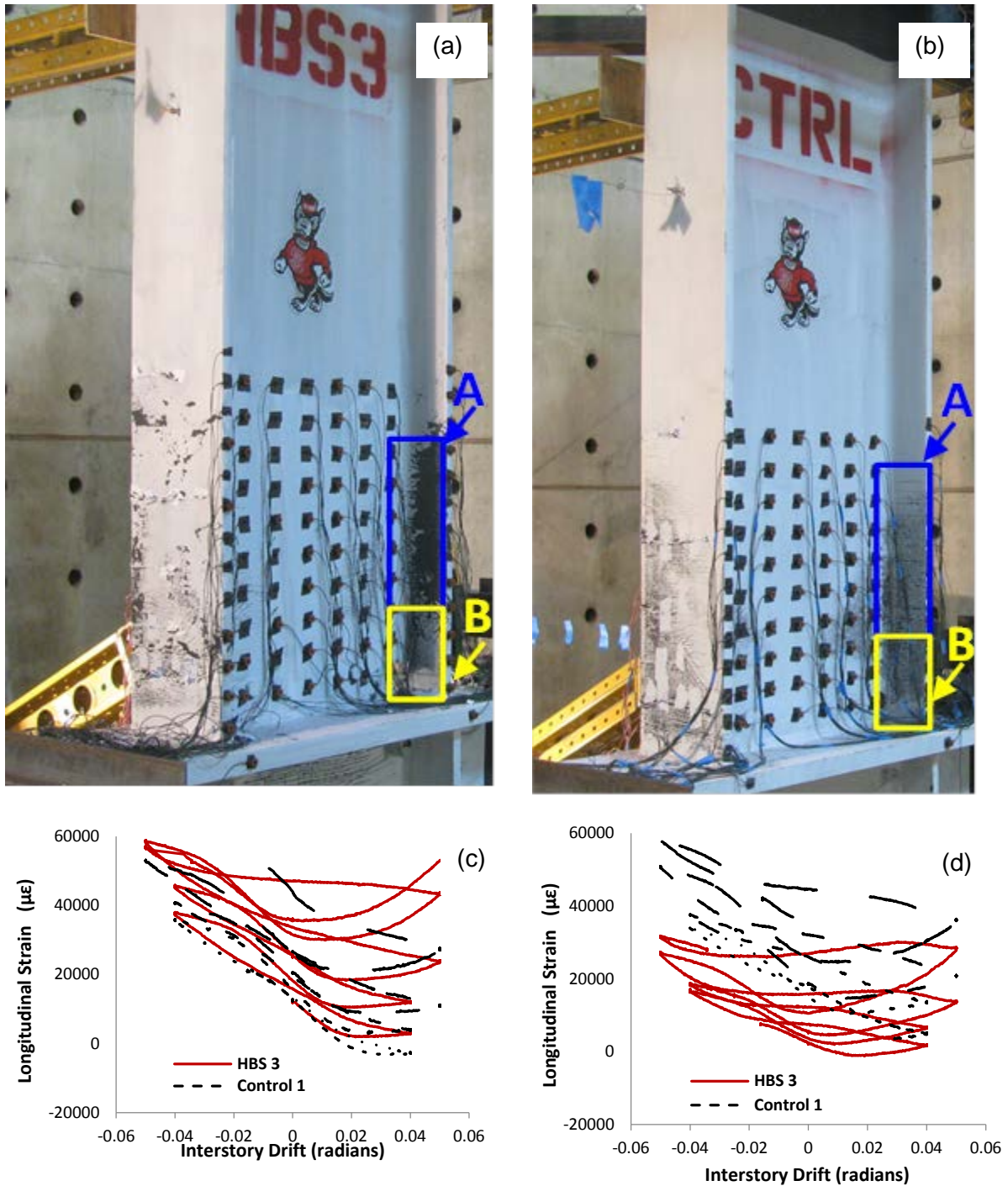


Fig. 9. Comparison of beam yielding for HBS 3 and Control 1, (a) Photograph of HBS 3 at 3% drift (b) Photograph of Control 1 at 3% drift (c) Recorded longitudinal strains along the side of the beam top flange 178 mm (7") from the column face for Control 1 and HBS 3 (d) Recorded longitudinal strains along the side of the beam top flange 13mm (0.5") from the column face for Control 1 and HBS 3

Table 2 presents a summary of the test results for HBS and control specimens. This table summarizes the plastic rotation contributions by the various components of the total rotation including panel zone shear, column flexural and beam flexural rotations. These components have been calculated using equations proposed by Popov et al. 1986[17]. From these calculations it can be seen that HBS specimens underwent higher amounts of inelastic panel zone deformation compared to the control specimen. For example in HBS 3 plastic panel zone rotation accounted for approximately 25% of the total plastic rotation while in the control specimen plastic panel zone rotation accounted for only 6% of the total plastic rotation. This difference in panel zone participation is related to higher than expected material strength in HBS connections which will be discussed more later.

Table 2 Summary of test results

Specimen	HBS 1	HBS 2	HBS 3	Control 1
Total maximum interstory drift (radians)	0.06	0.04	0.06	0.06
Total plastic rotation (radians)	0.046	0.026	0.049	0.049
Panel zone maximum plastic rotation (radians)	0.009	0.009	0.012	0.0029
Beam maximum plastic rotation (radians)	0.031	0.011	0.036	0.0432
Column maximum plastic rotation (radians)	0.006	0.006	0.0075	0.0028
M/M_p (at column face)	1.18	1.21	1.23	1.26
Failure Mechanism	Test terminated to prevent damage to experimental setup	Test terminated to prevent damage to experimental setup	Fracture initiating at a welding error between backing bar and beam flange	Test terminated to prevent damage to experimental setup

Table 2 also presents the ratio of the recorded moments at the column face to the plastic moment of the beam cross section at the column face. Maximum bending moments at the face of the column were 18-23% higher than the calculated plastic moment of the beam for HBS specimens and 26% higher for the control specimen. From this data it is apparent that the HBS specimens did not significantly reduce maximum bending moments at the column face as was expected. This can be explained by examination of Fig. 11 which shows a comparison of the stress-strain response of unconditioned A992 steel, furnace heat-treated A992 steel and induction heat-treated A992 steel. The induction annealed samples were taken from a beam flange which was subjected to an annealing cycle identical to that of the test specimens (Fig. 3a). The furnace annealed steel was taken from a beam flange, placed in an electric furnace and subjected to the thermal cycle shown in Fig.3a. The prescribed thermal cycle for the furnace heat annealed and induction annealed material were the same however, as can be seen in Fig.11 the tensile response is significantly different. Though both tensile specimens had similar proportional limits (furnace annealed $\sigma_0 = 275$ MPa, induction annealed $\sigma_0 = 281$ MPa) the post yield behavior is vastly different. The induction annealed material exhibits no yield plateau and work hardens at a fast rate achieving both a higher ultimate strength (furnace annealed $\sigma_u=414$ MPa, induction annealed $\sigma_u= 483$ MPa) and a reduced ductility. This significant variation in stress-strain behavior particularly the increase in the rate of work hardening and the increase in tensile strength led to the observed minimal reduction of bending moment in HBS specimens. Pre test analyses were conducted based on the tensile response of furnace annealed A992 coupons and as a result, these analyses under predicted the moment capacity of HBS moment connection specimens. Examination of the

induction heat-treatment apparatus and temperature time history data showed 2 main shortcomings of this methodology:

1. Due to the large volume of steel which was prescribed to be heated, the single induction coil used in the setup shown in Figs. 5a and 5b was insufficient to produce a uniform temperature distribution in the HBS.
2. The lack of adequate insulation prevented the desired slow cooling rate from being achieved. Analysis of temperature time history data have shown that the actual cooling rate of the HBS specimens were significantly faster than the rate prescribed.

The combination of these 2 shortcomings is believed to be the cause of the dramatic difference in stress strain behavior of the induction annealed and furnace annealed tensile specimens.

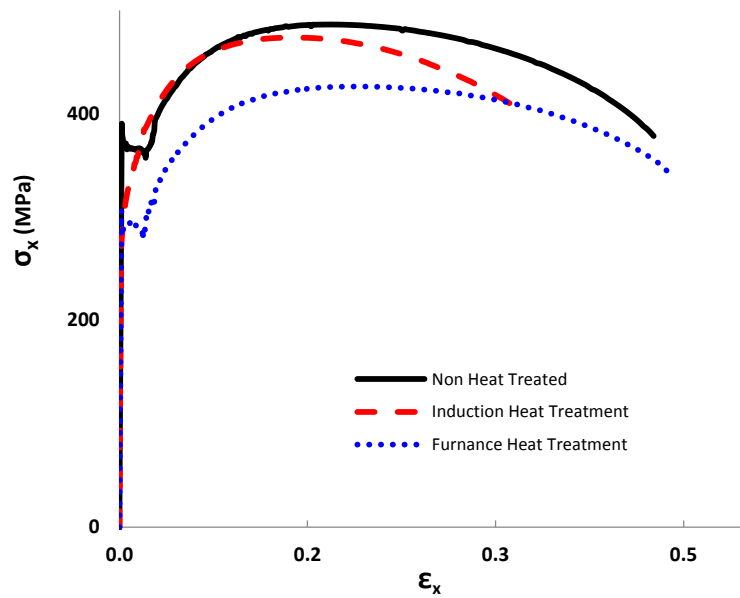


Fig. 10. Comparison of Uniaxial Stress Strain response of Heat-treated A992 Steel

The effect of the fast rate of work hardening of the induction heat-treated material on connection response is observed by comparing hysteresis loops from 1% to 4% story drift for HBS 2 and Control 1 as shown in Fig 12. In this figure a higher rate of increase in bending moment with increase in story drift is evident for HBS 2 compared to Control 1. This is can be observed by comparing the difference in peak bending moments of HBS 2 and control 1 at each drift angle. Note that difference in peak bending moments reduces with progressive cycles and by 4 % drift there is only a small difference in peak bending moments between HBS 2 and the control 1.

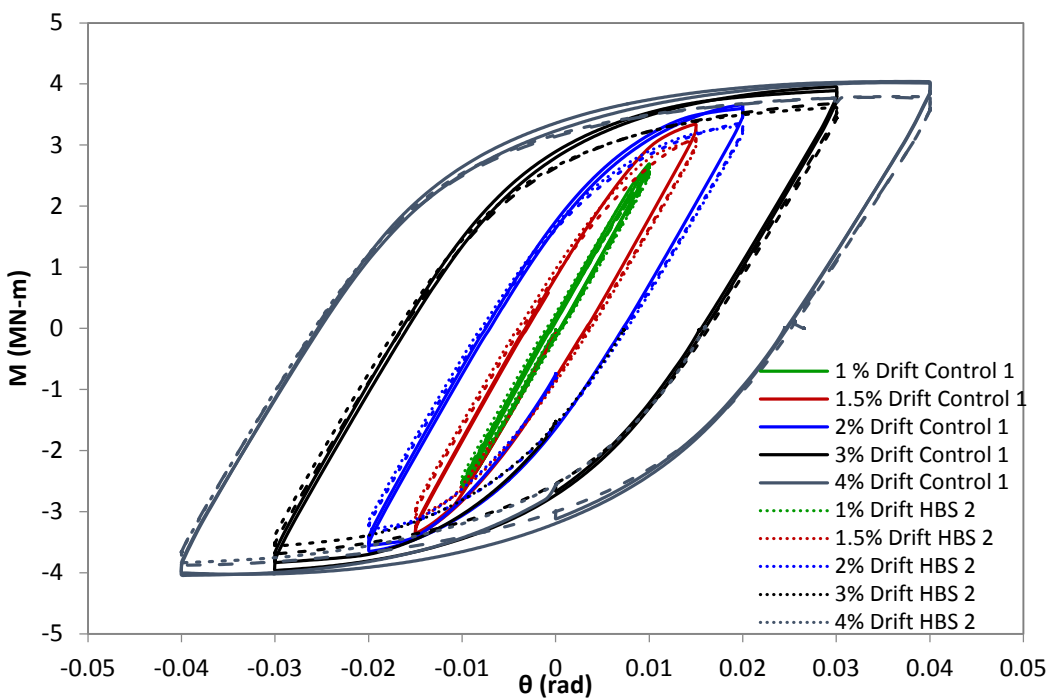


Fig. 9. Comparison of hysteresis loops from 1% to 4% story drift for HBS 2 and Control 1

5. Post-experiment microstructure analysis of Heat-treated A992 steel

Steel samples from the test specimens were studied using optical microscopy to analyze the effect of the heat-treatment on the material microstructure. Optical microscopy images of A992, furnace heat-treated A992 and induction heat-treated A992 steels are shown in Fig. 13. In these images it can be observed that the furnace heat-treatment (Fig. 13b) preserved the ferrite (light areas), pearlite (dark areas) microstructure seen in the A992 samples (Fig. 13a), but produced larger grains which are the expected effects of annealing heat-treatment. However, in the case of induction heat-treated A992 steel, larger ferrite grains are observed but polygonal ferrite is accompanied by widmanstatten ferrite or “widmanstatten ferrite side plates” which are the product of displacive phase transformation from austenite. Displacive phase transformation takes place without diffusion and preserves atomic correspondence between parent and product phases. The consequence is the introduction of invariant plane strain (increased strain energy) in the lattice which results in increased tensile strength and hardness. This is consistent with the results of tensile testing presented earlier and Vickers hardness measurements which are shown in Fig.13. Displacive phase transformations are typically the result of fast cooling rates from high temperatures where “reconstructive” transformations (diffusion controlled) are not given sufficient time to occur [18]. As such it is believed that the formation of widmanstatten ferrite in the induction heat-treated A992 steel is consistent with the observation of the beam flange cooling rates being substantially faster than the programmed cooling rates during induction heat-treatment of the full scale beam specimens as previously mentioned.

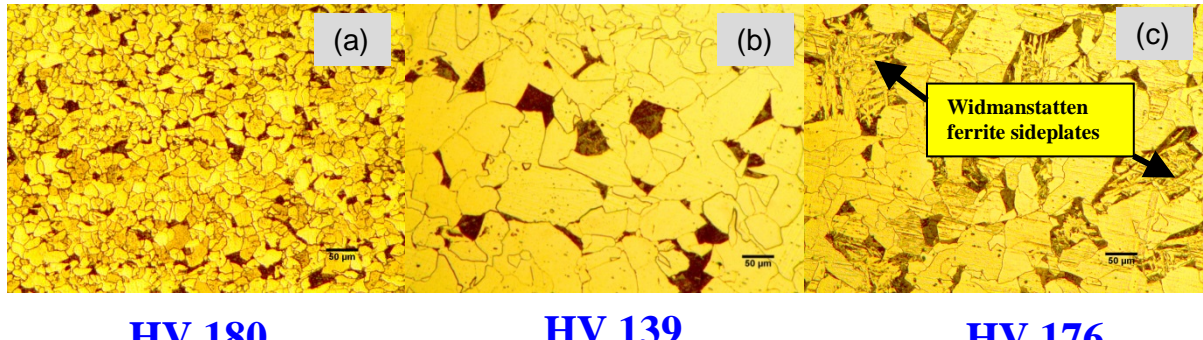


Fig. 10. Optical micro graphs and Vickers Hardness numbers of A992 Steel (a) Before heat-treatment (b) After furnace heat-treatment (c) After induction heat-treatment

6. Posttest FE Analysis

Three dimensional nonlinear finite element models were developed for HBS and WUF-W (control) connections using the commercial finite element analysis software ANSYS Mechanical ADPL [19]. Geometric and material nonlinearities were incorporated in the finite element models. An example of the finite element mesh and boundary conditions is shown in Fig.14a

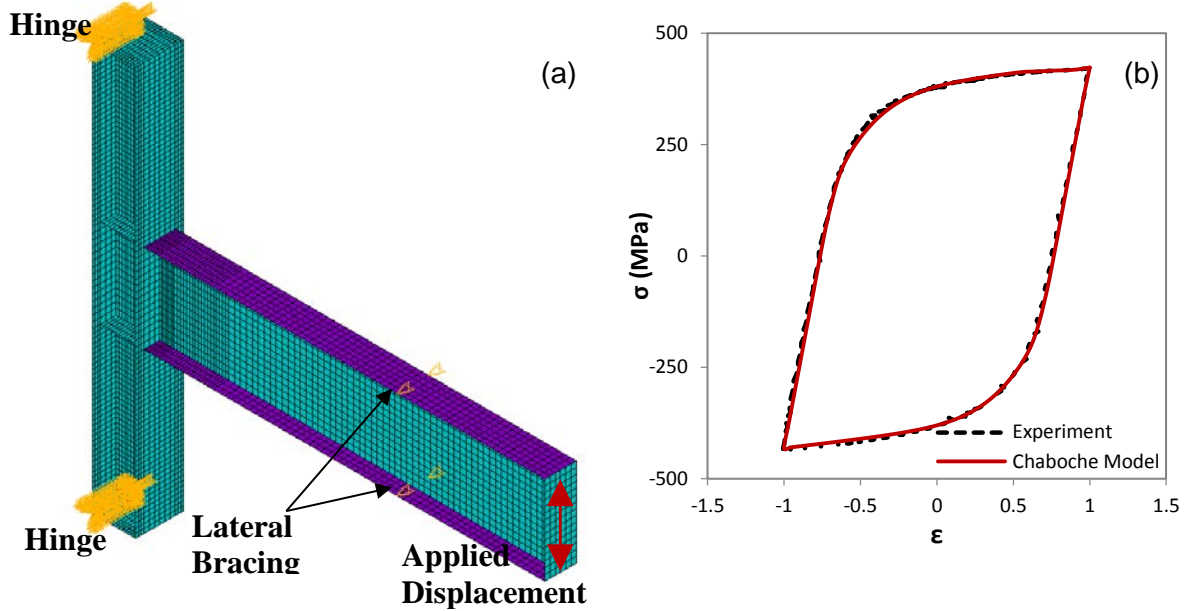


Fig. 13. (a) Finite element mesh and boundary conditions (b) Chaboche model simulation of A992 1% strain amplitude hysteresis curve

The FEA utilized quadratic shell elements (shell 281) and accounted for material nonlinearities through the Chaboche non-linear kinematic hardening model for the beam and column A992 steel material and a bilinear kinematic hardening model for the E71T-8 weld material. Chaboche material model parameters were obtained by fitting stable single amplitude hysteresis loops. Chaboche model prediction of 1% amplitude stress strain response of A992 steel is shown in Fig. 1b. Geometric nonlinearities were accounted for via a large displacement formulation which accompanied by small eccentricities/imperfections in the geometry allowed for the simulation of local buckling. Initial imperfections were obtained by first conducting an eigenvalue analysis of the perfect structure and then prescribing a scaled value of the first eigenmode displacement field as the initial

configuration of the structure. The scaling was chosen to represent realistic values of W-shape “out of squareness” based on ASTM A6 [20].

The predicted moment-rotation responses of HBS 3 and the control 1 are plotted against the recorded experimental responses in Fig. 15a and 15b. Longitudinal strain predictions along the width of the beam top flange 127mm (5in) away from the column flange for the control specimen are plotted and compared to the recorded strains in fig. 16. In addition, comparison between the predicted and experimentally observed plastic hinge formation and local flange buckling for control 1 is shown in Fig.17. These figures show good accuracy of the FE model in predicting the observed behavior of the test specimens.

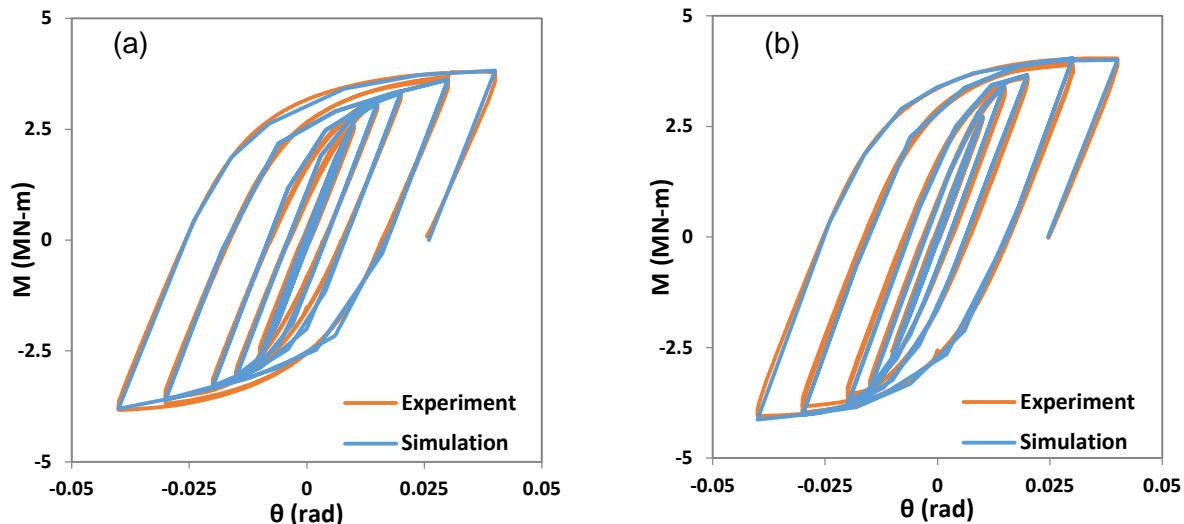


Fig. 14. Comparison of experimental and FE predicted moment rotation response for (a) HBS 3 and (b) Control 1

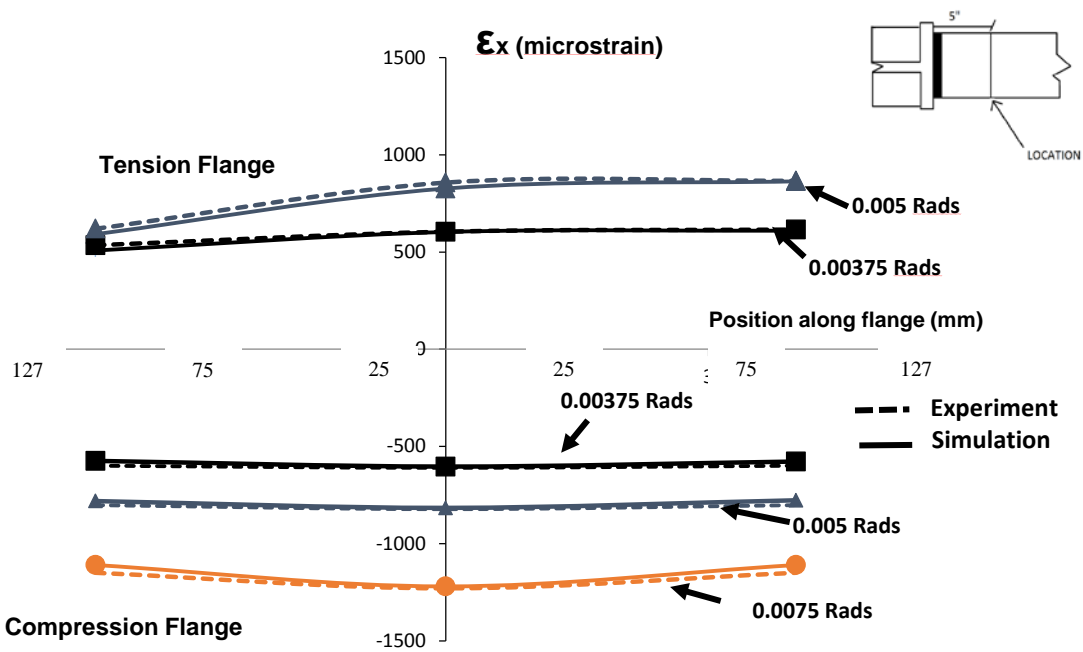


Fig. 15. Comparison of experimental and FE predicted longitudinal strain responses 127mm (5") from the column face for control 1

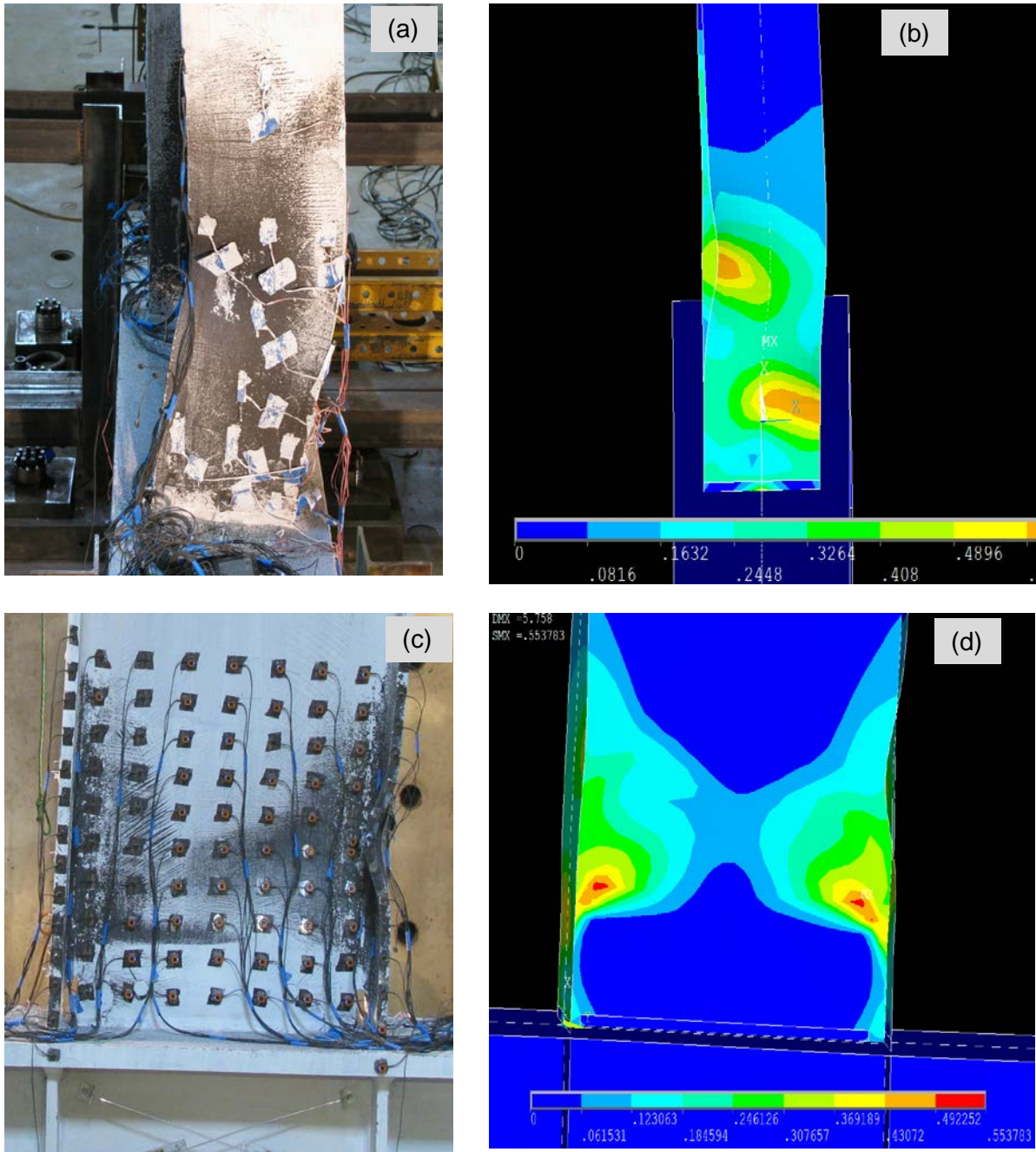


Fig. 16. Photograph of control 1 during loading cycles at 4% drift showing local flange buckling b) FEA prediction of deformation of control 1 top flange buckling at 4% drift c) Photograph showing plastic hinge formation of control 1 during loading cycles at 4% d) accumulated equivalent plastic strain solution for control 1

6.1 Effect of HBS material properties

To examine the effect of the induction heat-treatment on the response of HBS specimens, simulations were conducted using constitutive models calibrated from the furnace heat-treatment tensile stress-strain response and induction heat-treatment stress-strain response. Longitudinal strain predictions along the width of the beam top flange 50mm (2in) away from the column flange for these analysis are shown in Fig. 18. Note that this location is between the HBS and the column flange. Due to the faster rate of strain hardening and higher tensile strength, the induction heat-treatment produces larger strains outside of the heat-treated region than the furnace heat-treatment. This is due to the larger bending moments which were observed when the induction heat-treated material response was considered. The larger moments are produced from the faster work hardening rate of the induction heat-treated material in the plastic hinge. Note from the stress-strain curves in Fig. 11 that the induction heat-treated steel has a yield strength that is lower than the unheated steel, and as such yielding does initiate in the HBS. However, due to the fast rate of work hardening the moments increase rapidly in accordance with the material behavior.

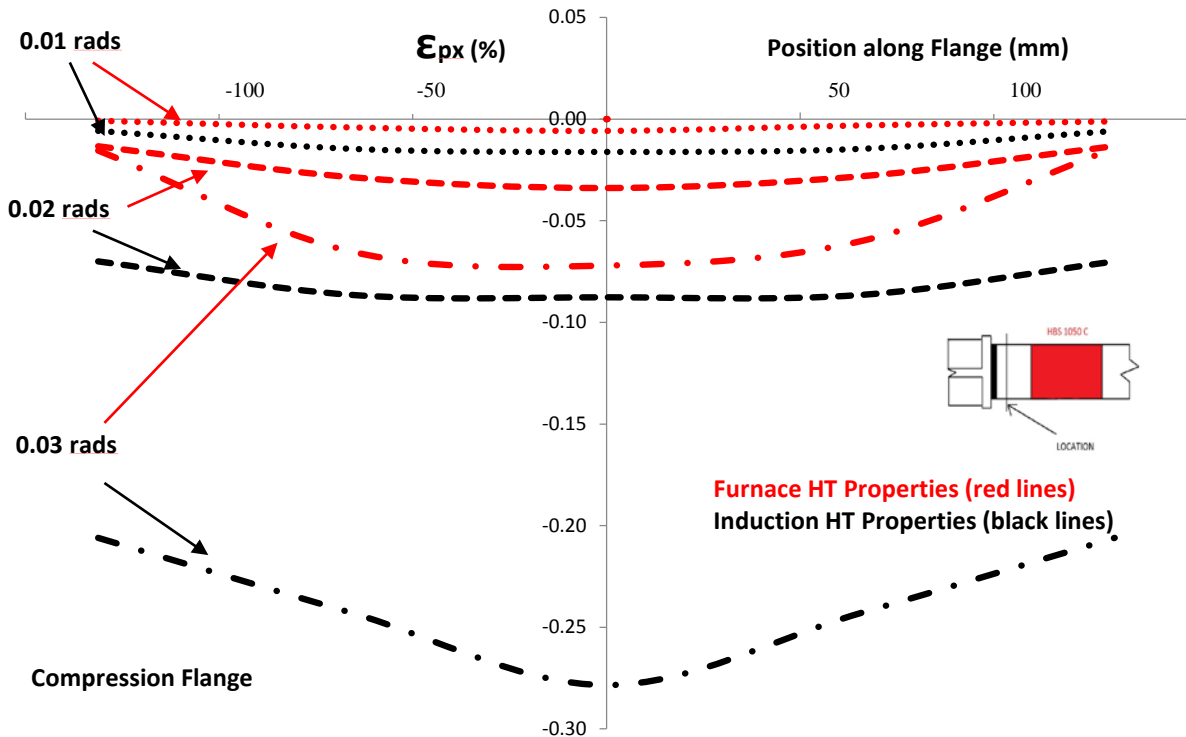


Fig. 17. FE analysis prediction of longitudinal strains along the width of the beam top flange 50mm (2in) away from the column flange for HBS specimens

6.2 Effect of welded shear tab

FE analysis was used to examine the strengthening effect of the welded shear tab on WUF-W connections. The presence of the shear tab was accounted for by increasing the thickness of the shell elements which model the beam web in the vicinity of the connection where the shear tab is located. Therefore the beam web was considered to be “thickened” by the shear tab. The plastic hinge formation and local flange buckling of a WUF-W connection with and without the presence of a welded shear tab is shown in Fig.19. As shown in the Fig.19a and 19b the welded shear tab has the effect of shifting the plastic hinge away from the connection. The consequence of this is that the plastic strain demands at the beam flange

weld toe are lowered as large deformations primarily due to local buckling are reduced in the vicinity of the connection. These lower strain demands are illustrated in Fig.19c and 19d where longitudinal plastic strain demands at the weld toe are plotted and compared for both simulations.

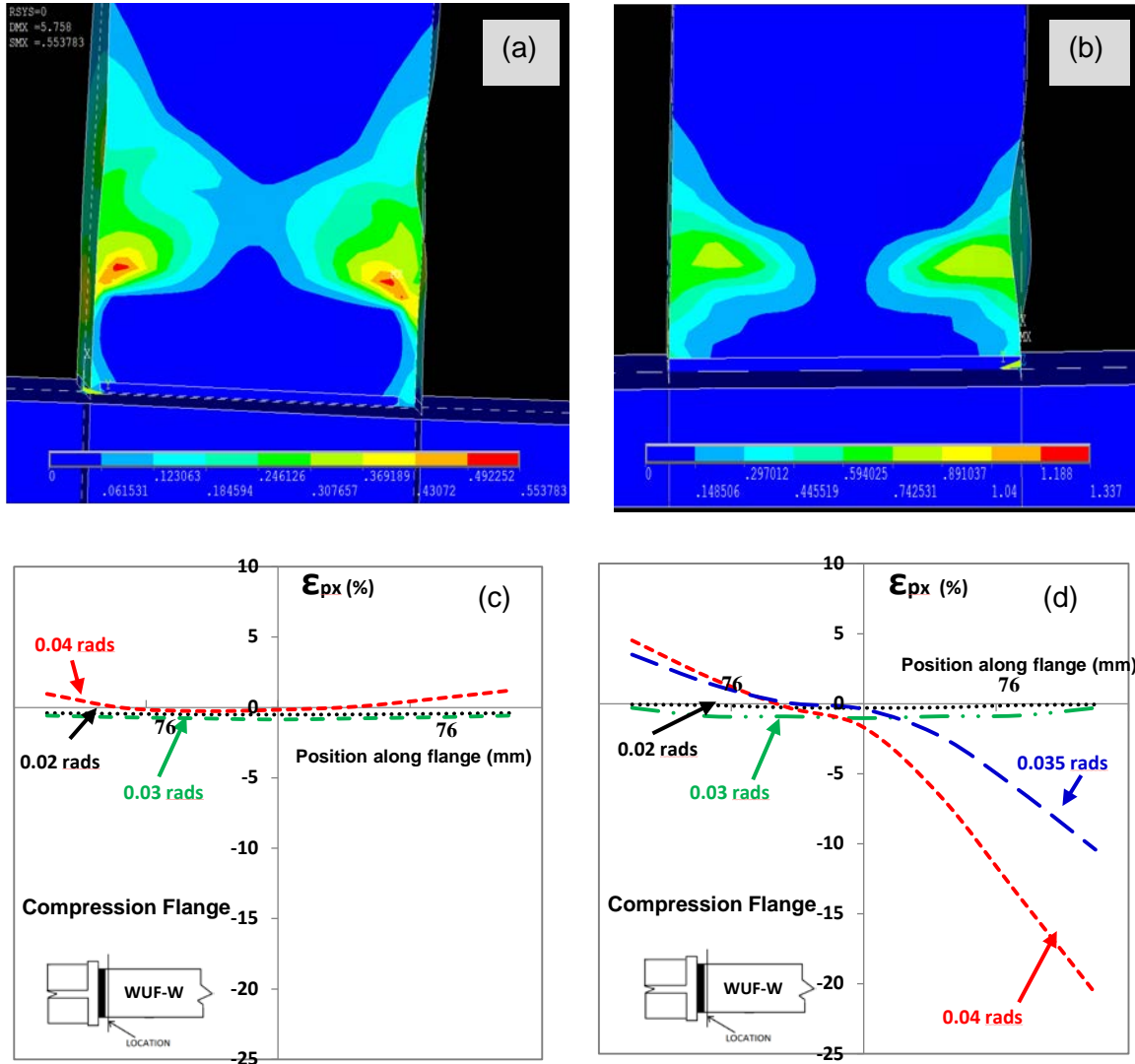


Fig. 18. Finite element simulation of the effect of the welded shear tab (a) accumulated equivalent plastic strain solution for WUF-W at 4% drift (b) accumulated equivalent plastic strain solution for WUF-W without welded shear tab at 4% drift (c) FE analysis prediction of longitudinal strains along the width of the beam top flange at the weld toe for WUF-W (d) FE analysis prediction of longitudinal strains along the width of the beam top flange at the weld toe for WUF-W without welded shear tab

7. Conclusions

A novel performance enhancement technique for welded unreinforced moment connections has been presented. It involves annealing heat-treatment of the beam flanges in specified areas to reduce material strength. Such a heat-treatment provides reduction of strain demands at the beam to column flange CJP welds through formation of the plastic hinge in the HBS. This weakening and consequent plastic hinge formation in the HBS is achieved without altering the elastic stiffness of the beam.

Strain measurements as well as M-θ rotation response comparisons of HBS specimens with a WUF-W specimen demonstrate the effect of the annealing heat-treatment technique on reducing strain demands at the welded connection and lowering beam moment strength. However, moment strength reduction of HBS connections was observed to be less than anticipated. This was due to fast rate of work hardening observed in tensile tests of material taken from beam flanges subjected to induction heat-treatment. This was caused by fast cooling rates from high temperatures during heat-treatment.

This shortcoming can be overcome through improved design of the induction heat-treatment setup including the use of more insulation to ensure slower cooling rates. Another option is to seek an alternative heating method for example the use of electrical resistance heating blankets which may provide better control of cooling rates and temperature distribution. Future experiments of HBS connections will involve the use of an improved heat-treatment methodology and also extend the use of the heat-treatment technique to other connection configurations for example, welded unreinforced flange bolted web connections as well as bolted unstiffened extended end plate moment connections.

Connections such as the RBS and HBS which show clear evidence of reducing strain demands at the welded connection (as compared to welded unreinforced connections) do not eliminate the need for careful welding and inspection practice. Finite element studies conducted by Engelhardt et al. 2000 [21] on RBS connections qualitatively capture the experimentally observed reduction in strain demands at the welded connection. These finite element studies show that although strain demands are lowered at the welded connection region, stresses are not significantly reduced. As a result, brittle fractures may still be observed if weld fracture mitigation techniques such as use of notch tough weld metal, removal weld tabs, backing bar and reduction of weld flaws through careful welding inspection (visual and ultrasonic) are neglected. The fracture of HBS 3 at the location of a welding error supports the observations of Engelhardt et al. 2000 [21].

Finally, it was observed from experiments and FE simulations that the WUF-W connection is reinforced by the welded shear tab. The welded shear tab strengthens the connection in a manner that promotes large deformations from yielding and buckling of the beam to occur away from the column face. This reduces strain demands at the beam flange CJP welds and HAZ.

8. References

- [1] Kunnath, S.K., & Malley J.O. "Structural Forum." *Journal of Structural Engineering* 126.1 (2000): 4-9.
- [2] Sabol, T.A., Engelhardt, M.D., Aboutaha, R.S., Frank, K.H., "Overview of the AISC Northridge Moment Connection Test Program", in Proceeding of the World Conference on Earthquake Engineering (11WCEE), 1996.
- [3] Richard, Ralph M., C. Jay Allen, and J. E. Partridge. "Proprietary slotted beam connection designs." *Modern Steel Construction* (1997): 28-33.

- [4] Houghton, D. L., Myers, S., and Nelson Houghton, Inc. (1997, August). Prototype Cyclic Testing of the Side Plate-Moment Connection System. In *Northridge Earthquake Research Conference*.
- [5] AISC/ANSI 358-10 (2010) Prequalified Connections for special and intermediate steel moment frames for Seismic Applications, Chicago.
- [6] Sumner, E. A. and Murray, T. M. (2002), "Behavior of Extended End-Plate Moment Connections Subject to Cyclic Loading," *Journal of Structural Engineering*, ASCE, vol. 128, no. 4, pp. 501-508.
- [7] Schneider, S.P. & Teeraprbwong, I. (2002) "Inelastic Behavior of Bolted Flange Plate Connections" *Journal of Structural Engineering*, Vol. 128, pp. 492-500.
- [8] Adan, M. S., and Gibb, W., (2009) "Experimental Evaluation of Kaiser Bolted Bracket Steel Moment-Resisting Connections," *Eng. J.*, 35(3), 128-139
- [9] Ricles, J.M., Mao, C., Lu, L.W., & Fisher, J.W. (2002). "Inelastic Cyclic Testing of Welded Unreinforced Moment Connections". *Journal of Structural Engineering*, Vol. 128, No. 4 pp. 40-49.
- [10] Lee, D., Cotton, S.C., Hajjar, J.F., & Dexter, R.J. (2005), "Cyclic Behavior of Steel Moment-Resisting Connections Reinforced by Alternative Column Stiffener Details, I. Connection Performance and Continuity Plate Detailing," *Engineering Journal*, 4th Quarter, pp. 189-213.
- [11] Hamburger, R. O., Krawinkler, H., Malley, J. O., and Adan, S. M. (2009). "Seismic design of steel special moment frames: a guide for practicing engineers," NEHRP Seismic Design Technical Brief No. 2, produced by the NEHRP Consultants Joint Venture, a partnership of the Applied Technology Council and the Consortium of Universities for Research in Earthquake Engineering, for the National Institute of Standards and Technology, Gaithersburg, MD., NIST GCR 09-917-3.
- [12] Iwankiw, N. R. and Carter, C. J. "The Dogbone: A New Idea to Chew On." *Modern Steel Construction*. April 1996. pp. 18-23.
- [13] Engelhardt, M., Winneberger, T., Zekany, A., & Potyraj, T. (1998). Experimental investigation of dogbone moment connections. *Engineering Journal*, 35(4), 128-139.
- [14] Kim, K-D & Engelhardt M.D. (2007). Nonprismatic beam element for beams with RBS connections in steel moment frames, *Journal of Structural Engineering* 133(2), 176-184.

- [15] Bramfitt, B.L. Annealing of Steel, *Heat Treating*, Volume 4, *ASM Handbook*, ASM International, 1991, p 42–55.
- [16] AISC/ANSI 341-10 (2010) Seismic Provisions for structural steel buildings, Chicago.
- [17] Popov, E.P., Amin, N. R., Louie, J.C., Stephen, R. M. "Cyclic behavior of large beam-column assemblies." *Engineering Journal* 23.1 (1986): 9-23.
- [18] Krauss, G.. *Steels: processing, structure, and performance*. ASM International, 2005.
- [19] ANSYS® Academic Research, Release 14.5, Help System, Structural Analysis Guide, ANSYS, Inc.
- [20] ASTM A370-10 Standard Test Methods and Definitions for Mechanical Testing of Steel Products.
- [21] SAC Joint Venture (2000) ‘‘Behavior and Design of Radius Cut Reduced Beam Section Connections’’ *Rep. No. SAC/BD-00/17*.

CHAPTER 3: An Innovative Seismic Performance Enhancement Technique for Steel Building Moment Resisting Connections Part II

Abstract

This study develops and experimentally validates an innovative technique for enhancing the seismic performance of steel beam to column moment connections. The technique involves reducing the strength of specified regions of the beam flanges by exposing them to high temperatures followed by slow cooling. Analogous to the reduced beam section (RBS) connection, yielding and plastic hinge formation is promoted in the heat-treated beam section (HBS). Moreover, because the elastic and inelastic modulus of the steel is unmodified by the heat-treatment and the beam cross section is not altered, a HBS connection does not sacrifice elastic stiffness or buckling resistance as does the RBS. Design of the HBS connection was performed through detailed finite element analysis and material testing. Two (2) large scale connections modified with the HBS technique were tested in this study. The test program showed that the proposed heat-treatment technique was successful in the promotion of yielding and plastic hinge development in the heat-treated regions with specimens attaining interstory drifts as high as 6% without weld or near weld fracture. Strength degradation due to beam buckling within the HBS was the observed failure mechanism in both specimens. Detail analyses of strain and beam deformation data are presented to explain the HBS connection plastic hinge formation and gradual strength degradation. Broader applications of the technique to other structural components are identified.

Keywords: Steel moment connection; seismic performance enhancement; beam plastic hinge; heat-treated beam section; reduced beam section

1. Overview of Steel Moment Connection advances since Northridge Earthquake

Extensive damage to steel moment resisting frame connections during the 1994 Northridge Earthquake instigated a comprehensive research effort led by the SAC joint venture intended to develop a broad and fundamental understanding of the seismic performance of moment frame connections [1]. A multitude of failure modes were observed in moment connections following the earthquake, the most common of which were fractures originating at or near the beam flange CJP welds which accounted for approximately 80% of the damage to welded steel moment frames [2]. In many cases these fractures propagated to other areas of the connection for example, column flanges, column web and beam web [3].

Initially, poor quality welds stemming from improper workmanship, use of welding electrodes which deposit weld metal with inherently low toughness, and a lack of careful inspection practice were thought to be the main causes for these brittle failures. However, studies which incorporated weld fracture mitigation measures alone showed that improvements in welding, inspection practice and weld metal are insufficient to guarantee adequate performance of these connections in high seismic areas [4, 5, 6]. One of these studies, performed by Stojadinovic et al. [4], evaluated the welded unreinforced flange-bolted web connection (WUF-B), which was one of the most commonly used moment resisting connections (prior to Northridge) due to their perceived ductility and economy [7, 8]. As a part of the study, moment connections were fabricated to pre-northridge standards and tested

to in an effort to recreate the brittle failures discovered after Northridge and in doing so confirm the reasons for these failures. Subsequently, connections fabricated using “notch tough” weld metal, improved welding procedure, improved welding inspection and more careful connection detailing were evaluated. The study showed the pre-Northridge connections to be brittle as was also shown by Engelhardt and Hussain [9] and Popov et al [3]. The WUF-B connections exhibited little to no ductility with fractures emanating from the beam flange to column flange CJP weld root or toe and propagating along different paths. Among the failures were divot pull outs of the weld and column flange material, crack propagation through the column flange and web, crack propagation through the beam web, beam flange gross section fractures at the weld toe and weld root [4].

The so called ‘SAC post-northridge’ connections tested by Stojadinovic et al. [4] displayed improved performance, however none of these connections were able to attain the required 0.03 radians plastic rotation in the standard proof test defined in the FEMA interim guidelines and the 1997 AISC Seismic provisions for steel buildings [4]. Careful examination of these connections through experimental and analytical studies, suggested that beam flanges were “overstressed” due to stress redistribution and stress risers imposed by the configuration of the connection which ultimately limited connection plastic rotation capacity [10].

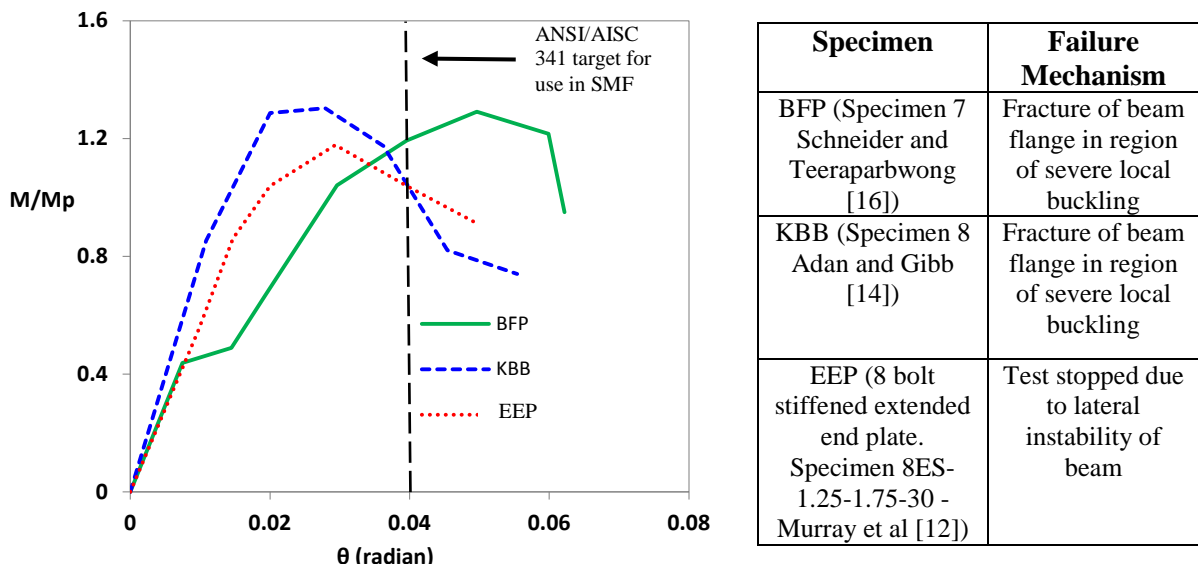


Fig. 1. Moment-rotation experimental backbone curves (in positive bending) of stiffened connections.

However, a study conducted by Xue et al. [11] showed evidence, albeit with a limited number of tests, that weld fracture mitigation strategies combined with a fully welded beam web could produce plastic rotations larger than 0.03 rads. Nonetheless, Stojadinovic et al. [4] concluded that weld fracture mitigation strategies alone are insufficient and that in future, moment connections intended for use in special moment frames (SMF) should incorporate both “weld mitigation measures as well as overstress mitigation measures”. As such, many subsequent research studies focused on lowering these stress and strain demands through various means. The fundamental change in the design philosophy of these moment connections to that of the pre-Northridge connection is the development of a plastic hinge away from the beam end intended to act as a reliable and ductile seismic fuse. In most of these connections the relocation of the plastic hinge is accomplished through strengthening

and stiffening the connection by adding endplates with stiffeners [12], cover plates [13], castings [14], haunches [15] etc. to encourage plastic hinging in the beam just beyond the strengthened region. The intent being that the strengthened connection would primarily remain elastic while plastic hinging of the beam takes place, thereby reducing the plastic strain demands and stress concentrations in the critical connection region.

Studies conducted by Sumner and Murray [12] demonstrated the use of extended end plate (EEP) connections with and without stiffeners to enhance the ductility of moment connections. Schneider and Teeraparbwong [16] and Sato et al. [17] demonstrated that carefully designed bolted flange plate (BFP) connections were successful in causing hinging of the beam section beyond the flange plate and that this led to a ductile and reliable failure mechanism. Adan and Gibb [14] evaluated proprietary cast high strength steel "Kaiser" bolted brackets (KBB) which were either bolted or welded to the beam flange and then bolted to the column flange. In this study it was demonstrated that similar to stiffened extended end plate and bolted flange plate connections the KBB strengthens the beam column connection region and forces plastic hinging, buckling and eventually fracture of the beam flange just beyond the end of the bracket.

Figure 1 shows experimental backbone curves for selected EEP, BFP and KBB connections from these studies. Moments have been normalized based on plastic moment capacities reported in the respective studies. Both moments and rotations were computed with respect to the column centerline. Note in Fig. 1 that all these connections were successful in achieving their plastic moment capacity and exceeded the 2010 ANSI/AISC 341 Seismic Provisions [18] performance criteria for use in SMF's. As a result, they are now

included in the 2010 ANSI/AISC 358 Prequalified Connections for Special and Intermediate Moment Frames for Seismic Applications [19]. It is also important to note that in the case of the BFP and to a lesser extent the KBB, plastic rotation is achieved through various mechanisms, for example beam flange and web yielding, panel zone yielding, small amounts of flange plate or Kaiser Bracket yielding and slip of beam flange and column flange bolts. This slip produces pinching of the hysteresis curves which can be identified in the backbone curve for the BFP connection by a reduction in stiffness at a rotation angle of about 0.01 rad followed by an increase of stiffness at approximately 0.015 rad. Slip can be a favorable energy dissipation mechanism but if excessive, p- δ effects may become significant due to large interstory drifts. Therefore, careful design and detailing of bolt holes is important to allow for both ease of field erection and preventing excessive rotations from slip. Note also that some of these strengthened connections displayed a variety of failure modes in laboratory experiments [14, 16]. As a result, in some cases limit state design may be tedious and the predictability of failure mechanisms is questionable.

Another ‘overstress’ mitigation technique is to weaken the beam adjacent to the connection so as to create a fuse for damage and energy dissipation in this weakened region. The reduced beam section (RBS) shown in Fig. 2a employs such a strategy and has been widely tested and adopted in the ANSI/AISC 358 [19]. When combined with an all welded connection (welded flange and web) the RBS successfully develops plastic hinging of the beam in the reduced section and as a result relieves the high inelastic strain demands at the beam flange groove welds, thereby reducing the likelihood of weld or near weld failures [20].

Experimental studies by Plumier [21], Engelhardt et al. [22], Chi and Uang [23] along with several others have demonstrated this improved ductility.

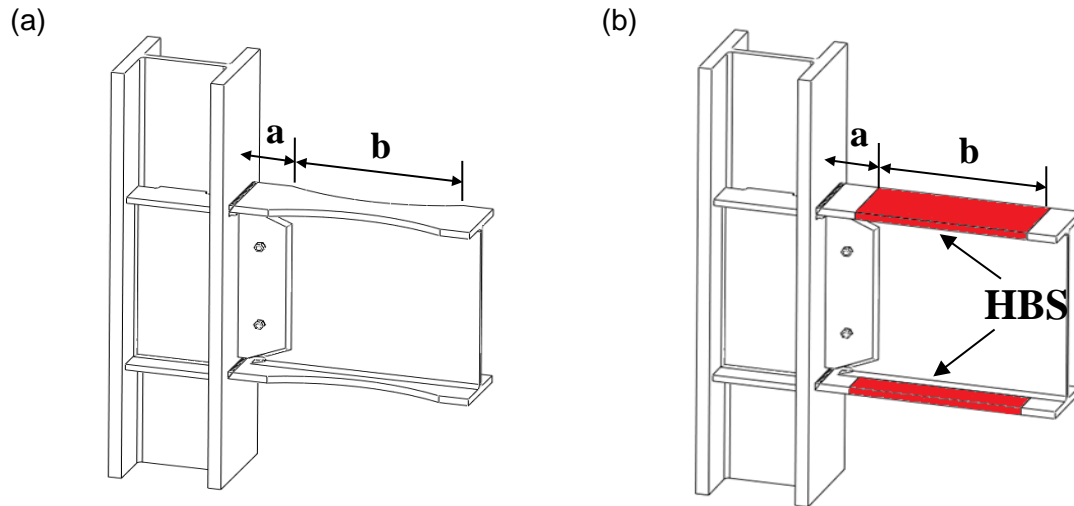


Fig. 2. Sketch of (a) Reduced Beam Section (RBS) and (b) Heat-treated Beam Section (HBS).

A consequence of the flange area reductions is the decrease in the elastic stiffness of frames employing such connections and as such, increases in maximum interstory drifts when subjected to lateral loads. Kim and Engelhardt [24] reported that flange reductions between 40 and 50% resulted in increased story drifts of 4.5 to 8%. In design practice this problem is suitably overcome by the use of larger beam sizes than would otherwise be necessary. An advantage of the RBS is that the flange width reduction may delay local flange buckling, but the consequential disadvantage is that the reduced flange stiffness lowers resistance to local web buckling and lateral torsional buckling [7]. However strength degradation associated with this reduced buckling resistance has been shown to be delayed in

RBS connections tested with concrete slabs [25] and in bare steel connections with lateral bracing at the reduced section [26]. Despite these drawbacks the RBS is widely considered to provide an attractive combination of performance, economy and simplicity (both in design and construction) when compared to strengthened connections, making it one of the most widely used connections in SMF's.

Studies conducted by Ricles et al. [6] and Lee et al. [27] showed that welded unreinforced flange-welded web connections (WUF-W) which combine the use of fracture tough weld metal, a modified access hole design, a CJP welded web and reinforcing fillet welds between the beam web and the shear tab could also successfully meet the aforementioned AISC performance criteria. It is noted that the WUF-W makes use of a stiffened web connection which in effect redirects stresses away from the beam flanges. This concept was previously validated on free flange moment connections by Choi et al. [28]. The WUF-W has also been prequalified in the 2010 ANSI/AISC 358[19] for use in SMFs. Fig. 3 shows experimental backbone curves for selected WUF-B, WUF-W and RBS connections from the studies mentioned above. Again, moments have been normalized based on plastic moment capacities reported in the respective studies. Both moments and rotations were computed with respect to the column centerline. In Fig. 3, significant performance improvements derived from almost 2 decades of research following Northridge are evident.

The above overview of special moment connections is not exhaustive as proprietary connections such as the Side PlateTM and Slotted WebTM have met ANSI/AISC performance specifications and have found widespread use in buildings in high seismic areas [29].

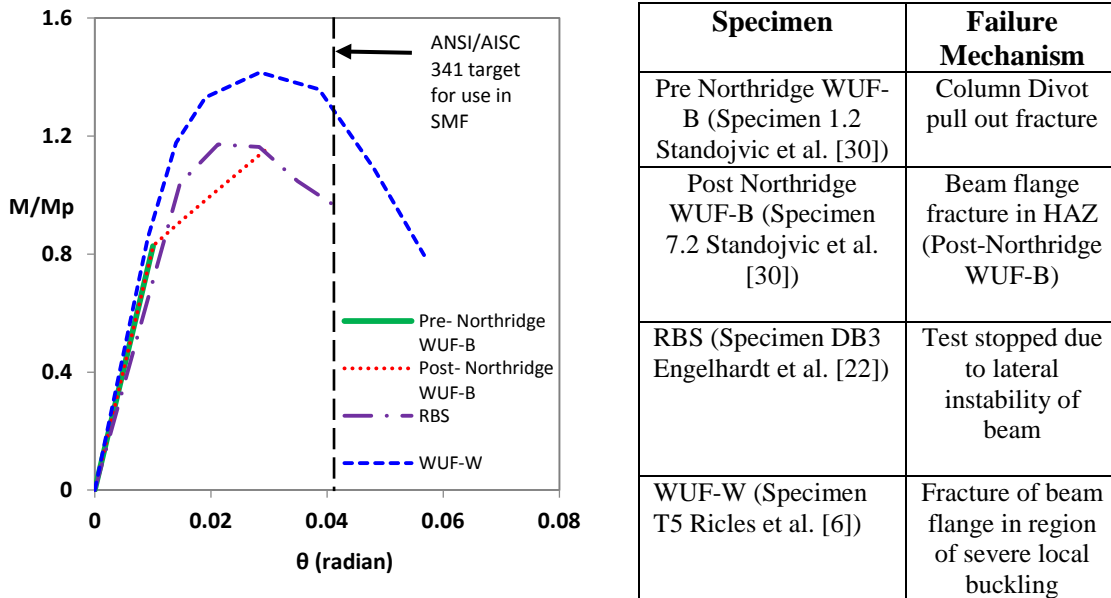


Fig. 3. Moment-rotation experimental backbone curves (in positive bending) of welded unreinforced connections.

As previously stated the performance (ductility), simplicity and economy offered by the RBS when compared to strengthened connections make it especially attractive for new construction. This study proposes an alternative connection strategy through beam weakening which offers comparable ductility to the RBS without the loss of elastic stiffness and buckling resistance as discussed in the following.

2. Introduction to the Novel Connection Concept

The proposed connection utilizes a similar ‘fusing’ mechanism to that of the RBS, however, weakening of the beam is achieved through a reduction in material strength as opposed to a reduction in flange area. This material strength reduction is achieved through high temperature heat-treatment (annealing) of the beam flanges in the areas highlighted red in Fig. 2b. The temperature history used in the heat-treatment process is shown in Fig. 4a

(details provided later) and the resulting softening of the A992 steel is shown in Fig. 4b. As a consequence of this softening, plastic hinging of the beam takes place in the heat-treated beam section (HBS).

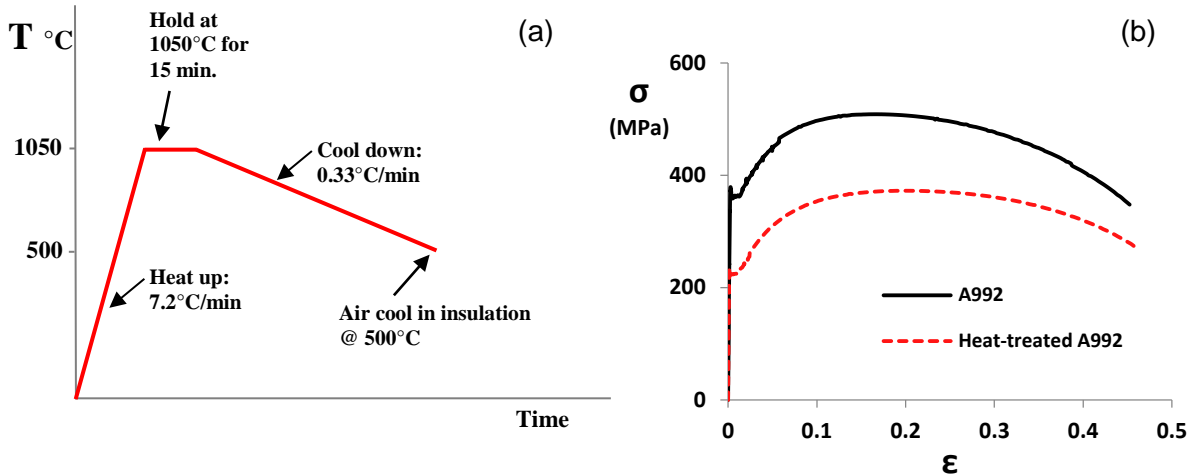


Fig. 4. (a) Temperature history of A992 heat-treatment (b) Engineering Stress-Strain response of A992 and heat-treated A992 steel

In a similar manner to the RBS, this connection provides a ductile seismic fuse through weakening, but because the elastic modulus of the HBS is unchanged, a connection modified with such a technique does not sacrifice elastic stiffness as does the RBS. Also, since the cross section of the beam is unaltered and the inelastic portion of the stress strain curve is not significantly modified (note the downward shift of the stress-strain curve in Fig. 4) the buckling resistance of this connection remains similar to that of a beam section before heat-treatment. Another advantage of the HBS connection is that the reduction of plastic hinge moments without the sacrifice of elastic stiffness may lead to more economical columns as

panel zone shear demands are lowered. In addition, lower beam flexural strength may lead to reduced column sizes without violating strong column weak beam (SCWB) criteria. The objective of this study was to experimentally validate the HBS concept. Two full scale experiments were conducted and the results are presented below along with details of the heat-treatment method and its development.

3. Heat-treatment thermal process

Annealing heat-treatment of steels is used in the processing and manufacturing of a wide variety of tools, components and equipment. It usually involves heating the steel to a particular temperature followed by a “soak” period and subsequent cooling at a prescribed rate (Fig. 4a). The parameters of the annealing cycle are determined primarily based on the chemical, mechanical and metallographic properties of the alloy prior to annealing and the desired post anneal properties [31]. The body centered cubic to face centered cubic phase transformation that iron undergoes above the lower critical temperature results in the nucleation and growth of new crystal grains upon heating and cooling. Careful control of the heating and subsequent slow cooling typically leads to a courser (larger grain size) grain structure from the annealing process. This coarsening of the grain structure through annealing is primarily responsible for the reduction in strength of A992 steel¹ (Fig. 4b) which is consistent with the well-established Hall-Petch relationship [32]. Optical Microscopy images of A992 steel samples before and after annealing are shown in Fig. 5, where coarsening of the grain structure can be seen.

¹ In this study full annealing is the technique utilized as opposed to *recrystallization* annealing which is typically used to reduce hardness and recover ductility by reducing the defect density in parts which have been heavily cold worked.

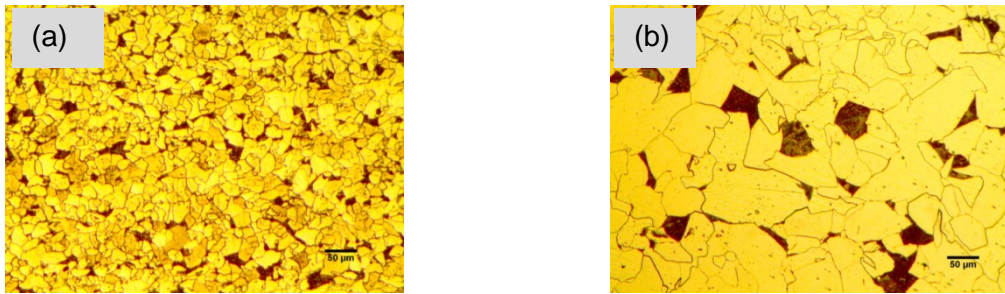


Fig. 5. Optical micro graphs of A992 Steel (a) Before heat-treatment (b) After heat-treatment at 1050°C cooled at 20°C/hr to 500°C followed by air cooling. Nital etch. Original Magnification: 100x.

As previously noted weakening of the beam flanges is achieved through a high temperature heat-treatment/annealing process in which the steel is raised to a temperature of 1050 °C and slow cooled to 500 °C after which the steel is left cool in still air to room temperature (Fig. 4a). This process has been designed to reduce the yield and tensile strength of A992 steel by approximately 35% and 25%, respectively. This strength reduction is reflected in the stress strain curves shown in Fig. 4b and summarized along with other material properties in table 1. Design of this thermal cycle was aided by a parametric study conducted to determine the effect of peak temperature, soak time and cooling rate on the tensile properties of A992. This study was conducted by heat-treating coupons machined from the flange of a W8X39 wide flange member. The heat-treatment was performed in an electric furnace and tested in uniaxial tension in accordance with ASTM A370 [33]. The results are plotted in Fig. 6a and 6b where it is observed that peak temperature and cooling rate had significant influence on the stress-strain response. It can be seen from both these figures that with higher peak annealing temperatures and slower cooling rates the tensile response is softened (yield strength and tensile strength are lowered). It is also observed that

for the ranges of temperatures and cooling rates considered there is no effect on the Elastic Modulus or the strain at maximum stress (uniform elongation). The effect of the heat-treatment on fracture strain or material ductility is also insignificant as can be seen in Fig. 6. The sensitivity of strength to peak temperature is explained by the fact that upon austenizing (heating above the upper critical temperature) the growth rate of austenite grains is a thermally activated process so an increase in austenizing temperature (with all other parameters unchanged) results in larger austenite grains.

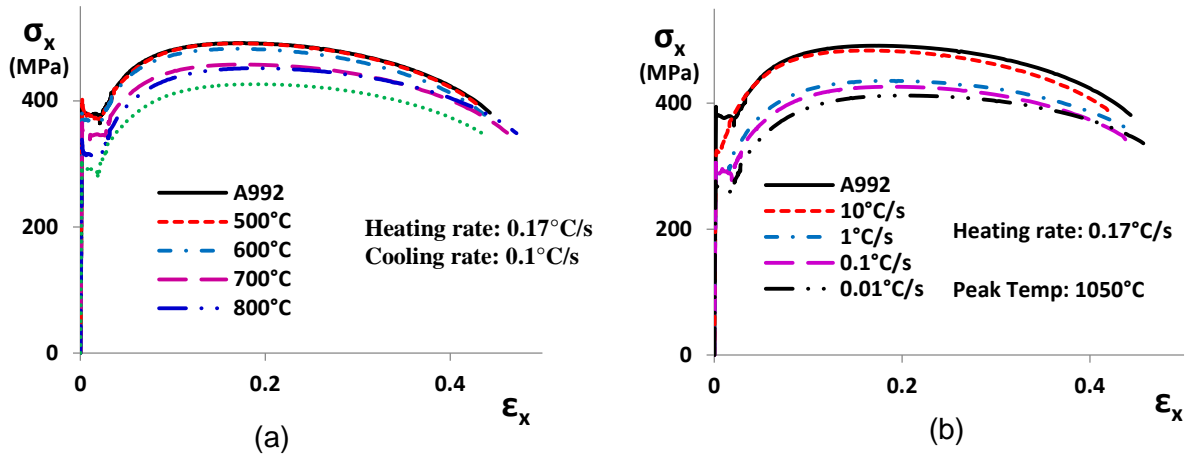


Fig. 6. Uniaxial stress strain responses of heat-treated A992 Steel, (a) effect of peak temperature, (b) effect of cooling rate

Table 1 Summary of material properties of A992 before and after heat-treatment

Material Property	A992	Heat-treated A992
Average Grain Diameter (μm) (ASTM Size Description)	22.1 (Fine)	56.5 (Medium)
σ_y (ksi)	52.5	32.4
σ_u (ksi)	73.8	54.1
Average Charpy V Notch Toughness @ 70°F (ft-lb)	72	69
Average HV (Vickers Hardness #)	180	125

Material was obtained from the flange of a W30x148 member

Austenite grain boundaries tend to be favorable nucleation sites for allotriomorphic ferrite during phase transformation, and so larger austenite (parent phase) grains tend to lead to larger ferrite grains (product phase) [34]. Also grain growth suppressing alloying elements such as niobium, vanadium and aluminum which are often used in A992 steel are less effective at inhibiting growth of austenite grains with increasing temperature. These elements form submicroscopic carbides, nitrides and carbon nitrides which remain undissolved in austenite at high temperatures. These precipitates segregate to grain boundaries during high temperature processing of steels and suppress grain growth through a process known as Zener pinning. However, if the temperature is raised above the ‘grain-coursing temperature’ these precipitates dissolve into austenite and no longer resist grain growth. At this stage there is an abrupt increase in the austenite grain growth rate [32].

Slow cooling during phase transformation facilitates the nucleation and growth of course grained equiaxed ferrite and pearlite with course inter-lamellar spacing from the

austenite parent phase. Analogous to dendritic growth during solidification, slower cooling rates during solid state phase transformation tends to yield larger grain sizes due to the available thermodynamic driving force for grain growth (reduction in grain boundary energy) [32]. Careful control of the cooling rate was found to be essential in facilitating purely diffusional phase transformations and promoting the formation of polygonal ferrite and pearlite microstructures. Coupons cooled in still air from high annealing temperatures were observed to form widmanstatten ferrite and banite microstructures which led to higher tensile strength and lower ductility when compared to nonheat-treated coupons.

4. HBS Connection Design Development

Similar to the RBS, 3 parameters are needed for design of the HBS connection (see Fig. 2), the distance from the column flange to the start of the HBS (dimension a), the length of the HBS (dimension b) and the desired tensile properties of the beam flanges in the HBS. The results of the afore-mentioned parametric study were paired with finite element analysis (FEA) carried out using ANSYS Mechanical ADPL. The FEA was used to evaluate the 3 main input parameters (dimension a, dimension b and the tensile stress-strain properties of the HBS). The FEA utilized quadratic shell elements (shell 281) and accounted for material nonlinearities through the Chaboche non-linear kinematic hardening model for the beam and column material and a bilinear kinematic hardening model for the E71T-8 weld material. Geometric non-linearity's were accounted for using a large-displacement formulation. The beam flanges and web were assumed to be welded to the column flange in these simulations. The numerical model was first validated against the RBS connection experimental responses from the literature [22]. Subsequently analysis of the HBS connection was performed in

order to determine parameters “a”, “b” and the desired material strength reduction of the beam flanges in the HBS, for performance evaluation as discussed below. More detail descriptions on the finite element modeling and the constitutive model used are presented in [35].

The FEA study revealed that dimensions similar to those specified in 2010 ANSI/AISC 358 for RBS parameters “a” and “b” provides desirable performance for the HBS connection. Distance “a” was kept as small as possible to maximize moment reductions at the face of the column without causing high strain demands at the beam flange complete joint penetration (CJP) welds. While dimension “b” was proportioned so as to provide a large region over which yielding of the beam flange is promoted. This allows a wide distribution of plasticity which helps to provide high energy dissipation, stable hysteretic behavior and lowers strain demands in the HBS region. When combined with the same dimensions for “a” and “b”, the tensile properties of heat-treated A992 steel shown in Fig. 4b were found to provide similar strength (moment capacity) reduction to RBS flange area reductions of 40%.

Results of these FEA analysis are shown in Fig. 7 in which comparisons are made between the global and local responses of RBS and HBS connections having the same beam and column sizes and the same dimensions for parameters “a” and “b” along with similar reductions in moment capacity in the weakened section. Fig. 7b shows the moment-rotation envelop (in positive bending) comparison in which it is observed that the HBS connection provides improved elastic stiffness (~7% increase) and delayed onset of strength degradation as compared to the RBS. In this figure moments have been normalized to the plastic moment capacity of the unweakened crosssection adjacent to the column face and rotations

are computed at the face of the column. Note also that the HBS connection provides relocation of the plastic hinge similar to that of the RBS connection as indicated in Figs. 7c

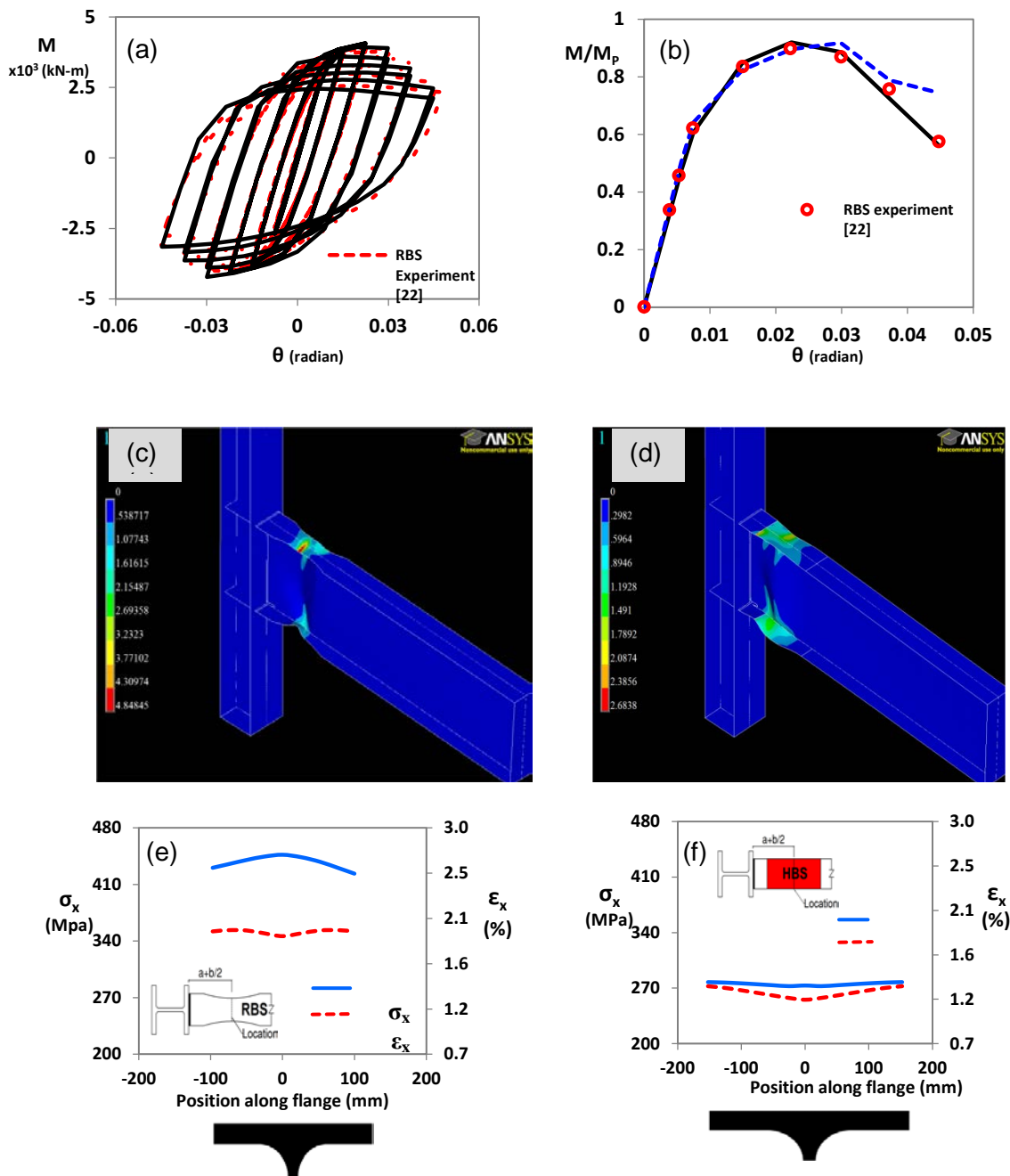


Fig. 7. Finite element analysis of RBS and HBS connections, (a) comparison of experimental and analytical results for specimen DB 3 Engelhardt et al. [22] (b) comparison of $M-\theta$ envelop (Moments are normalized to the plastic moment capacity of the beam at the face of the column), (c) equivalent plastic strain solution of RBS @ 4.5% story drift (d) equivalent plastic strain solution of HBS @ 4.5% story drift, (e) longitudinal stress and strain at the center of the RBS @ 2% story drift (f) longitudinal stress and strain at the center of the HBS @ 2% story drift.

and 7d which shows a contour plot of the equivalent plastic strain responses for both connections. From comparison of Figs. 7e and 7f it is observed that though both the RBS and HBS create a fuse through weakening, in a strict sense, there is a difference in the local stress and strain state within the weakened region in both connections. For example at 2% drift the longitudinal stresses and strains in the RBS are higher than those in the HBS as can be observed by comparing these figures. This can be explained by considering that in the case of the RBS yielding is promoted in the reduced flange section due to higher effective stresses in this area (relative to the unreduced section adjacent to the column) resulting from the area reduction. However, in the HBS, stresses in the weakened region are lowered due to the reduction in material strength. This stress reduction provides added benefit in terms of local buckling resistance, especially if this technique is applied to flanges and webs of sections with slender elements. Further, it is noted that the HBS provides a constant reduction of material strength over the entire weakened region while the strength reduction in the RBS is concentrated in the center of trimmed flange. As a result of this, inelastic action in the form of yielding is distributed over a larger flange area in the HBS as compared to the RBS (Figs. 7c and 7d); this reduces strain demands despite providing a similar ‘fuse’ mechanism through weakening.

5. Heat-treatment method for full scale beams

In the current study heat-treatment of the beam flanges was performed after fabrication of the beam was complete but prior to field welding the beam to column. Heat-treatment was accomplished via the use of electric surface heating pads which were attached to both the outside and inside surfaces of the beam flanges as shown in Figs. 8a and 8c. These heating

pads are constructed from a nickel-iron alloy electric resistance heating wire woven through ceramic beads which were sized based on the dimensions of the heat-treated region. Power is supplied to the heating pads via a portable power console and type K thermocouples were used to measure temperatures and provide continuous feedback to the power console controller. The heat-treatment set-up was completed by enclosing the beam flange and part of the beam web with 2 layers of 2" high density ceramic fiber insulation blankets as shown in Fig. 8b.

No heat sinks were needed to prevent heat conduction to regions of the beam outside of the HBS. FEA was used to perform thermal simulations to analyze temperature distribution during heating and cooling [36]. These analyses predict that regions outside the HBS remain at temperatures below 500°C during the heat-treatment process (see Fig. 8d) and as a result, no significant change in strength is expected in these areas. This can be deduced from the results of tensile tests conducted on coupons subjected to peak temperatures of 500°C and 600°C shown in Fig. 6a. This was also confirmed via tensile testing of coupons taken from the beam flange adjacent to the HBS during the development of the full scale heat-treatment process. Thermal analysis predictions were later confirmed by temperature measurements made using type K thermocouples and infrared thermometers during the heat-treatment of beam specimens. No distortion of the beam sections were observed after the completion of the full scale heat-treatment process.

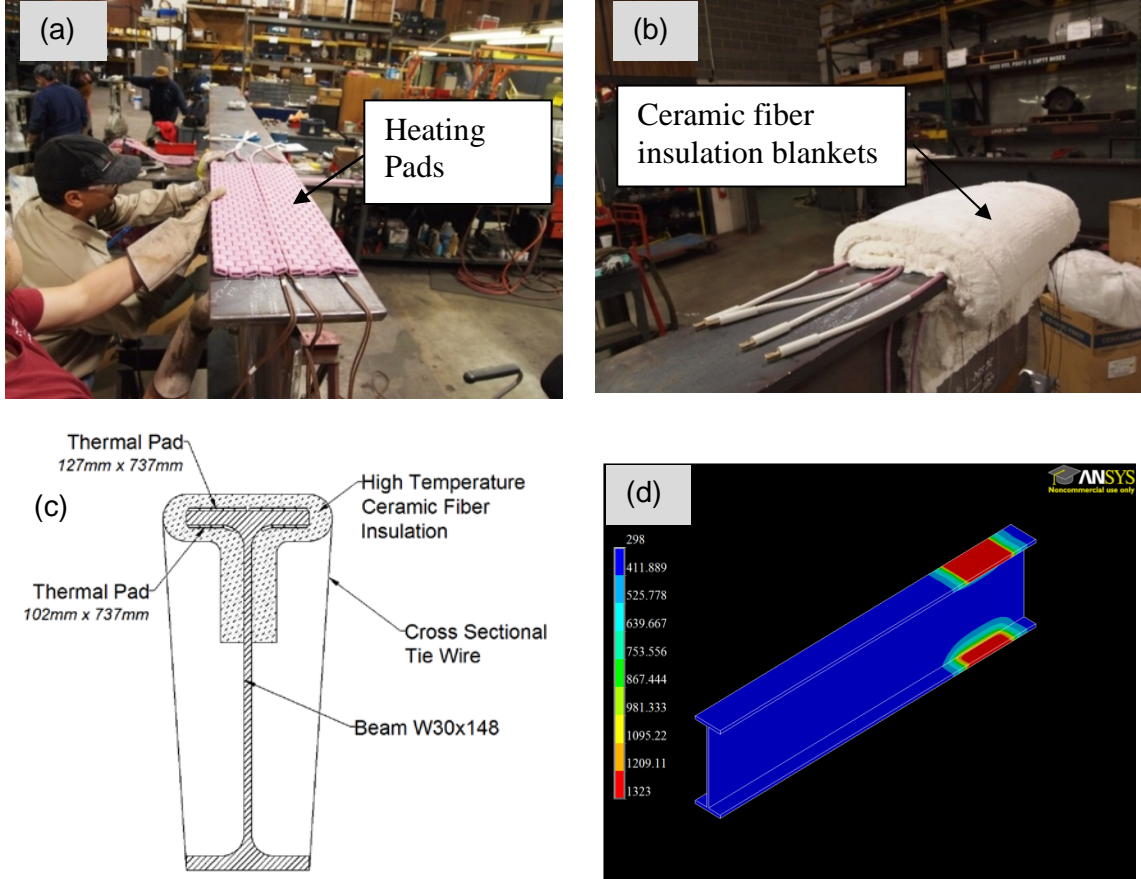


Fig. 8. Heat-treatment setup (a) photograph showing electric surface heating pads during installation on a beam flange, (b) photograph showing insulation of beam flange for well controlled heating and cooling, (c) schematic showing section view of heat-treatment setup, and (d) contour plot from thermal finite element analysis [36] of temperature (absolute scale) distribution during heating of the beam.

6. Connection Design and Experimental Setup

Two identical large scale specimens (HBS 5 and HBS 7) were tested to validate the HBS concept. See Figs. 9a and 9c for the test setup. In these specimens the HBS was combined with an all welded connection in which the beam flanges and web were connected to the column flange using complete joint penetration welds. These details are consistent with current design and construction practice for RBS connections utilized in SMFs. The beam

and column sections and lengths were chosen to be similar to those of specimen DB5 studied by Engelhardt et al. [22].

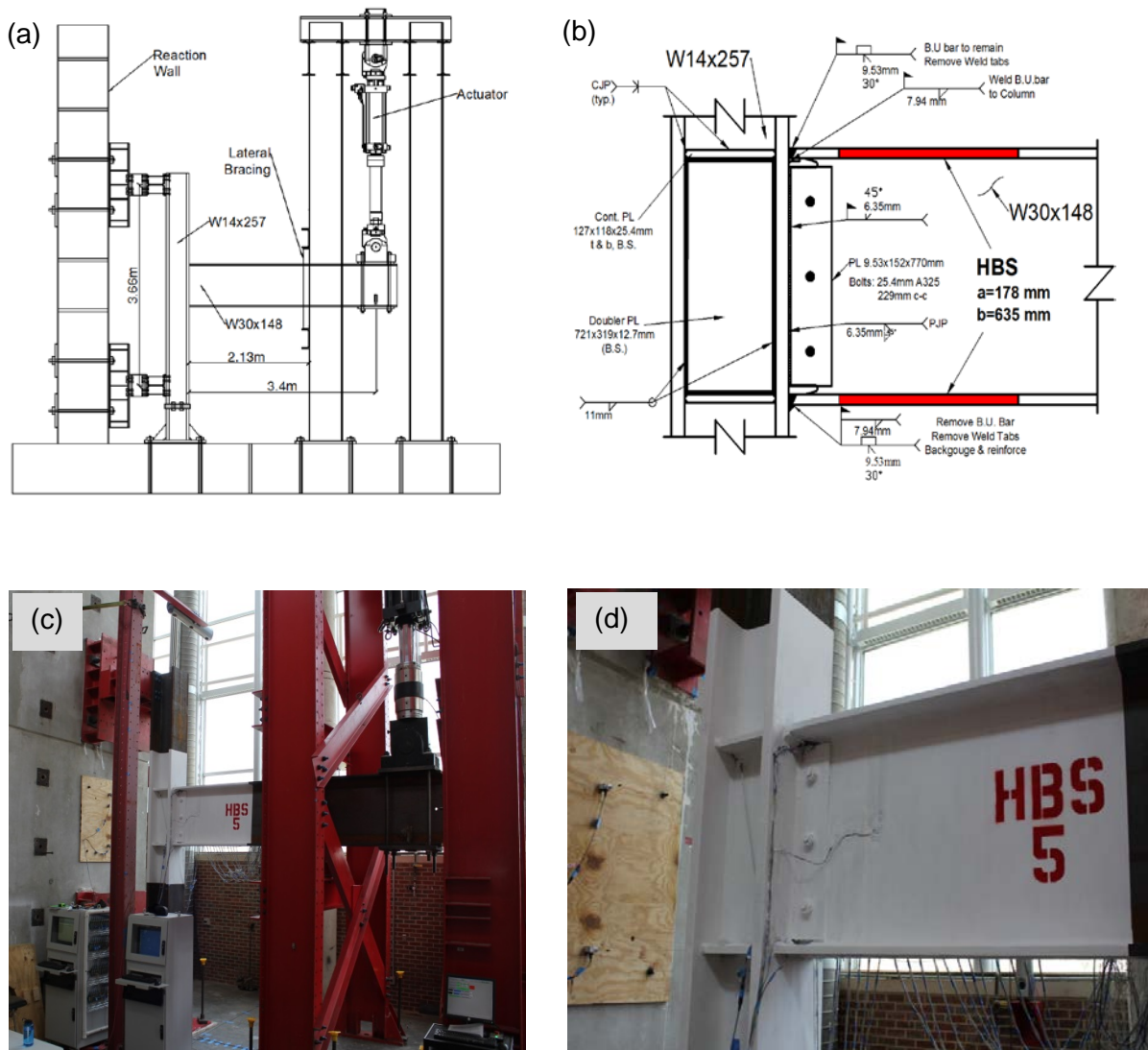


Fig. 9. HBS test setup and connection details a) sketch of the test setup, b) sketch of the connection details, c) photograph showing test setup and, d) photograph of HBS 5 connection prior to testing

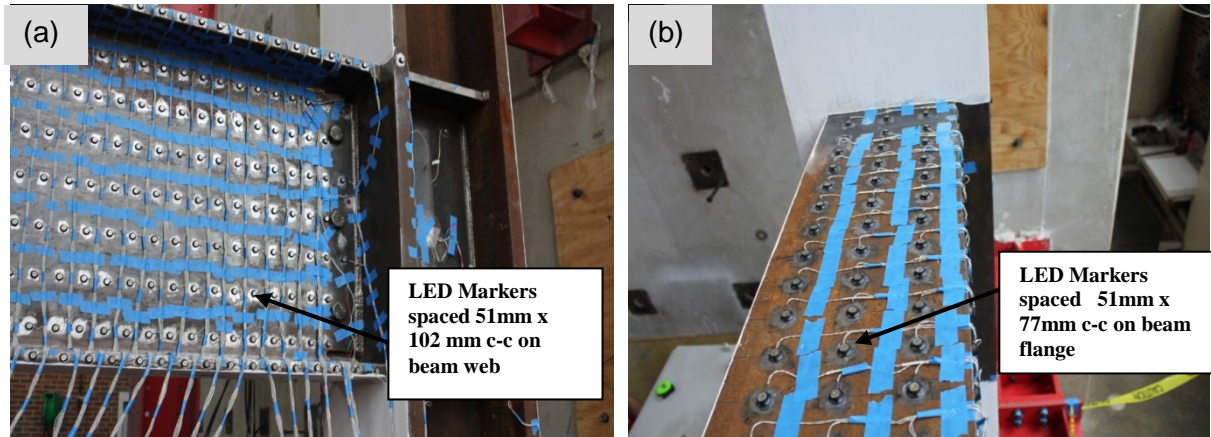


Fig. 10. Instrumentation of HBS 5, a) LED markers placed on beam web and the sides of beam top and bottom flanges, and b) LED markers placed on beam top flange

However, the column panel zone was reinforced with two-12.7 mm (1/2 inch) doubler plates which were designed to promote strong panel zone behavior and ensure that most of the inelastic action was obtained from the beam. By doing this, large plastic rotation demands are placed on the beam which allows better evaluation of the ductility and energy dissipation provided by the HBS. These connection details are shown in Fig. 9b.

Connection welding was performed outdoors with the column oriented vertically by a welder qualified in accordance with the requirements of AWS D1.1-10 and AWS D1.8-09. Welding was accomplished with self-shielded flux cored arc welding (FCAW) process. E70-T6 electrodes were used for beam flange welds, while E71-T8 electrodes were used for the beam web weld and the reinforcing fillet welds. Both of these electrodes were specified by the manufacturer to deposit metal with a minimum Charpy V-notch toughness of 27 J (20 ft.-lbs.) at -28 °C (-20°F) . The bottom flange backing bar was removed and a reinforcing weld was placed at the root of the groove weld.

The top flange backing bar was left in place, however a fillet weld was provided between the backing bar and the column flange. Weld tabs from the top and bottom beam flange groove welds were removed by carbon air arc gouging. No vertical weld tabs were used for the beam web CJP welds. Finally, all CJP welds were ultrasonically (UT) tested by a certified welding inspector (CWI) in conformance with AWS D1.1-10 and AWS D1.8-09.

7. Instrumentation

Each specimen was equipped with strain gauges along the beam flanges to monitor longitudinal flange strains, at various locations including the weld toe and HBS region. String and linear potentiometers were used to monitor displacements and rotations in the column, beam and panel zone. A calibrated load cell in the hydraulic actuator provided readings of force response during the experiment. All specimens were painted with hydrated lime prior to testing to visually indicate regions of yielding.

The Optotak Certus HD three-dimensional (3D) position system produced by Northern Digital Incorporated was used to capture the positions of markers placed along the beam flanges and web as shown in fig. 10. Two Optotak cameras were used which were able to capture the motion of markers placed on the top and sides of the beam top flange, the beam web and the side of the beam bottom flange. Position time history data obtained from this system was post processed to calculate displacements and strains in areas of interest. Accuracy of the Optotak system was illustrated by Goodnight et al. [37] where the strain measurements obtained from the Optotak system were found to closely match those measured by traditional instruments (strain gage and extensometer) for a tensile test of a steel bar. The Optotak system provides the advantage of being able to record large cyclic inelastic

strains while electrical resistance strain gages may either exhibit gradual strain drift or fail to remain adhered.

8. Test Results

8.1 Global response of HBS connections

Testing was conducted at the North Carolina State University Constructed Facilities Laboratory (CFL) on an exterior type sub-assemblage (single cantilever). Loads were applied at the beam tip in accordance with the 2010 ANSI/AISC 341 [18] seismic provisions Appendix S loading protocol consisting of quasi-static increasing amplitude displacement cycles. Figure 11 shows the moment- rotation response of both specimens. These global responses of HBS connections show wide hysteresis loops indicating good energy dissipation. Both specimens exceeded the 2010 AISC Seismic Provisions (ANSI/AISC 341-10) SMF qualifying 4% interstory drift angle without significant strength loss. Strength degradation due to local flange, web and lateral torsional buckling initiated during the 2nd cycle of loading at 4% drift (see Fig. 11a) and continued during later loading cycles. Loading of HBS 5 was terminated after sustaining 2 loading cycles at 5% drift due to a fracture in the location of significant flange buckling. Loading of HBS 7 was terminated before starting the 2nd loading cycle at 6% story drift (see Fig. 11b) due to significant strength loss as a result of lateral buckling and twisting of the beam.

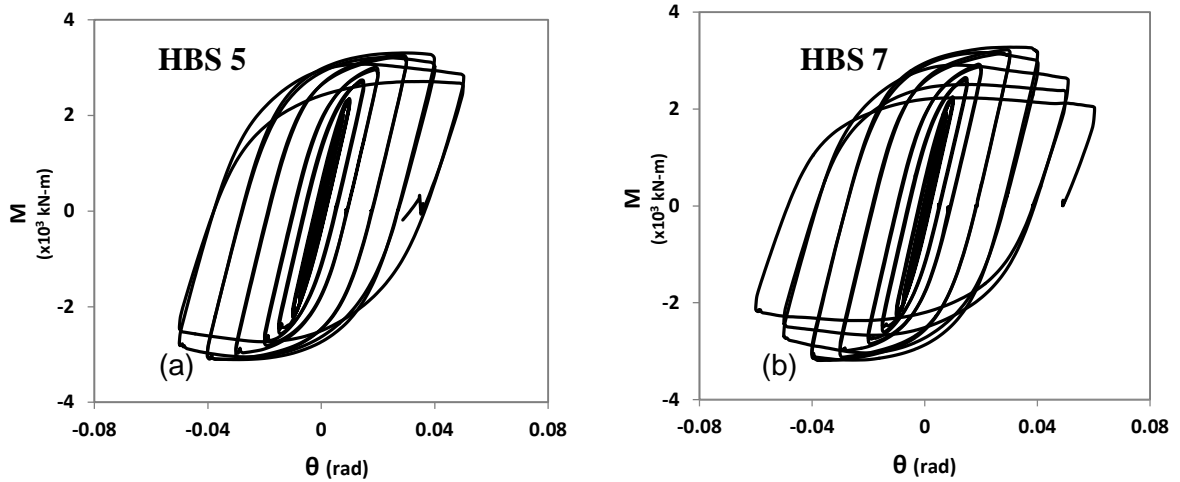


Fig. 11. Moment-rotation responses of HBS connections, a) HBS 5 and, b) HBS 7

The response of the HBS 7 is further analyzed by plotting the moment-plastic rotation curves for each component of the connection assembly which were calculated using data measured by instrumentation during the test and equations proposed by Popov et al. [38]. These graphs as shown in Fig. 12 indicate that panel zone shear and column flexural deformations contributed only to the elastic behavior of the sub-assemblage and as a result, inelastic action was entirely confined to the beam. The contributions of panel zone shear and column flexural deformations to the total rotation of the connection are observed to diminish as loading amplitudes are increased.

This is illustrated in Fig. 13 which presents bar graphs of the total rotation contributions (elastic + plastic) of each component to the total connection rotation for both specimens. The trends observed in both graphs confirm the expectation for beam hinge rotations to dominate the deformations by a continuously greater magnitude as imposed drift

angles are increased in ductile connections with strong panel zones designed to satisfy strong column weak beam criteria.

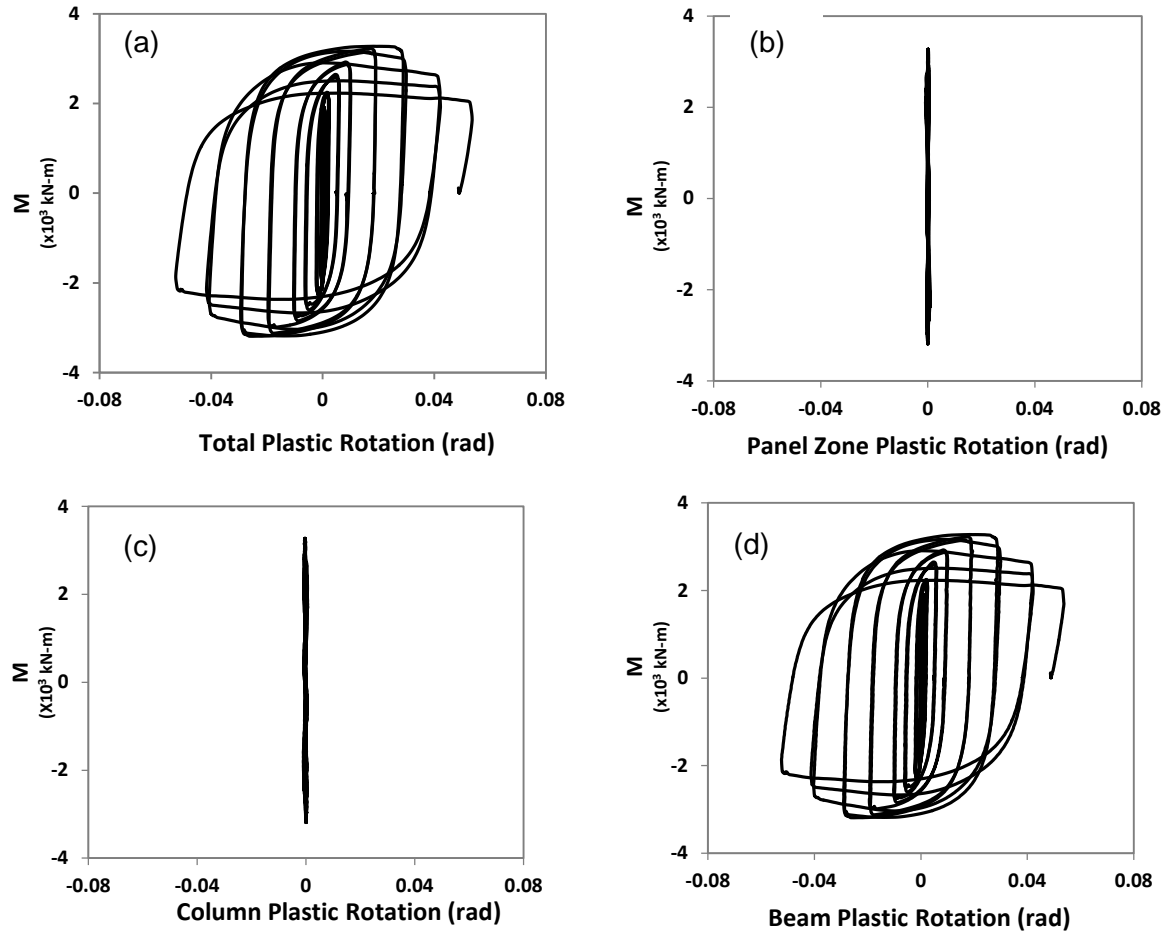


Fig. 12. Plastic rotation contributions by components of HBS 7, (a) total connection plastic rotation, (b) panel zone shear plastic rotation (c) column flexural plastic rotation and, (d) beam plastic rotation

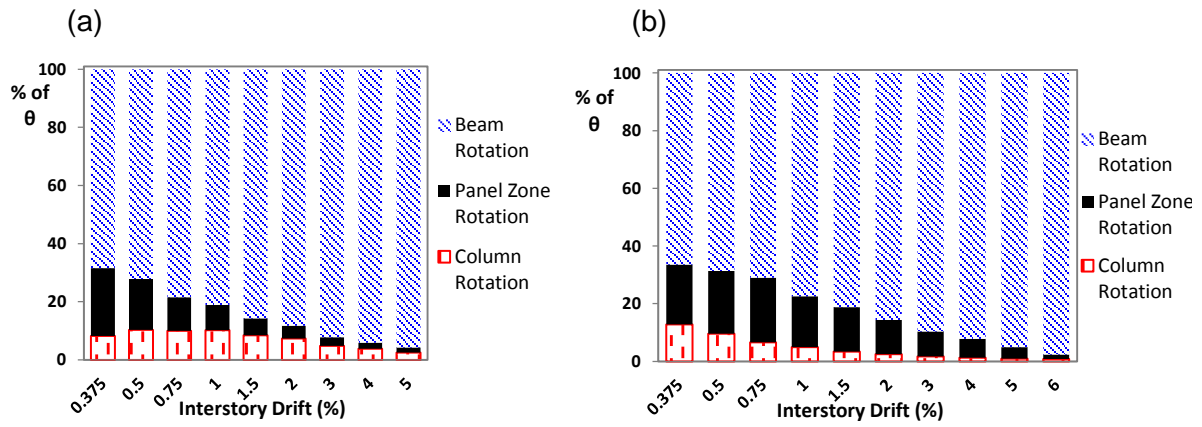


Fig. 13. Total rotation contributions of HBS connections, (a) HBS 5 and, (b) HBS 7

8.2 Plastic hinge formation in HBS Connection

Figure 14 illustrates the progression of inelastic action along the beam flange via bar graphs in which the distribution of longitudinal tensile strains (normalized by the yield strain) along the centerline of the beam flange at various stages of the loading history are plotted. Bars highlighted in red represent the strains in the heat-treated (weakened) regions. Strains were calculated by post processing data obtained from 3D noncontact spatial displacement measurement sensors placed along the beam flange as shown in Fig. 10. These plots demonstrate proof of the HBS concept and the following observations have been made:

1. Flexural yielding of the beam flange initiated within the HBS as evidenced by strains recorded at 1% interstory drift (Fig. 14a) and flaking of white wash observed during testing (Fig. 15a).
2. As loading amplitudes were increased, strains within the HBS and near the column face increased and the distribution of strain within the heat-treated areas were influenced by the moment gradient. It is of note that the beam tested had a length of 3.4m (134 inches)

corresponding to a moment frame with a clear span of approximately 6.8m (22 feet). This relatively short span results in a large moment gradient which when combined with the strain hardening of the heat-treated material results in some limited yielding near the column face. However this was not observed to have a detrimental effect on the performance of the HBS connections as no weld or near weld failures were observed.

3. As the loading progresses from 2% to 4% drift, strains within the HBS increase significantly while strains adjacent to the column face grow slightly (see Fig. 14b-14d). Also at 4% drift large strains are distributed over a significant length of the HBS region. These indicate that large displacements imposed at the beam tip are mostly accommodated by inelastic flexural action in the HBS through gradual formation of the plastic hinge.

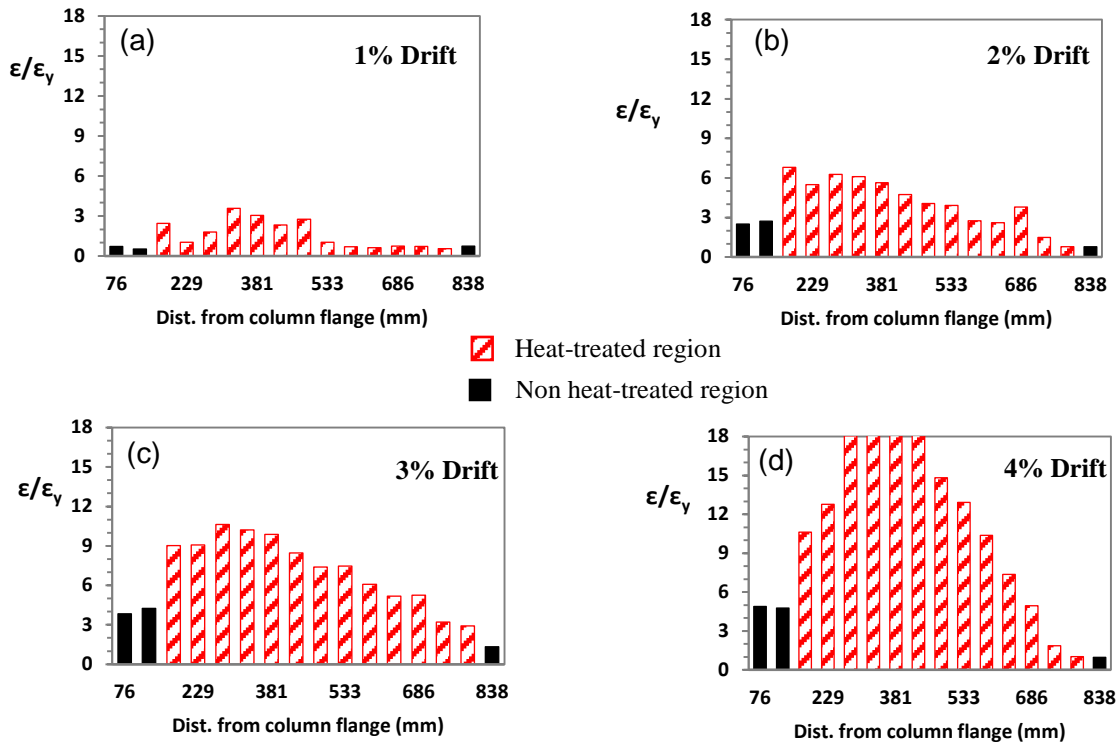


Fig. 14. Recorded longitudinal strains along the center of top flange of the beam from HBS 5.

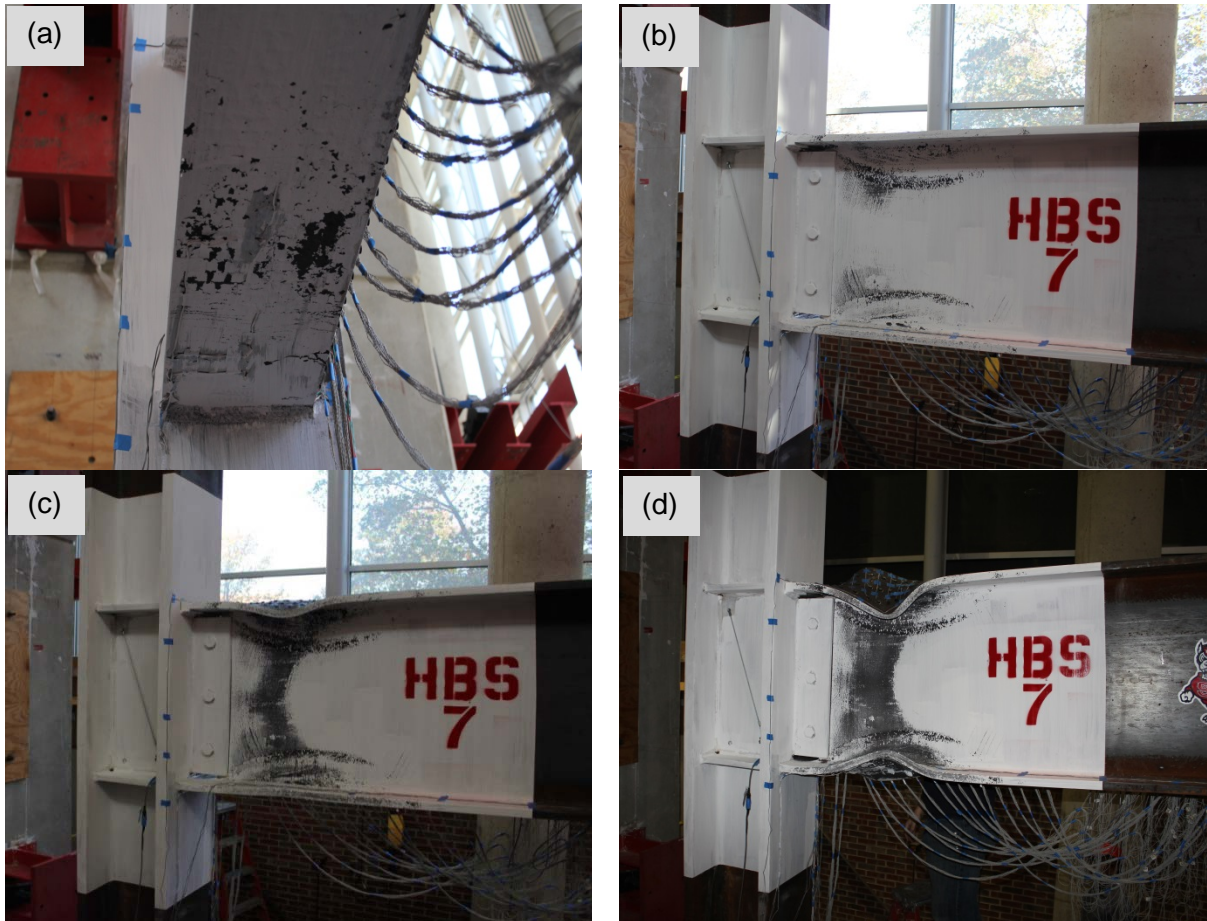


Fig. 15. Yielding and plastic hinge formation of HBS 7, (a) view of beam bottom flange at 1 % Drift, (b) Connection at 3% drift, (c) Connection at 4% drift and, (d) Connection at 6% drift.

8.3 Failure Mechanism of HBS connections

As previously stated, strength degradation of both specimens began during the 2nd cycle of loading at 4% drift when significant local beam web, flange and lateral torsional buckling was observed (see Figs. 11 and 15c). To demonstrate the progressive strength degradation mechanism, beam cross-sections located at 406 mm away from the column flange (within the HBS) are plotted using the recorded vertical and horizontal positions of

Optotrak markers of HBS 5 at various peak drift rotations as shown in Fig. 16 . Dotted lines have been traced between data points to make evident the progressive buckling of the beam.

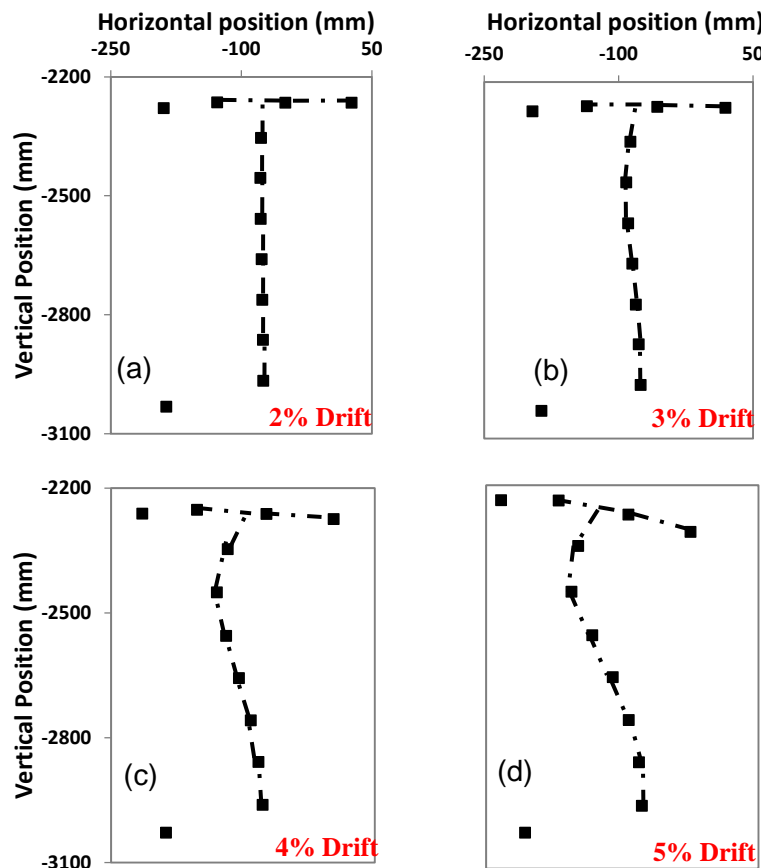


Fig. 16. HBS 5 progression of beam web and flange buckling recorded 406mm away from the column flange at interstory drifts of (a) 2%, (b) 3%, (c) 4% and, (d) 5% (Beam is in positive bending i.e. top flange in compression).

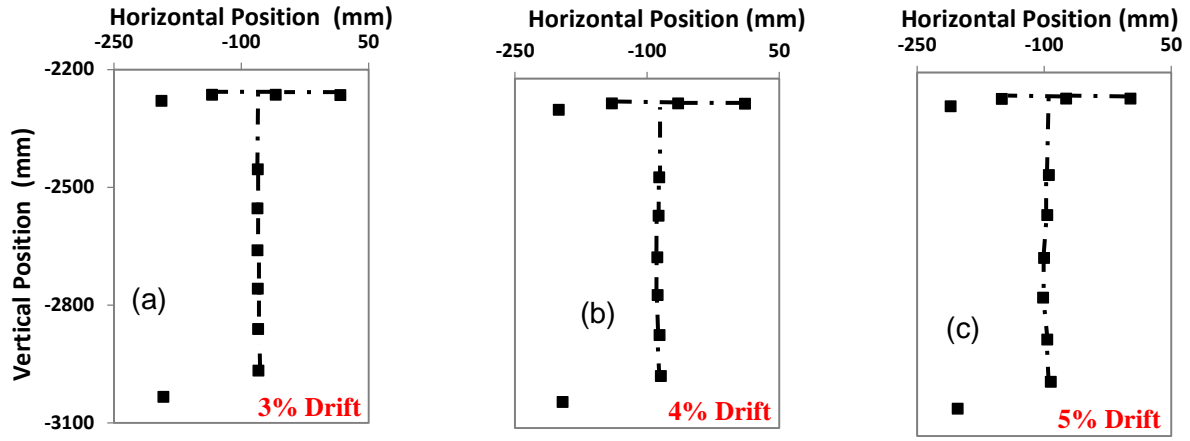


Fig. 17. HBS 5 progression of beam web and flange buckling recorded 106mm away from the column flange of HBS 5 at interstory drifts of (a) 3%, (b) 4% and, (c) 5% (Beam is in positive bending i.e. top flange in compression).

In this figure it is observed that the degradation mechanism appears to have been initiated by slight local buckling of the beam web in the plastic hinge during loading cycles at 3% interstory drift (Fig. 16b). This local web buckling was soon followed by local flange buckling and twisting of the beam as the loading amplitude was increased (Fig. 16c). The amplitudes of flange and web buckling gradually increased with the rotation amplitude resulting in the observed strength degradation (Fig. 11 and 16). This progressive strength degradation mechanism was observed in both test specimens. Testing of HBS 7 was stopped as a result of this significant strength loss. In the case of HBS 5, rupture of the beam flange at the region of largest buckling amplitude is believed to be a result of large strain due to localized bending of the beam flange resulting from the afore described degradation mechanism rather than an axial stress effect. This was also observed in extended end plate (EEP) and welded unreinforced flange-bolted web (WUF-B) connections modified with the HBS technique [39, 40].

Figure 17 shows a series of similar beam cross-section plots of markers located 106 mm away from the column flange (between the column flange and the HBS). Comparison of beam cross-sections in Fig. 17 to those in Fig. 16 with the same drift reveals that in addition to reducing strain demands near the column face as previously discussed (Fig. 14), the HBS was also successful in shifting large deformations due to beam web and flange buckling away from the beam flange CJP welds. Inspection of Figs. 16d and 17c shows that at 5% drift only very slight lateral deformations are evident close to the column flange while significant lateral displacement and twisting of the beam are observed in the plastic hinge. Post-test measurements (Fig. 18) showed flange buckling amplitudes between 114 mm (4.5 inches) and 152 mm (6 inches) and web buckling amplitudes between 80 mm (3 inches) and 127 mm(5 inches) in the two specimens. These large buckling amplitudes were located approximately 420 mm (16.5 inches) from the column flange.



Fig. 18. Photograph showing post-test local flange buckling amplitude of HBS 7 (after 1 cycle of 6% drift).

8.4 Comments on a possible design method of HBS connections

The limited number of tests conducted in this program is insufficient to develop a design method for HBS connections. However, analysis of the available experimental data shows that a design methodology similar to that currently used for RBS connections may be adopted. Table 2 presents data on the magnitudes of bending moments developed in both specimen beams. These were compared to the estimated plastic moment capacity of the unweakened beam section adjacent to the column flange calculated from measured tensile coupon data. Bending moments developed in the middle of the HBS were compared to the estimated plastic moment capacity based on estimated tensile properties obtained from prior tensile testing of coupons extracted from undamaged heat-treated beam flanges.

Table 2 Bending moments developed in HBS test specimens

Specimen	[*] F_y Beam	M_p (kN-m)	M_{p-HBS} (kN-m)	M_{max} (kN-m)	M_{max-HBS} (kN-m)	M_{max}/ M_p	M_{max-HBS}/ M_{p-HBS}
HBS 5 W30 x148	362	2966	2109	3118	2664	1.26	1.05
HBS 7 W30 x148	344	2819	2005	3037	2595	1.29	1.08

M_p = plastic moment of beam based on flange tensile coupon data

M_{p-HBS} = plastic moment at center of HBS region based on estimated flange yield stress

M_{max} = maximum moment developed at column face

$M_{max-HBS}$ = maximum moment developed at center of HBS region

*Flange yield strength determined from tensile coupons tested in accordance with ASTM A370

Maximum bending moments at the face of the column were 5-8 percent higher than the plastic moment capacity while bending moments at the center of the HBS were 26-29% higher than the plastic moment capacity of the weakened section indicating significant work hardening. These results are comparable with RBS test data presented in Engelhardt et al. [22]. Therefore a design methodology in which the parameters of the HBS are selected so as to limit the bending moments at the column face to a desired factor of the plastic moment capacity can be developed. Note that the proposed heat-treatment may also be applied to the beam web in addition to the flanges if design scenarios require larger reduction of moments at the column flange.

9. Conclusion

The experimental validation of an innovative seismic performance enhancing technique for welded steel moment connections has been presented. The technique involves weakening regions of the beam flanges away from the welded joint by exposing them to high

temperatures followed by slow cooling. Consequently, under simulated seismic loading, plastic hinging of the beam takes place in the heat-treated beam section (HBS). All welded connections enhanced with the HBS displayed ductile seismic response, which exceeded the 2010 AISC Seismic Provisions (ANSI/AISC 341-10) SMF qualifying 4% interstory drift angle without much strength loss. Test data also shows that the HBS was successful in shifting the majority of inelastic action and lateral deformation due to local flange and web buckling away from the welded joint.

Based on the results of this preliminary study the HBS concept shows promise as a means of providing a simple, ductile, seismic fuse without sacrificing elastic stiffness or buckling resistance. As a result, other applications of this concept may appear fruitful where these characteristics are desired. For example, this concept has also been successfully used to enhance the seismic performance of extended end plate (EEP) and welded unreinforced flange bolted web (WUF-B) moment connections [39, 40]. This technique may also prove useful in enhancing the seismic performance of link to column connections in eccentrically braced frames or providing low yield strength steel for use in steel plate shear walls. Given the wide scope of possible applications of this technique, future studies are needed to implement it to end uses where it may provide the optimal combination of performance and economy.

Despite, the promising results presented in this study, more analytical and experimental investigation is needed for further development and eventual industry implementation of HBS moment connections. Experimental studies are needed to evaluate the suitability of this technique for a range of beam and column sections, especially larger and heavier sections

which experience more severe strain concentrations during seismic loading [41]. Numerical and analytical parametric studies may be paired with such experimental investigations to develop reliable design methods for accurately predicting strength and performance limit states of HBS moment connections.

10. References

- [1] Kunnath, S.K., & Malley J.O. "Structural Forum." *Journal of Structural Engineering* 126.1 (2000): 4-9.
- [2] Youssef, N.F.G., Bonowitz, D., & Gross, J.L. 1995. A Survey of Steel Moment-Resisting Frame Buildings Affected by the 1994 Northridge Earthquake. Report NISTIR 5625. National Institute of Standards and Technology NIST Gaithersburg, Maryland.
- [3] Popov, E.P., Yang, T., & Chang, S., (1998) "Design of steel MRF connections before and after 1994 Northridge earthquake," *Engineering Structures*, 20(12), 1030-1038.
- [4] Stojadinovic, B., Subhash C.G., Lee, K-H, Margarian, A.G., & Choi, J-H (2000), "Parametric Tests on Unreinforced Steel Moment Connections," *Journal of Structural Engineering*, Vol. 126, pp. 40-49.
- [5] Han, S.W., Kwon, G.U., & Moon, K.H., (2007), "Cyclic Behavior of Post-Northridge WUF-B connections," *Journal of Constructional Steel Research*, 63, pp. 365-374.
- [6] Ricles, J.M., Mao, C., Lu, L.W., & Fisher, J.W. (2002). "Inelastic Cyclic Testing of Welded Unreinforced Moment Connections". *Journal of Structural Engineering*, Vol. 128, No. 4 pp. 40-49.
- [7] Bruneau, M., Uang, C.M., & Whittaker, A. (1998). *Ductile design of steel structures*. New York: McGraw Hill Companies.
- [8] Krawinkler, H. & Popov, E.P., (1982) "Seismic Behavior of Moment Connections and Joints," *Journal of the Structural Division*, Vol. 108, pp. 373-390.
- [9] Engelhardt, M. & Husain, A.S., (1993) "Cyclic-Loading Performance of Welded Flange-Bolted Web Connections" *Journal of Structural Engineering*, 119(12), 3537-3550.
- [10] Barsom, J.M. & Pellegrino, J.V. (2002) "Failure Analysis of Welded Steel Moment – Resisting Connections" *Journal of Materials in Civil Engineering*, 14(1), 44-49.

- [11] Xue, M., Kaufmann, E.J., Lu, L. & Fisher, J.W., (1996) "Achieving Ductile Behavior of Moment Connections-Part II" *Modern Steel Construction* June 1996.
- [12] Sumner, E.A., & Murray, T.M. (2002). "Behavior of extended end-plate moment connections subject to cyclic loading" *Journal of Structural Engineering*, Vol. 128, No. 4 pp.501-508.
- [13] Engelhardt , M.D. & Sabol, T.A. 1994. Testing of Welded Steel Moment Connection in response to the Northridge Earthquake. Progress report to AISC committee on special moment-resisting frame research, October.
- [14] Adan, S.M., & Gibb, W. (2009). "Experimental evaluation of Kaiser Bolted Bracket steel moment-resisting connections," *Engineering Journal*, 181-195.
- [15] Uang C.M., Yu, Q.S., Noel, S. & Gross, J. (2000) "Cyclic testing of steel moment connections rehabilitated with RBS or welded haunch" *Journal of Structural Engineering* 126(1) pp. 57–68.
- [16] Schneider, S.P. & Teeraprbwong, I. (2002) "Inelastic Behavior of Bolted Flange Plate Connections" *Journal of Structural Engineering*, Vol. 128, pp. 492-500.
- [17] Sato, A., Newell, J., & Uang, C.M. (2007) "Cyclic Testing of Bolted Flange Plate Steel Moment Connection for Special Moment Frames" Report No. SSRP-07/10 Department of Structural Engineering, University of California, San Diego, Lo Jolla, CA.
- [18] AISC/ANSI 341-10 (2010) Seismic Provisions for structural steel buildings, Chicago.
- [19] AISC/ANSI 358-10 (2010) Prequalified Connections for special and intermediate steel moment frames for Seismic Applications, Chicago.
- [20] SAC Joint Venture (2000) "Behavior and Design of Radius Cut Reduced Beam Section Connections" *Rep. No. SAC/BD-00/17*.
- [21] Plumier, A. (1997). "The Dogbone: Back to the Future" *Engineering Journal*, 2nd Quarter, Vol. 34, No.2, 1997.
- [22] Engelhardt, M., Winneberger, T., Zekany, A., & Potyraj, T. (1998). Experimental investigation of dogbone moment connections. *Engineering Journal*, 35(4), 128-139.
- [23] Chi, B., Uang, C.M. (2002), "Cyclic Response and Design Recommendations of Reduced Beam Section Moment Connections with Deep Columns," *Journal of Structural Engineering*, Vol. 128, pp. 464-473.

- [24] Kim, K-D & Engelhardt M.D. (2007). Nonprismatic beam element for beams with RBS connections in steel moment frames, *Journal of Structural Engineering* 133(2), 176-184.
- [25] Jones, S.L., Fry, G.T., & Engelhardt, M.D., (2002), "Experimental Evaluation of Cyclically Loaded Reduced Beam Section Moment Connections." *Journal of Structural Engineering*, Vol. 128, pp. 441-451.
- [26] SAC Joint Venture (2000) "Cyclic Response of RBS Moment Connections: Loading Sequence and Lateral Bracing Effects" *Rep. No. SAC/BD-00/22*
- [27] Lee, D., Cotton, S.C., Hajjar, J.F., & Dexter, R.J. (2005), "Cyclic Behavior of Steel Moment-Resisting Connections Reinforced by Alternative Column Stiffener Details, I. Connection Performance and Continuity Plate Detailing," *Engineering Journal*, 4th Quarter, pp. 189-213.
- [28] SAC Joint Venture (2000) "Parametric Tests on the Free Flange Connections" *Rep. No. SAC/BD-00/02*.
- [29] FEMA-350, 2000, *Recommended Seismic Design Criteria for New Steel Moment-FrameBuildings*, prepared by the SAC Joint Venture for the Federal Emergency Management Agency, Washington, DC.
- [30] SAC Joint Venture (2000) "Parametric Tests on Unreinforced Connections Volume 1-Final Report" *Rep. No. SAC/BD-00/01*.
- [31] Bramfitt, B.L. Annealing of Steel, *Heat Treating*, Volume 4, *ASM Handbook*, ASM International, 1991, p 42–55.
- [32] Krauss, G.. *Steels: processing, structure, and performance*. ASM International, 2005.
- [33] ASTM A370-10 Standard Test Methods and Definitions for Mechanical Testing of Steel Products.
- [34] Siwecki, T., & Engberg, G.. "Recrystallization controlled rolling of steels." *Proceedings: Thermomechanical Processing in Theory, Modelling, and Practice* (1996).
- [35] Morrison, M. and Hassan, T., "Influence of cyclic loading history on the local behavior of welded unreinforced flange moment connections ,” under preparation.
- [36] Quayuum, S. & Hassan, T. "Thermal analysis of heat-treated beams for HBS connection," (Unpublished results), NC State University, 2011.

- [37] Goodnight, J.C., Kowalsky, M.J. & Nau, J.M. "Effect of Load History on Performance Limit States of Circular Bridge Columns." *Journal of Bridge Engineering* 18.12 (2013): 1383-1396.
- [38] Popov, E.P., Amin, N. R., Louie, J.C., Stephen, R. M. "Cyclic behavior of large beam-column assemblies." *Engineering Journal* 23.1 (1986): 9-23.
- [39] Morrison, M., Schweizer, D., Quayyum, S., Hassan, T. (2014) "Experimental Validation of an Improved Extended End-Plate Moment Connection and Addressing Further Development," to be submitted to *Journal of Constructional Steel Research*
- [40] Morrison, M., Schweizer, D. Hassan, T. (2014) "Seismic enhancement of welded flange-bolted web (WUF-B) moment connections" to be submitted to *Journal of Structural Engineering*
- [41] SAC Joint Venture (1998) "Strength and Ductility of FR Welded-Bolted Connections"
Rep. No. SAC/BD-98/01

CHAPTER 4: Seismic Enhancement of Eight Bolt Extended End Plate Moment Connections Part I: Numerical Modeling and Design Development

Abstract

The eight bolt stiffened extended (8ES) end plate connection is one of the prequalified connections in the AISC 358 Standard for special moment frames (SMFs) in seismic regions. In 8ES connection, a stiffener plate is welded between the end plate and the beam flanges to strengthen the extended portion of the end plate. In addition to stiffening and strengthening the end plate, this stiffener forces plastic hinging of the beam to take place away from the connection region and promotes uniform distribution of beam flange forces to the connecting bolts. In some experimental studies, this connection showed good performance in terms of energy dissipation and ductility, whereas premature rupture of beam flange at the toe of the stiffener have also been observed due to high stress concentration in this region. The study reported herein performed detailed finite element analysis to understand the failure mechanisms of the eight bolt unstiffened and stiffened extended end plate moment connections. Based on observations made during this study, an improved unreinforced eight bolt extended end plate connection is proposed. In the modified design, the end plate stiffeners were excluded from the connection so as to eliminate the stress concentration associated with the stiffener, and the bolts were rearranged into a hexagonal pattern to ensure uniform distribution of bolt forces. In addition, to reduce the high strain demands at the beam flange to end plate CJP welds a recently validated connection overstress mitigation technique called the heat-treated beam section (HBS) was introduced to shift the plastic hinge away from the beam flange to end plate welds. Finally a technique for delaying the onset of

strength degradation was also included in the proposed connection. The technique called Web Stiffener (WS) involves attaching a steel plate to the beam web in the expected plastic hinge region which delays the onset of web local buckling. The modified connection with these performance enhancing techniques showed improved fatigue failure resilience and buckling failure resilience when compared to the 8ES connection.

Keywords: Extended end plate connection, seismic performance, hexagonal bolt arrangement, end plate stiffener, stress concentration

1. Introduction

In bolted extended end plate (BEEP) moment connections a steel plate is shop welded to the end of a beam which is then field bolted to the connecting members. Though shop fabrication of BEEP connections may be more costly than field welded connections, they offer the advantage of eliminating the difficulties associated with field welding and may provide rapid erection of moment frames [1]. Simulated seismic testing of BEEP connections have shown them to be capable of providing considerable ductility and seismic resilience and as a result, BEEP moment connections have been included in the 2010ANSI/AISC 358 [2] prequalified connections for special and intermediate moment frames for seismic applications. The 2010ANSI/AISC 358 [2] prequalifies three types of BEEP connections, the four bolt unstiffened (4E) four bolt stiffened (4ES) and the eight bolt stiffened (8ES) (Fig. 1).

The cyclic performances of the prequalified BEEP connections have been evaluated through numerous large scale experimental and analytical studies. Early cyclic testing by

Tsai and Popov [2] Ghobarah *et al.* [4], Koral *et al.* [5], and Murray and Meng [6] on four bolt unstiffened (Fig. 1a) and four bolt stiffened (Fig. 1b) extended end plate connections showed that when properly designed, these connections can provide excellent performance under large load reversals. The findings of these studies indicate that in general, best results are obtained when connection elements such as the end plate, end plate stiffener and bolts are designed to undergo limited inelastic action forcing most of the damage to occur in the beam. More recent studies by Sumner and Murray [7], and Sumner *et al.* [8] corroborate these findings for the four bolt unstiffened extended end plate connections and also showed that eight bolt stiffened extended end plate connections could provide sound seismic performance. Test results from these studies have been used in the prequalification of BEEP connections and in the development and verification of design equations for seismic applications [1, 2, 9].

In stiffened connections (4ES and 8ES) a triangular stiffener is welded between the outer surface of the beam flange and the extended portion of the end plate. This stiffener serves the main purpose of increasing the strength and stiffness of the end plate. Experimental and analytical studies show that bolt force distribution is more uniform and end plate deformations as well as prying forces are reduced with the addition of the stiffener [3, 10]. End plate design equations in the 2010ANSI/AISC 358 standard which are derived from yield line analysis of the end plate account for this added strength and as a result, four bolt stiffened (4ES) connections require thinner end plates than do four bolt unstiffened (4E) connections with all else being equal [1, 8]. In addition to added strength and stiffness, stiffened connections form plastic hinges at the base of the stiffener away from the beam

flange to end plate welds reducing the inelastic strain demands in this vulnerable region [9].

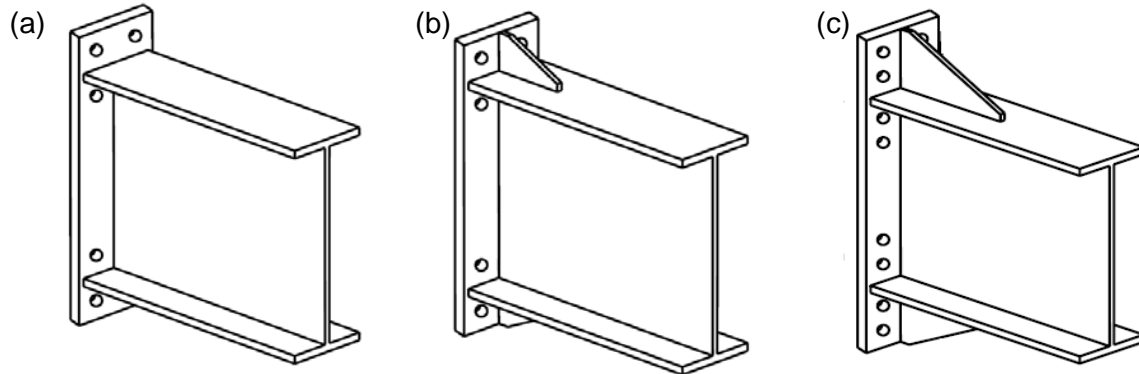


Fig. 1. ANSI/AISC 358 Prequalified Extended End Plate Connections (a) Four bolt unstiffened (4E), (b) four bolt stiffened (4ES), (c) eight-bolt stiffened (8ES) [9].

Although, some investigations on stiffened (4ES and 8ES) BEEP connections [6, 7] have shown ductile behavior and good energy dissipation, other studies [4, 11, 12] report premature failure of the weld between the beam flange and the stiffener or fractures initiating at the beam flange to end plate CJP welds followed by gross section fractures of the stiffener. In one study [13], fracture was reported to have initiated at the toe of the weld between the end-plate stiffener and the beam flange and was attributed to the stress concentration in this region. This stress concentration results from the geometric discontinuity introduced by the stiffener and may be exacerbated by the presence of weld defects some of which may not be detected by welding inspection practice [14, 15]. Careful detailing, fabrication and inspection of stiffened BEEP connections can reduce the likelihood of failures arising from this stress concentration, however the seismic performance uncertainty and added complexity to design,

fabrication and inspection associated with stiffened BEEP connections provides the motivation for the current study involving a detailed examination of eight bolt extended end plate connections ultimately leading to the development of an improved eight bolt *unstiffened* extended end plate connection.

The overall goal of this research effort is to obtain a better understanding of the seismic behavior and failure mechanisms of eight bolt extended end plate moment connections, and by so doing, develop an eight bolt unstiffened extended end plate connection that is both fatigue failure resilient and buckling resilient. This connection eliminates both the unfavorable stress concentration due to the end plate stiffener in the 8ES connection and the non-uniform distribution of bolt forces that ultimately led to brittle failures in previously studied 8-bolt unstiffened 4 wide (8E-4W) connections (Fig.15) [8, 9]. Furthermore, the proposed connection reduces additional welding and fabrication associated with the end plate stiffener while also providing more usable floor space above the concrete slab.

In this article, detailed finite element modelling (FEM) of extended end plate connections is described and validated with data from the literature. The finite element model is then used to investigate the influence of details such as bolt configuration and end plate stiffener on the seismic performance and potential failure mechanisms of the connection in question. Key observations from this study led to a proposed hexagonal bolt arrangement that provides uniform distribution of bolt forces for unstiffened 8 bolt extended end plate connections.

Subsequently, the hexagonal bolt pattern is extended to a heavier beam section where large strain demands at the beam flange to end plate CJP welds motivate the introduction of a recently validated connection overstress mitigation technique [16]. This technique involves subjecting selected regions of the beam flange to high temperatures followed by slow cooling resulting in reduced strength of steel in the heat-treated beam section (HBS). This reduction in strength promotes yielding and plastic hinging within the HBS in a manner similar to the reduced beam section (RBS) and by so doing, reduces inelastic strain demands at the beam flange to end plate welds. An 8 bolt extended end plate connection modified with the hexagonal bolt pattern and HBS eliminates entirely the necessity for the end plate stiffener and demonstrates potential applicability to a wide range of available beam sections.

Finally, a technique for delaying the onset of strength degradation was also included in the proposed connection. This technique involves welding a steel plate to the beam web in the expected plastic hinge region which stiffens the beam web and delays the onset of web local buckling. In previous studies, web local buckling has been identified as a “trigger” that eventually leads to strength degradation in deep beam sections subjected to large loading reversals [17, 18]. The addition of the proposed *Web Stiffener* (WS) was found to be effective in delaying the onset and slowing the rate of strength degradation without affecting the low cycle fatigue failure resilience and bolt force distribution in the proposed connection. Finite element modeling and development of the proposed connection is described in detail where each of the afore-mentioned performance enhancement techniques is clearly shown to have a pronounced effect on bolt force distribution, low cycle fatigue failure resilience, plastic hinge formation, and strength degradation due to local buckling.

It must be mentioned that during the development of the proposed connection, Kiamanesh *et al.* [19] investigated a circular bolt arrangement for eight bolt extended end plate connections which is similar to the hexagonal bolt arrangement proposed in this study. In the study by Kiamanesh *et al.* [19] finite element analysis (FEA) was used to show that a circular bolt arrangement was effective at reducing hysteresis pinching and improving connection strength and energy dissipation when compared with the rectangular bolt arrangement without the end plate stiffener. The study concludes that these benefits are appreciable in connections with large bolt diameters and end plate thicknesses and in general are a result of the more uniform distribution of bolt forces.

The study reported herein presents the systematic development of the proposed bolt arrangement through careful examination and observations of the behavior of eight bolt stiffened (8ES) and eight bolt 4 wide (8E-4W) extended end plate connections. The final bolt arrangement concept is arrived at based on considering the following:

1. The influence of the proximity of the bolt group to the beam tension flange on bolt force distribution
2. The influence of the end plate stiffener on bolt force distribution
3. The influence of bolt arrangement on the stiffness of the end plate region between the beam flange and the bolt group and the consequential effect on bolt force distribution

In addition, the current study addresses other key considerations for optimal connection performance and design such as plastic hinge formation, low cycle fatigue and buckling resilience, and the applicability of the proposed connection to different member sizes.

2. Finite Element Modeling and Analysis of Extended End plate Connections

Finite element modeling (FEM) has been useful in providing insight on the behavior and failure mechanisms of moment resisting connections. However, the simulation responses from FEM will be useful only when all the components of the assembly and their interactions are modeled appropriately. Literature shows successful simulation of several experimental responses for different types of moment resisting connections [10, 21, 22], and based on the failure mechanisms observed from simulated responses, modifications were proposed to the existing connections which were later experimentally validated [10, 21, 23]. Likewise, extended end plate connections have been studied by using finite element modeling [9, 10, 19, 22, 24-36] and good correlations were observed between the experiment results and simulated responses under monotonic loading conditions in some studies [24-27, 31-32]. Starting with Krishnamurthy in 1978 [33], most of the finite element analysis was focused on the monotonic response simulation, or parametric studies to understand the behavior of the connection under monotonic loading conditions. Simulation of extended end plate connections under cyclic loading is limited in the literature [19, 22, 34, 35] and few studies show reasonable correlation with experimental responses [22, 35]. Compared to other types of moment connection such as welded unreinforced flange welded web (WUF-W) connection and reduced beam section (RBS) connection, simulation of extended end plate moment connection is more challenging because of the complexities due to the contact interaction between the various connection components and the effects of bolt pre-stress/pretension. In this study detailed modeling of extended end plate connections was

undertaken using advanced finite element modeling techniques. A brief description of the finite element modeling scheme adopted in this study is presented next.

2.1 Finite element modeling details

Three dimensional nonlinear finite element models were developed for extended end plate connections by using the finite element analysis software ANSYS. Geometric, contact and material nonlinearities were incorporated in the finite element models. Fig. shows an example of the finite element mesh generated for an eight bolt stiffened extended end plate connection. The beam, and column were modeled and discretized by eight noded solid brick elements (SOLID 185). In order to precisely model the bolts and their interaction with the end plate, the bolts and endplate were discretized with twenty noded solid brick elements (SOLID 186).

The interaction between the end plate and column flange, bolt head and end plate, bolt nut and column flange, and bolt shank and circular holes in the end plate and column flange were modelled by small sliding contact surfaces. Surface-to-surface contact elements (CONTA 174) and target elements (TARGE 170) were used to generate the contact regions. The penalty stiffness contact algorithm with a penalty stiffness factor of 0.1 was found to ensure acceptably small values of contact penetration whilst alleviating numerical convergence difficulties. It should also be noted that the approach utilized for modelling bolts in this study resulted in no displacement boundary conditions being specified for the bolts. Therefore, rigid body motion was circumvented by ensuring that small gaps between contact pairs resulting from numerical round offs during meshing were closed prior to application of

pretension loads by using contact surface offsets.

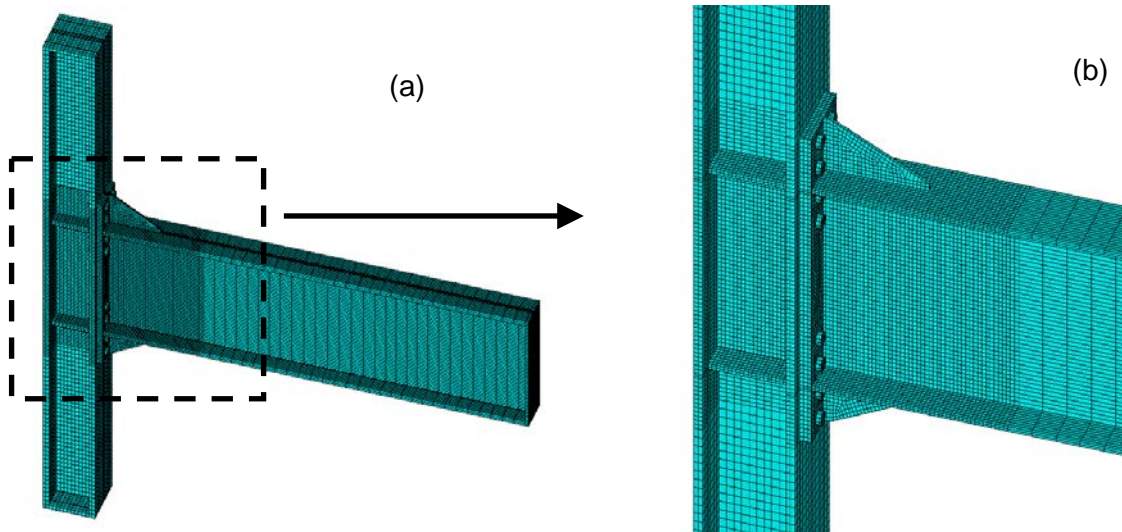


Fig. 2. (a) Finite element mesh of an eight bolt stiffened (8ES) extended end plate connection
(b) Close up view of finite element mesh

The AISC LRFD specified minimum bolt pretension forces [37] were modeled by using two ANSYS features, the PRETS179 pretension element and the PSMESH pretension meshing command. When pretension loading is applied, this element (PREST 179) simulates the reduction of effective length (length between the underside of the bolt head and nut) that takes place during tightening of the fastener in order to generate the required clamping forces. In the simulation, the pretension load is applied during the first load step and stored as an initial displacement before the application of loads at the beam tip. This allows for the simulation of fluctuations to the initial pretension load due to the deformations and interactions of the assembly. It should be noted however, that the bolt threads were not modeled in this study i.e. the bolt nut was glued to the bolt shank. Thus the complex

nonlinear behavior that arises between the threads of the bolt shank and nut were not captured.

2.2 Material models

Finite element models accounted for material nonlinearity through rate-independent metal plasticity theory based on the von mises yield criterion, additive strain decomposition and associated flow rule. The Chaboche non-linear kinematic hardening model [38] was used for cyclic analysis. Chaboche material model parameters were obtained by fitting stable single amplitude hysteresis loops. The distinguishing feature of the Chaboche model is the superposition of non-linear kinematic hardening rules according to Eq. 3 and Eq. 4. This allows for accurate simulation of hysteretic loop shape and therefore plastic modulus over a wide strain range and various loading paths. A summary of the nonlinear kinematic hardening parameters used for cyclic analysis is provided in table 1 and a brief description of the Chaboche [38] model is given below.

The yield criterion:

$$f(\underline{\sigma} - \underline{\alpha}) = \left[\frac{3}{2} (\underline{s} - \underline{a}) \cdot (\underline{s} - \underline{a}) \right]^{\frac{1}{2}} = \sigma_0 \quad (1)$$

where $\underline{\sigma}$ is the stress tensor, $\underline{\alpha}$ is the current center of the yield surface in the total stress space, \underline{s} is the deviatoric stress tensor, \underline{a} is the current yield surface center in the deviatoric space, and σ_0 is the radius of the yield surface. The rate-independent plastic strain increment is calculated using the associated flow rule:

$$d\underline{\varepsilon}^p = d\lambda \frac{\partial f}{\partial \underline{\sigma}} = \frac{3}{2} dp \frac{\underline{s} - \underline{a}}{\sigma_0} \quad (2)$$

The superimposed kinematic hardening rule is given by:

$$d\bar{a} = \sum_{i=1}^n d\bar{a}_i \quad (3)$$

$$d\bar{a}_i = \frac{2}{3} C_i d\bar{\varepsilon}^p - \gamma_i \bar{a}_i dp \quad (4)$$

Each of the superposed kinematic hardening rules has a strain hardening term (1st term in Eq. 4) and a dynamic recovery term (2nd term in Eq. 4). C and γ are material parameters obtained from fitting a stable single amplitude stress-plastic strain curve from a uniaxial cyclic material test.

In the finite element modeling of the extended end plate connection, ASTM A992 and A572 Gr.50 steels were used as beam and column materials, whereas ASTM A36 was used as the end plate material. Bolts were modeled using either ASTM A490 or A325 bolts. Chaboche model parameter determination requires that the stable hysteresis loop of the cyclic stress-strain response be known. In this case, stable hysteresis loops were obtained from single amplitude strain controlled cyclic test of ASTM A992, ASTM A572 Gr.50 and ASTM A36 steel coupons. Chaboche parameters were determined from a hysteresis loop of strain controlled experiment of ASTM A992, ASTM A572 Gr.50 [39] and ASTM A36 [39] steels. The nonlinear kinematic hardening parameters (shown in Table1) were determined by using a genetic algorithm based optimization method.

Table 1 Nonlinear kinematic hardening parameters for different steels

Parameters	ASTM A36	ASTM A572 Gr.50	ASTM A992	ASTM A490
E (MPa)	186861	191505	199948	199948
σ_0 (MPa)	261.5	251.7	238.6	777.7
C_1 (MPa)	119996.4	125415.7	383336.8	204615.8
C_2 (MPa)	10873.1	28868.4	280782.1	152250.1
C_3 (MPa)	537.8	2675.2	50780	101318.5
C_4 (MPa)	68.9	144.8	1958.3	32219.2
γ_1	1036	4585	21081.2	4143
γ_2	129	324	6256.2	285
γ_3	5	42	515	107
γ_4	0	0	13.2	0

Simulations were made at the material level with obtained parameters for validation. As shown in Fig., the simulated responses were in good agreement with the experimental responses. The connection between the beam flanges and end plate was modeled with groove welds using the material properties of E70 weld metal obtained from FEMA-355B [14] and implemented in the FE simulation through bilinear material model as shown b. For determining the material properties of ASTM A325 and A490 bolts, uniaxial tests were performed [40] and Chaboche model parameters (shown in Table 1) were obtained through fitting the monotonic stress-strain curve.

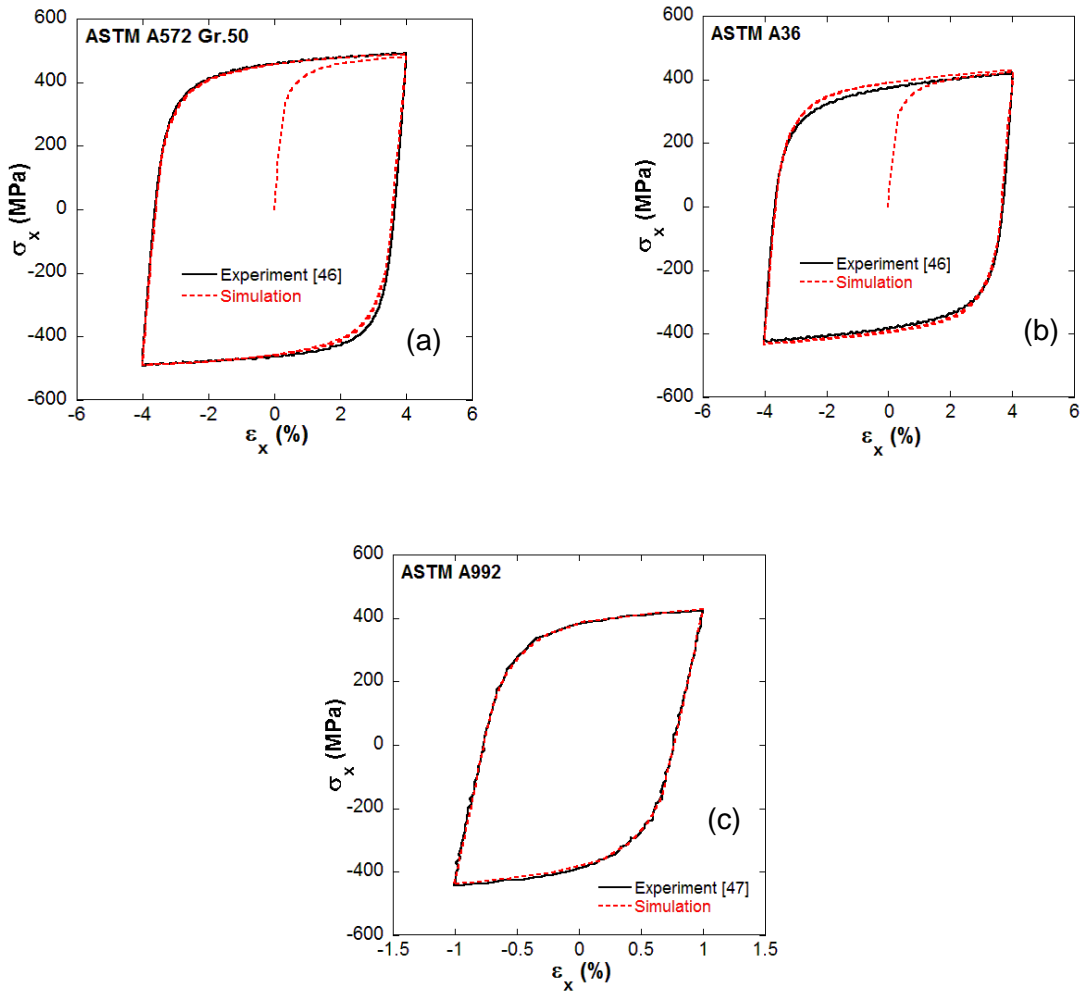


Fig. 3. Experimental and simulated response of strain controlled hysteresis loop with Chaboche model parameters. (a) ASTM A572 Gr.50 steel, (b) ASTM A36 steel, (c) ASTM A992 steel.

2.3 Loads and Boundary Conditions

In the finite element modeling of the extended end plate moment connection, the boundary conditions were applied such that it mimics the boundary conditions applied in the experimental setup for seismic testing of extended end plate connection used by Sumner *et*

al. [8]. The boundary conditions implemented in the finite element simulations are shown in Fig. a. The top and bottom of the column flange nodes were hinged (x, y and z-direction of the nodal displacements were restrained) near the column end stiffeners.

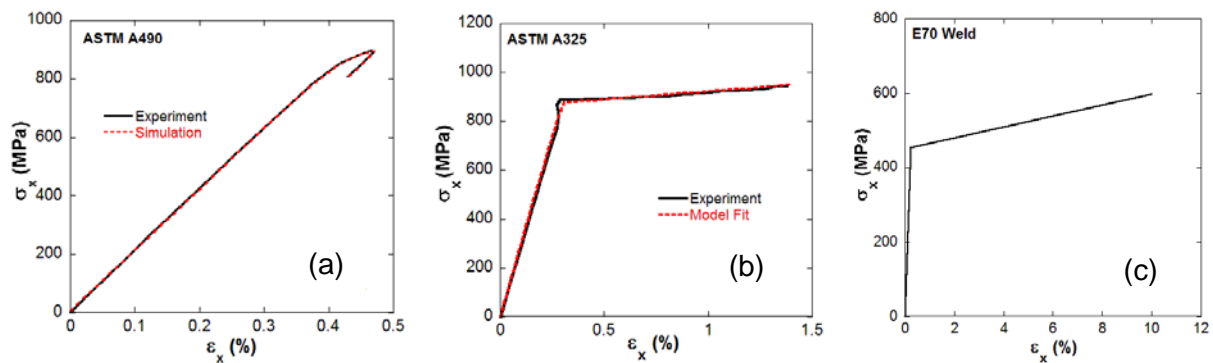


Fig. 4. (a) Experimental monotonic stress-strain response and simulated response for ASTM A490 bolt with Chaboche model parameters, (b) Experimental monotonic stress-strain response [40] and simulated response for ASTM A325 bolt with Chaboche model parameters, (c) bilinear model for E70 weld obtained from the reported yield and tensile strength data [14].

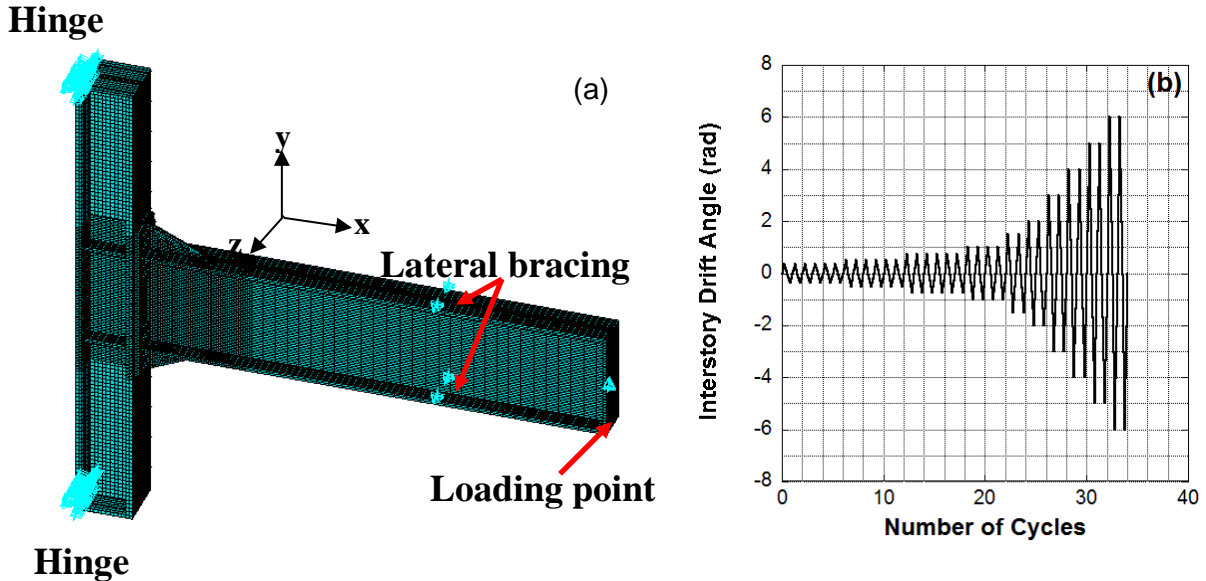


Fig. 5. (a) Boundary conditions adopted in the seismic analysis of extended end plate connection, (b) SAC loading protocol [41].

Lateral displacements were restrained close to the loading point at the beam tip as shown in Fig. a. Vertical displacement was applied at the central nodes located on the stiffener plate at the free end of the beam so as to simulate the displacement controlled actuator loading during the test. All beam-column assemblies were analyzed with a displacement-based SAC loading protocol of SAC/BD-97/02 [41] consisting of a series of prescribed quasi-static cyclic displacements to the end of the beam as shown in Fig. 5b [41].

3. Validation of Finite Element Model

In this study, the finite element model was validated against the experimental responses of the four bolt unstiffened (4E) and eight bolt stiffened (8ES) extended end plate connections tested by Sumner *et al.* [8], where the connections' performance was evaluated under SAC loading history as shown in Fig. b. Fig. shows a comparison of the simulated and

experimental moment-rotation responses of 4E and 8ES specimens tested by Sumner *et al.* [8] where it is observed that the hysteresis loop shape and peak moments in each cycle are simulated with reasonable accuracy. Plastic hinge formation and local buckling is also simulated with good accuracy as shown in Figs. 7 and 8.

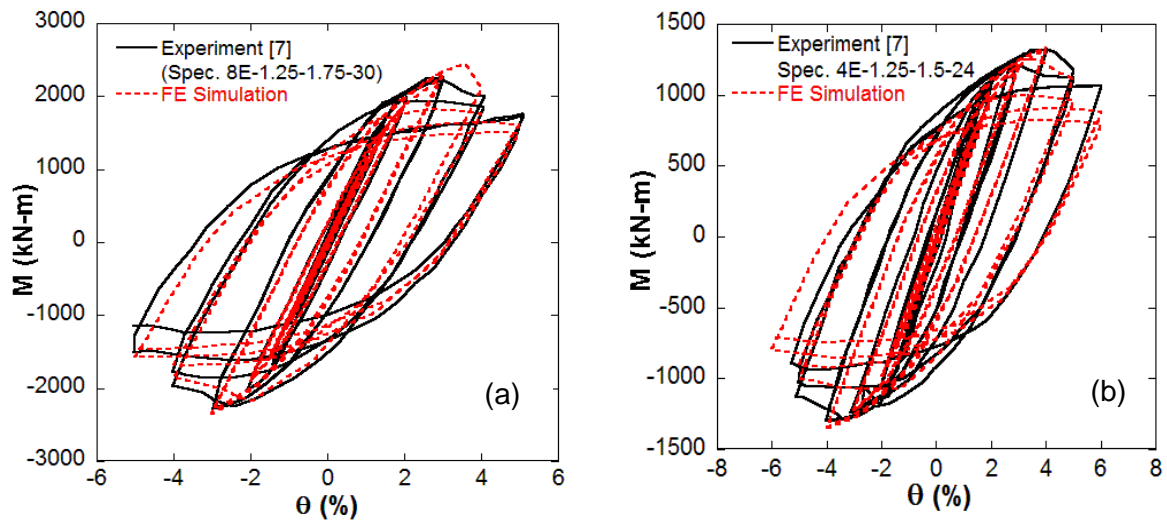


Fig. 6. Comparison between experimental and simulated moment-rotation response of (a) eight bolt stiffened (8ES), and (b) four bolt unstiffened (4E) extended end plate connections tested by Sumner *et al.* [7].

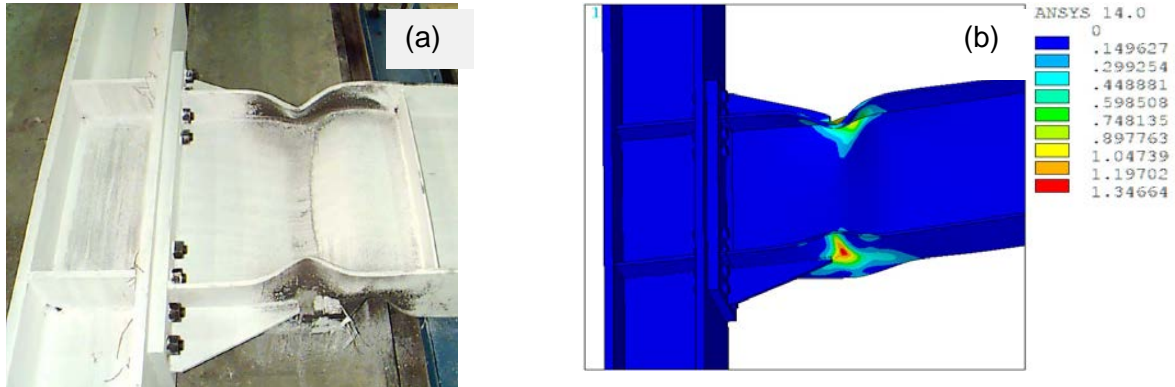


Fig. 7. Comparison of experimental and simulated deformed shape for 8ES specimen tested by Sumner *et al.* [7] a) Post-test photograph of specimen 8E-1.25-1.75-30 b) Accumulated equivalent plastic strain FE prediction showing plastic hinge formation at the base of the endplate stiffener

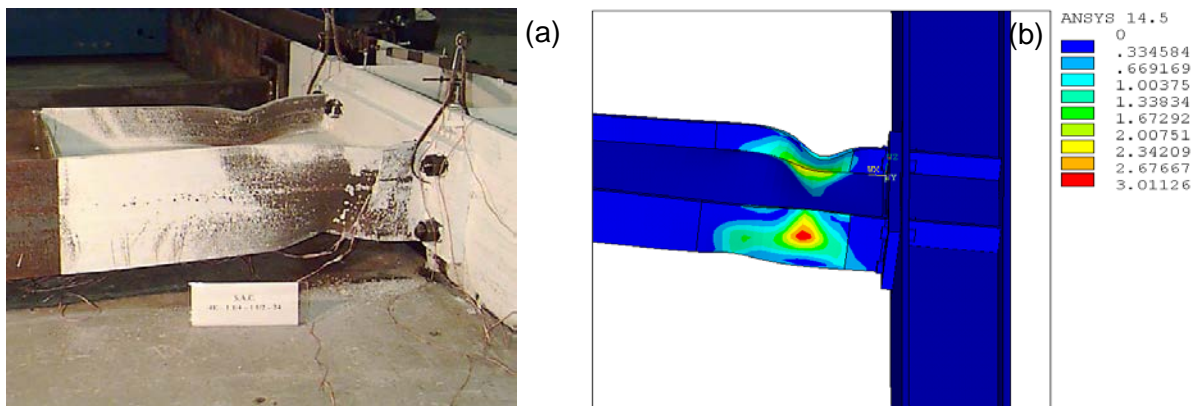


Fig. 8. Comparison of experimental and simulated deformed shape for 8ES specimen tested by Sumner *et al.* [7] a) Post-test photograph of specimen 4E-1.25-1.5-24 b) Accumulated equivalent plastic strain FE

Figure 9 shows a comparison of bolt strain responses obtained from the experiments and simulation of an interior bolt from the 8ES connection tested by Sumner *et al.* [8]. In the experiment (Fig. 9a) the strain in the bolt cycled within the pretension strain range with a

slight decrease in the bolt strain during cycling. Similar observations were made from the finite element analysis results (Fig. 2b).

In summary, the developed finite element models show good accuracy in predicting experimental responses of interest and are used to investigate the failure mechanism of other types of extended end plate connections in the following.

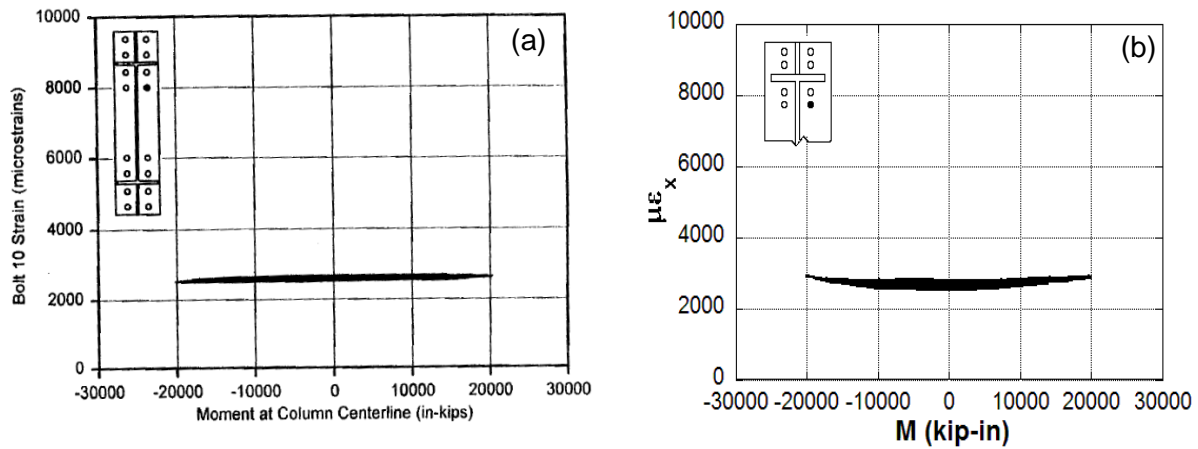


Fig. 9. Comparison of experimental and simulated bolt strains for 8ES specimen tested by Sumner et al. [7]. (a) Experimental response, (b) simulated response.

4. Finite Element Analysis of Extended End plate Connections

In this part of the study, detailed finite element analysis was performed on eight bolt extended end plate connections with different bolt arrangements in order to investigate the failure mechanisms and develop an enhanced eight bolt extended end plate connection. An exterior sub-assemblage consisting of a W14×193 (ASTM A992) column with a single W30×99 (ASTM A992) beam attached to the flange was chosen for this analysis. The end plate material used was ASTM A36 which was bolted to the column flange with ASTM

A490 or A325 bolts. Bolts were given a pretension as specified in the AISC LRFD specification [37]. The column was reinforced with 19.05 mm continuity plates and a 9.525 mm doubler plate. Lateral supports were provided for the beam at a distance of 1.25 m, 2.46 m and 5.72 m from the centerline of the column [8]. The loading was applied to the beam at a distance of 6.13 m from the centerline of the column. All the connections were analyzed under displacement controlled cyclic loading in accordance with the SAC loading protocol [41] as shown in Fig. 5a. The following four types of connection configurations were considered consisting of eight bolts at each flange with different arrangements of bolts.

- i. Eight bolt stiffened connection (8ES): four rows of two bolts at each flange, two rows above and two rows below the flange with end plate stiffener (Sumner *et al.* [8]).
- ii. Eight bolt 4 wide unstiffened connection (8E-4W): two rows of four bolts at each flange, one row above and one row below the flange without end plate stiffener (Sumner *et al.* [8]).
- iii. Eight bolt unstiffened connection (8E): four rows of two bolts at each flange, two rows above and two rows below the flange without end plate stiffener.
- iv. Modified eight bolt unstiffened connection (8EUH): four rows of two bolts at each flange, two rows above and two rows below the flange in a hexagonal pattern without end plate stiffener.

The results of the finite element analysis on these connection configurations are presented next.

4.1 Eight Bolt Stiffened Extended End plate Connection (8ES)

The eight bolt stiffened extended end plate connection (8ES) analyzed in this part of the study was identical to that presented in section 3, however the beam and column materials were modelled as ASTM A992 steel. This was done to facilitate comparison with newly developed designs in which A992 material will be used. The connection had an end plate thickness of 44.45 mm which was bolted to the column flange with 31.75 mm diameter ASTM A490 bolts. The bolts were arranged in four rows of two bolts at each flange, two rows above and two rows below the flange. There was a 12.7 mm thick end plate stiffener placed at the extended portion of the end plate which was welded to the end plate and the beam flange. The material properties used for the end plate stiffener was ASTM A36.

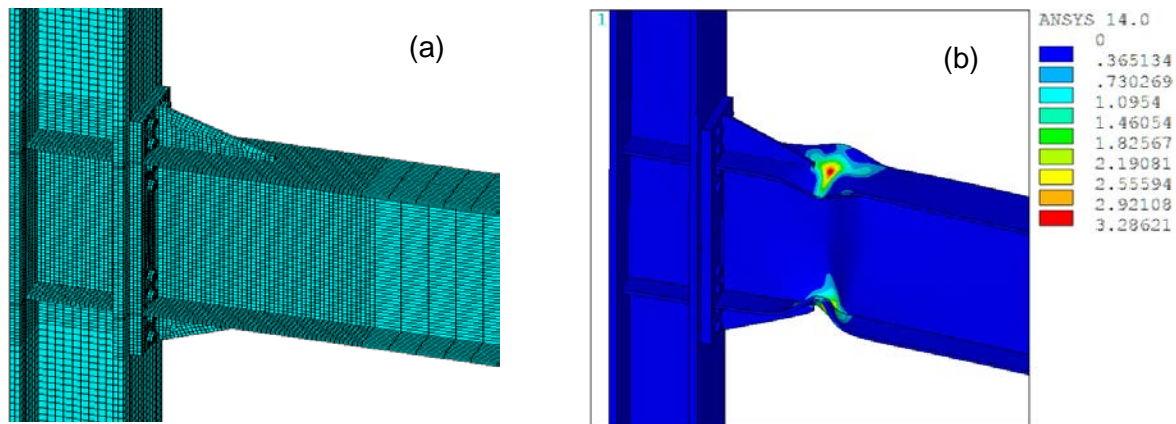


Fig. 10. Eight bolt stiffened extended end plate connection (8ES). (a) FE mesh, (b) accumulated equivalent plastic strain contour showing formation of plastic hinge after cyclic loading up to 6% interstory drift.

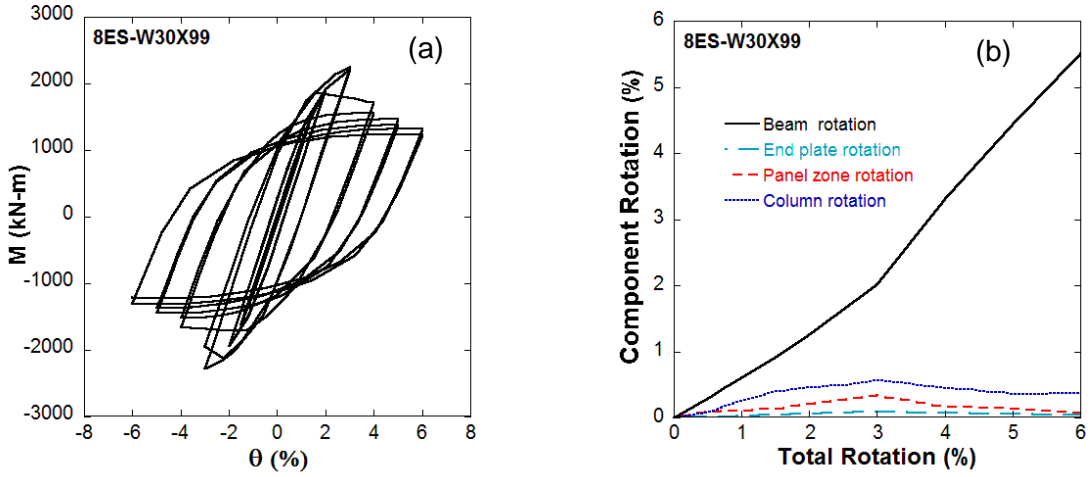


Fig. 11. Cyclic response of 8ES connection. (a) Moment-rotation hysteresis response, (b) rotation contribution of connection components.

The finite element mesh of the connection is shown in Fig. 10a. In the figures and discussion, this connection has been denoted as 8ES-W30×99, where the beam size analyzed is also indicated. The connection showed ductile behavior forming a plastic hinge at a distance of 492 mm away from the face of the column which was at the base of the end plate stiffener as can be seen in Fig. 10b. The moment-rotation plot of the connection (shown in Figure 11a) showed initiation of strength degradation in the 2nd cycle of 3% interstory drift which became significant (30%) during loading cycles at 4% interstory drift. As the loading cycles progressed, strength of the connection was reduced by 40% at 6% interstory drift, due to local buckling of the beam. The contributions of the beam, panel zone, column and end plate to the maximum interstory drift (6%) were: $\theta_b=5.51\%$, $\theta_{pz}=0.07\%$ $\theta_c=0.37\%$ $\theta_{ep}=0.05\%$ (shown in Figure 12b). These contributions indicate that the beam flexural hinging accounted for most of the connection rotation.

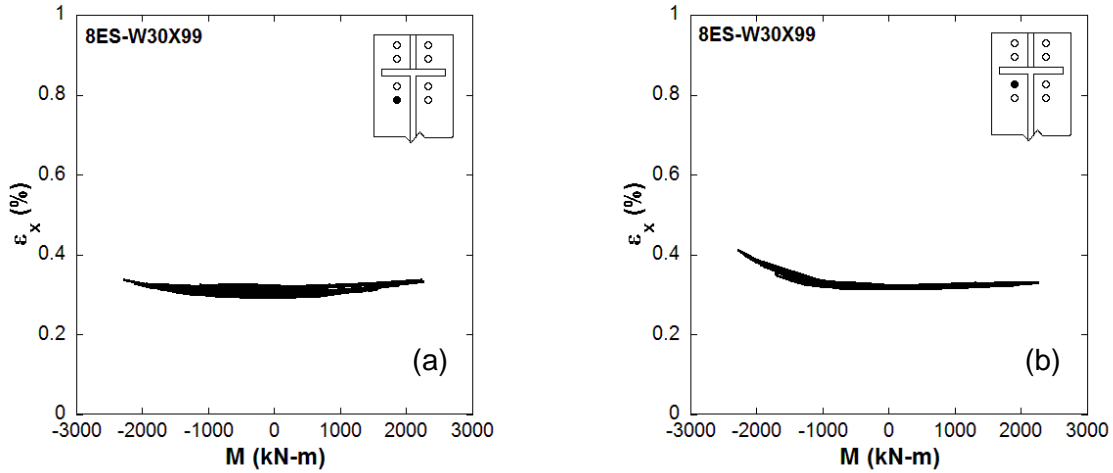


Fig. 12. Bolt strains for 8ES configuration during loading cycles at the top flange of the beam.

It is to be noted here that the contributions from panel zone, column and end plate in the rotation capacity of the connection started to decrease when the beam started to buckle locally, indicating a noticeable increase in the beam's participation in the rotation of the connection (Fig. 11b).

Bolt strain responses were in the elastic range, but small relaxation in the bolt strains was observed during cycling (Fig. 12). It is also noted that bolt strain distribution between the inner and outer row of bolts remained fairly uniform. As will be discussed in more detail later, uniform distribution of bolt strains and forces between the inner and outer row of bolts is a result of the improved local end plate rigidity provided by the stiffener which consequently reduces endplate deformations and promotes uniform bolt force distribution [3].

Throughout the loading cycles, the axial strains in both the top and bottom flange groove welds remained at or just below the yield strain as shown in Fig. 13. These low strain demands are due to significantly reduced local deformations at the weld joint as a result of the end plate stiffener which redirects force flow away from the beam flange-to-end plate welded connection region. As a result, plastic hinge formation takes place at the toe of the end plate stiffener and the beam flange to end plate connection remains essentially undamaged (Fig. 10b and 13).

However, an unfortunate consequence of this plastic hinge relocation is the introduction of a stress concentration at the toe of the stiffener. This results from the sharp change in the principal stress direction in this region as stresses flow from the beam flange into the stiffener. Upon yielding this stress concentration causes high strain rates with continued cycles resulting in a strain concentration in this region. This is illustrated in Fig. 14 where von mises stresses (Fig. 14a) and strains (Fig. 14b) are plotted along the center of beam starting at the beam flange-to-endplate CJP weld toe. The stress concentration at the toe of the stiffener is clearly discernable (note the sudden jump in stressses at approx 500mm away from the CJP welds) in Fig. 14a during cycles at 0.5% drift where the response is elastic. Note that as loading progresses from 2-4% drift, a rapid increase in plastic strain is observed with comparably small increases in stress.

In the presence of pre existing flaws in the stiffener-to-beam flange weld or the stiffener to end plate weld, this stress concentration may provide the driving force for the propagation of a brittle crack. Also, with several repeated cycles in the inelastic range the strain concentration will limit the fatigue life of the connection. Therefore, despite the

benefits obtain from the stiffener in terms of strengthening the endplate, improving local endplate rigidity, promoting uniform bolt force distribution and relocation of the plastic hinge away from the CJP welds, this consequential stress concentration may reduce the ductility of the connection as observed in some experiments [11-13]. It should be noted that the stress and strain distributions in Fig. 14 are presented for qualitative discussion only. The 90° reentrant corner at the base of the stiffener which is a fictitious geometrical detail arising from modelling simplifications creates a theoretical stress singularity where mesh refinement will not result in convergence of the FE stress and strain predictions. Therefore these results are used only to identify trends in the stress and strain responses and not for accurate quantitative predictions.

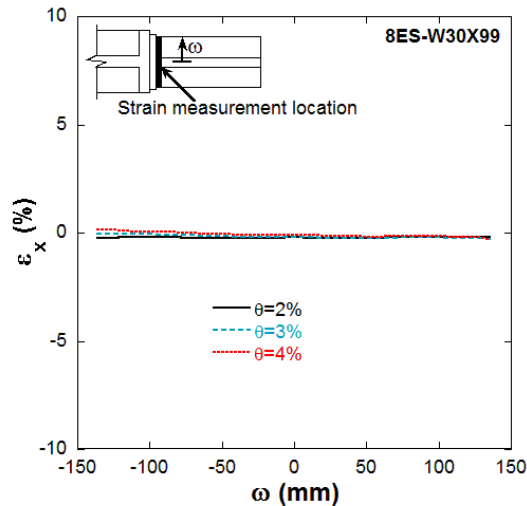


Fig. 13. Axial strain profile along the width of beam bottom flange at the weld toe for 8ES connection.

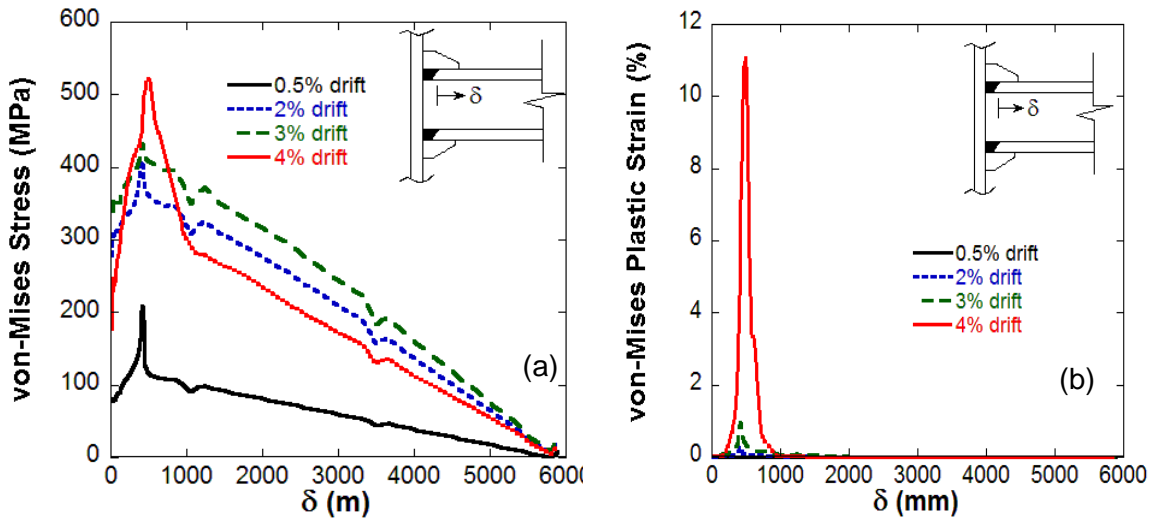


Fig. 14. (a) Von-Mises stress distribution along the beam centerline (b) Von-Mises (Equivalent) plastic strain distribution along the beam centerline

4.2 Eight Bolt 4 Wide Unstiffened Extended End plate Connection (8E-4W)

Similar to 8ES, the eight bolt 4 wide unstiffened extended end plate connection (8E-4W-W30×99) utilizes eight bolts at each flange for connecting the beam to the column, but the bolts are arranged in two rows instead of four rows unlike 8ES connection. Each row has four bolts, one row above and one row below each beam flange. As previously mentioned, this connection configuration was tested by Sumner *et al.* [8], and suffered from non-ductile failure modes including bolt rupture and end plate tearing. Figure 15a shows the FE mesh used for 8E-4W connection which is identical in geometry to specimen 4W-1.25-1.125-30 tested by Sumner *et al.* [8], however as with the previously discussed 8ES connection, the beam and column materials were modelled as ASTM A992 steel. Figure 15b shows the accumulated equivalent plastic strain contour plot for the 8E-4W connection at 3% interstory drift under SAC loading. Divergence of the FE solution was encountered during loading cycles at 3% interstory drift which prevented the analysis of this connection at higher drift

angles. However, the FE model captured qualitatively the failure mechanisms reported from experimental testing of this connection [8].

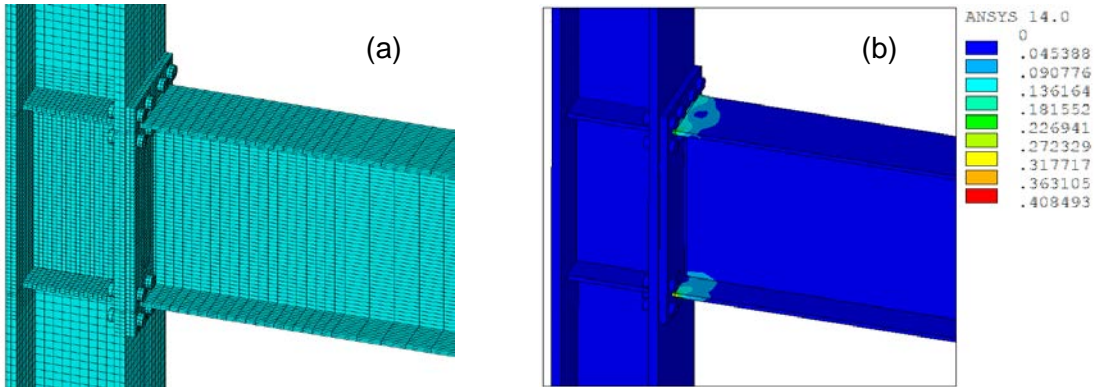


Fig. 15. FE Simulation of Eight bolt 4 wide unstiffened extended end plate connection (8E-4W-30x99). (a) FE mesh, (b) accumulated equivalent plastic strain contour showing at 3% interstory drift angle.

Initial yielding of the beam flanges was observed during loading cycles at 1% interstory drift in the beam flanges close to the weld. During loading cycles at 2% interstory drift, additional yielding of the beam flanges was observed with small amount of yielding of beam web, panel zone and end plate. During cycling at 3% interstory drift, severe yielding of the beam flanges at the toe of the CJP welds as shown in Fig. 16 where flexural strains as high as 10% were predicted.

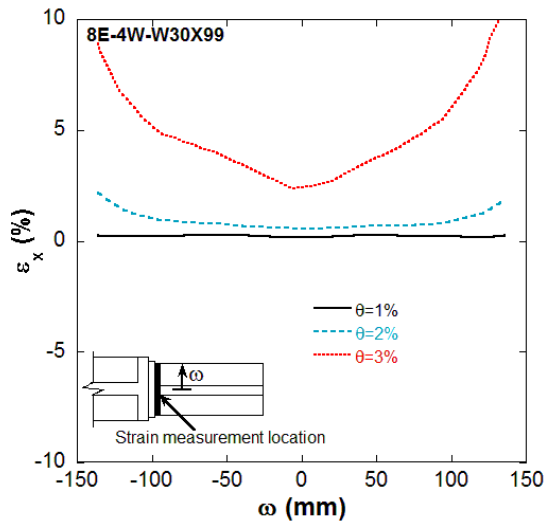


Fig. 16. Axial strain profile along the width of beam flange at the weld toe for 8E-4W-W30x99 connection.

Non-uniform distribution of forces between the inner and outer bolts below the beam flange was captured by the simulation (Fig. 17). During the 2nd cycle of loading at 3% interstory drift angle, the two bolts closest to the beam web on the inside of the beam flange showed large strain increases and permanent set. Large inelastic strains and eventual rupture of these bolts were observed during experimental testing of this connection by Sumner et al. [8].

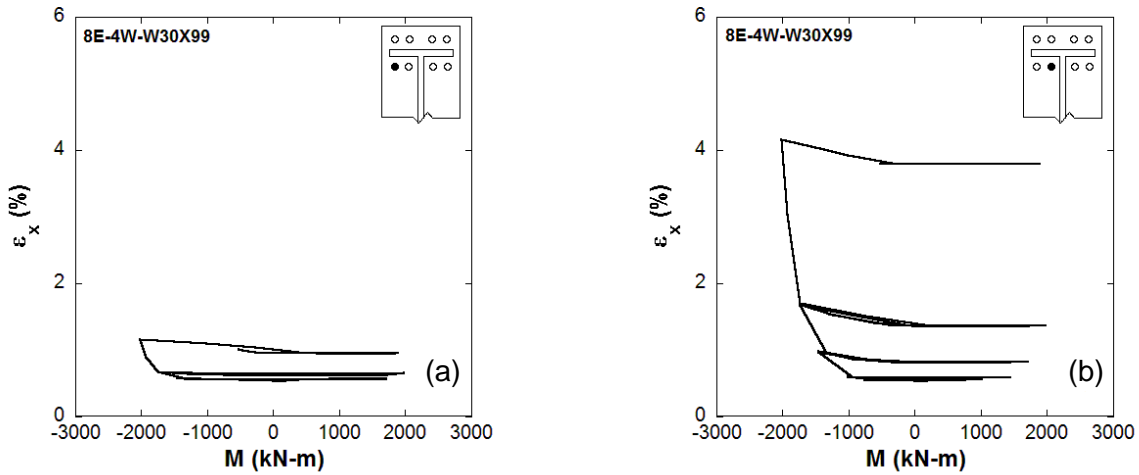


Fig. 17. Simulated bolt strains for 8E-4W under SAC loading cycles at the top flange of the beam.

End plate tearing between the two inner bolts of the tension flange was reported to have taken place just after bolt rupture during testing of this connection. In the FE simulation, strain concentrations were observed at the location of the rupture as shown in Fig. 18a . It should be noted that the 8E-4W-W30×99 connection evaluated here was designed for 110% of the expected plastic moment capacity of the beam which is the same design load used for the 8ES. The plate thickness was determined based on yield line analysis and the bolts selected based on the assumption that no prying forces would develop. This design process resulted in the use of a thinner end plate than was used for the 8ES-W30×99 connection presented before. The 8E-4W connection was also tested and analyzed using A325 bolts in lieu of A490 bolts which were used for 8ES connection[8].

Despite the fact that both connections (8ES and 8E-4W) were designed with the intent of forcing most of the inelastic action into the beam, significant inelastic action and

eventual failure occurred in the bolts and endplate of the 8E-4W-W30×99 connection. This appears to have been caused by an unfavourable load path which placed very high demands on the inner bolts located nearest to the center of the beam flange (Fig. 17b) and on the endplate region adjacent to the beam flange (Fig. 18a).

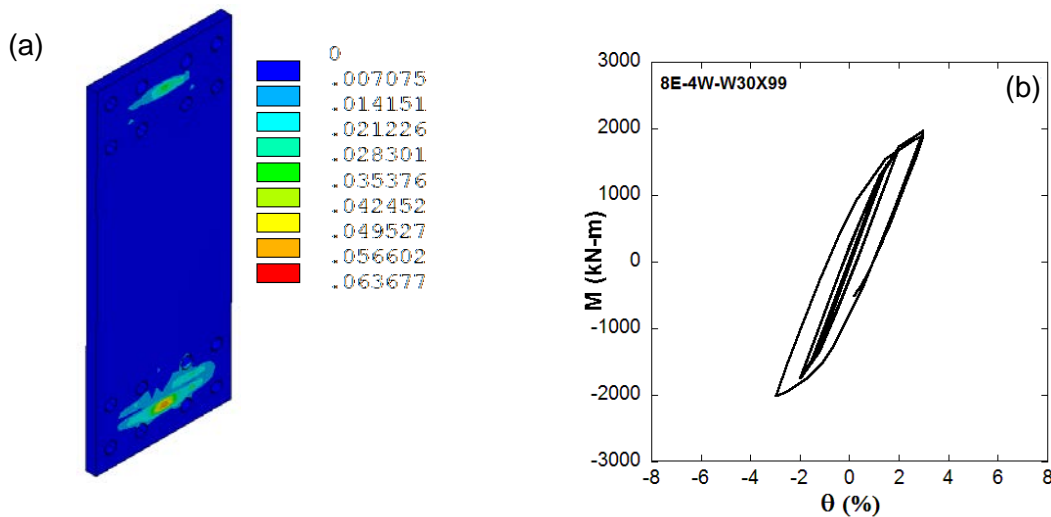


Fig. 18. FE Simulation of 8E-4W-W30×99 (a) Accumulated equivalent plastic strain contour of end plate at the end of 3% interstory drift angle, (b) moment-rotation hysteresis response of 8E-4W connection.

4.3 Eight Bolt Unstiffened Extended End plate Connection (8E)

In this section the influence of end plate stiffener on the performance of the 8ES connection will be demonstrated. To do so, the end plate stiffener in 8ES connection was removed and the connection was analyzed under SAC loading. In the discussion, this connection has been denoted as 8E-W30×99. The finite element mesh and the accumulated equivalent plastic strain contour for 8E-W30×99 connection are shown in Fig. 19. The accumulated equivalent plastic strain contour plot shows the local buckling and plastic hinge

formation which unlike the 8ES-W30×99 connection forms close (100 mm) to the column face. The consequence of this is larger strain demands placed on the beam flange-to-endplate CJP welds (compare Fig.13 and Fig. 20). Moreover, with the end plate stiffener removed, the strain distribution in the bolts is no longer uniform as was demonstrated both experimentally [8] and through FE analysis (Fig. 12) for the 8ES-W30×99 connection. The reduced local endplate rigidity as a result of the stiffener removal places higher strain demands (approximately 40%) on the bolts located nearest to the beam flange (compare Fig.12b with Fig. 21b).

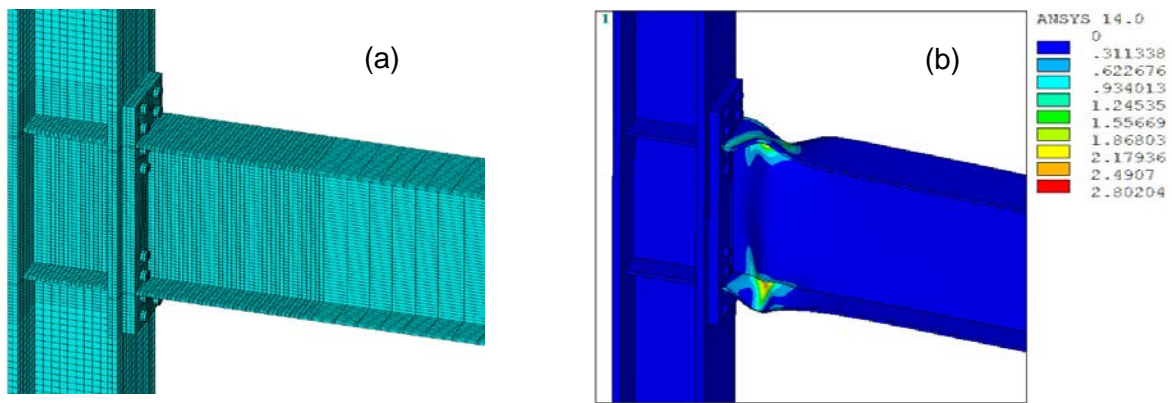


Fig. 19. FE Simulation of Eight bolt unstiffened extended end plate connection (8E-W30×99). (a) FE mesh, (b) accumulated equivalent plastic strain contour showing formation of plastic hinge after cyclic loading up to 6% interstory drift.

Based on these observations and those made during the FE evaluation of the 8E-4W-W30x99 connection a new bolt configuration, designed to provide a more efficient load path is proposed as described in the following section.

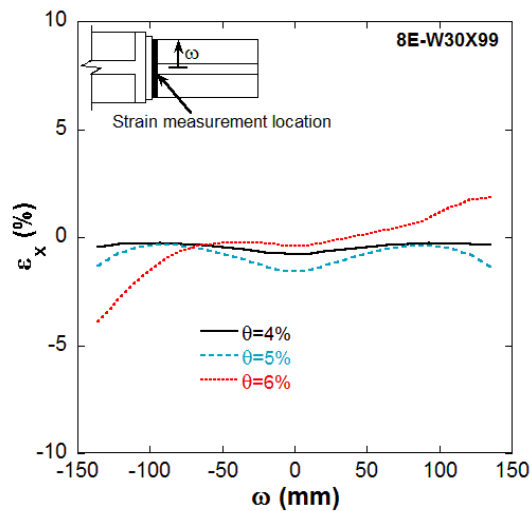


Fig. 20. Axial strain profile along the width of beam bottom flange at the weld toe for 8E-W30x99 connection.

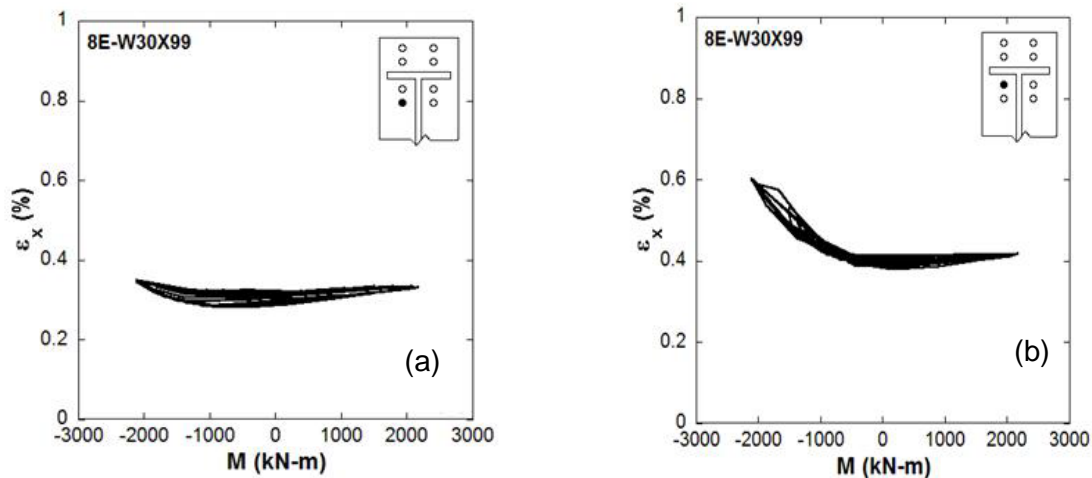


Fig. 21. Simulated bolt strains for 8E configuration under SAC loading cycles at the top flange of the beam.

4.4 Eight Bolt Unstiffened Modified Extended End plate Connection (8EUH)

The preceding sections demonstrated the effect of end plate stiffener which promoted uniform distribution of bolt forces and relocation of the plastic hinge away from the beam

flange to end plate CJP welds. However, the stiffener also introduces a stress concentration at the toe of the stiffener may lead to premature fractures and reduced connection ductility [11-13]. In addition, the end plate stiffener may increase construction cost because of the fabrication and welding required to attach the stiffener to the beam flanges and end plate. Moreover, as the stiffener extends out into the floor space, it is not preferred by the architects for building construction.

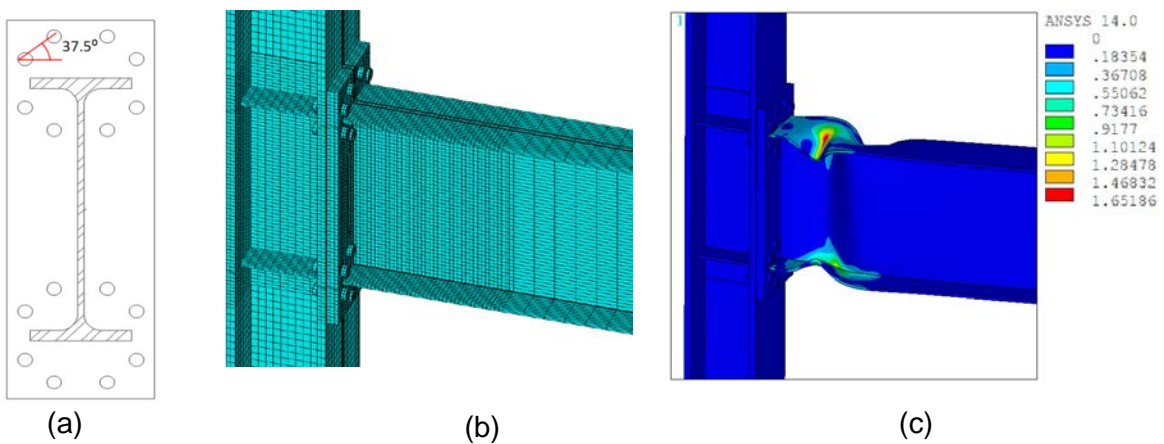


Fig.22. (a) Proposed bolt rearrangement in a hexagonal pattern, (b) FE mesh with the modified bolt arrangement for 8EUH configuration of the connection, (c) accumulated equivalent plastic strain contour of 8EUH connection at 5% drift

To eliminate the triangular stiffeners (and the associated stress concentration) in 8ES connection, the bolts need to be arranged so as to create a favorable load path to promote equal participation among the entire bolt group. However, in the preceding two sections it was demonstrated that the 8E and 8E-4W bolt arrangements are not effective in this regard. In both configurations it was shown that the bolts nearest the beam flange-to-web

intersection resist a larger share of the tensile force. This is due to greater endplate rigidity in this region and not prying action of the end plate [3].

Based on this observation, a hexagonal bolt arrangement is proposed in this study. Essentially, in the hexagonal bolt arrangement, the bolts nearest the beam flange-to-web intersection are shifted away, and the bolts farthest from the flange-to-web intersection are shifted closer. By doing this, beam flange and web forces are uniformly distributed amongst the bolt group. Through finite element analysis utilizing a trial and error process, an angle of 37.5° between the top and bottom layers of bolts was found to be optimal (See Fig. 22a).

The eight bolt extended end plate connection with this modified bolt configuration was analyzed under SAC loading to investigate its seismic performance and will be referred to as 8EUH-W30x99 in the following discussion. The FE mesh and the accumulated equivalent plastic strain contour plot of the 8EUH-W30x99 connection at 5% drift are shown in Fig. 22. The moment-rotation response (shown in Fig. 23a) showed initiation of strength degradation in the 2nd cycle of 4% interstory drift which became significant (34% strength loss) during loading cycles at 5% interstory drift.

The contributions of the beam, panel zone, column and end plate during loading at the maximum interstory drift angle of 6% were: $\theta_b = 5.55\%$, $\theta_{pz} = 0.26\%$, $\theta_c = 0.1\%$, $\theta_{ep} = 0.08\%$ (shown in Fig. 23b). This distribution of component rotation is similar to that of the 8ES-W30x99 connection where the beam accounted for most of the connection rotation. It is to be noted here that the contributions from panel-zone, column and end plate in the rotation capacity of the connection started to decrease after 4% interstory drift when the beam started to buckle locally and connection strength loss became significant resulting in a sharp increase

in the beam's flexural hinge rotation.

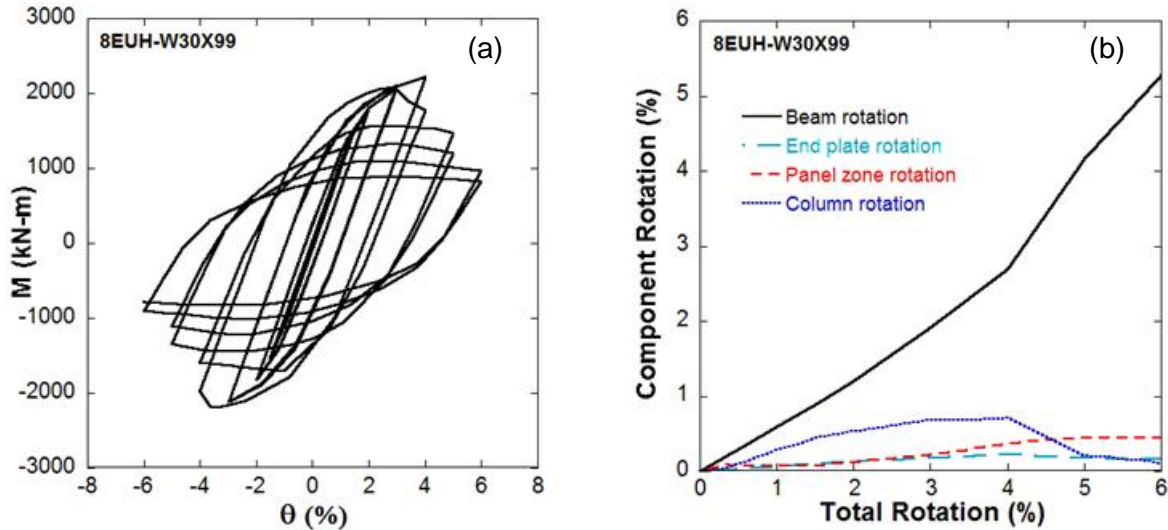


Fig. 23. Cyclic response of 8EUH configuration of connection. (a) Moment-rotation hysteresis response for cyclic loading up to 6% interstory drift, (b) rotation contribution of connection components.

Bolt strain responses of the 8EUH-W30x99 connection shown in Fig. 24 indicates that the hexagonal bolt pattern is effective in distributing tensile forces uniformly to the connecting bolts and as a result lowers the strain demands on the bolts located nearest the beam flange-to-web intersection (compare Fig. 24 with Fig. 21b and Fig. 17b). Note that the only differences between the 8E-W30x99 and 8EUH-W30x99 connections were the bolt arrangement and end plate width, all other parameters remained unchanged. As shown in Fig. 24, strains in bolts below the flange showed similar trends during the loading cycles. Bolt strains remained in the elastic range with a gradual decrease of pretension strain with progression of loading cycles. In addition, as illustrated in the Fig. 25a strain concentrations

at the weld toe remain relatively low compared to the 8E-4W connection throughout the loading history.

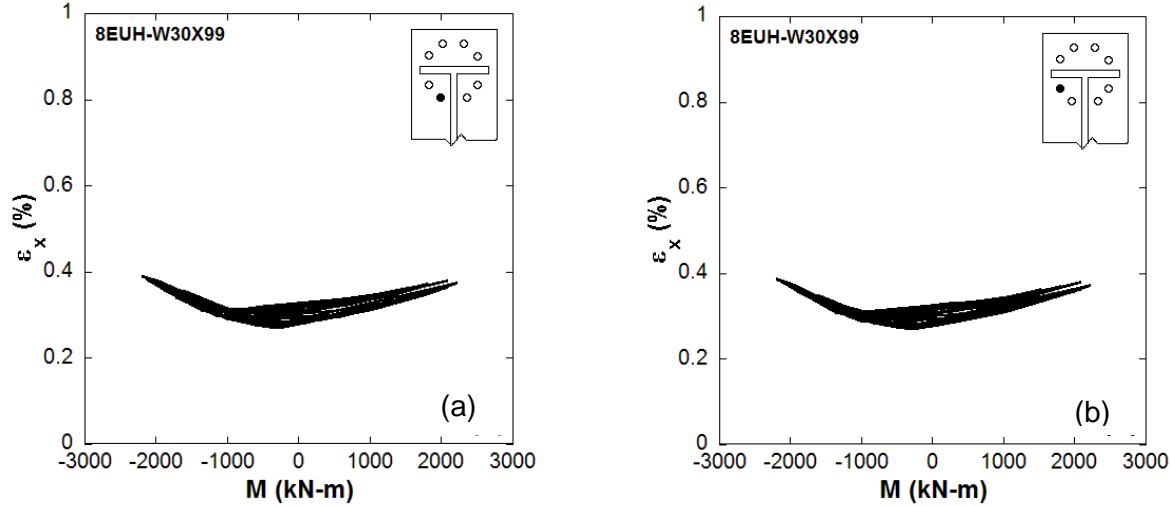


Fig. 24. Bolt strains for 8EUH-W30x99 during loading cycles at the top flange of the beam.

4.5 Comparison of 8ES, 8E-4W and 8EUH Connections

A comparison of the moment-rotation envelopes of the analyzed 8 bolt extended end plate connections is presented in Fig. 25b. It can be observed that the connection with the modified bolt arrangement showed better performance than the other configurations of the connection in terms of strength degradation. For 8EUH-W30x99 configuration, the connection started to lose strength during loading at 4% interstory drift, whereas the connection with stiffener (8ES-W30x99) started to lose strength during loading at 3% interstory drift. The 8E-W30x99 connection also showed good performance in terms of strength degradation, but showed higher bolt strains and higher strain demands at the CJP

weld toe.

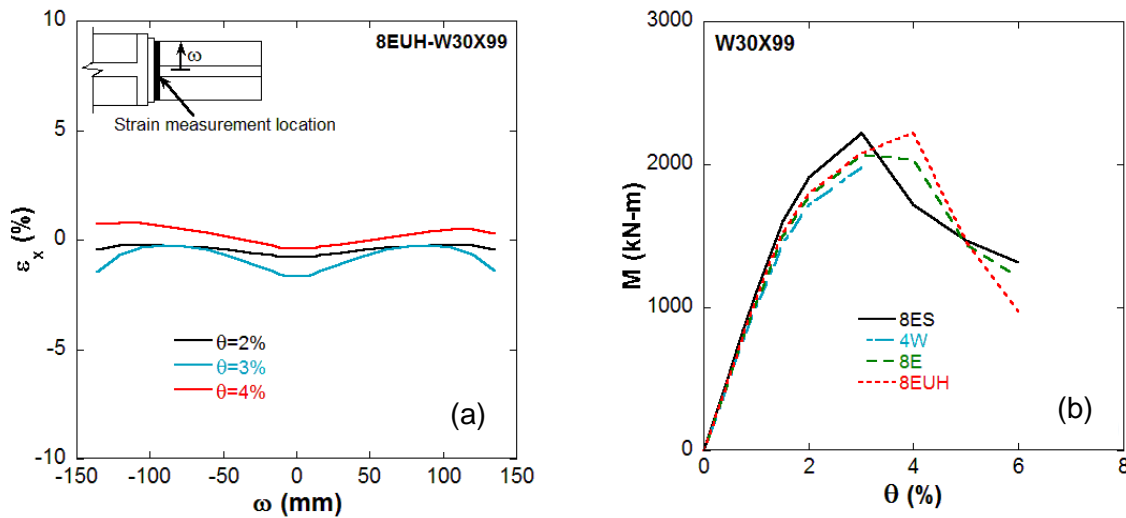


Fig. 25. (a) Axial strain profile along the width of beam bottom flange at the weld toe for 8EUH configuration of the connection, (b) moment-rotation envelopes of the extended end plate connections for different bolt arrangements.

It must be mentioned here that although the proposed hexagonal bolt arrangement provides optimal performance at an angle of 37.5° between top and bottom bolt layers, some flexibility in the bolt orientation is required for practical design and construction of this connection. In some cases the presence of either thick column webs or doubler plates will make it difficult or impossible to build a connection to this exact specification. As a result, a range of angles were studied to investigate the variability in the bolt force distribution, and it was observed that relatively uniform distribution of bolt forces can be obtained in the range of 35° - 45° angles between the inner and outer layers of bolts.

4.6 Further Development of the Modified Eight Bolt Unstiffened Extended End plate Connection (8EM)

In the preceding sections development of a modified unstiffened eight bolt extended end plate connection (which will be referred to as 8EM in the following) was presented. The connection was developed through first validating a FE model of the existing 8 bolt stiffened extended end plate connection with experimental data from the literature [8] and then analyzing the effect of the endplate stiffener and bolt arrangement on the failure mechanisms of the connection. From this analysis an unreinforced 8 bolt extended end plate connection with a hexagonal bolt arrangement was proposed. By removing the endplate stiffener, the associated stress concentration is alleviated and by rearranging the bolts in the hexagonal pattern bolt forces are more evenly distributed. As a result this connection displayed improved global and local seismic performance to that of the 8ES-W30x99, 8E-4W-W30x99, 8E-W30x99 connections. However this analysis was performed on a W30x99 beam and a W14x146 column and as such the effect of beam size was not explored. In this section the 8EM will be extended to heavier and deeper beam sections which experience more severe strain concentrations during seismic loading [42].

The 8EM is applied to two connections involving larger members for further study. The first connection includes a W30x148 beam connected to W14x257 column section. The column panel zone was reinforced with doubler plates to prevent excessive shear distortions. The member lengths and boundary conditions were kept same as earlier presented connections. The second connection includes a W36x170 beam connected to a W14x257 column section. This connection was also reinforced with doublers plates and member

lengths and boundary conditions were also unchanged. In absence of a design procedure to select the end plate thickness for these 8EM connections, the end plate thickness was selected using the existing design equations for the 8ES connections in ANSI/AISC 358-10. It is noted that this process was followed in section 4.4 during the initial evaluation of the 8EUH connection on the W30x99 beam. Based on the uniform distribution of bolt force provided by the 8EM connection each bolt was designed according to the AISC LRFD specifications [37] to resist an equal share of the tensile force component of the expected maximum moment couple at the column face.

In both connections the beam and column material was modelled as ASTM A992 and the end plate material was modelled as ASTM A36. Design equations required an end plate thickness of 47.625 mm which was bolted to the flange of the column with 38.1 mm diameter A490 bolts for both assemblies. The bolts were given a pretension load of 658 kN as specified in the AISC LRFD specification. The columns were reinforced with 25.4 mm continuity plates and a 25.4 mm doubler plate. The connections were analyzed under the simulated seismic loading shown in Fig. 5b.

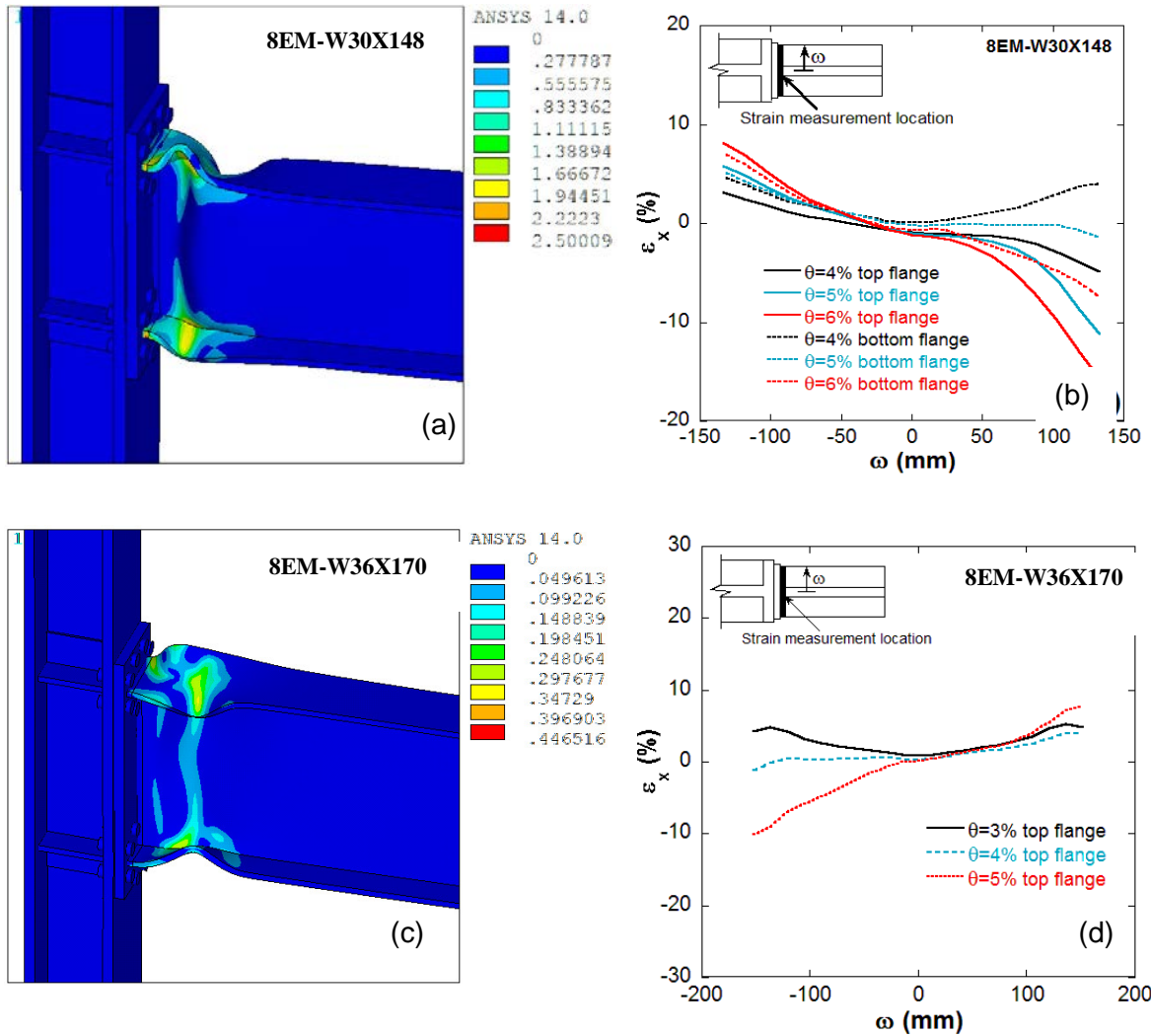


Fig. 26. FE simulation of 8EM connection. (a) Equivalent plastic strain contour for 8EM-W30x148 (b) Axial strain profile along the width of the beam flange for 8EM-W30x148 (c) Equivalent plastic strain contour for 8EMH-W36x170 (d) Axial strain profile along the width of the beam flange for 8EMH-W36x170

The equivalent plastic strain contour and the moment-rotation response for the eight bolt modified extended end plate connection (8EM) with W30×148 beam section is shown in Fig. 26a while the corresponding plot for the 8EM connection with W36x170 beam section is shown in Fig. 26c. Both connections showed local and global buckling of the beam flanges

and web leading to formation of plastic hinge at a distance of approximately 145 mm away from the end plate. Bolt forces were observed to be uniform as demonstrated in Fig. 27 which shows the inner and outer bolt strains for bolts below the top flange.

However, in both connections the location of the plastic hinge led to large strain demands at the beam flange-to-end plate CJP welds as demonstrated in Figs. 26b and 26d. It was observed that tensile strains were approximately 5% during loading cycles at 4% interstory drift and approached 10% for loading cycles at 5% and 6% interstory drift.

Although it has been noted [3, 9] that shop welded EEP connections without web access holes are less vulnerable to weld fractures, the metallurgical notch created by hardening of the HAZ is well known to be a factor in the reduction of the fatigue life of low alloy steel welded joints [43]. Based on this premise a recently validated technique [16] to lower the strain demands at the welded joint is proposed to reduce the risk on weld HAZ failures in this connection. This technique promotes plastic hinging of the beam away from the welded joint by selectively reducing the material strength of the beam flanges.

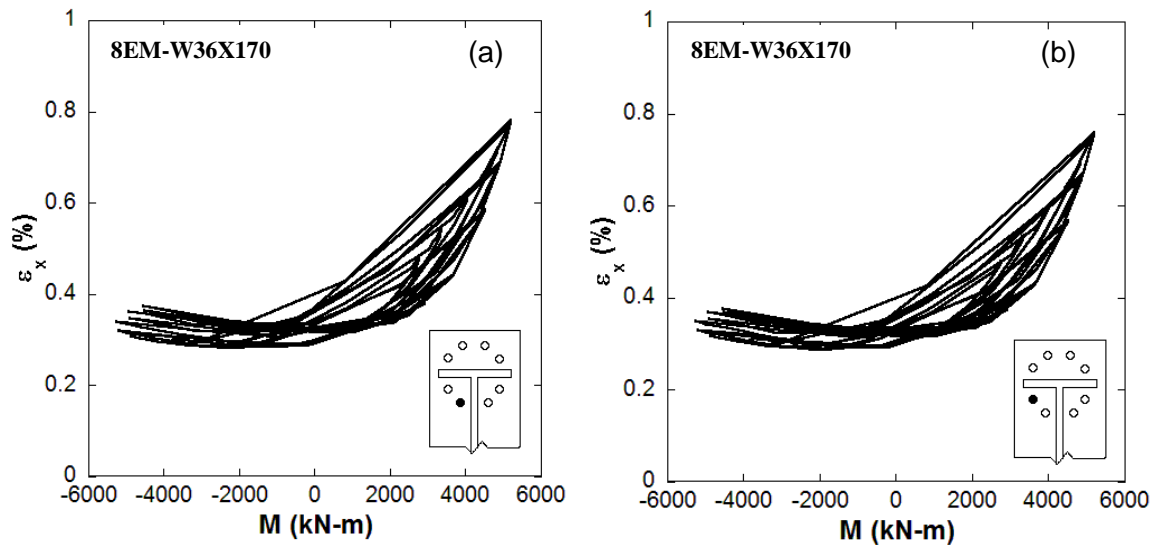


Fig. 27. Bolt strains for 8EM-W36x170 connection during loading cycles at the top flange of the beam

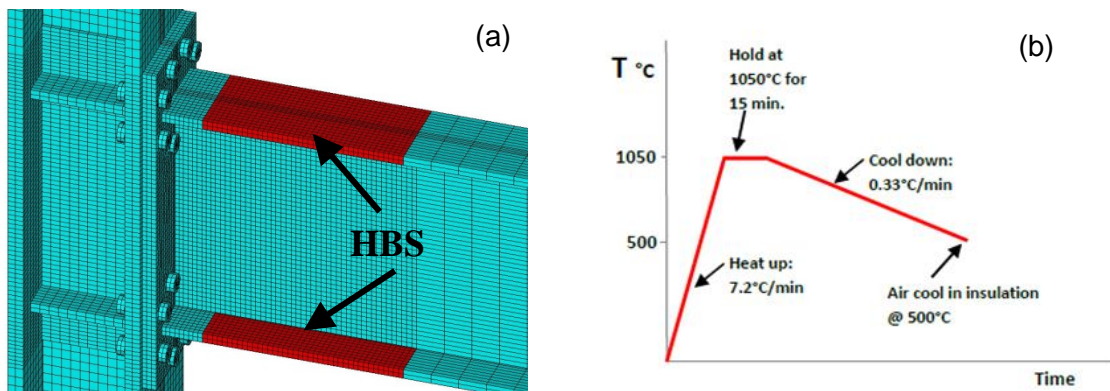


Fig. 28. HBS applied to modified extended end plate connection for seismic performance enhancement. (a) FE mesh for 8EMH connection (b) Temperature-Time history applied to HBS

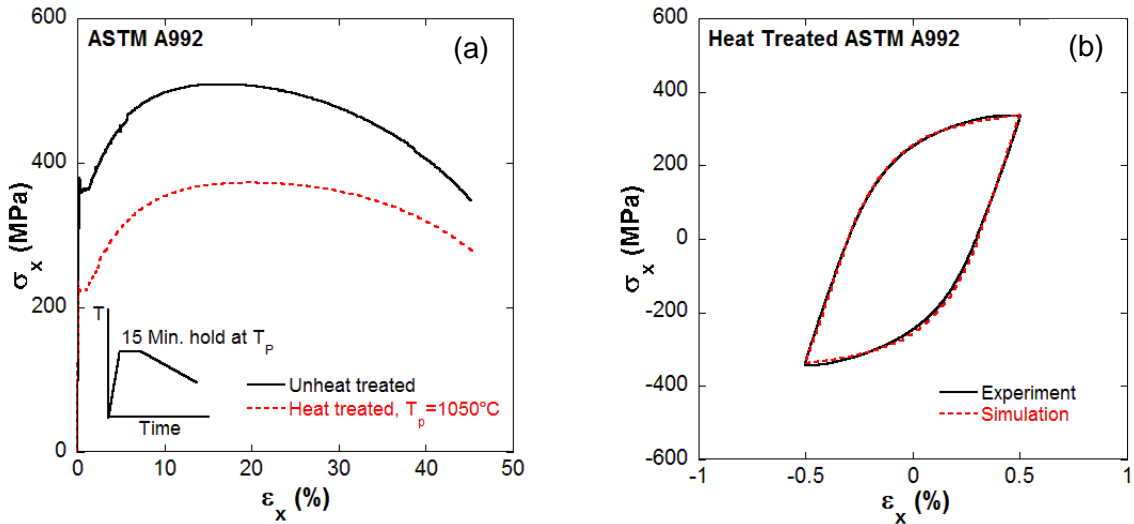


Fig. 29. (a) Monotonic stress-strain response of A992 and heat-treated A992 steel (b) Experimental and simulated response of strain controlled hysteresis loop with Chaboche parameters for heat-treated ASTM A992 steel.

Material strength reduction is achieved through high temperature heat-treatment (annealing) of the beam flanges in the areas highlighted red in Fig. 28a. The temperature-time history used heat-treat the beam flanges is shown in Fig. 28b and the resulting strength reduction is shown in Fig. 29a. As a consequence of this softening, plastic hinging of the beam takes place in the heat-treated beam section (HBS). Therefore, large displacements applied at the beam tip are mostly accommodated by yielding and plastic hinging of the HBS which reduces inelastic strain demands at the weld HAZ. In a similar manner to the RBS, this connection provides a ductile seismic fuse through weakening, but because the elastic modulus of the HBS is unchanged, a connection modified with such a technique does not sacrifice elastic stiffness as does the RBS.

Chaboche model parameters were determined from cyclic strain controlled experiments performed on heat-treated ASTM A992 steel. Simulations were made at the material level as shown in Fig. 29b. The 8EM connection with a W30x148 beam and W36x170 beam modified with HBS were analyzed under the simulated seismic loading. This connection has been denoted as 8EMH. The equivalent plastic strain contour plot along with the moment-rotation response of both connections is shown in Fig. 30. In both cases the connections show wide hysteresis loops and strength degradation initiation after loading cycles at 3% interstory drift. By comparing Figs. 26a and 26c with Figs. 30a and 30b it can be observed that the plastic hinge is shifted to the HBS region (in both connections) and by so doing, the strain demands at the beam flange-to-end plate CJP welds are reduced (compare Figs. 26b and 26d with Figs. 31a and 31b). Figures 32 and 33 show the bolt strains in the 8EMH connections where it can be observed that bolt strains remained uniform with the addition of the HBS, in fact, bolt strains are reduced by the introduction of the HBS (compare Figs. 27 and 32).

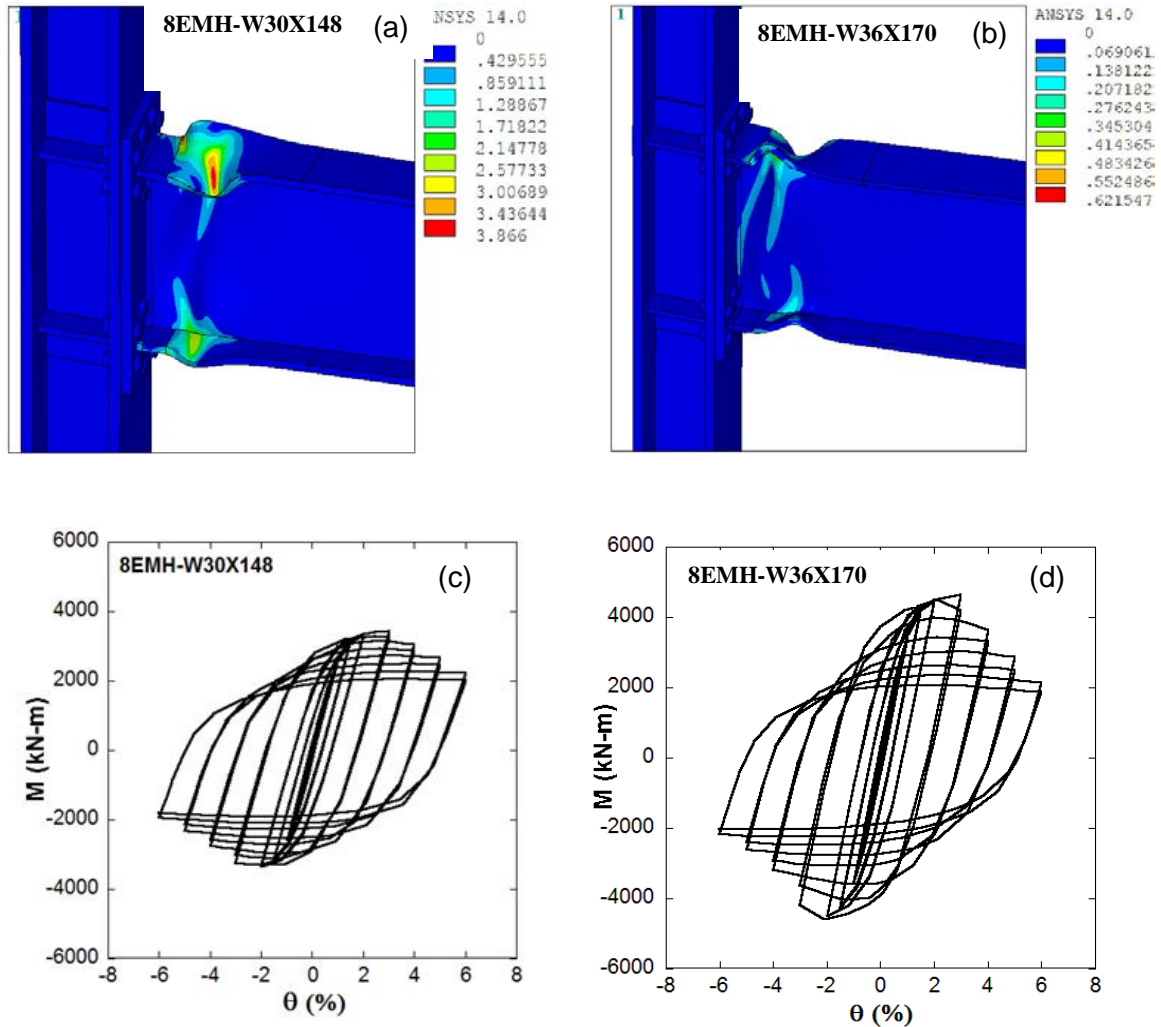


Fig. 30. Cyclic response of 8EMH connection. (a) Equivalent plastic strain contour for 8EMH-W30x148 (b) Equivalent plastic strain contour for 8EMH-W36x170 (c) Moment-rotation response up to 6% interstory drift angle for 8EMH-W30x148 (d) Moment-rotation response up to 6% interstory drift angle for 8EMH-W36x170

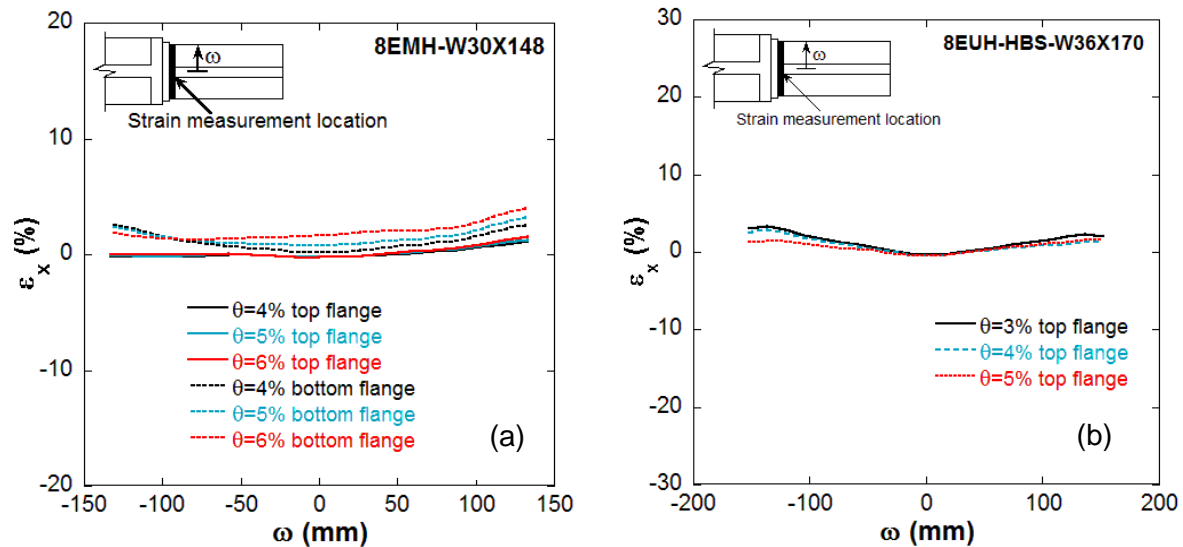


Fig. 31. Axial strain profile along beam flange-to-end plate CJP weld toe (a) 8EMH-W30x148 (b) 8EMH-W36x170

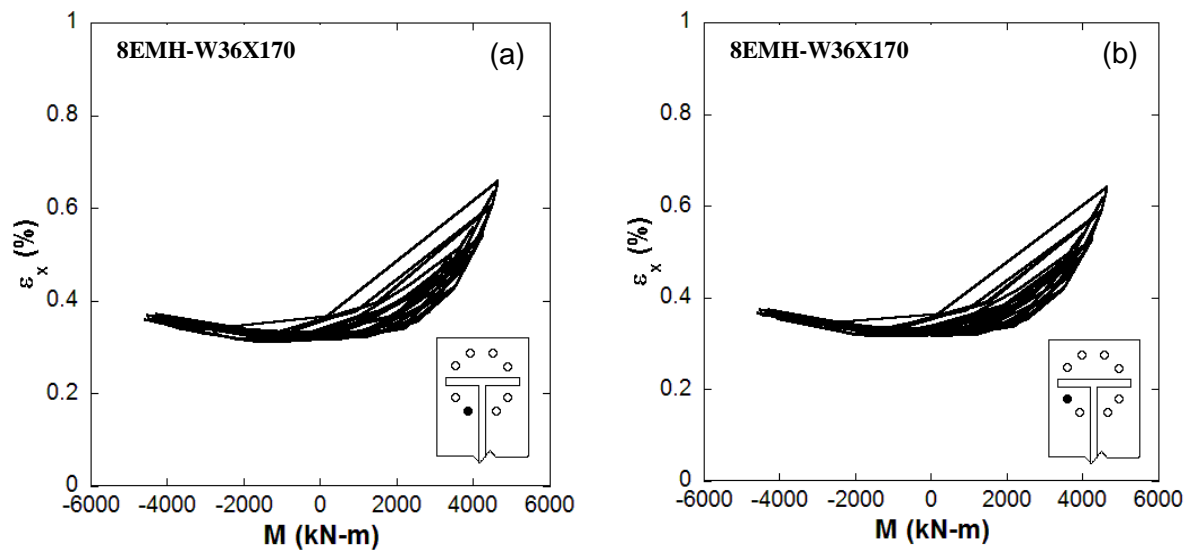


Fig. 32. Bolt strains for 8EMH -W36×170 connection.

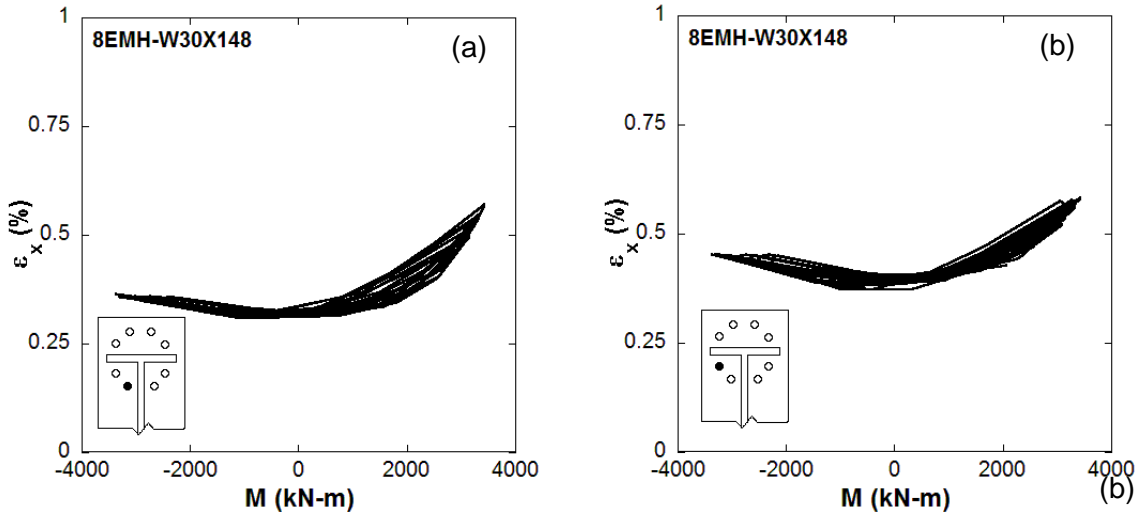


Fig. 33. Bolt strains for 8EMH -W30×148 connection.

A comparison of the moment-rotation envelopes for the 8ES and 8EUH connections (Fig. 21 25b) shows that the initiation of strength degradation was delayed by the removal of the end plate stiffener. However, despite this delay, the strength degradation rate was rapid. As a result the strength degradation mechanism (which was similar in all the previously analyzed connections) was investigated to determine whether a feasible method could be used to delay its onset and slow its rate.

The strength degradation mechanism was observed to be initiated by local buckling of the beam web followed by local flange buckling and then lateral torsional buckling of the beam in the plastic hinge. This mechanism as observed in the 8EMH connection with a W30x148 beam is illustrated in Fig. 34 where the cross section of beam in the plastic hinge is plotted during loading cycles at 3% and 4% interstory drift.

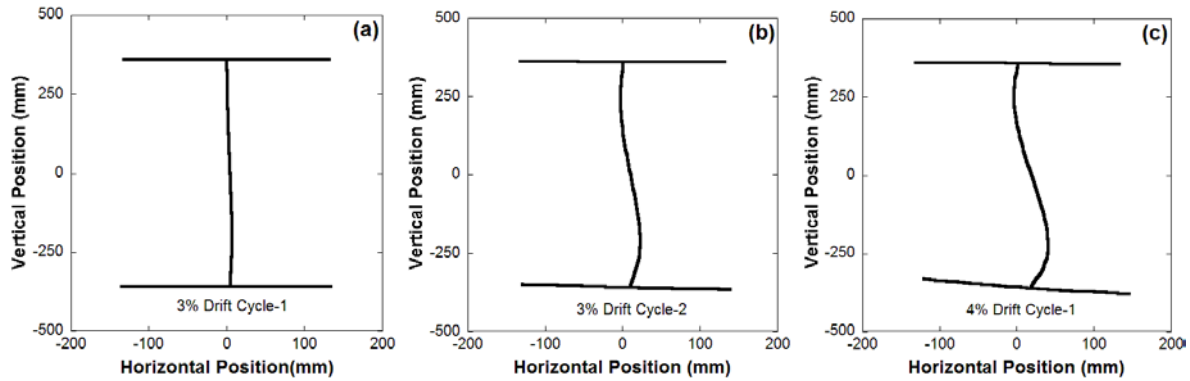


Fig. 34. Local buckling of beam web and flanges at different loading cycles for 8EMH-W30x148 connection.

It was observed that the beam web started to buckle during the first cycle of 3% story drift (Fig. 33a), however no strength degradation was observed. During the second cycle of loading at 3% storey drift, the web of the beam started to twist which initiated lateral-torsional buckling of the beam and this in turn led to strength degradation of the connection. As the load amplitude was further increased, the lateral torsional buckling became more pronounced and strength degradation increased significantly. Similar observations were also made by [16-18, 44-46] where they observed that strength degradation is caused by either local lateral buckling or local lateral torsional buckling of the beam in the plastic hinge. Since lateral torsional buckling for the 8EMH connection was initiated by local web buckling of the beam, incorporating a web stiffener may delay the strength degradation of the connection by delaying the initiation of web buckling as well as lateral torsional buckling.

A finite element analysis was performed on the 8EMH connection by incorporating a “web stiffener” on each side of the beam web. This connection configuration is denoted as 8EMH-W. The web stiffener consisted of a 6.35 mm thick plate attached to the beam web

and extending from the face of the end plate to the end of the heat-treated region as shown in Fig. 18a. In the numerical analysis the plate was considered to be in full contact with the beam web, in other words the plate provided thickening of the beam web in the plastic hinge region.

The equivalent plastic strain contours and the moment rotation response of this connection are shown in Fig. 35b and Fig. 36a. These responses show that the plastic hinge still forms in the HBS (Fig. 18b) and there was no noticeable strength degradation up to 6% interstory drift (Fig. 19a). As a result, the axial strains at the weld toe remained low throughout the loading history (Fig. 19). Moreover, the connecting bolts were equally effective in resisting the beam flange and web forces as a result of the modified bolt arrangement (Fig. 20).

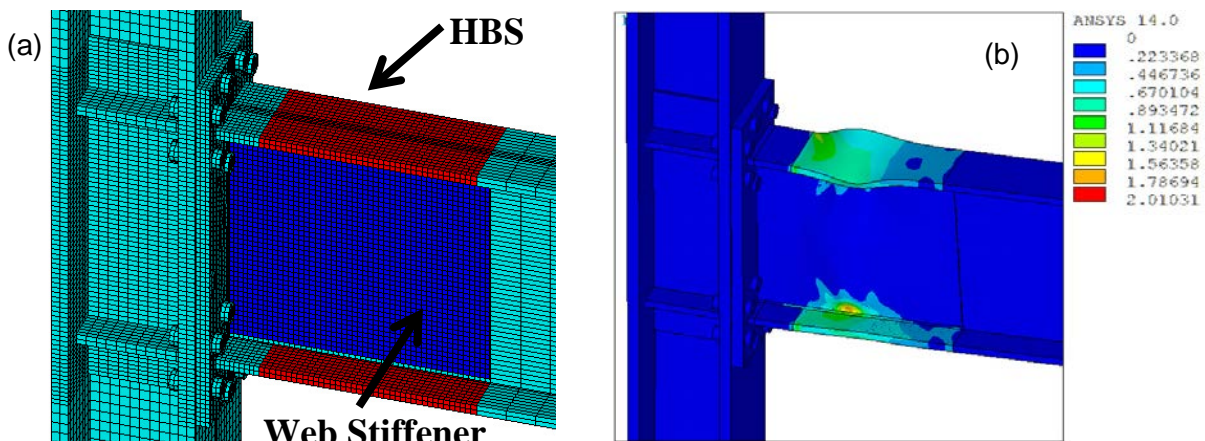


Fig. 35. (a) FE mesh of modified extended end plate connection (8EMH-W) with heat-treatment and web stiffener (b) Equivalent plastic strain contour plot showing formation of plastic hinge in the heat-treated region of the beam flanges of 8EMH-W connection at 5% drift.

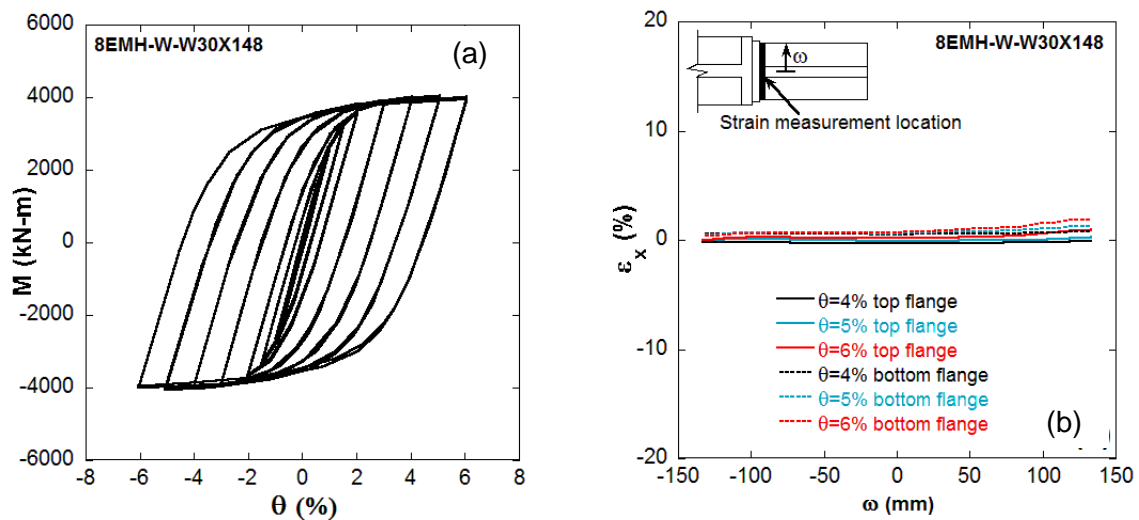


Fig. 36. Cyclic response of 8EMH-W-W30-148 connection up to 6% interstory drift (a) Moment-rotation hysteresis response; (b) Axial strain profile along beam flange at the weld toe.

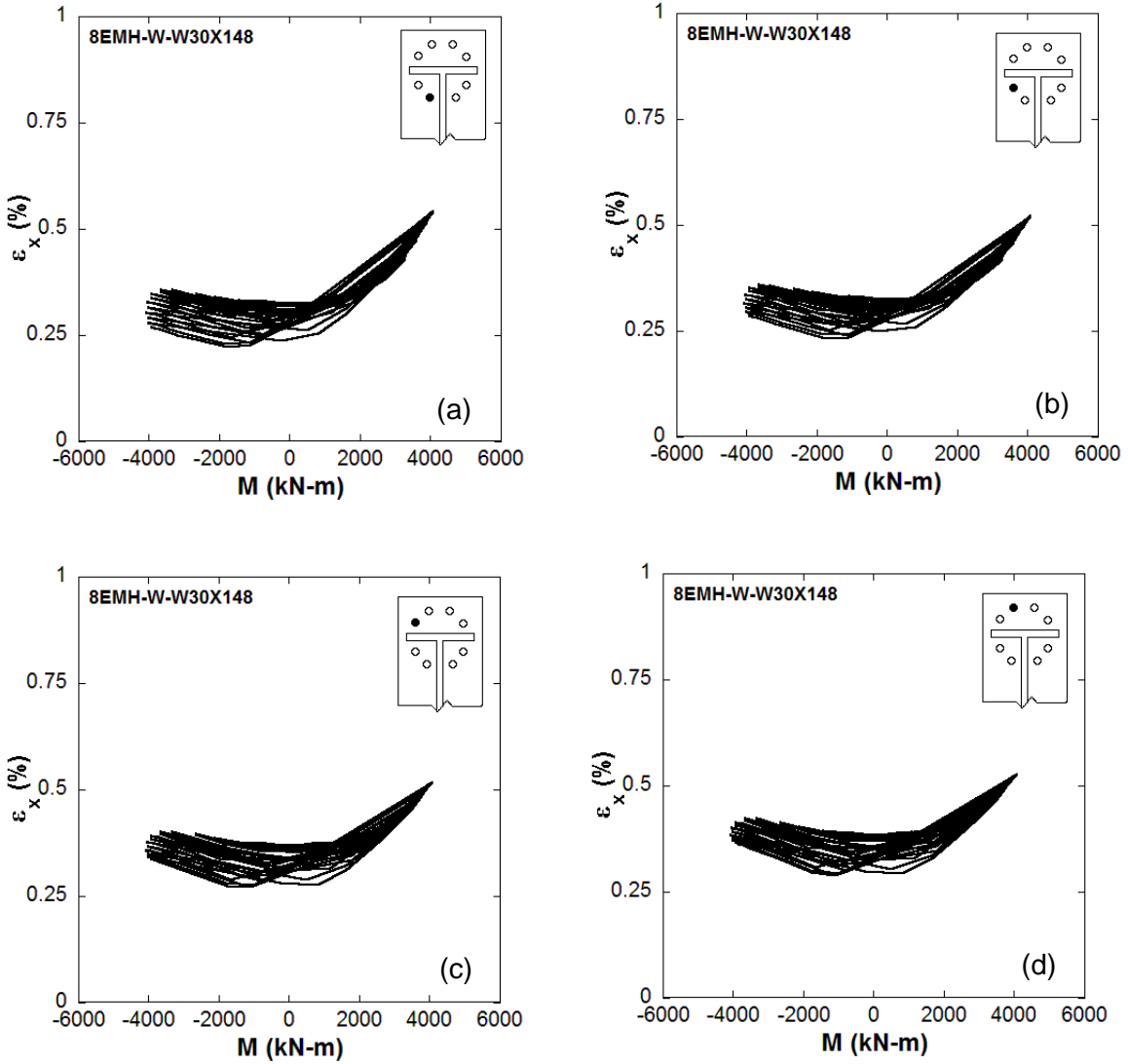


Fig. 37. Bolt strains for 8EMH-W-W30x148 connection.

A comparison of the moment-rotation envelope of the 8ES, 8EMH and 8EMH-W connection with W30×148 beam section is shown in Fig. 38a. It is evident that 8EMH-W connection shows a marked improvement compared to the 8ES and 8EMH connections in terms of strength degradation. The 8EMH-W was also investigated for the W30×99 beam

section (Fig. 38b) where significant improvements in the delay of strength degradation and the reduction in the rate of strength degradation were observed. Based on these observations, it is apparent that the proposed design of extended end plate connection with hexagonal bolt arrangement, heat-treated beam section and web stiffener can improve the seismic resilience of the extended end plate connection when compared to the existing stiffened 8 bolt extended end plate connection design (8ES).

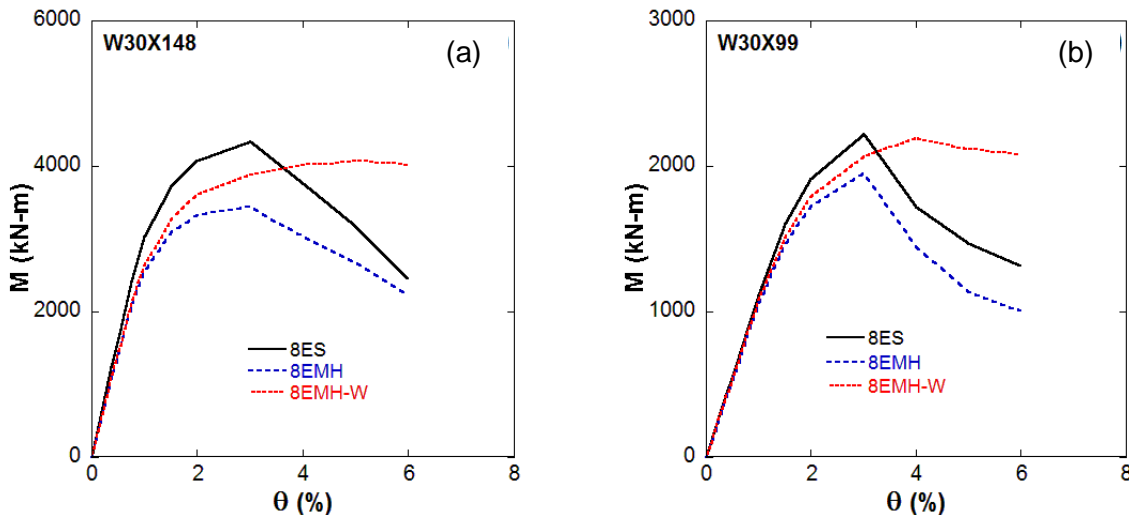


Fig. 38. Moment-rotation envelopes of different configurations of the extended end plate connections. (a) W30×148 beam section (b) W30×99 beam section.

5. Conclusions

In this study an improved unreinforced 8 bolt extended end plate moment connection has been proposed. The proposed design consists of rearranging the bolts into a hexagonal pattern to distribute the flange forces evenly to the connecting bolts, heat-treating the beam flanges to ensure formation of plastic hinge away from the connection region, and adding

stiffeners on both the sides of the beam web to delay the onset of strength degradation. The performance of the proposed connection has been evaluated under simulated seismic loading and compared with the prequalified stiffened 8 bolt extended end plate connection. The connection showed significant improvement over the stiffened 8 bolt extended end plate connection in terms of fatigue failure resilience, buckling resistance, and energy dissipation. To conclude, the modified design of extended end plate connection demonstrates potential to be used as a viable alternative to the conventional stiffened extended end plate connection where the uncertainty and unfavorable failure mechanisms associated with the end plate stiffener can be eliminated.

6. References

- [1] Murray TM, Sumner EA. AISC design guide series 4, Extended end-plate moment connections, Chicago, 2003.
- [2] AISC/ANSI 358-10 (2010) Prequalified Connections for special and intermediate steel moment frames for Seismic Applications, Chicago.
- [3] Tsai K, Popov EP. Cyclic behavior of end-plate moment connections. Journal of Structural Engineering 1990; 116.11:2917-2930.
- [4] Ghobarah A, Osman A, Korol RM. Behaviour of extended end-plate connections under cyclic loading. Engineering Structures 1990; 12.1:15-27.
- [5] Korol RM, Ghobarah A, Osman A. Extended end-plate connections under cyclic loading: behavior and design. Journal of Constructional Steel Research 1990; 16(4):253-279.
- [6] Murray TM, Meng RL. Seismic loading of moment end-plate connections: Some preliminary results. Connections in Steel Structures III: Behavior 1996; Strength and Design: 361.
- [7] Sumner EA, Murray TM. Behavior of extended end-plate moment connections subject to cyclic loading. Journal of Structural Engineering 2002; 128.4:501-508.

- [8] SAC/BD-00/21. Cyclic testing of bolted moment end-plate connections. by Sumner EA, Mays T, Murray TM.
- [9] Sumner EA. Unified design of extended end plate moment connections subject to cyclic loading. Ph.D. Dissertation, Virginia Polytechnic Institute and State University, Blacksburg, VA, 2000.
- [10] Mays TW. Application of the finite element method to the seismic design and analysis of large moment end-plate connections. Ph.D. Dissertation, Virginia Polytechnic Institute and State University, Blacksburg, VA, 2000.
- [11] Adey BT, Grondin GY, Cheng JJR. Cyclic loading of end plate moment connections. Canadian Journal of Civil Engineering 2000; 27:683-701.
- [12] Shi G, Shi Y, Wang Y. Behaviour of end-plate moment connections under earthquake loading. Engineering structures 2007; 29.5:703-716.
- [13] Guo B, Gu Q, Liu F. Experimental behavior of stiffened and unstiffened end-plate connections under cyclic loading. Journal of Structural Engineering 2006; 132.9:1352-1357.
- [14] FEMA-355B. State of the Art Report on Welding and Inspection, prepared by the SAC Joint Venture for the Federal Emergency Management Agency, Washington, DC, 2000.
- [15] SAC/BD-00/21. Round robin testing of ultrasonic testing technicians, by Shaw RE, Jr.
- [16] Morrison, M., Schweizer, D., and Hassan, T. "An innovative seismic performance enhancement technique for steel building moment resisting connections." *Journal of Constructional Steel Research* 109 (2015): 34-46.
- [17] SAC/BD-00/21. Steel moment resisting connections reinforced with cover and flange plates, by Kim T, Whittaker AS, Bertero VV, Gilani ASJ, Takhirov SM.
- [18] Uang CM, Fan CC. Cyclic stability criteria for steel moment connections with reduced beam section. Journal of Structural Engineering 2001; 127.9:1021-1027.
- [19] Kiamanesh R, Abolmaali A, Razavi M. Effect of circular bolt pattern on behavior of extended end-plate connection. Journal of Structural Engineering 2012; 139.11:1833-1841.
- [20] AISC/ANSI 341-10. Seismic provisions for structural steel buildings, Chicago, 2010.

- [21] Mao C, Ricles JM, Lu LW, Fisher J. Effect of local details on ductility of welded moment connections. *Journal of Structural Engineering* 2001;127.9:1036-1044.
- [22] Meng W, Shi Y, Wang Y, Shi G. Numerical study on seismic behaviors of steel frame end-plate connections. *Journal of Constructional Steel Research* 2013; 90:140-152.
- [23] Ricles JM, Fisher JW, Lu LW, Kaufmann EJ. Development of improved welded moment connections for earthquake-resistant design. *Journal of Constructional Steel Research* 2002;58:565-604.
- [24] Ahuja V, Kukreti AR, Murray TM. Analysis of stiffened end-plate connections using finite element method. Research Report No. FSEL/MBMA 82-01, Fears Structural Engineering Laboratory, School of Civil Engineering and Environmental Science, University of Oklahoma, Oklahoma, 1982.
- [25] Ghassemieh M, Kukreti AR, Murray TM. Inelastic finite element analysis of stiffened end-plate moment connections. Research of Civil Engineering Laboratory, School of Civil Engineering and Environmental Science, University of Oklahoma, Norman, Oklahoma, 1983.
- [26] Bahaari MR, Sherburne AN. Structural behavior of end plate bolted connections to stiffened columns. *Journal of Structural Engineering* 1996; 122.8:925-935.
- [27] Bahaari MR, Sherbourne AN. Computer modeling of an extended end-plate bolted connection. *Computers and Structures* 1994; 52:879-893.
- [28] Choi CK, Chung GT. Refined three-dimensional finite element model for end-plate connection. *Journal of Structural Engineering* 1996; 122.11:1307-1316.
- [29] Bose B, Wang ZM, Sarkar S. Finite-element analysis of unstiffened flush end-plate bolted joints. *Journal of Structural Engineering* 1997; 123:1614-1621.
- [30] Bursi OS, Jaspart JP. Basic issues in the finite element simulation of extended end plate connections. *Computers and Structures* 1998; 69.3:361-382.
- [31] Maggi YI, Goncalves RM, Leon RT, Ribeiro LFL. Parametric analysis of steel bolted end plate connections using finite element modeling. *Journal of Constructional Steel Research* 2005; 61:689-708.
- [32] Díaz C, Victoria M, Martí P, Querin OM. FE model of beam-to-column extended end-plate joints. *Journal of Constructional Steel Research* 2011; 67.10:1578-1590.

- [33] Krishnamurthy N. A fresh Look at Bolted End-plate Behavior and Design. AISC Engineering Journal 1978; 15.2:39-49.
- [34] Lim C, Choi W, Sumner EA. Low cycle fatigue life prediction using a four-bolt extended unstiffened end plate moment connection. Engineering Structures 2012; 41:373-384.
- [35] Gerami M, Saberi H, Saberi V, Daryan AS. Cyclic behavior of bolted connections with different arrangement of bolts. Journal of Constructional Steel Research 2011; 67:690-705.
- [36] Kim J, Yoon JC, Kang BS. Finite element analysis and modeling of structure with bolted joints. Applied Mathematical Modeling 2007; 31:895-911.
- [37] AISC. Manual of steel construction load and resistance factor design. 13th ed. Chicago, IL, 2006.
- [38] Chaboche JL. Constitutive equations for cyclic plasticity and cyclic viscoplasticity. International Journal of Plasticity 1989; 5.3:247-302.
- [39] Kaufmann EJ, Metrovich BR, Pense AW. Characterization of cyclic inelastic strain behavior on properties of A572 Gr. 50 and A913 Gr. 50 rolled sections. ATLSS Report No. 01-13, Lehigh University, 2001.
- [40] Wade PM. "Characterization of high-strength bolt behavior in bolted moment connections." Master's Thesis, North Carolina State University, Raleigh, NC, 2006.
- [41] SAC/BD-97/02. Protocol for fabrication, inspection, testing and documentation of beam-column connection tests and other experimental specimens, by Clark P, Frank K, Krawinkler H, Shaw R, 1997.
- [42] SAC Joint Venture (1998) "Strength and Ductility of FR Welded-Bolted Connections" Rep. No. SAC/BD-98/01
- [43] Hoeppner, D. W. (Ed.). (1978). *Fatigue testing of weldments* (Vol. 648). ASTM International.
- [44] Stojadinovic B. Stability and low-cycle fatigue limits of moment connection rotation capacity. Engineering structures 2003; 25.5:691-700.

[45] Okazaki T, Liu D, Nakashima M, Engelhardt MD. Stability requirements for beams in seismic steel moment frames. *Journal of Structural Engineering* 2006; 132.9:1334-1342.

[46] Yin S, Corona E, Ellison MS. Degradation and buckling of I-beams under cyclic pure bending. *Journal of engineering mechanics* 2004; 130.7:809-817.

CHAPTER 5: Seismic Enhancement of Eight Bolt Extended End Plate Moment Connections Part II: Experimental Validation and Addressing Further Development

Abstract

Extended end plate (EEP) moment resisting connections provide the advantage of eliminating field welding and by virtue of this, facilitate fast field erection of building frames. Currently, EEP connections have been prequalified for use in the ANSI/AISC 358 standard. For seismic applications rolled wide flange sections with a depth greater than 24" necessitate the use of a stiffened 8 bolt configuration. In this connection the stiffener serves the purpose of strengthening the end plate, distributing flange forces uniformly amongst the bolt group and promoting the formation of a plastic hinge away from the welds connecting the beam flange to the end plate. The study reported herein proposes an unstiffened 8 bolted end plate connection in which the bolt arrangement is modified so as to promote uniform distribution of flange force among the bolt group and plastic hinge formation is promoted by reducing the strength of steel over specified regions of the beam flanges by exposing the regions to high temperatures followed by slow cooling. Finally, strength degradation due to local web and flange buckling in the plastic hinge region is delayed via the addition of a web stiffener. Development of the proposed connection through detailed finite element studies was presented in an earlier article. Here, the results of full scale testing are presented and analyzed to demonstrate the seismic performance of the proposed connection. Connection behavior is further analyzed through post experiment finite element analysis. Future analytical as well as experimental needs for further development of the proposed connection

are discussed.

Keywords: Steel moment connection; extended end plate connection; seismic performance enhancement; beam plastic hinge; reduced beam section, web stiffener

1. Introduction

In bolted extended end plate moment connections (BEEP) a steel plate is shop welded to the end of a beam which is then field bolted to the connecting members. Though shop fabrication of BEEP connections may be more costly than field welded connections, they offer the advantage of eliminating the difficulties associated with field welding and may provide rapid erection of moment frames [1]. Simulated seismic testing of BEEP connections have also shown them to be capable of providing significant ductility and seismic resilience and as a result, BEEP connections have prequalified for use in special moment frames (SMF) in the 2010ANSI/AISC 358 prequalified connections for special and intermediate moment frames for seismic applications. The 2010ANSI/AISC 358 prequalifies 3 types of BEEP connections, the four bolt unstiffened, four bolt stiffened and the eight bolt stiffened extended end plate connections. In the stiffened connections a gusset plate is welded to the extended portion of the end plate and to the outer surface of the beam flange. This stiffener has been found to strengthen and stiffen the extended portion of the endplate usually resulting thinner end plates in current design practice [2]. The stiffener also promotes yielding and plastic hinge formation at the base of the stiffener away from the beam flange to end plate CJP welds [3]. Investigations on 8 bolted and 4 bolted stiffened extended end plate

connections [4, 5, 6] have shown ductile performance and good energy dissipation. However, in other studies [7, 8, 9, 10] premature failure of the weld between the beam flange and the stiffener or fractures initiating at beam flange to end plate CJP welds followed by gross section fractures of the stiffener have been observed. In one study [11] fracture was reported to have initiated at the toe of the weld between the end-plate stiffener and the beam flange and was attributed to the stress concentration in this region. This stress concentration results from the geometric discontinuity introduced by the stiffener and may be exacerbated by the presence of weld defects some of which may not be detected by welding inspection practice [12]. Careful detailing, fabrication and inspection of stiffened BEEP connections may reduce the likelihood of failures arising from the stress concentration induced by the flange stiffener, however the seismic performance uncertainty and added complexity to design, fabrication and inspection associated with stiffened BEEP connections has motivated the development of an 8 bolt unstiffened extended end plate connection in which 3 novel seismic performance enhancing techniques have been introduced. This connection was developed through detailed finite element simulations in a companion article by Quayyum et al. [13]. In that paper, the 8 bolted extended endplate moment connection was studied in detail to access the influence of the flange stiffeners, bolt arrangement, plastic hinge formation and other parameters on connection failure modes and ductility.

The study presented herein describes the results of full scale testing of the connection proposed by Quayyum et al. [13]. Experimental development as well as measured global and local experimental responses will be discussed. Connection performance is further analyzed

through post-test finite element simulations; also, analytical as well as experimental needs for further development of this connection will be addressed.

2. Review of proposed novel performance enhancing techniques

In the companion paper by Quayyum et al. [13] details of the conceptual and finite element development of the proposed modified 8 bolt extended end plate connection are presented, however they are briefly summarized here as follows. The first of the 3 performance enhancing modifications is the removal of the end plate stiffener and rearrangement of the bolts in a hexagonal pattern as shown in Fig. 1 and Fig. 4d. Finite element analysis (FEA) showed that the end plate stiffener creates a stress concentration at the toe of the weld between the stiffener and the beam flange. To avoid this stress concentration the stiffener was removed, however in order to ensure uniform bolt force distribution rearrangement of the bolt group was necessary. The proposed hexagonal pattern was found to be effective in promoting uniform force distribution amongst the bolt group reducing the likelihood of non-ductile failure modes such as bolt rupture and end plate fractures [6].

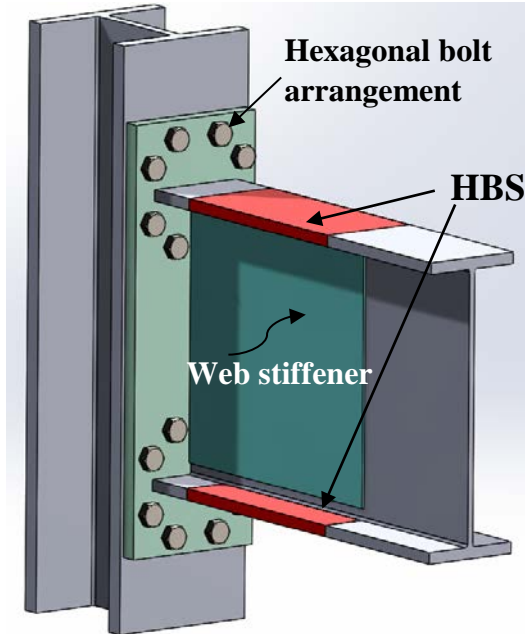


Fig. 1. Sketch of Modified BEEP Connection

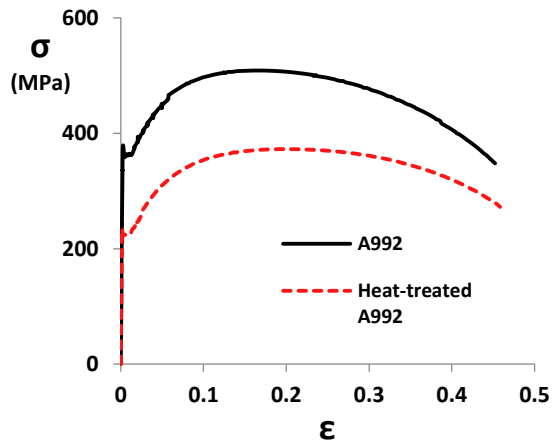


Fig. 2. Engineering stress-strain response of A992 and heat-treated A992 steel

To further enhance performance, high temperature heat-treatment of the beam flanges was added to the proposed connection. This heat-treatment involves subjecting selected regions of the beam flange to high temperatures followed by slow cooling and by so doing reduces the strength of steel in the heat-treated beam section (HBS). Details of the heat-treatment and its effect upon a wide range of material properties are presented elsewhere [14] however, the uniaxial stress strain response comparison of an A992 steel coupon before and after heat-treatment is shown in Fig. 2. As can be seen from this figure the yield and tensile strength of the material is reduced by 38% and 25% respectively while the elastic modulus and ductility remain unaffected. This reduction in strength promotes yielding and plastic hinging within the HBS in a manner similar to the reduced beam section (RBS). However, a connection modified with the HBS does not sacrifice elastic stiffness or buckling resistance

as does the RBS. The HBS technique was previously validated on welded flange-welded web (all welded) moment connections by Morrison et al. [14].

Finally, a technique for delaying the onset of strength degradation was included in the proposed connection. This technique involves welding a steel plate to the beam web and endplate in the expected plastic hinge region which stiffens the beam web and delays the onset of web local buckling. In the companion study web local buckling was observed to be the first mode of instability that eventually led to lateral torsional buckling and strength degradation. The addition of the proposed “web stiffener” was found to be effective in delaying the onset and slowing the rate of strength degradation [13].

The connection which was proposed in the companion paper was called 8EMH-W [13], however the testing of this connection was included as a part of a broad experimental program in which the test specimen was assigned the name HBS 4 and will be referred to as such in the following.

3. Connection Design and Experimental Setup

One large scale specimen (HBS 4) was tested to evaluate all 3 performance enhancing modifications. The test setup and details of the test specimen are shown Figs. 3 and 4. The connection was fabricated by an AISC certified commercial fabricator. All welds were made in the fabrication shop in the down hand position and welding was accomplished using gas shielded metal arc welding (GMAW) with E71T-1C-H8 electrodes (Lincoln ultra core 71C) which is specified to meet all the requirements of AWS D1.8. The beam flange was welded to the endplate with complete joint penetration welds (CJP) similar to the AWS prequalified TC-U4b-GF weld. These welds were made without an access hole and backing bar, however

an 8mm (5/16 inch) backing fillet weld was provided. This weld detail is similar to that used in other BEEP studies [2] and results in a small region of the CJP weld (directly above the beam web) that is uninspected by the ultrasonic technique.

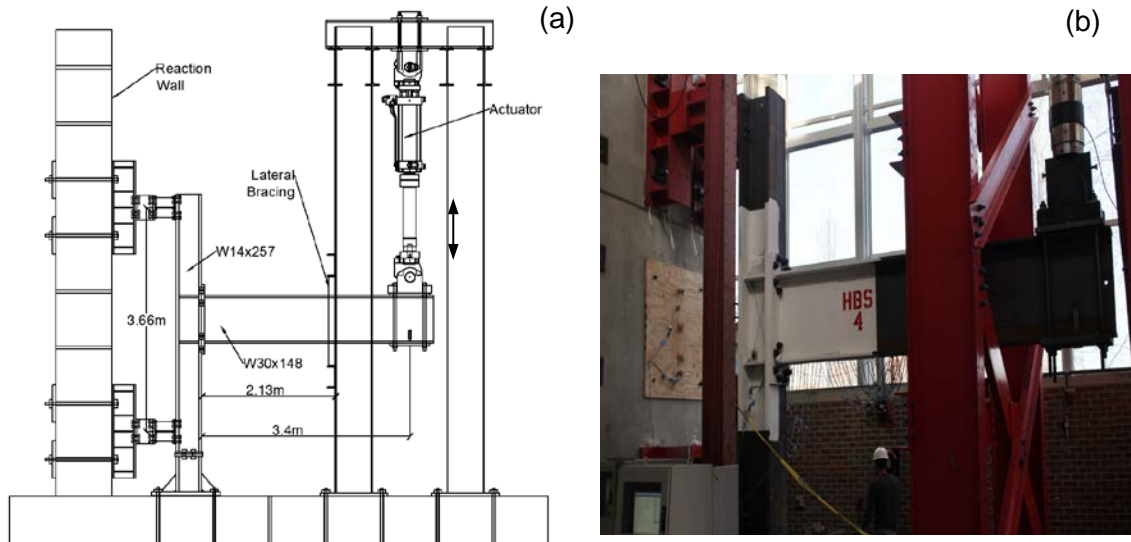


Fig. 3. HBS 4 Test setup a) sketch of test setup, b) photograph showing test setup

The beam web was welded using a CJP weld, which was used in lieu of fillet welds to facilitate the fit up and welding of the web stiffeners as shown in Figs. 4a and 4c. As may be inferred from Fig. 4c the web stiffener plate adjacent to the root of the bevel was used as a backer for the beam web CJP weld. Fillet welds were used to connect the web stiffeners to the end plate and to the beam web as shown in Fig. 4a.

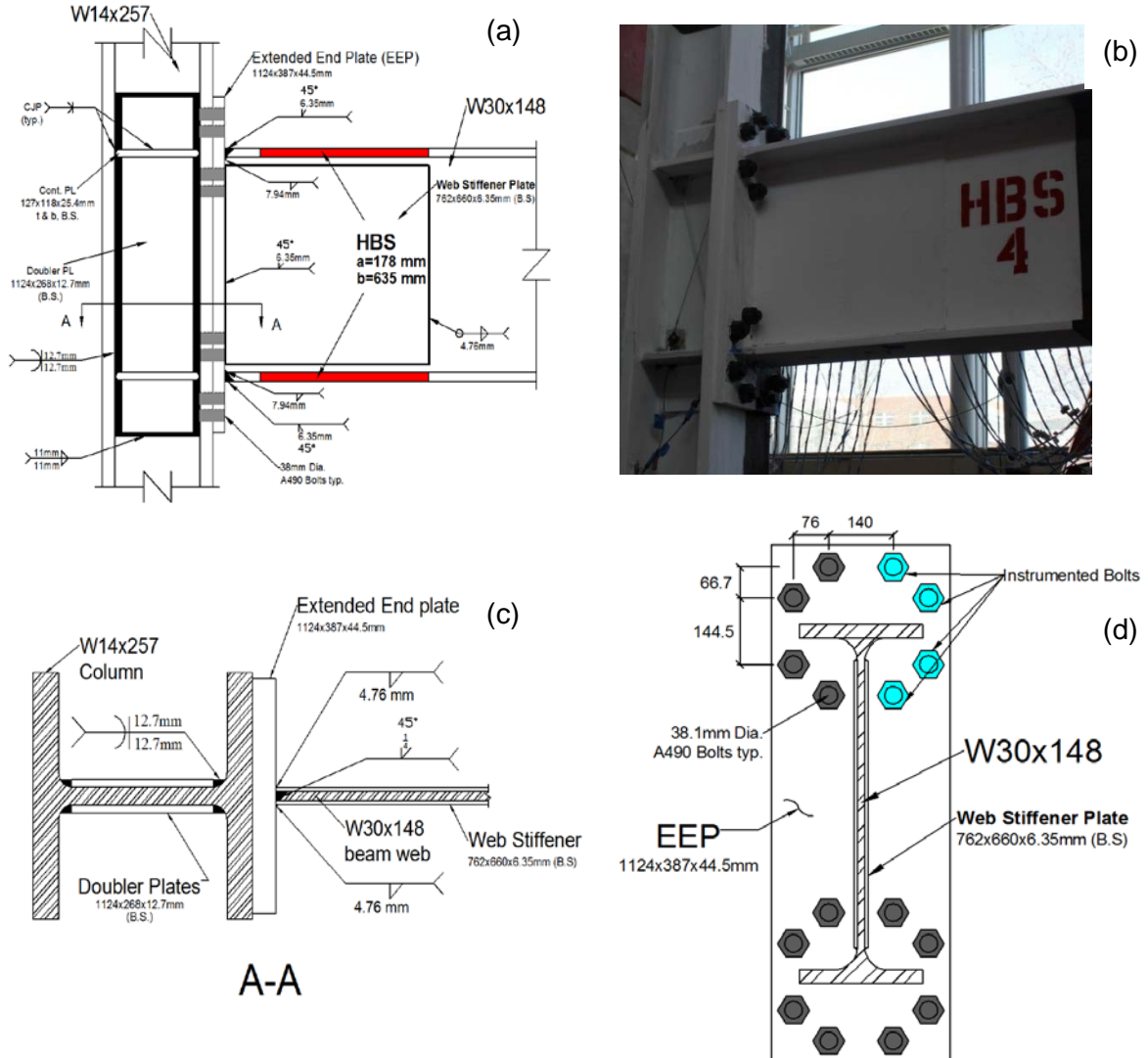


Fig. 4. HBS 4 connection details a) elevation of connection, b) photograph of HBS 4 connection prior to testing, c) section A-A showing connection of beam web and web stiffeners to endplate, d)elevation of end plate showing modified bolt arrangement

These welds resulted in distortion of the web stiffener plates which adversely affected their effectiveness in delaying the onset and retarding the progression of local buckling as will be discussed later. Finally, the column was reinforced with two-12.7 mm (1/2 inch) doubler

plates which were designed to promote strong panel zone behavior in order to ensure that most of the inelastic action was confined to the beam.

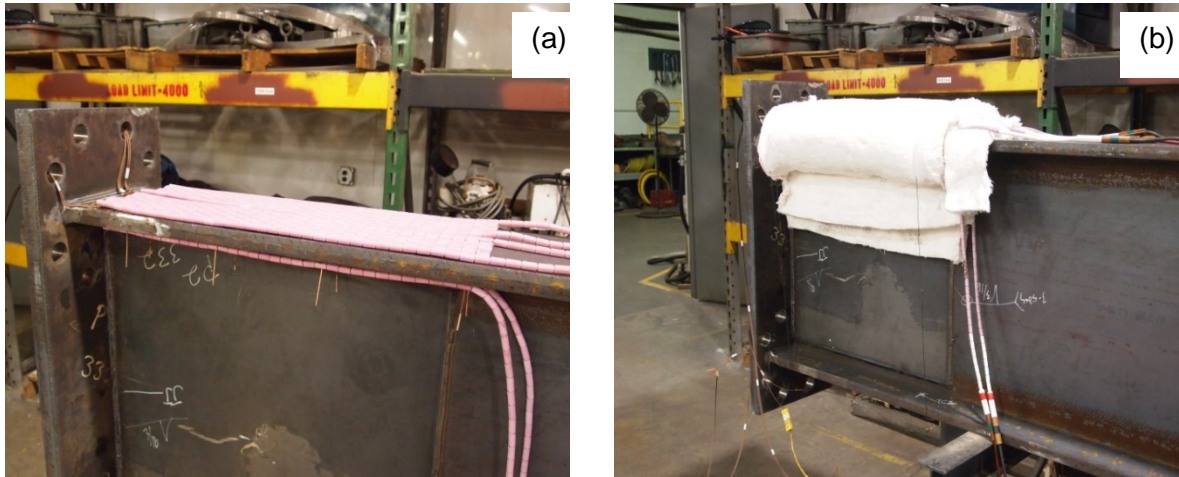


Fig. 5. Heat-treatment setup (a) photograph showing electric surface heating pads during installation on a beam flange, (b) photograph showing insulation of beam flange for well controlled heating and cooling

Upon completion of fabrication, selected regions of the beam flanges were heat-treated. The locations of the heat-treated beam sections (HBS) are shown in Fig. 4a and were decided upon numerically through finite element simulations [13, 14]. Heat-treatment was performed using electrical resistance ceramic mat heating pads as shown in Fig. 5a. Heating pads were sized according to the required dimensions of the HBS and were installed on the inner and outer surface of the beam flanges. The heating pads were connected to a power supply and type K thermocouples were used to monitor temperatures and provide continuous feed back to the power supply. Two (2) layers of 50 mm (2 inch) high density ceramic fiber insulation blankets were wrapped around the beam flanges as shown in Fig. 5b to provide

well controlled heating and cooling. More details about the heat-treatment setup and procedure are provided in Morrison et al. 2014 [14].

The assembly of the beam and column was made with the column in the vertical “upright” position. Bolts were installed and ‘tightened’ using the turn-of-nut method. The turn-of-nut procedure was first verified by tightening bolts from the same batch of those used in the test specimen in a Skidmore Wilhelm bolt tension calibrator to the minimum pretension specified by the AISC LRFD Specification (AISC 2005).

4. Instrumentation

The test specimen was equipped with strain gauges along the beam flanges to monitor longitudinal flange strains at various locations including the beam flange to endplate weld toe and HBS region. Bolt response was of particular interest; as such, 4 of the 16 bolts (see Fig 4d.) were instrumented by installing a strain gauge in the center of the unthreaded portion of each bolt shank. String and linear potentiometers were used to monitor displacements in the column, beam and panel zone. A calibrated load cell in the hydraulic actuator provided readings of force response during the experiment. All specimens were painted with hydrated lime prior to testing to visually indicate regions of yielding.

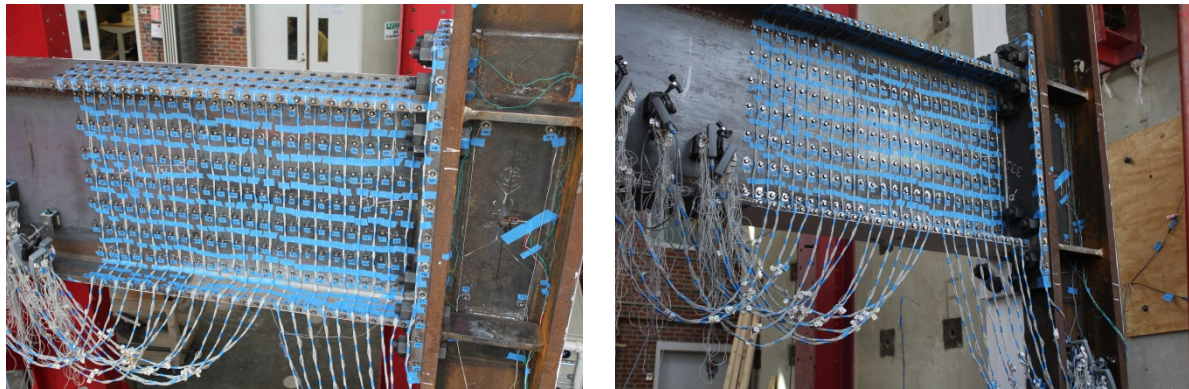


Fig. 6. Instrumentation of HBS 4, a) LED markers placed on beam top flange, beam web and web stiffeners, b) LED markers placed on the sides of beam top and bottom flange, beam web and webstiffners

The Optotrak Certus HD three-dimensional (3D) position system produced by Northern Digital Incorporated was used to capture the positions of markers placed along the beam flanges and web as shown in Fig. 6a and 6b. Two Optotrak cameras were used which were able to capture the motion of markers placed on the top and side of the beam top flange, the beam web and the side of the beam bottom flange. Position time history data obtained from this system was post processed to calculate displacements and strains in areas of interest. The Optotrak system provides the advantage of being able to facilitate the calculation of large cyclic inelastic strains while electrical resistance strain gages may either exhibit gradual strain drift or fail to remain adhered.

5. Test Results

5.1 Global response of modified Extended End plate connection

Testing was carried out at the North Carolina State University Constructed Facilities Laboratory. Loads were applied at the beam tip in accordance with the 2010 ANSI/AISC 341 seismic provision Appendix S loading protocol consisting of quasi-static increasing

displacement cycles. Figure 7a shows the moment-rotation response of HBS 4. The global response is characterized by wide hysteretic loops indicating good energy dissipation. The specimen exceeded the 2010 AISC Seismic Provisions (ANSI/AISC 341-10) special moment frame (SMF) qualifying 4% interstory drift angle without significant strength loss. Slight strength degradation began during the 1st loading cycle at 4% interstory drift and progressed during later loading cycles at 5% and 6% interstory drift. Loading was terminated during the second cycle at 6% story drift due to fracture in the location of significant beam flange buckling (see Fig. 13b)

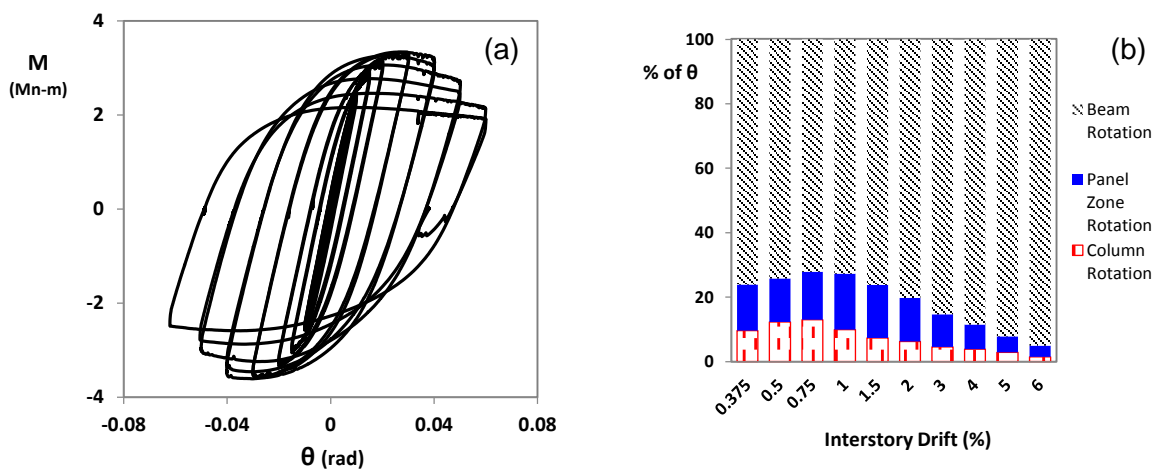


Fig. 7. a) Moment Rotation Response b) Total Rotation Contributions

The response of HBS 4 is further analyzed by plotting the total rotation contributions and the moment-plastic rotation curves for each component of the connection assembly which were calculated using data measured by instrumentation during the test and equations proposed by Popov et al. [15]. These graphs as shown in Fig. 7b and Fig. 8a-d indicate that

panel zone shear and column flexural deformations contributed only to the elastic behavior of the sub-assemblage and as a result, inelastic action was entirely confined to the beam. It is of note that end plate separation from the column flange was not recorded, however given the strong plate approach adopted in this modified BEEP connection, endplate inelastic flexural deformations and end plate separation are expected to be negligible.

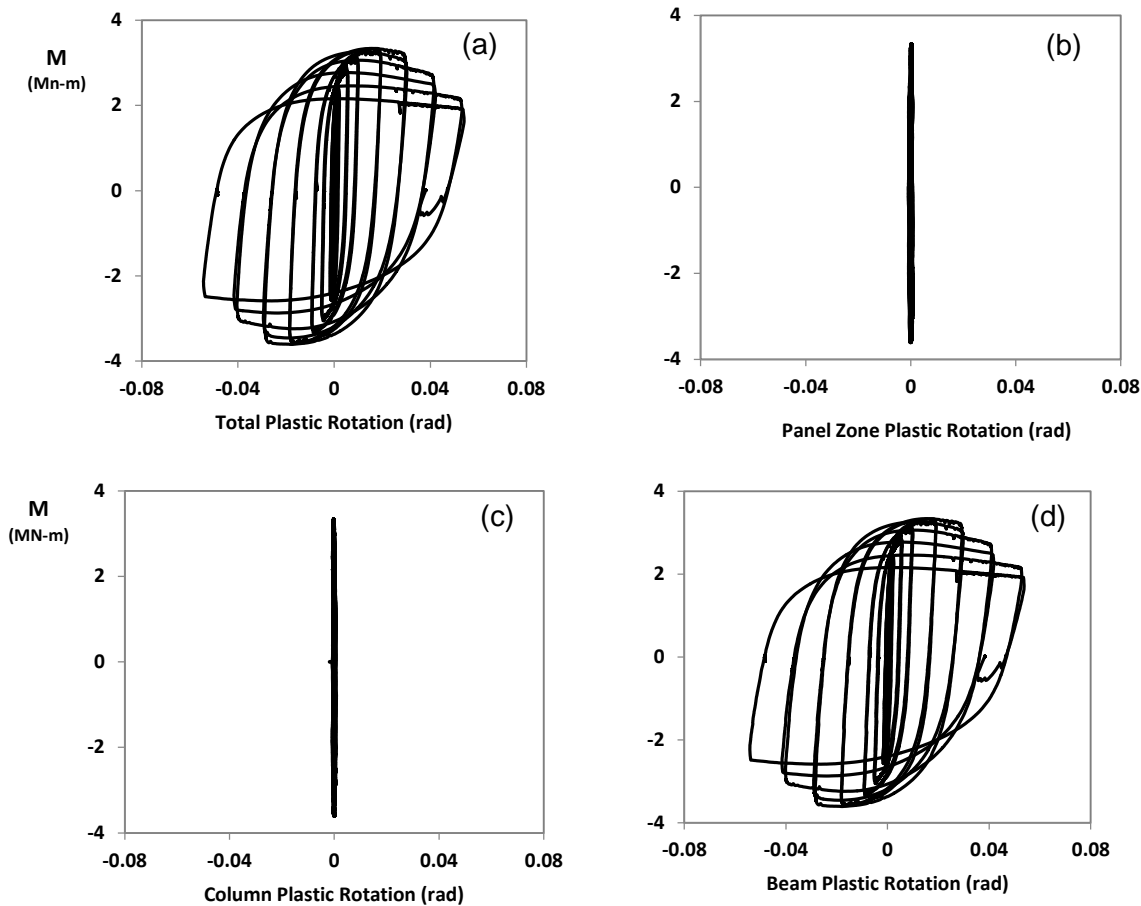


Fig. 8. Plastic rotation contributions by components of HBS 4, (a) total connection plastic rotation, (b) panel zone shear plastic rotation (c) column flexural plastic rotation and, (d) beam plastic rotation

5.2 Plastic hinge formation in the modified BEEP connection

Figure 9a-d illustrates the progression of inelastic action along the beam flange via bar graphs in which the distribution of longitudinal tensile strains (normalized by the yield strain) along the centerline of the beam flange at various stages of the loading history are plotted. Bars highlighted in red represent the strains in the heat-treated (weakened) regions. Strains were calculated by post processing data obtained from 3D noncontact spatial displacement measurement sensors placed along the beam flange as shown in Fig. 6a.

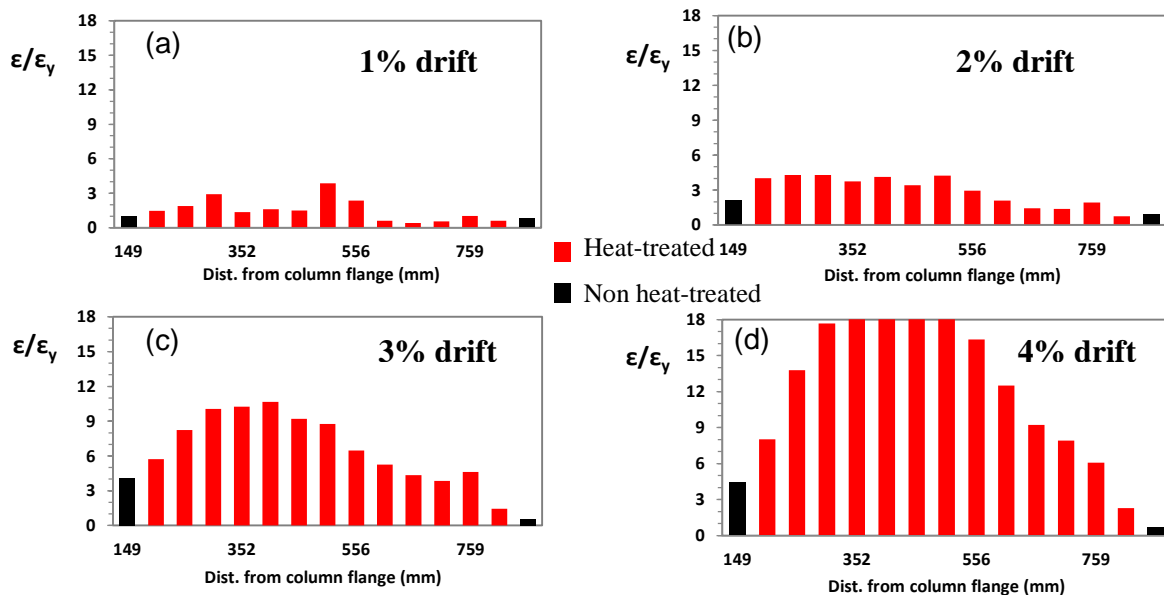


Fig. 9. Recorded longitudinal strains along the center of top flange of the beam from HBS 4

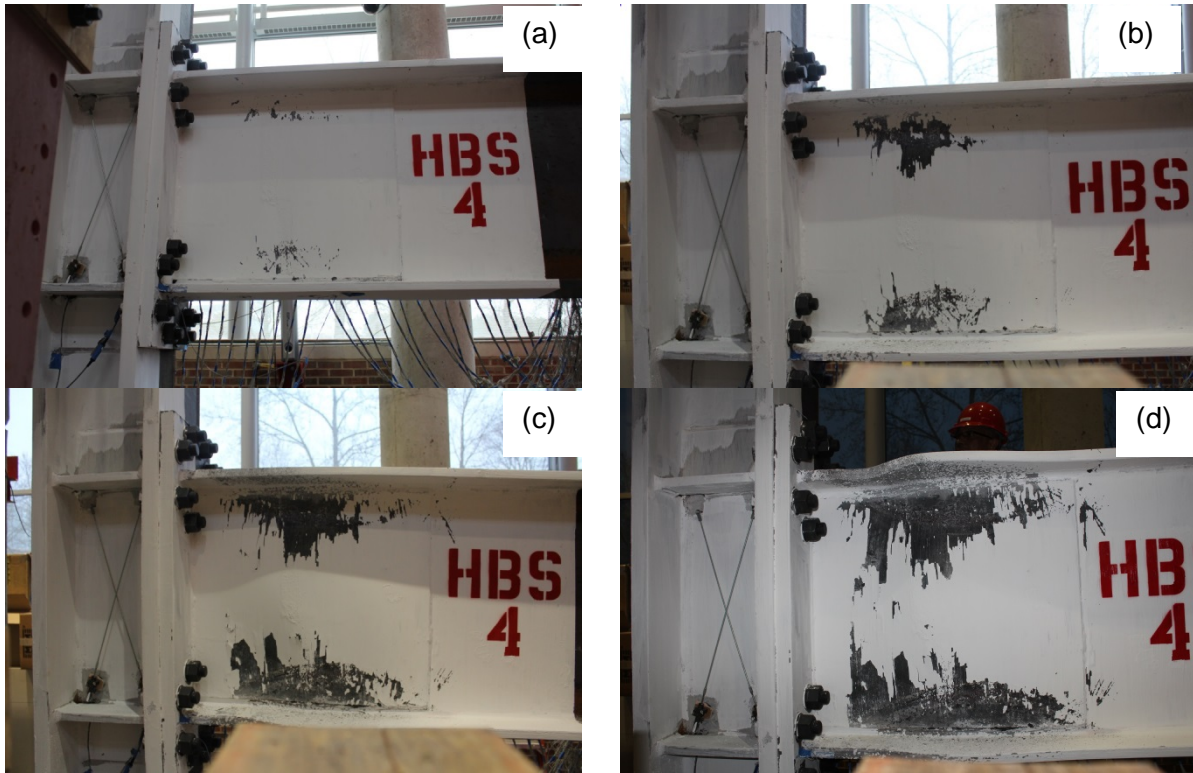


Fig. 10. Progression of yielding and plastic hinge formation in HBS 4 a) 1% drift b) 2% drift c) 3% drift and d) 4% drift

These plots illustrate the influence of the HBS in promoting majority of the inelastic action away from the beam flange to endplate welds. Similar observations have been made in all welded connections modified with HBS [14]. The strain profiles indicate that flexural yielding initiates in the heat-treated areas at 1% drift. As loading is continued longitudinal strains increase more in the heat-treated areas than in the unheat-treated regions adjacent to the beam flange to end plate welds. It is important to note that the beam length of 3.4m (134in) used in this test corresponds to a moment frame with a clear span of 6.8m (22 feet). This relatively short span results in a large moment gradient which is reflected in the strain profiles. As drift angles increase from 3% to 4% longitudinal strain in the heat-treated

regions increase significantly while strains outside of the heat-treated areas grow only slightly. This demonstrates that the large displacements imposed at the beam tip are mostly accommodated by flexural deformation in the HBS to gradually form the plastic hinge. The progression of the plastic hinge formation is also qualitatively reflected in the photographs shown in Figs 9a-d, where it is observed that flaking of the white wash takes place away from the beam flange to end plate junction during loading cycles from 1% to 4% interstory drift.

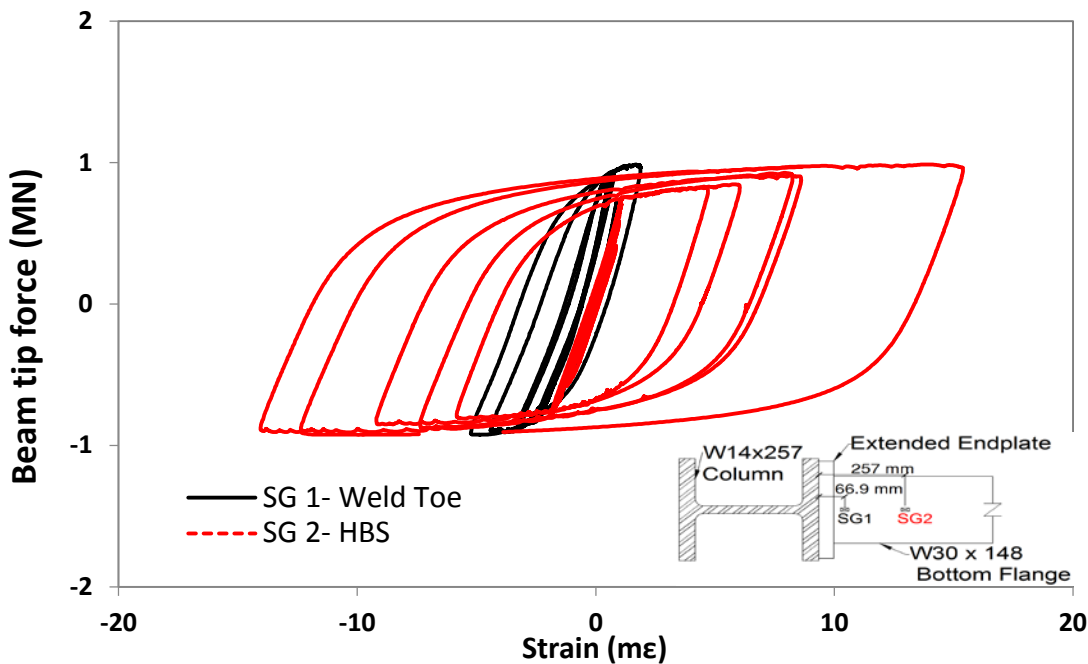


Fig. 11. Measured flexural strains from strain gages placed on the bottom flange of HBS 4. Strains are shown from the beginning of test to the second cycle of 3% drift.

The beam tip load vs. longitudinal strains recorded from strain gages placed on the beam bottom flange at the weld toe and in the HBS region are shown in Fig.10. This figure

further highlights the performance of the HBS in shifting inelastic action away from the beam welds. Here it can be inferred that the HBS acts like a damper for the connection providing energy dissipation in a location free of stress and strain concentrations (prior to the onset of local buckling) and resistant to fracture. As a result, locations which are relatively less ductile or fatigue resilient (e.g. the beam flange to endplate welds) are exposed to lower strain demands providing enhanced connection performance.

5.3 Bolt response in the modified Extended End plate connection

The measured axial strains vs column centerline bending moment is shown in Fig. 12 for the 4 bolts which were instrumented with strain gages. In general bolt axial strain behavior is characterized by increased stains during tensile excursions (i.e. negative bending of the beam) followed by a reduction in strain when the loading is reversed. In all cases a gradual relaxation of the bolt strains was observed with progressive loading. Note that the recorded tensile strains from the initial tightening of the bolts differ which reflects the variability in pretension forces that may be encountered when using the turn of nut method.

Comparison of the inner and outer bolts (bolts 1 and 2) located above the top flange Figs. 12a and 12b shows approximately a 10% difference in the peak tensile strain response of these bolts throughout the loading history. Both bolts relaxed to approximately 75% of their pre-tension strain at the end of the test. The bolts located below the flange Figs. 12c and 12d displayed larger strains (especially bolt 4) indicating that these bolts resisted a larger portion of the tensile forces. The difference in peak tensile strains between the inner and outer bolts (bolts 3 and 4) was approximately 10%. In particular bolt 4 showed a sharp increase in strain with applied moment. This was expected due to the relative proximity of

this bolt to the stiff beam web to flange junction. The welding of the beam web, web stiffeners and beam flange in this region stiffens the endplate and attracts larger forces to the bolts nearest to this area. This behavior was captured by pretest finite element analyses [13] and though bolt 4 did experience slightly larger strains than the other instrumented bolts, no permanent set in bolt strains was observed nor was this behavior found to be detrimental to connection performance.

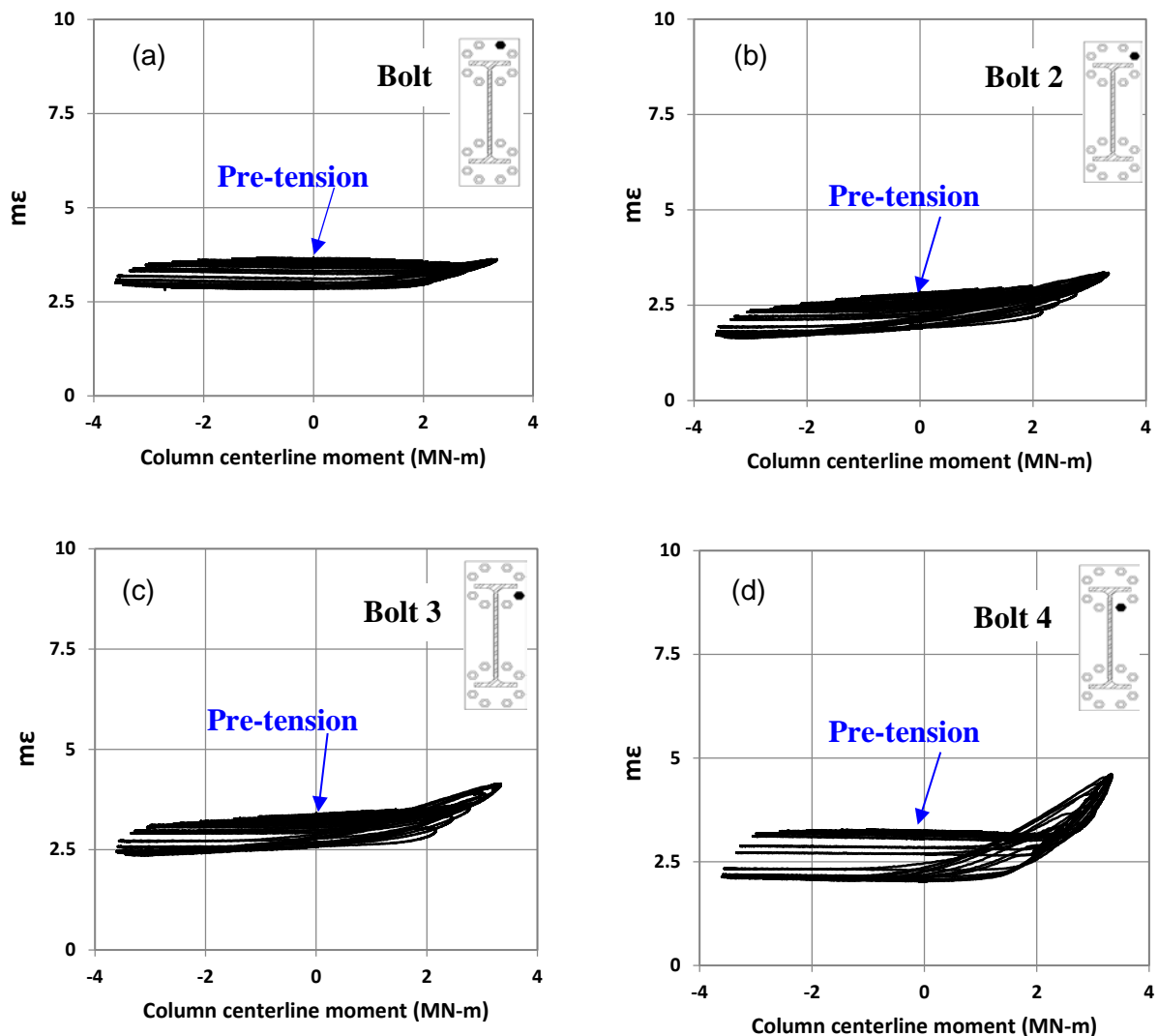


Fig. 12. Recorded axial bolt strain vs column centerline moment

5.4 Failure Mechanism

Loading of the HBS 4 was terminated due to a fracture in the beam flange at the location of significant local buckling as shown in fig. 13a and 13b. This flange buckling mechanism appeared to have initiated during loading cycles at 3% drift and strength of the

connection progressively deteriorated during loading cycles at 4%, 5% and 6% drift. The initiation of this strength degradation mechanism at 3% drift was unexpected based on pre-test FEA which did not include web stiffener distortion (Fig.15a).

As mentioned before the edges of the web stiffener were continuously connected to the beam web and end plate with (4.76mm) fillet welds. These welds resulted in distortion (bowing outward) of the web stiffener plates. Based on pretest measurements obtained from the optotrak markers placed on the beam web and on the web stiffener plates it is estimated that at the center of the plates there was a maximum 19mm gap between the beam web and the web stiffeners. At this point it was realized that the web stiffener design will need modifications in future studies.

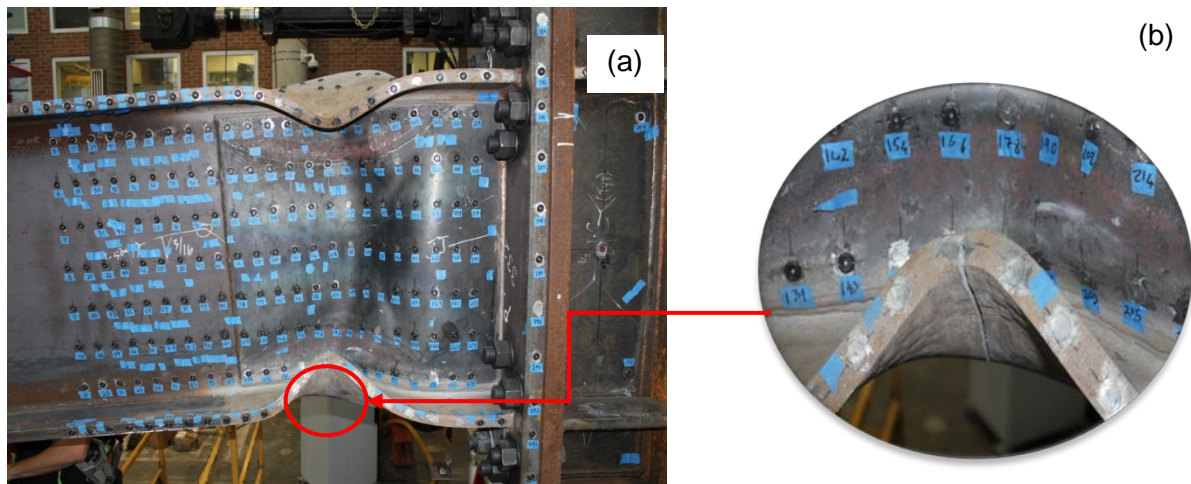


Fig. 13. Local buckling failure of HBS 4: a) Post test photograph showing flange and web local buckling b) Photograph showing fracture of beam flange in the crest of flange buckle

During loading cycles at 1.5 % drift loud noises similar to those created during a fast fracture were heard. It is believed that these noises were created from impact occurring between the web stiffeners and the beam web. This impact was due to the buckling of the web stiffeners which was visually observed during loading cycles at 2% drift and continued for the remainder of the test. This early initiation of buckling limited the effectiveness of the web stiffeners in delaying the onset of beam local web buckling and strength degradation and will be discussed further in the following section.

6. Post-test FEA and discussion

In order to more closely analyze the behavior of HBS 4, posttest FEA was conducted using general purpose finite element software ANSYS. The features of the finite element model including the element type, material model and material parameters were kept same as those presented in the pre-test numerical study [13]. However, an attempt was made in the post test FEA to model the welding induced initial distortions in the web stiffener plates as shown in fig. 14a. Estimates of geometry of the web stiffener plates were obtained from the pretest displacement fields recorded by the Optotruk system. As noted previously Optotruk sensors were placed on the web stiffener plates and on the beam web (Fig. 6). Using the nominal thickness of the web stiffener plate and assuming no distortion in the beam web, estimates of the initial gap between the beam web and the web stiffener as well as the “distorted shape” of the web stiffener could be made and included in the post test FEA. Welding induced residual stresses and strains were not included in the model. Also, no geometric imperfections were included in the modelling of the beam and column.

A comparison between the FEA prediction and the observed moment- rotation response is shown in Fig. 14b. The FEA prediction is in good overall agreement with the experiment response both in terms of peak strength prediction and the rate of strength degradation. The predicted deflected shape is compared with a photograph of the test specimen during cycles at 6% drift in Figs. 14c and 14d. Predictions of the top flange buckling amplitudes are also compared with the measured top flange deflections Figs. 14e and 14f. These comparisons show that local deformations including buckling modes are reasonably predicted by the FEA model.

The finite element model was used to analyze the effect of the initial distortion of the web stiffener plates on the initiation and rate of strength degradation of HBS 4. Presented in Fig. 15a is a comparison of the moment vs. interstory drift envelop in negative bending for a pre-test simulation including perfect geometry of the web stiffener plates (full initial contact between the web stiffener and the beam web), a post-test simulation including welding induced distortion of the web stiffener plates, and a post-test simulation with no web stiffener plates. As expected these results show that the welding induced distortions limited the effectiveness of the web stiffener plates.

From comparison of both post-test simulations (with and without the web stiffener) it is observed that web stiffener increases the moment capacity and slows the initial rate of strength degradation between 3% and 4% interstory drift. However, the rate of strength degradation between 4% and 6% is unaltered resulting in a strength loss of approximately 27% during cycles at 6% drift. This is approximately twice the amount of strength loss predicted by the pre-test simulations. This accelerated strength loss is accompanied by larger

amplitudes of local flange buckling and larger plastic strains as shown in Fig. 15b and 15c which compares the equivalent plastic strains for pre and post test simulations of HBS 4.

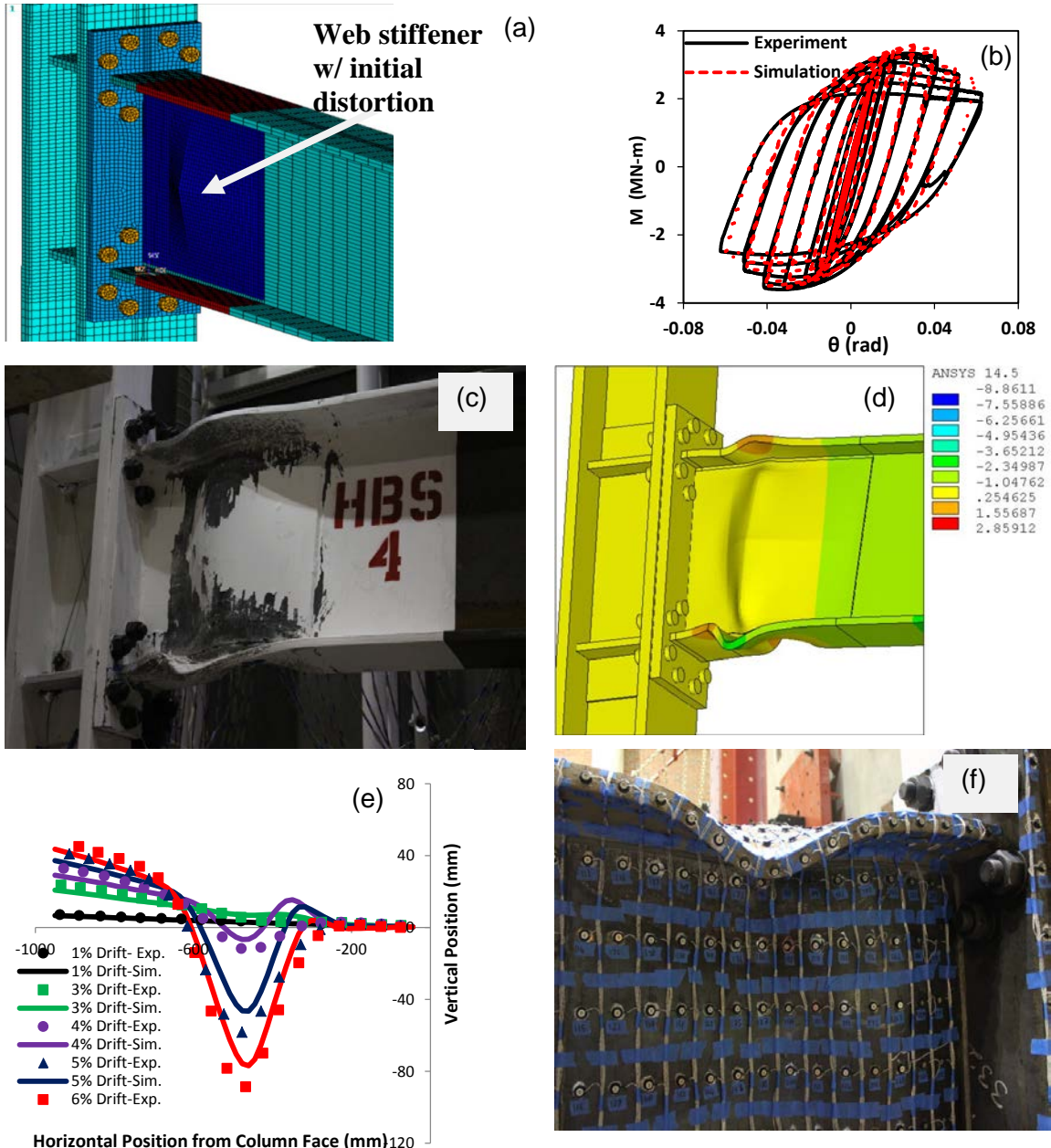


Fig. 14. Validation of post-test FEA of HBS 4 a) FEA discretization including initial distortion of web stiffener plates b) Comparison between FEA prediction and the recorded moment-rotation response c) Photograph of HBS 4 during loading cycles at 6% d) FEA prediction of deformation at 6% drift e) Comparison between FEA predictions and recorded top flange vertical displacements during various stages of loading history f) Photograph of HBS 4 top flange during loading at 4% drift

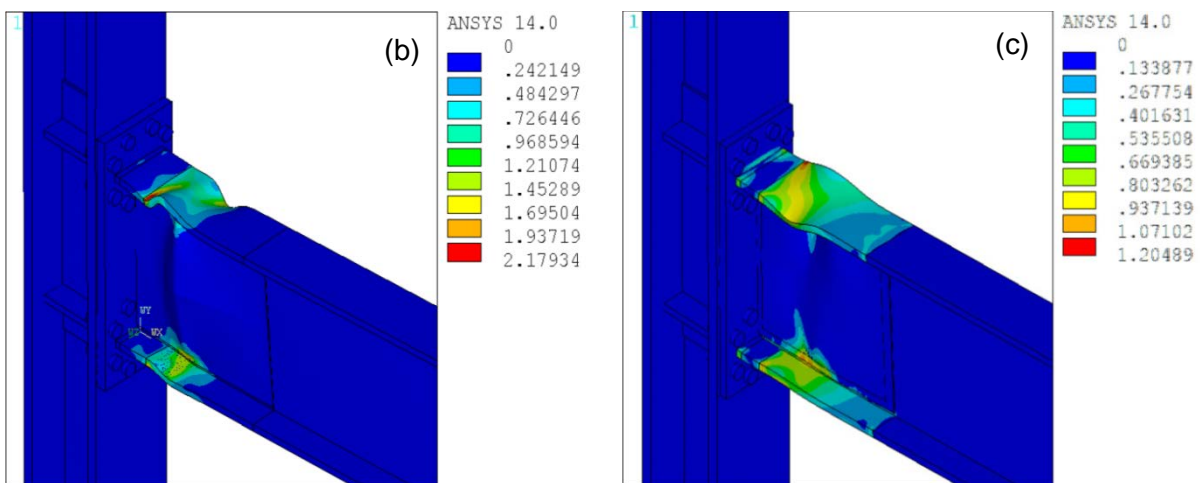
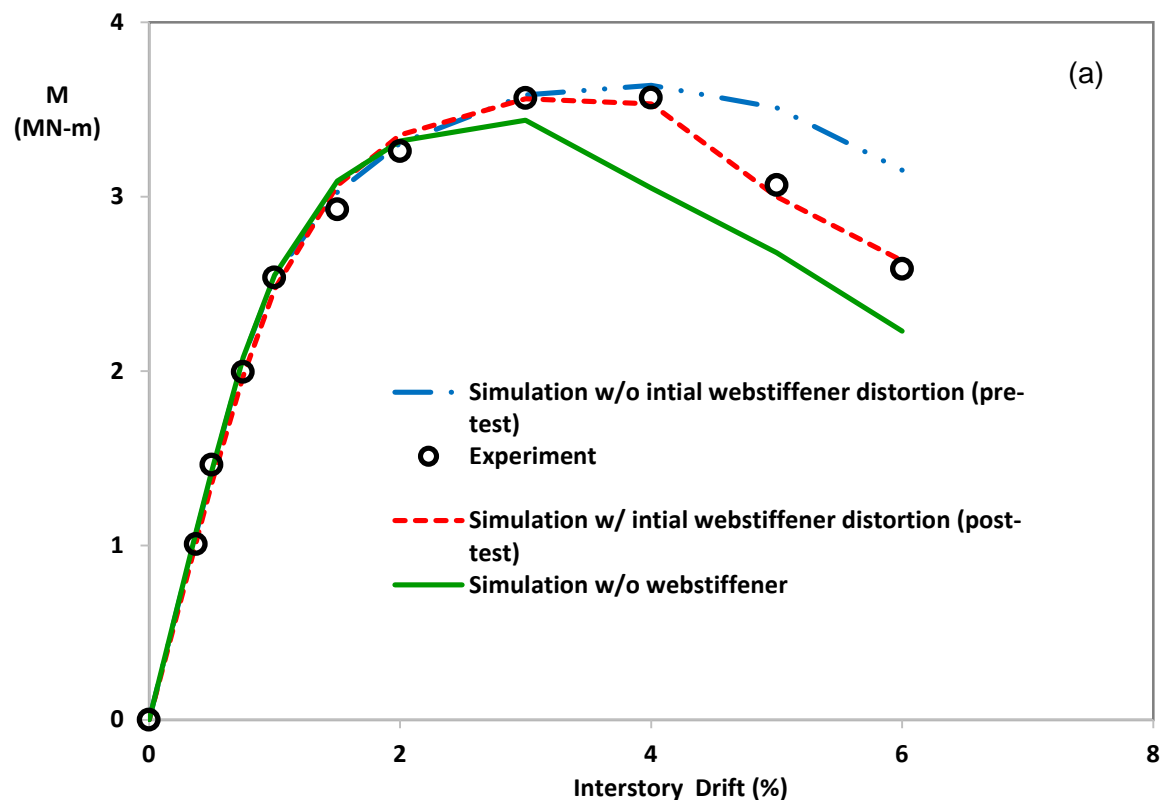


Fig. 15. Post-test FEA Simulation results showing the effect of initial web stiffener plate distortion: a) moment rotation envelop b) Accumulated equivalent plastic strain prediction at 5% drift for HBS 4 (post-test simulation with initial web stiffener distortion) c) Accumulated equivalent plastic strain prediction at 5% drift for HBS 4 (pre-test simulation without initial web stiffener distortion)

7. Future development of Modified Extended End Plate Connections

Due to limited resources only 1 test specimen was evaluated in this study. This test specimen included 3 modifications all of which were judged to have had an influence on overall the performance of the connection. However, it is practically impossible to accurately access and quantify the effect of each modification on various performance parameters including ductility, strength, buckling resilience, reliability etc. from the result of one full scale test. As such future development of the modified BEEP connection should involve more experiments in which each performance enhancing modification can be studied individually to more narrowly quantify and analyze its effect. For example, in the FEA development of the modified BEEP connection it was found that the combination of a ‘strong’ end plate with the arrangement of bolts in the proposed hexagonal pattern significantly reduced strain demands in the bolts and endplate, however plastic hinging of this connection forms at the beam end and as a result high strain demands are placed on the beam flange to end plate welds. This motivated the use of the HBS as opposed to the currently used flange stiffener to shift plastic hinging away from the beam end without introducing stress or strain risers. Shifting the plastic hinge away from the beam end in such a manner reduces strain demands at the welded joint and so it is believed that this provides more reliable connection performance.

However, experimental evaluation of the modified unstiffened BEEP connection without the HBS may demonstrate that this connection can meet or exceed the performance requirements for use in SMF’s outlined in the AISC seismic provisions. This assertion is

made based on the following factors which may contribute to enhanced ductility of EEP connections:

1. EEP connections are shop welded in more favorable conditions (year round) when compared to field welded connections, thus eliminating some problems related with field welding. In particular, shop welding ensures adequate access to perform welding and also to make sound visual inspections during and after welding. It is also possible to make all welds in the preferred ‘down hand’ position which is not possible in field welded connections such as the WUF-W or RBS.
2. Due to the fact that EEP connections are shop welded, no weld access holes are required to make flange to endplate welds. This reduces the inevitable stress and strain concentrations introduced by access hole cuts. It must be noted that as a consequence of the elimination of the access hole, the beam flange to end plate weld directly above the beam web is a partial-joint-penetration weld. However, this has not proved to be detrimental to connection performance in published experimental studies.

The combination of these factors with the use of ‘notch-tough’ low hydrogen welding electrodes with specified minimum Charpy V-notch toughness, strict quality control practices such as the careful cleaning and preparation of the weld root opening, careful visual inspection of root and subsequent weld passes, removal of weld run off tabs, compliance with AWS specified minimum preheat temperatures etc., may provide adequate ductility to modified 8 bolt EEP connections precluding the need for either reinforcing the connection or weakening the beam. Such a connection may prove to be more economical than the currently

prequalified 8 bolt stiffened extended end plate connection and as such, future studies to evaluate its seismic performance are warranted.

7.1 Future work on web stiffener

In the current study the web stiffener plates seemed to provide some resistance to strength degradation but not to the extent that was predicted by pre-test analysis. It is noted here that the web stiffener concept may be extended to field welded connections in which a fuse is provided, for example the RBS and the recently validated HBS [14] connection. However, given the lessons learned in this current study, more consideration should be given to the attachment of the web stiffener. Further FEA studies evaluating various attachment details e.g. use of plug welds and slot welds to provide more attachment points between the beam web and the web stiffener plates, thus improving the overall stiffness of the assembly may be useful towards more successful implementation of this technique. Thermo mechanical simulations to include the effect of welding induced distortions and residual stresses may provide useful insight in this process.

In addition, compact wide flange sections readily achieve rotation capacities of 3 [16] or greater before the onset of significant local buckling and resulting strength loss. As such, carefully constructed moment connections utilizing these sections readily achieve the 2010 AISC Seismic Provisions (ANSI/AISC 341-10) special moment frame (SMF) qualifying 4% interstory drift angle without more than 20% loss of nominal moment capacity. Therefore, the web stiffener technique may provide more added value to built-up beams with slender webs in which rotational capacities are reduced.

7.2 Design Development

Given that the proposed modified EEP connection deviates significantly from the configuration of existing prequalified EEP connections, design methodologies for the practical use of modified EEP connections in moment frames also need to be established, in particular the limits of beam and column size including flange thickness, depth etc. Also design equations or tables to proportion and configure the modified endplate are needed. In the current study design of the endplate was partly guided by using equations based on yield line analysis to select trial endplate sizes. FEA was then used to optimize the design of the endplate and bolt arrangement. This type of exercise is not well suited for design practice and therefore future studies need to be conducted to develop prescriptive design procedures for the proposed modified 8 bolt unreinforced EEP connection.

8. Conclusion

The test results of a modified 8 bolted un-stiffened extended end plate connection has been presented. Three (3) performance enhancement techniques were utilized in this connection. These include the removal of the flange stiffener and rearrangement of the bolts in a hexagonal pattern, heat-treatment of the beam flanges in specified regions adjacent to the connection, and the welding of steel plates called ‘web stiffeners’ to the beam web. The modified BEEP connection displayed ductile seismic response which exceeded the 2010 AISC Seismic Provisions (ANSI/AISC 341-10) SMF qualifying 4% interstory drift angle without much strength loss. Test data shows that the use of a strong end plate with a modified bolt arrangement performed well in distributing bolt forces uniformly amongst the bolt group while the HBS was successful in shifting the majority of inelastic action away from the beam

flange to end plate welds. These observations are consistent with pre-test FEA predictions. The web stiffener, did not perform as predicted by pre-test FEA, however this discrepancy was shown by post-test FEA to be attributable to the presence of welding induced distortions of the web stiffener plates. This indicated that an improved web stiffener design will require the use of slot or plug welding in addition to fillet welding around the edges.

Though the excellent seismic performance of HBS 4 shows the promise of the modified BEEP connection, future effort is needed to optimize this connection for both performance and economy. In addition, prescriptive design procedures for seamless inclusion of this connection in current seismic design practice and for prequalification in the ANSI/AISC 358 standard are required.

9. References

- [1] Murray, T. M., and Sumner, E. A., (2003). AISC design guide series 4, Extended end-plate moment connections, Chicago.
- [2] Sumner E.A. Unified design of extended end plate moment connections subject to cyclic loading. Ph.D. Dissertation, Virginia Polytechnic Institute and State University, Blacksburg, VA, 2000.
- [3] Mays TW. Application of the finite element method to the seismic design and analysis of large moment end-plate connections. Ph.D. Dissertation, Virginia Polytechnic Institute and State University, Blacksburg, VA, 2000.
- [4] Tsai, Keh-Chyuan, and Egor P. Popov. "Cyclic behavior of end-plate moment connections." *Journal of Structural Engineering* 116.11 (1990): 2917-2930.
- [5] Sumner, E.A., & Murray, T.M. (2002). "Behavior of extended end-plate moment connections subject to cyclic loading" *Journal of Structural Engineering*, Vol. 128, No. 4 pp.501-508.
- [6] SAC/BD-00/21. Cyclic testing of bolted moment end-plate connections. by Sumner, E.A., Mays, T., Murray, T.M.

- [7] Korol RM, Ghobarah A, Osman A. Extended end-plate connections under cyclic loading: behavior and design. *Journal of Constructional Steel Research* 1990;16(4):253-279.
- [8] Ghobarah, A., A. Osman, and R. M. Korol. "Behaviour of extended end-plate connections under cyclic loading." *Engineering Structures* 12.1 (1990): 15-27.
- [9] Adey BT, Grondin GY, Cheng JJR. Cyclic loading of end plate moment connections. *Canadian Journal of Civil Engineering* 2000;27:683-701.
- [10] Shi Gang, Yongjiu Shi, and Yuanqing Wang. "Behaviour of end-plate moment connections under earthquake loading." *Engineering structures* 29.5 (2007): 703-716.
- [11] Guo, Bing, Qiang Gu, and Feng Liu. "Experimental behavior of stiffened and unstiffened end-plate connections under cyclic loading." *Journal of Structural Engineering* 132.9 (2006): 1352-1357.
- [12] FEMA-355B, 2000, *State of the Art Report on Welding and Inspection*, prepared by the SAC Joint Venture for the Federal Emergency Management Agency, Washington, DC
- [13] Quayyum, S., Hassan, T. (2014) "An improved unstiffened 8 bolt extended end-plate moment connection for special and intermediate moment frames, Part I: Numerical modelling and Development" *Submitted to Journal of Constructional Steel Research*
- [14] Morrison, M.L., Schweizer, D.Q., Hassan, T., (2014) "An Innovative Seismic Performance Enhancement Technique for Steel Building Moment Resisting Connections." *Submitted to Journal of Constructional Steel Research*
- [15] Popov, E.P., Amin, N. R., Louie, J.C., Stephen, R. M. "Cyclic behavior of large beam-column assemblies." *Engineering Journal* 23.1 (1986): 9-23.
- [16] Bruneau, M., Uang, C.M., & Whittaker, A. (1998). *Ductile design of steel structures*. New York: McGraw Hill Companies.

CHAPTER 6: Seismic Enhancement of Welded Unreinforced Flange Bolted Web Moment Connections

Abstract

Widespread damage to welded unreinforced flange-bolted web (WUF-B) steel moment connections during the 1994 Northridge earthquake led to intensive experimental and analytical research study of this connection. Ultimately, after improvements to weld metal, weld practice and connection details, the post-Northridge WUF-B connection was not able to attain sufficient ductility for use in special moment frames (SMF). This study presents detailed FE analysis of post Northridge WUF-B connections to better understand the mechanisms which limited connection ductility in laboratory tests. Observations made from the FE analysis led to the development and numerical study of a modified WUF-B connection which combines a new bolted web design originally proposed by Lee and Kim (2006), in which beam web shear and bending moments are transferred through a slip critical bolt assembly. This design is combined with a recently developed and validated technique to promote plastic hinging of the beam by selectively reducing the material strength of the beam flanges away from the connection joint. The proposed connection provides the benefit of reduced field welding and UT inspection without sacrificing connection ductility and seismic performance. Finally, the proposed connection is experimentally validated through full scale seismic testing. The test program showed that the proposed modifications were successful in enhancing the seismic performance of WUF-B connections. The pilot test specimen exceeded the 2010 ANSI/AISC Seismic Provision SMF qualifying 4% interstory drift angle without significant strength loss. No weld or near weld cracks were observed. Instead, failure of the

connection at 5% interstory drift resulted from large local buckling deformation in the plastic hinge away from the welded joint.

Keywords: Steel moment connection; seismic performance enhancement; beam plastic hinge; heat-treated beam section; reduced beam section; modified WUF-B

1. Introduction

Prior to the 1994 Northridge Earthquake welded unreinforced flange bolted web connections (WUF-B) were one of the most commonly used moment connections in earthquake prone regions of the United States [1]. Investigations after the Northridge Earthquake uncovered wide spread damage to WUF-B connections in the form of weld or near weld fractures with little evidence of inelastic action [1]. The widespread use of the WUF-B for several years prior to Northridge has been attributed to its perceived performance (ductility) and economy [2]; in addition, the WUF-B, which was commonly referred to as the “prescriptive connection”, was prequalified for seismic applications in the 1988 Uniform Building Code (UBC) and later adopted into the 1992 AISC Seismic Provisions[3]. This prequalification was based upon non standardized laboratory testing carried out during the 1970’s and 1980’s [4-6]. However, an objective review of results from these and other laboratory tests of WUF-B connections preceding the Northridge earthquake reveals that the performance of WUF-B connections showed considerable inconsistency [7], and perhaps was given perfunctory treatment by building code officials and structural engineers.

Early testing done by Popov and Stephen [4], in which direct comparisons were made between WUF-B connections and all welded connections (welded flange welded web) showed this variability. In this study, eight specimens were tested, two of which were all-welded connections, five were WUF-B connections and one in which no web connection was provided. The 2 all welded specimens produced similar ductile behavior and formed full beam end plastic hinges prior to the termination of loading, however in all but 1 case the WUF-B specimens failed by weld or near weld fractures. Subsequent studies by Popov et al. (1986) [5], Popov and Tsai (1988)[6], and Engelhardt and Hussain (1993) [7] showed this erratic behavior in which failures modes were mostly weld or near weld fractures and in many cases were described as being abrupt failures in which little inelastic action is evident. Based on the analysis of results from several experimental studies on WUF-B connections Engelhardt and Hussain (1993) [7] suggested that the performance of these connections was subpar based on the existing acceptability criteria (1992 AISC Seismic provisions) and that the effect of web connection details (for example the addition of supplemental fillet welds between the corners of the shear tab and the beam web) were disguised by the variability in the performance of flange welds. Several experimental studies conducted after the Northridge earthquake [8, 9, 10, 11, 12] in which the performance of pre Northridge WUF-B connections were evaluated, showed similar brittle behavior with many connections essentially displaying linear (moment-rotation) behavior to failure at very low drift angles. This evidence provides insight to the widespread damage to WUF-B connections during the Northridge Earthquake.

Post Northridge studies showed that improvements to weld metal, welding practice and welding inspection (weld fracture mitigation techniques) could significantly enhance the performance of welded steel moment connections. In particular, studies by Ricles et al. 2000 [13] showed that use of ‘notch-tough’ weld metal deposited from E70TG-K2 electrodes along with improved details such as removal of the backing bar significantly improved the ductility and changed the failure mechanism from brittle fractures in the weld (observed in assemblies joined by low toughness E70T4 electrodes), to ductile failures in the base metal away from the welded joint in pull plate test assemblies.

Subsequent tests on full scale beam to column subassemblies by Stojadinovic et al. 2000 [12, 14] showed that the use of notch tough electrodes combined with various improvements to WUF-B connection detailing, improved the connection performance and ductility. However despite these improvements the so-called SAC post –Northridge connection (Fig.1a) did not exceed the 1997 AISC seismic provision 0.03 rad total plastic rotation performance requirement for use in special moment frames. The study did however provide informative and insightful results about the behavior and failure mechanism of WUF-B connections constructed with sound welding practice and consumables. Most notably, the failure mode change from brittle weld metal fractures (observed in pre-Northridge WUF-B connections) to ductile tearing followed by fast fracture of the base metal nucleating between the edge of the weld fusion zone and the base of the weld access hole (where the access hole meets the beam flange) as shown in Fig. 1b.

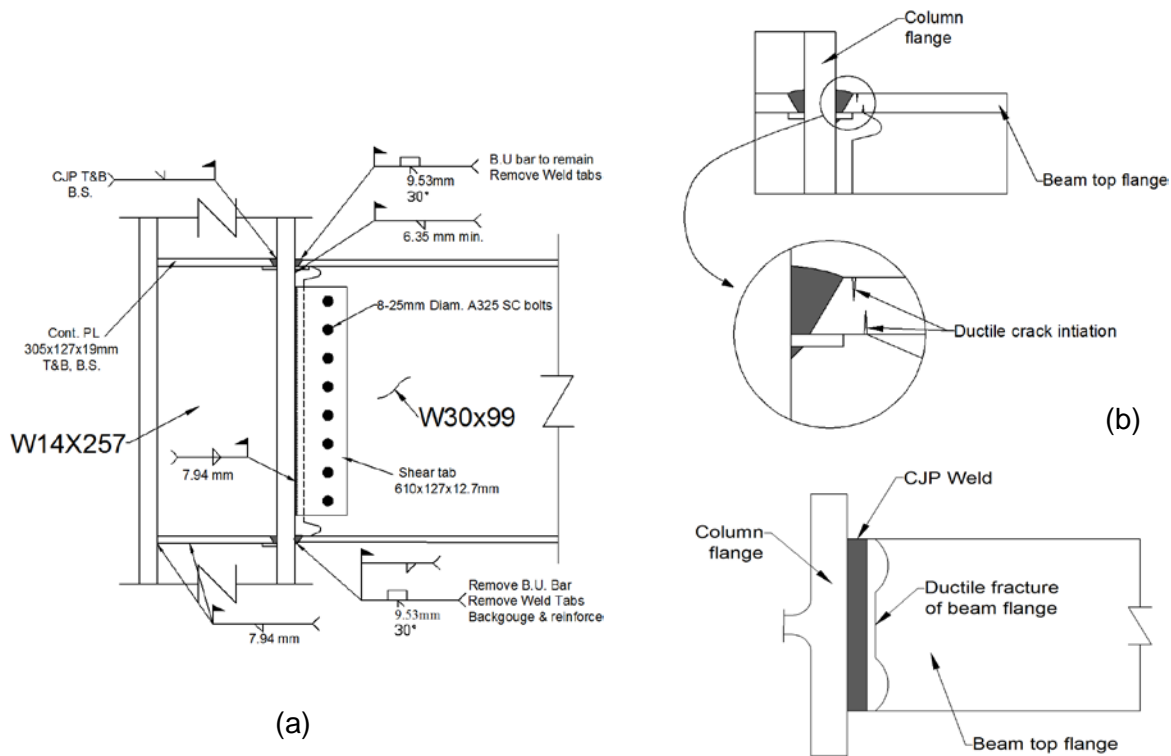


Fig. 1. Post Northridge WUF-B (specimen 6.1 [14]) (a) Connection details (b) Sketch of ductile fracture failure of specimen 6.1[14]

This failure mechanism was repeated for several specimens and was independent of the beam and column sizes which were tested [14]. Similar failures were also observed in WUF-B specimens tested by Chen et al. 2005[15] and Han et al. 2007[16]. The later of these two studies tested WUF-B connections with an improved access hole geometry designed to lower stress and strain concentrations. Failures at the access hole similar to those observed in other WUF-B studies [14,15] suggests that the controlling failure mechanism may not be very sensitive to access hole design. The results of these studies clearly show that in the case of WUF-B connections weld fracture mitigation strategies alone (improved weld metal and

weld details) are insufficient to meet the performance requirements for use in special moment frames. As stated by Stojadinovic et al. 2000 [14], moment connections intended for use in special moment frames (SMF) should incorporate both “weld fracture mitigation measures and flange overstress mitigation measures”.

An overstress mitigation measure which has found wide spread use in current practice is the reduced beam section (RBS). In the RBS, the beam is weakened by selective trimming of the flanges adjacent to the connection so as to create a fuse for damage and energy dissipation in this weakened region. However, combination of the RBS with a bolted web connection has yielded mixed results. In some studies [17, 18], despite suffering eventual weld or near weld failures, they have demonstrated significant ductility and energy dissipation achieving 4% interstory drift or higher. However, the results of a study by Lee at al. 2005 [19] conducted to directly compare the performance of RBS connections with bolted webs (RBS-B) and welded webs (RBS-W) revealed that the former were unable to attain 4% interstory drift. In repeated test RBS connections with bolted webs failed due to premature fractures of the beam flanges at the access hole. As a result of this, RBS connections with bolted webs have not been prequalified for use in special moment frames. The performance and observed failure mechanisms of WUF-B and RBS-B connections in lab testing provide evidence of a mechanistic flaw as predicted below, which limits the ductility of these unreinforced connections.

In several studies [16] and [19- 21] it has been pointed out that slip of the web bolts is observed early in the inelastic cycles which results in reduction of connection moment strength. More importantly, slippage of the web bolts means that there will be rigid rotation

of the beam web (in the connection region) and redistribution of web bending stresses to the flange. It is believed that this stress redistribution places higher demands on the beam flange adjacent to the connection leading to a higher incidence of near weld failure [22]. Higher strain demands in the beam flanges adjacent to the connection were recorded in RBS-B connections when compared to RBS-W connections tested by Lee et al. [19] which provide evidence of this redistribution.

Perceptions about the debilitating effect of bolt slippage on the performance of WUF-B and RBS-B connections have been developed mainly through qualitative comparison of bolted web and welded web specimens in experimental studies [4, 18, 19]. However, the effect has not been quantified in detail experimentally or analytically. In this study, detailed numerical analysis has been conducted to quantify the effect of the bolted web attachment on global and local responses of WUF-B connections. By accurately predicting global and local responses, improved understanding of connection behavior and failure mechanisms is attained. This facilitated the development and experimental validation (through full scale testing) of a new and improved design to enhance seismic performance as presented subsequently.

2. Finite Element Modeling of WUF-B Connections

Finite element modelling has been useful in understanding the behavior and failure mechanisms of welded steel moment connections and has been shown to predict with good accuracy the measured global and local responses [26]. Studies by [9], [21] and [27- 30] have examined WUF-B connections with close attention paid to various aspects of the connection behavior and details. These studies have been instrumental in the development of improved

connection details and in better understanding the influence of parameters, such as panel zone strength/stiffness, beam depth, beam and column flange thickness, access hole geometry etc. on connection behavior. However, these studies have all made various degrees of simplifying assumptions in modelling the beam web connection. In some studies the beam web was modelled to be monolithic with the shear tab [28, 30] while in the most recent of the cited studies [21] the bolt shank was assumed to bear directly against the bolt hole, as such, additional demand from bolt slippage was not included in any of these studies.

With the goal of analyzing precisely the effect of the bolted web attachment on global and local connection responses and failure mechanisms, this study involved detailed modelling of the WUF-B connection including the web attachment as described in the following.

2.1 Finite Element Modelling

2.1.1 Global Model

Three dimensional nonlinear finite element models were developed for WUF-B connections using the commercial finite element analysis software ANSYS Mechanical ADPL [31]. Geometric, material and contact nonlinearities were incorporated in the finite element models. An example of the finite element mesh and boundary conditions is shown in Fig. 2a and Fig. 2b.

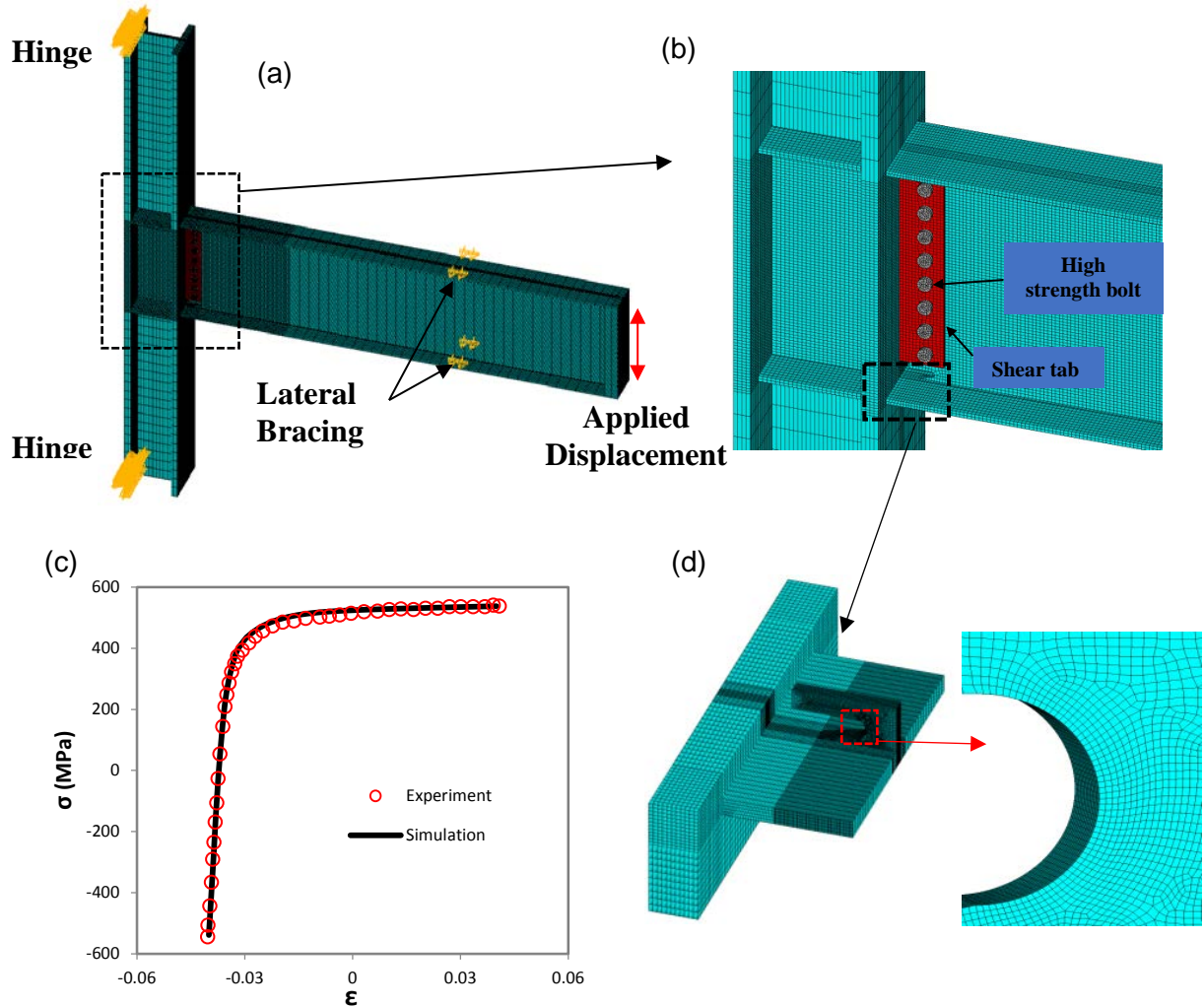


Fig. 2. Finite element mesh (a) Specimen 6.1 [12] mesh and boundary conditions (b) Close up view of specimen 6.1[12] mesh (c) fitted ASTM A572 gr 50 hysteresis curve for determining Chaboche model parameters (Experimental data from [32]), and (d) FE submodel mesh

The beam, column, shear tabs and continuity plates were modeled with 8 noded solid hexahedral elements (SOLID185) with selective reduced integration scheme. To enable accurate modelling of the bolted shear tab, the bolts were modelled with 20 noded solid hexahedral elements (SOLID186). The heads and nuts of the bolts were modelled as solid disks having a thickness equal to that of the nominal bolt thickness specified in the RCSC

Specification [33]. The disk model is a simplification to the actual hexagonal shape however it closely represents the circular contact surface located on the underside of the bolt head and nut which produces the annular distribution of contact pressure (produced by bolt tightening) on the faying surfaces demonstrated by Polyzois and Frank 1986 [34]. The AISC LRFD specified minimum bolt pretension forces [35] were generated via a “pretension element” (PREST 179) which inserts one dimensional zero length elements at the nodes of a specified cross section of the bolt shank. When pretension loading is applied, this element (PREST 179) simulates the reduction of effective length (length between the underside of the bolt head and nut) that takes places during tightening of the faster, in order to generate the required clamping forces. In the simulation, the pretension load/clamping force is applied during the first load step and stored as an initial displacement before the application of loads at the beam tip. This allows for the simulation of fluctuations to the initial pretension load due to the deformations and interactions of the assembly. It should be noted however, that the bolt threads were not modeled in this study i.e. the bolt nut was glued to the bolt shank. Thus the complex nonlinear behavior that arises between the threads of the bolt shank and nut were not captured. Similar approaches to modelling structural bolts have been used in previous studies on bolted connections [36-39].

The interactions between the bolts, shear tab and beam web were modelled using deformable surface to surface sliding contact pairs (CONTA174). Coulomb friction was used to model the sticking/sliding interactions of the faying surfaces. The limiting coefficients of static friction for the assumed faying surface conditions were obtained from the AISC LRFD Specification [35]. During model development it was found that the augmented lagrangian

contact algorithm yielded better numerical stability and less sensitivity to the specified contact stiffness than the pure penalty method. Therefore, despite the extra computational effort required (due to iterative contact traction augmentations), improved conditioning and reduced sensitivity were the basis for choosing this contact algorithm. It should also be noted that the approach utilized for modelling bolts in this study resulted in no displacement boundary conditions being specified for the bolts. Therefore, rigid body motion was circumvented by ensuring that small gaps between contact pairs resulting from numerical round offs during meshing were closed prior to application of pretension loads by using contact surface offsets.

2.1.2 Material and Geometric nonlinearities

Finite element models accounted for material nonlinearity through rate-independent metal plasticity theory based on the von mises yield criterion, additive strain decomposition and associated flow rule. A multilinear kinematic hardening model calibrated from uniaxial monotonic tensile tests [32] was used for monotonic simulations. While the Chaboche nonlinear kinematic hardening model [40] was used for cyclic analysis. Chaboche material model parameters were obtained by fitting stable single amplitude hysteresis loops as shown in Fig. 2d. The distinguishing feature of the Chaboche model is the superposition of nonlinear kinematic hardening rules. This allows for accurate simulation of hysteretic loop shape and therefore plastic modulus over a wide strain range and various loading paths. A summary of the nonlinear kinematic hardening parameters used for cyclic analysis is provided in table 1.

Geometric nonlinearities were accounted for via a large displacement formulation which accompanied by small eccentricities/imperfections in the geometry allowed for the simulation of local buckling. WUF-B connections contain eccentricity due to the offset of the shear tab from the centerline of the column and so no additional imperfections were necessary to perturb local buckling. However, in the case of all welded connections (welded flange-welded web), initial geometric imperfections were introduced to perturb local buckling. Due to the symmetry of the mesh, boundary conditions, loads and resulting deformations, local buckling could not be simulated and unrealistically high values of peak strength were predicted when initial geometric imperfections were not considered. Initial imperfections were obtained by first conducting an eigenvalue analysis of the perfect structure and then prescribing a scaled value of the first eigenmode displacement field as the initial configuration of the structure. The scaling was chosen to represent realistic values of W-shape “out of squareness” based on ASTM A6 [41] tolerances. Similar approaches have been used in other studies [28] and [42-44].

Table 1 Nonlinear Kinematic hardening model material parameters

Parameters	ASTM A572 Gr.50	ASTM A490	E70 Weld*
E (MPa)	199948	199948	199948
σ_0 (MPa)	251.7	777.7	572
C_1 (MPa)	125415.7	204615.8	1450
C_2 (MPa)	28868.4	152250.1	
C_3 (MPa)	2675.2	101318.5	
C_4 (MPa)	144.8	32219.2	
γ_1	4585	4143	55
γ_2	324	285	
γ_3	42	107	
γ_4	0	0	

*Parameters obtained from [45]

2.1.3 Sub model and Cyclic Void Growth Damage Model

Sub models of both the top and bottom beam flange to column flange connections were developed to study with better accuracy and resolution local stress and strain responses in the weld toe and access hole region of WUF-B connections. Since the weld root was not the location of interest, the left in place backing bar and reinforcing fillet weld were not modelled at the top flange. An example of the sub model mesh used for the beam bottom flange to column flange connection is shown in Fig 2d. Stress and strain indices from this sub model were used as inputs to a cyclic void growth model (CVGM) proposed by Kavinde and Deierlein [23], to predict the initiation of ductile macroscopic cracks which were observed during laboratory tests [12]. The CVGM requires that a particular damage criterion is satisfied over a certain minimum volume of material which is characteristic of the scale of physical events leading to the formation of the crack. This minimum volume is termed as the characteristic volume or *characteristic length* [23]. The submodel mesh in the locations of interest such as the root of the weld access hole and beam flange beneath access hole cut have been refined to an element edge length of 0.2 mm to be approximately equal to the average characteristic length reported by Kanvinde and Deierlein 2006 [23] for A572 Gr 50 steel. Details on how this characteristic length is determined are reported in [23].

It should be noted that manufacturing and welding induced residual stresses or stress concentrations created by preexisting voids or cracks were not considered in the sub-model. Heterogeneity of the material properties in the heat affected zone (HAZ) [35] was also excluded. As a result of these idealizations, it was found that the chosen mesh density produced small stress and strain gradients across elements in the areas of interest. Also,

inelastic mesh convergence studies showed very little change in stresses and strains as elements were refined to this size. As a result, the accuracy of predictions made by this model is somewhat less sensitive to the characteristic length and mesh size than in other scenarios [46] where structural details and modelling of preexisting flaws may generate steeper stress and strain gradients.

To date several journal articles discussing the CVGM details, development and applications have been published [23, 46-50]. However, for completeness a brief description of the model and its basic equations is presented here.

The CVGM is a continuum level model for prediction of ductile fracture in metals subjected to ultra-low cycle fatigue (ULCF) loading. It is developed based on the semi-empirical equation proposed by Rice and Tracey 1969 [51] for the void growth rate of a spherical void in an infinite solid subjected to remote normal stresses and strain rates:

$$\frac{dR}{R} = C e^{1.5T} d\varepsilon_p \quad (1)$$

Where R = average void radius C = material constant, $T = \frac{\sigma_m}{\sigma_e}$ (ratio of mean stress to effective stress, also called stress triaxiality), $d\varepsilon_p$ = increment of equivalent plastic strain

For ductile fracture initiation, void growth is assumed to be the controlling mechanism in the development of a macroscopic crack and with this assumption Eq.1 is integrated to develop the following failure criterion based on a critical void ratio being attained over a given characteristic length:

$$VGI_{cyclic} > VGI_{cyclic}^{critical} \quad \text{for } l \geq l_{characteristic} \quad (2)$$

Where,

$$VGI_{cyclic} = \sum_{Tensile\ Cycles} \int e^{1.5T} d\varepsilon_p - \sum_{Compressive\ Cycles} \int e^{1.5T} d\varepsilon_p \quad (3)$$

And,

$$VGI_{cyclic}^{critical} = VGI_{monotonic}^{critical} e^{-\lambda \varepsilon_p^{accumulated}} \quad (4)$$

Where, $VGI_{monotonic}^{critical}$ is obtained from the following failure criterion establish for monotonic loading:

$$VGI_{monotonic} = \int_0^{\varepsilon_p} e^{1.5T} d\varepsilon_p > VGI_{monotonic}^{critical} \quad (5)$$

The parameter λ is a material dependent parameter which represents the degradation of material resistance to ductile fracture due to cyclic loads and $\varepsilon_p^{accumulated}$ is the equivalent plastic strain that has accumulated up to the beginning of each tensile excursion of loading.

$VGI_{monotonic}^{critical}$ and λ are calibrated by experimental testing of notched bar specimens subjected to monotonic and cyclic loading histories respectively. FE analysis of these test specimens is then conducted to extract stresses and strains needed for model calibration. These model parameters for A572 grade 50 steel used in the study reported herein were obtained from [23]. The reader is referred to [23] for a more detailed discussion of the CVGM and its parameter determination.

It should be emphasized that the CVGM model is developed to predicted ultra-low cycle fatigue (ULCF) failure. ULCF failure occurs at larger inelastic strains and lower cycle counts as compared to low cycle fatigue failures and displays common characteristics with ductile fracture from monotonic loading [23]. It is employed for use in this study because failures observed in lab testing of WUF-B connections seem to fall in the category of ULCF

based on the low number of cycles to fracture, large inelastic strains recorded near the fracture location and the reported appearance of the fracture surface [12]. These failures are somewhat common in structures subjected to earthquake induced loading histories which impose large ductility demands but low number of cycles.

Also it is noted that the void growth rate equation proposed by Rice and Tracey 1969 [51] which forms the basis of the CVGM is based on the assumption of “high triaxiality” where dilatational void growth (rather than shape change) dominates. Consequently, Kanvinde and Deierlein [23] state that the validity of the CVGM is “questionable” for low-triaxialty fracture ($T < 0.3$) where void shearing rather than void growth controls fracture. Finite element analysis showed that tensile stress tri-axialities at various locations of the weld access holes in WUF-B connections fluctuated between 0.8 and 1.2 throughout the loading history. This suggests that the CVGM is appropriate for analysis and predictions of ductile fractures initiating in this region.

Finally, it should be stated that the numerical model utilized in this study does not address crack propagation; instead the CVGM is used to predict the initiation of a macroscopic crack based on existing stress and strain conditions. The CVGM is thus ‘decoupled’ from the FE analysis and does not affect the global or local response predictions. As a result, loss of connection strength due to ductile tearing and fast fracture is not captured.

2.2 Validation of Numerical Modelling

2.2.1 Simulation of slip in a simple bolted assembly

Numerical modelling was conducted with the primary goal of understanding the effect of the bolted web attachment on connection performance. In particular, bolt slippage and its associated effects were of concern. Therefore, prior to the modelling of WUF-B connections, the bolt modelling technique described above was first applied to a simple double shear bolted plate assembly (tested by Huang et al. 2010 [52]) to determine whether experimentally observed slip loads could be simulated. The FE mesh, applied loads and boundary conditions used are shown in Fig. 3a. Due to symmetry, only half the test assembly was modelled. In Fig. 3b the load- displacement response at the tip of the connected plate is plotted where it can be observed that the sudden change in stiffness due to bolt slippage is captured and the predicted slip load is in good agreement with experimental observations. The model also captures the subsequent increase in stiffness due to bolt bearing, note that the diameter of the bolt holes were modeled to be 3.175 mm (1/8 in) larger than the bolt shank.

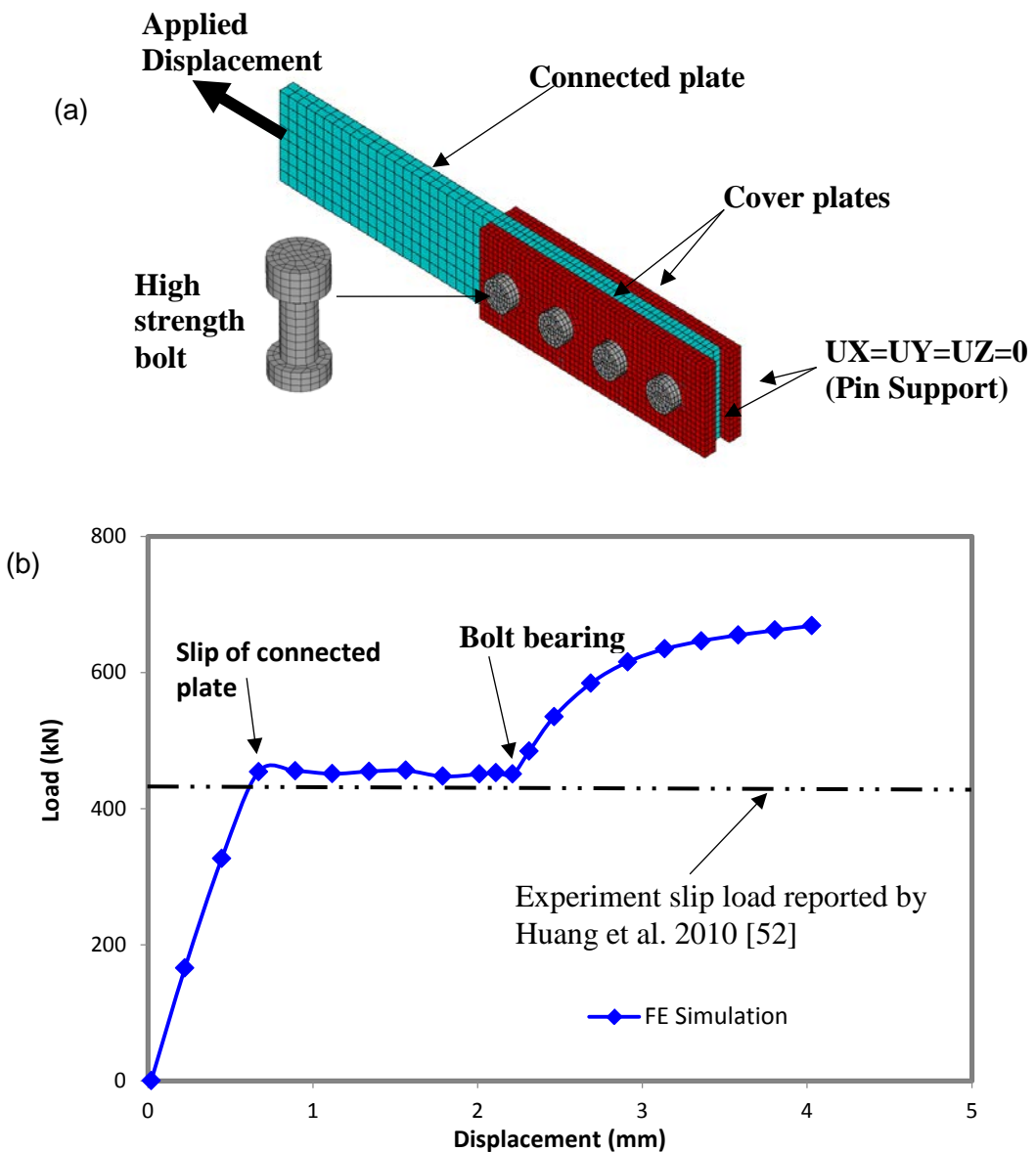


Fig. 3. Finite element analysis of a bolted plate assembly, (a) FE mesh of plate (b) Load-displacement response

2.2.2 Simulation of Post Northridge WUF-B connection

For validation and analysis of WUF-B connections specimen 6.1 tested by Stajodonivic et al. [12] was modelled. The connection details are shown in Fig 1a.

Experiment support conditions were simulated by applying hinge supports at the column ends and roller supports to the beam flanges near the point of loading (for lateral bracing) as shown in fig 2a. Displacements were applied at the beam tip according to the SAC loading protocol shown in Fig. 4a. The predicted moment-rotation response of specimen 6.1 is plotted against the recorded experimental response in Fig. 4b. Moments and rotations are calculated at the column centerline. To obtain the close agreement between the predicted and recorded responses shown in Fig. 4b two modeling considerations were found to be especially important:

1. Detailed modelling of the bolted shear tab web connection and
2. The use of a robust and properly calibrated constitutive model.

To demonstrate the importance of these considerations, simulated moment-rotation responses in which simplifications were made to the web connection details and material constitutive behavior are plotted against the experimental response and shown in Figs. 4c and 4d. In the simulation shown in Fig. 4c the web connection detail was simplified to assume the beam web to be monolithic with the shear tab i.e. the beam web was simply glued to the shear tab and no bolts or contact elements were incorporated. This resulted in over prediction of moment responses. The simulation shown in Fig 4d includes detailed modelling of the web connection using the techniques described in the previous section (see section 2.1.1), however, a multilinear kinematic hardening model calibrated from uniaxial monotonic tensile tests of A572 gr 50 steel [32] was used for the beam and column material. This resulted in

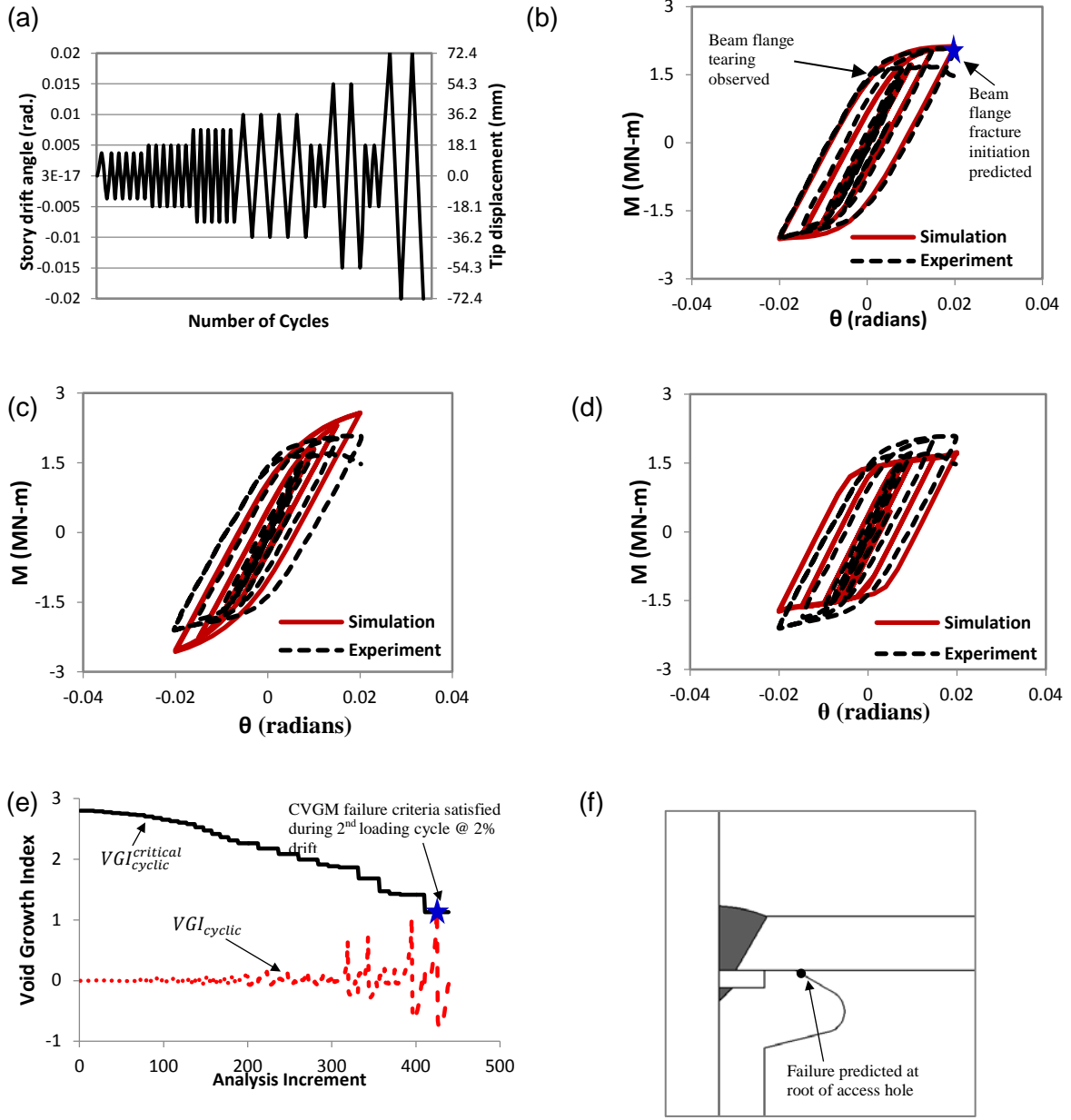


Fig. 4. Finite element analysis of WUF-B connection specimen 6.1 [12] (a) load history (b) comparison of experimental and analytical results for specimen 6.1 [12] (c) comparison of experimental and analytical results for specimen 6.1 with modelling simplification of web connection (d) comparison of experimental and analytical results for specimen 6.1 with multilinear constitutive model calibrated from monotonic tensile test data (e) Void growth indices for CVGM failure prediction (f) Sketch showing location of CVGM failure prediction

under prediction of moment responses. Comparison of Figs. 4c and 4d with Fig. 4b underscores the importance of modelling detail for accurate FE simulations. The evolution of the void growth indices (for the CVGM) which were calculated from stress and strain data extracted from the submodel of specimen 6.1 are shown in Fig. 4e. The location considered is the center of the access hole root at the beam top flange as shown in Fig. 4f. This and other locations such as the center and edges of the beam flange at the weld toe were evaluated for satisfaction of the CVGM failure criteria, however failure was predicted earliest in this location which is in agreement with the experiment observations [12]. It is interesting that in the study conducted by Stajodonivic et al. [12] two specimens (6.1 and 6.2) of identical geometry both suffered failures at the top flange. The FE global and submodels showed (albeit relatively small in magnitude) consistently higher plastic strains demands at the top flange access hole as compared to the bottom flange access hole for this specimen. As a result, the CVGM predicted failure to occur at the top flange first. At the time of writing it is unclear what accounts for this consistent difference in strains at the top and bottom flange access holes.

It is pointed out that for validation purposes the access hole geometry of specimen 6.1 was modelled to be similar to that reported in [12] as shown in the sketch in Fig. 4f. However for later comparative study of WUF-B connections with other connection designs, the improved access hole detail shown in Figs. 2c, 10a and 10b which is now widely used for WUF-W and RBS connections was considered.

3. Monotonic Analysis and comparative study of WUF-B connections

Monotonic analysis was conducted on WUF-B connections to better understand the mechanisms that lead to the failures commonly observed in experimental studies [12, 15, 16]. While it is recognized that global and local responses to cyclic and monotonic loading are different, monotonic loading responses are easier to interrupt while still representing the basic mechanisms that govern the inelastic behavior of the connection.

The monotonic moment vs rotation response of WUF-B connections was first simulated and compared to that of an all welded connection (welded flange welded web) of identical geometry. The WUF-B connection studied here is identical in geometry to specimen 6.1 which was analyzed under cyclic loading for validating the modeling technique implemented in this study. Displacements were applied to the beam tip incrementally up to a total connection rotation of 0.04 radians at the column centerline. The simulated moment-rotation response of both the WUF-B and all welded connections are plotted and compared in Fig. 5a. In the figure, moments and rotations are calculated at the column face to allow for easy comparison of connection responses with well-known strength indices used in design.

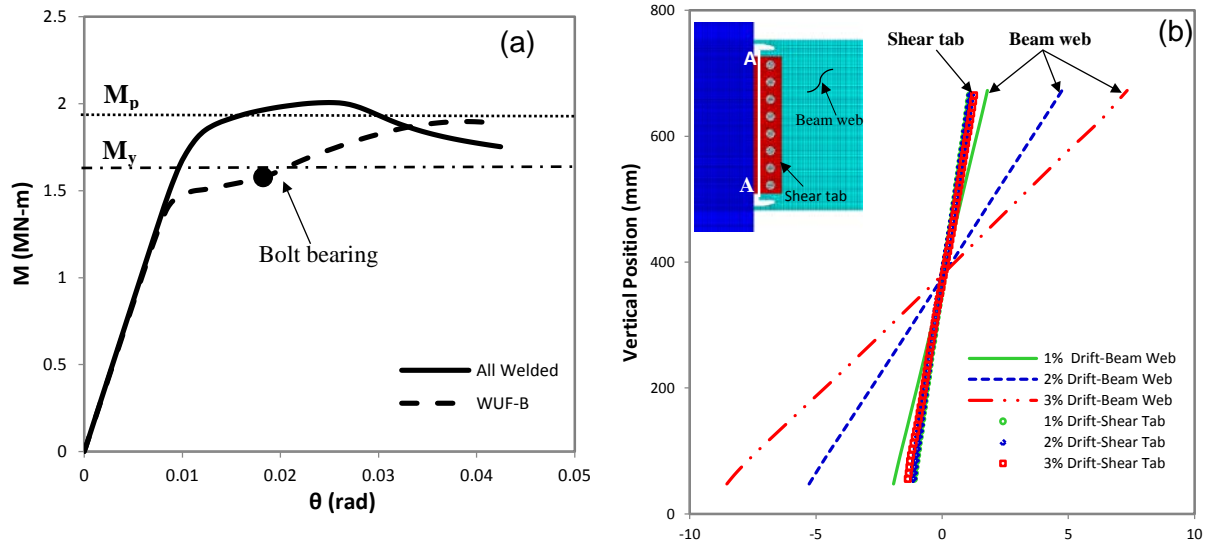


Fig. 5. Comparison of finite element monotonic response prediction for WUF-B and all welded moment connection (a) moment-rotation responses (b) Horizontal nodal displacements on the vertical edge of the beam web adjacent to the column flange (along line A-A) and horizontal displacements of the adjacent nodes on the shear tab for WUF-B connection

From Fig. 5a it is observed that initially both connections display similar linear behavior with comparable elastic stiffness. However, the onset of nonlinear behavior occurs earlier and more abruptly for the WUF-B connection. This sudden change in stiffness occurs at a smaller bending moment than the calculated yield moment of the beam cross-section at the column face and appears to be the result of bolt slippage and subsequent yielding of the beam flanges. The WUF-B connection displays very low post yield stiffness until approximately 0.02 radians rotation when the outer two bolts begin to bear against the holes of the shear tab and beam web. At this point there is a discernible increase in stiffness and the connection resistance continues to increase up to 0.04 radians; followed by a slight decrease in resistance due to local buckling prior to the termination of loading. As shown in Fig. 5a

this WUF-B connection does not attain the calculated plastic moment capacity (M_p) of the beam section at the column face, which is consistent with the observation made in the cyclic testing of specimen 6.1 [12].

On the other hand, the all welded connection displays the “characteristic” response of fully restrained steel moment connections. The onset of nonlinear behavior begins at the calculated yield moment and the connection displays gradual reduction of stiffness thereafter. In contrast to the WUF-B connection, the all welded connection exceeds the calculated plastic moment capacity at the column face. The onset of strength degradation occurs earlier in the all welded connection due to the larger stresses developed in the beam web adjacent to connection (the reason for which will be discussed later). As a result, web local buckling is initiated which triggers flange local buckling and twisting of the cross section leading to strength degradation.

From the afore-described moment-rotation response it is clear that bolt slippage has a debilitating effect on the global behavior of the WUF-B connection. Bolt slippage also has detrimental effects on the local stresses and strains in the connection region. To illustrate web bolt slippage progression, Fig. 5b compares the horizontal nodal displacements on the vertical edge of the beam web adjacent to the column flange with the horizontal displacements of the adjacent nodes on the shear tab at various stages of the loading history. Note the increasing displacements of the beam web which vary linearly with depth, compared with the very small (almost unnoticeable) displacements of the shear tab. This illustrates the slippage of the beam web with progression of loading. Note that even after the bolts begin to bear against the holes of the shear tab and beam web (at approximately 0.02

radians rotation see Fig. 5a) additional increase in relative displacements between the web and shear tab takes place due to the deformation of the outer two bolt holes. The simulated bolt slippage bears close resemblance to the reported behavior in several experimental studies [4, 16, 21].

Figure 6a shows the contour plot of the beam flexural stress distribution in the WUF-B connection at a moment equal to the yield moment (M_y) of the beam cross-section at the column face. The nodal averaged flexural stresses acting on the centerline of the beam cross section 762mm (30in), 178mm (7in) and 127mm (5in) from the face of the column (sections 1, 2 and 3) are plotted against those predicted by classical beam theory in Fig. 6b, 6c, and 6d. These figures show the effect of the afore-described bolt slippage on the bending stress distribution near the connection. As a result of bolt slippage, bending stresses gradually redistribute from the beam web into the flanges near the connection. Note from the contour plot (Fig. 6a) that this stress redistribution takes places adjacent to the weld access hole, causing most of the web flexural stresses to flow “through” the weld access hole into the flanges, placing large demands in this region. Note from Fig. 6d that the stresses on the beam flange exceed those predicted by classical beam theory by over 20%.

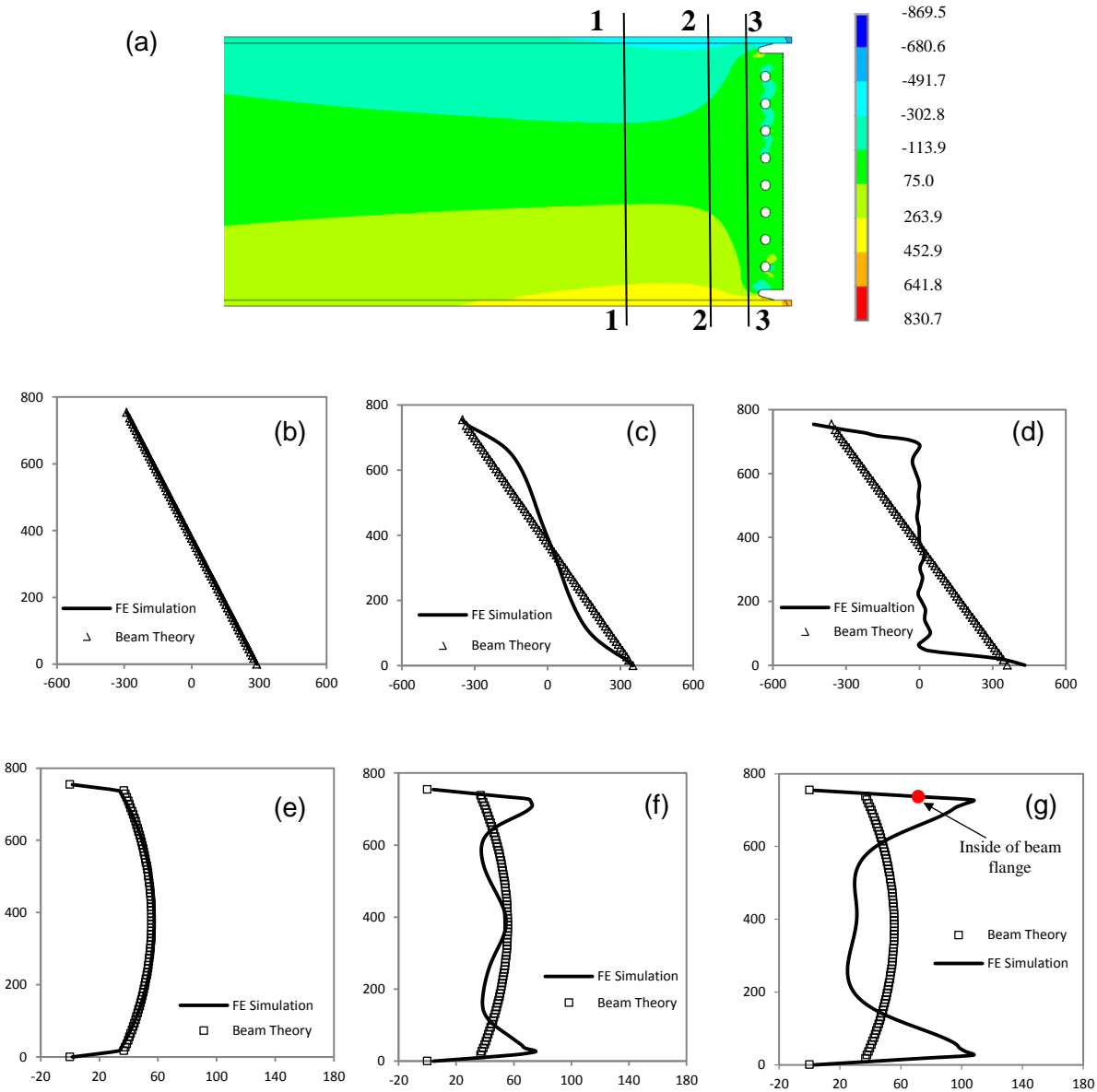


Fig. 6. Finite element analysis of WUF-B connection (a) contour plot of longitudinal stress distribution in beam (b) longitudinal stress along beam depth at section 1-1 (c) longitudinal stress along beam depth at section 2-2 (d) longitudinal stress along beam depth at section 3-3 (e) vertical shear stress along beam depth at section 1-1 (f) vertical shear stress along beam depth at section 2-2 (g) vertical shear stress along beam depth at section 3-3

The nodal averaged vertical shear stresses acting on the centerline of the beam at corresponding locations to those shown for bending stresses are plotted and compared to classical theory predictions for the WUF-B connection in Figs. 6e, 6f and 6g. Note that at cross-sections close to the connection (Figs. 6f and 6g), shear stress distribution deviates significantly from that predicted by classical theory. This has been mentioned in several other studies [4, 12, 22, 27, 28 and 53]. As will be shown later, redistribution of shear stresses adjacent to the connection is not unique to the WUF-B. However, it does appear that higher shear stresses are carried by the flanges of WUF-B connections than all welded connections (compare Figs. 6g and 7e). An unfortunate consequence of this stress redistribution is local bending of the beam flanges which creates severe stress and strain gradient across the flange width (see Fig. 10a) and through the flange thickness and places additional stress and strain demands particularly in the access hole region and at the weld root.

For purpose of comparison, the flexural stress contours in the beam of the all welded connection at a moment equal to the yield moment (M_y) of the beam cross-section at the column face is plotted in Fig. 7a. The nodal averaged flexural stresses acting on the centerline of the beam cross section 762mm (30in), 178mm (7in) and 127mm (5in) from the face of the column (sections I, II and III) are plotted against those predicted by classical beam theory in Fig. 7b, 7c, and 7d. In contrast to the WUF-B connection, close agreement is obtained between the flexural stress distributions of the all welded connection and those predicted by classical beam theory at all locations. The slight disturbance to the stress distribution near to the top and bottom flanges in Fig. 7c and 7d is created by the access hole and will be discussed further later.

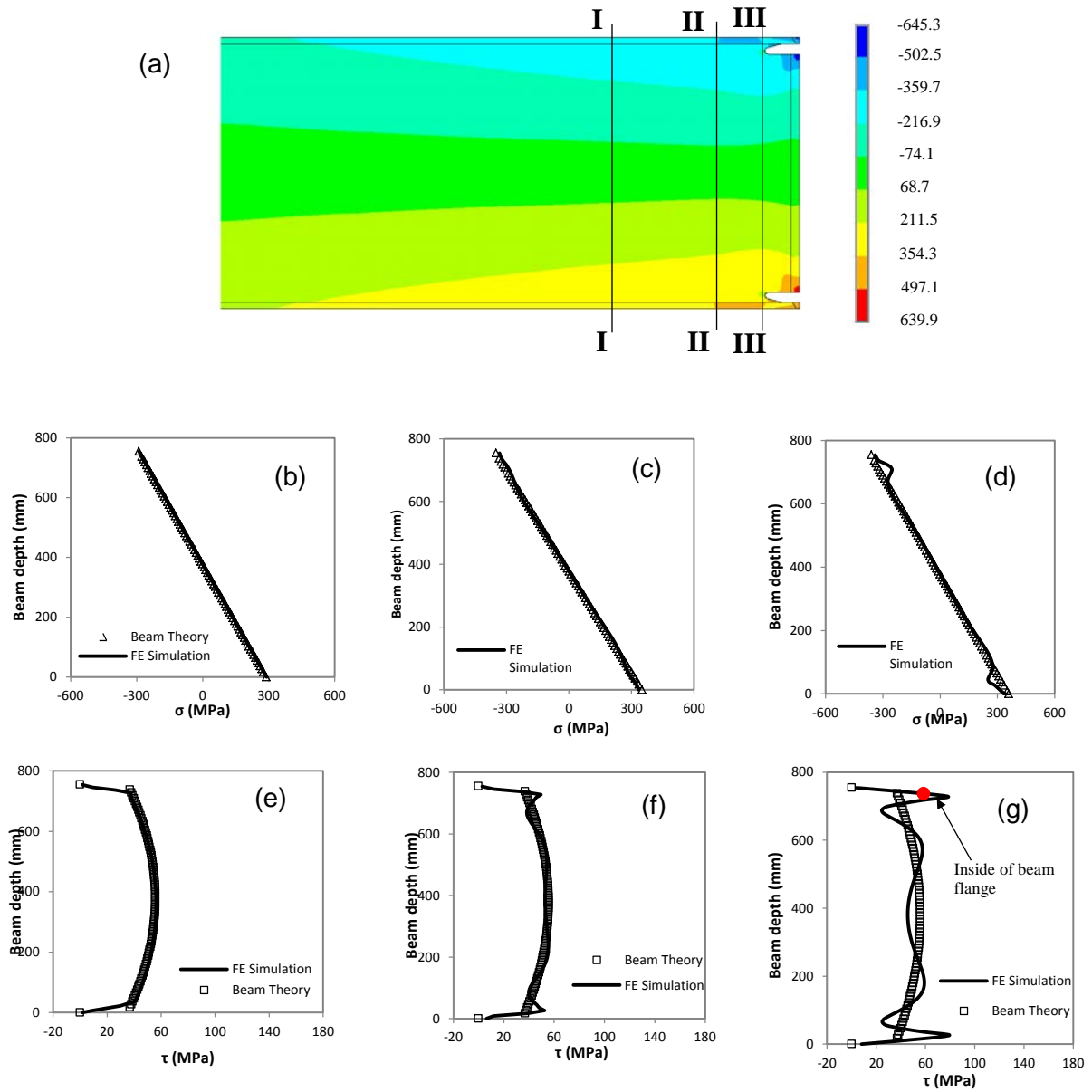


Fig. 7. Finite element monotonic response of WUF-B connection at yield moment (M_y) (a) contour plot of longitudinal stress distribution in beam, (b) longitudinal stress along beam depth at section I-I, (c) longitudinal stress along beam depth at section II-II, (d) longitudinal stress along beam depth at section III-III, (e) vertical shear stress along beam depth at section I-I, (f) vertical shear stress along beam depth at section II-II, and (g) vertical shear stress along beam depth at section III-III.

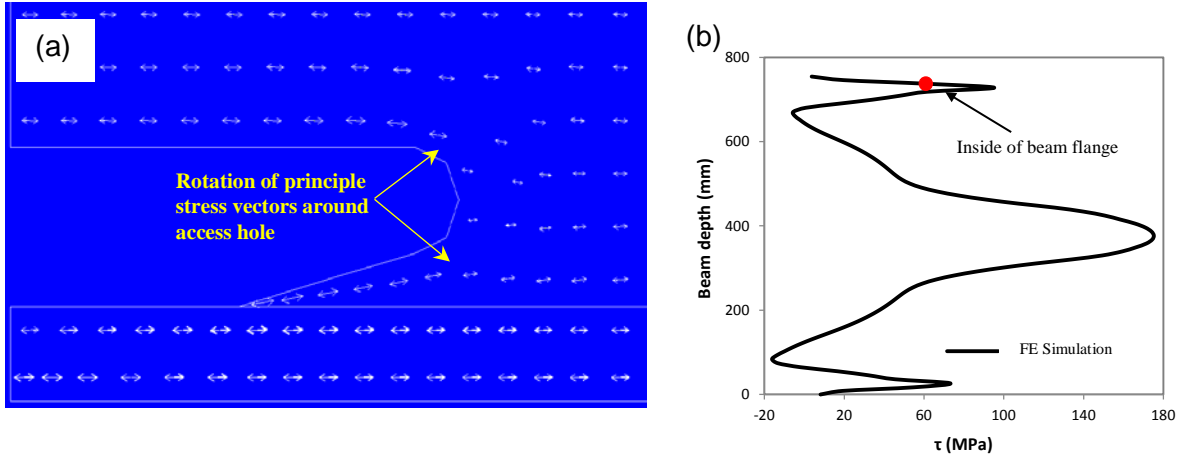


Fig. 8. (a) Principle stress vector plot around access hole (b) Vertical shear stress along beam depth at section II-II at 0.02 rad story drift

The nodal averaged vertical shear stresses acting on the centerline of the beam at corresponding locations to those shown for bending stresses are plotted and compared to classical theory predictions for the all welded connection in Figs. 7e, 7f and 7g. The shear stress distribution near the connection Figs. 7f and 7g deviates from classical theory predictions resulting in higher shear stresses at the top and bottom of the beam web, and in the beam flange. Note that the prying effect discussed earlier for WUF-B connection is still present in all the welded connection. This is a performance debilitating condition triggered by 2 effects. The first and more dominant trigger arises from boundary restraints to column deformation, Poisson deformation, and shear warping deformation. Boundary effects have been mentioned in other studies [14, 27, 28 and 53]. Note that the prying forces acting on the beam flanges created by stress redistribution near the connection are affected by the stiffness of the flange. This observation has led to the development of connections such as the slotted web [53] and free flange [54] which essentially decouple the beam flange from the web for a

sufficient distance away from the connection region. Consequently, the flange stiffness/ability to resist prying forces is significantly reduced which in turn lowers the vertical shear force carried by the beam flanges in the connection region.

Despite the presence and adverse effects of shear stress redistribution and consequent prying forces on the beam flanges in WUF-B and all welded connections, it should be pointed out that this effect is blunted when the flanges undergo wide spread yielding causing a reduction in flange stiffness near the connection. Such a scenario is depicted in Fig. 8b where the nodal averaged shear stresses in the all welded connection 5in. from the column face are plotted when the connection is at 0.02 radians story drift. When this figure is compared with Fig. 7g it can be observed that despite an increase in the applied shear of about 20% (see Fig. 5a) the increase in flange shear stress is minimal and much of the additional vertical shear is now redistributed to the central portion of the beam web. Similar observations have been made by El Tawil et al. [28].

The second and milder trigger to shear stress redistribution is the disturbance to the stress field caused by the access hole. To illustrate this effect, consider an all welded connection in which the column elastic flexural modulus is set to be several orders of magnitude higher than that of the beam ($\{EI\}_{column} = \{1000 * EI\}_{beam}$). Also consider the beam to be subjected to pure bending with an applied moment just slightly lower than the yield moment (i.e. linearly distributed couples forces are applied at the beam tip) and with Poisson ratio equal to zero. In this condition the shear stress redistribution due to boundary restraints is eliminated by removing or making insignificant column deformations, Poisson deformations and deformations due to shear warping. A vector plot of the principle stress

distribution in the beam for this “theoretical” scenario is shown in Fig. 8a. Note that at every point except around the access hole the principle stress vectors are horizontal indicating pure tension stress states. However, at the access hole the principle stress angles rotate which introduce self-equilibrated shear stresses around the top and bottom flange access holes. This creates mild prying effects on the beam flanges the magnitude of which is dependent on the shape, size and location of the access hole.

4. Seismic Enhancement of WUF-B moment connections

From the above comparison of the WUF-B to the all welded connection it is apparent that although more pronounced in the WUF-B, both connections suffer the debilitating shear stress redistribution and prying effects on the beam flanges. However, the more stark contrast between the two connections is the redistribution of bending stress (due to bolt slippage) in the WUF-B connection which is not observed in the all welded connection. This results in beam flanges of the WUF-B connection being subjected to larger bending stresses than those in the all welded connection. Upon yielding these stress concentrations become strain concentrations which grow rapidly with applied displacements at the beam tip and soon lead to ductile rupture at the toe of the access hole. This mechanism has been deduced from both cyclic analysis of the WUF-B connection which was presented earlier (see section 2.2.2) and monotonic analysis which will be discussed more later.

To improve upon the performance of the WUF-B without sacrificing its attractive features (i.e. less field welding and faster erection), two performance enhancement techniques are being proposed. The first performance enhancement technique is a modified bolt design originally proposed by Lee and Kim [24] in which the bolts are designed to

transfer web bending moments and shear forces through friction. To more efficiently resist the web bending moments, the bolts are rearranged to be located toward the outer edges of the beam web as shown in Fig. 8a. This creates a stiffer web connection thereby reducing the redistribution of stresses to the beam flange.

To reduce the strain concentrations that are created in the weld access hole and weld HAZ, a recently validated technique [25] to promote plastic hinging of the beam by selectively reducing the material strength of the beam flanges away from the connection joint is also incorporated. This material strength reduction is achieved through high temperature heat-treatment (annealing) of the beam flanges in the areas highlighted red in Fig. 9a and 9c. The temperature history used in the heat-treatment process is shown in Fig. 10a and the resulting strength reduction is shown in Fig. 10b. As a consequence of this softening, plastic hinging of the beam takes place in the heat-treated beam section (HBS). Therefore, large displacements applied at the beam tip are mostly accommodated by yielding and plastic hinging of the HBS. This reduces inelastic strain demands at the weld access hole and weld HAZ. In a similar manner to the RBS, this connection provides a ductile seismic fuse through weakening, but because the elastic modulus of the HBS is unchanged, a connection modified with such a technique does not sacrifice elastic stiffness as does the RBS. Also, since the cross section of the beam is unaltered and the inelastic portion of the stress strain curve is not significantly modified (note the downward shift of the stress-strain curve in Fig. 8e) the buckling resistance of this connection remains similar to that of a beam section before heat-treatment.

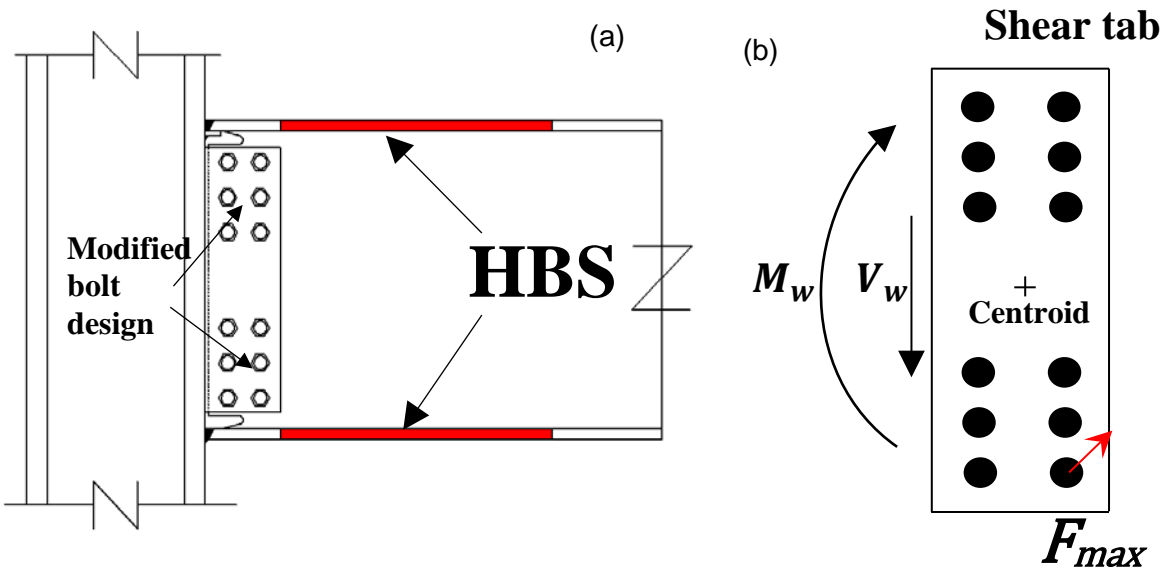


Fig. 9. (a) WUF-B connection with proposed modifications including modified bolt design and HBS, and (b) Free body diagram of shear tab (only one bolt force vector is shown for clarity)

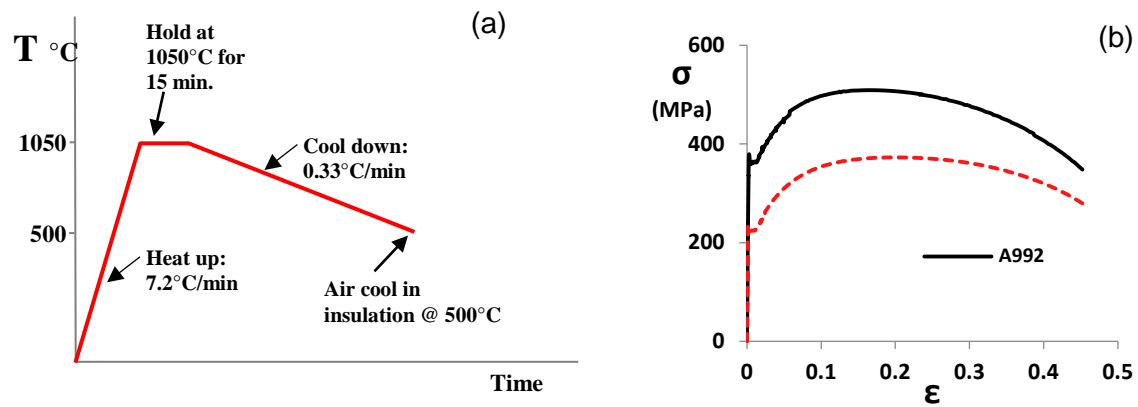


Fig. 110. (a) Temperature history of A992 steel heat-treatment (b) Engineering stress-strain response of A992 and heat-treated A992 steel

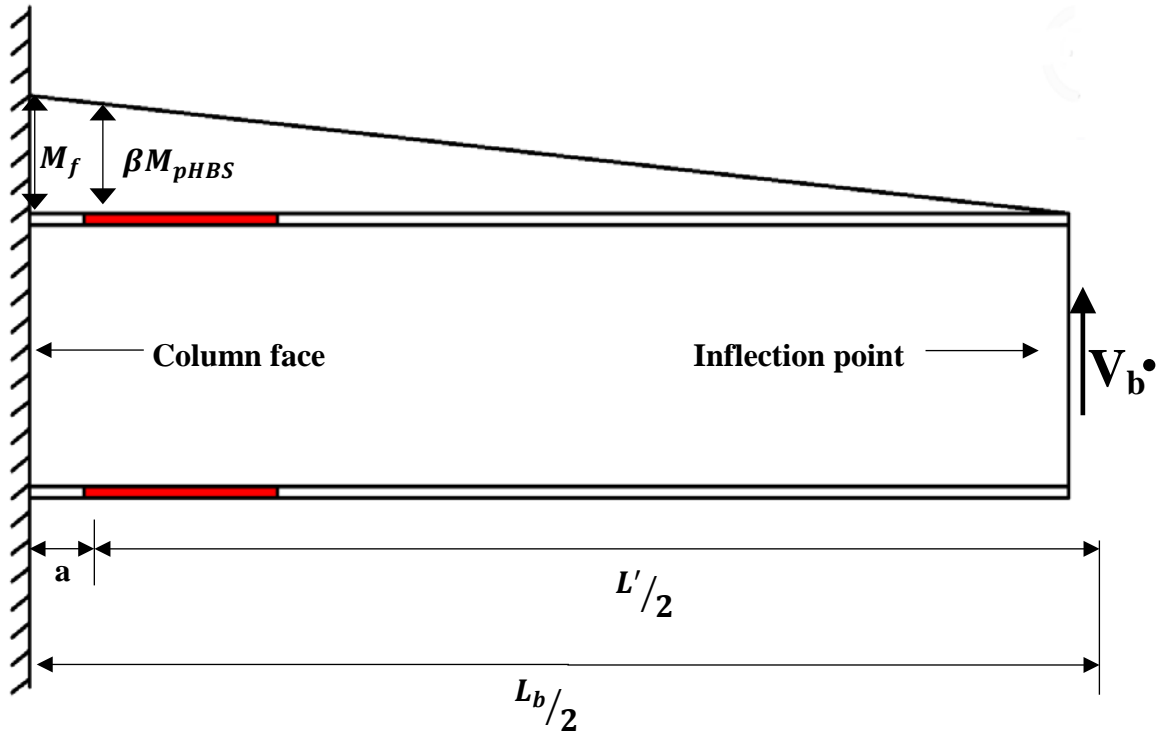


Fig. 11. Seismic moment distribution for design force determination

4.1 Overview of Connection Design

The following design of the proposed connection is similar to that proposed by Lee and Kim [24] where the modified bolt arrangement was applied to RBS connections. The design procedure is re-presented here with some modifications.

Step 1:

Calculate Probable maximum bending moment and beam shear at the column face

Based on the seismic moment distribution shown in Fig. 11, the probable maximum bending moment at the column face (M_f) and beam shear (V_b) can be computed as:

$$M_f = \beta M_{pHBS} (L_b / L') \quad (6)$$

Where

$$M_{pHBS} = F_{yfHBS} b_f t_f (d_b - t_f) + \frac{1}{4} F_{ywHBS} t_w (d_b - 2t_f)^2 \quad (7)$$

$$V_b = 2M_{pHBS}/L' \quad (8)$$

β is a material strain hardening parameter recommended to be taken as 1.15 based on the findings of Morrison et al. [25]. F_{yfHBS} and F_{ywHBS} are the flange and web yield strength in the HBS, b_f is the beam flange width, t_f is the beam flange thickness, t_w is the web thickness, d_b is the beam depth, L_b is the beam clear span length and L' is the distance between the plastic hinges formed on either end of the beam.

Step 2: Determination of shear and bending moments acting on Shear tab

Figure 9b shows a free body diagram of the shear tab. M_w and V_w are the beam web bending moment and beam web shear force to be resisted by the shear tab. Note that the shear tab detail proposed by Lee and Kim [24] involves the use of two shear tab plates located at top and bottom corners of the beam web. One shear tab with bolts located at the top and bottom corners is recommended here so as to simplify construction and provide additional lateral stiffness to resist web local buckling.

Lee and Kim [24] estimated from their numerical studies that the beam flanges carry half the beam shear. However FE analysis of all welded connections modified with the HBS showed that the web may resist as much as 75% of the beam shear. More research is necessary to refine such an estimate over a wide range of beam sizes; however, with the current knowledge it is recommended that the web connection be designed to resist 75% of the beam shear.

$$V_w \approx \frac{3}{4} V_b \quad (9)$$

Moments acting of the shear tab may be estimated in the same manner as previously proposed [24]:

$$M_w \approx \left(\frac{I_w}{I_w + I_f} \right) \times M_f \quad (10)$$

Step 3: Select shear tab thickness

Lee and Kim [24] recommended sizing the thickness of the shear tab based on the Von Mises yield criterion. Shear and normal stresses were calculated by assuming uniformly distributed shear V_w and normal forces acting on the shear tab. However, given the very complex stress states at the boundary of the shear tab and column face, this simplification may be unconservative. In addition, based on observations from our numerical studies, the shear tab provides lateral support to the beam web which prevents excessive local deformations near the connection region during buckling at large displacement load cycles. Hence it is recommended that the shear tab be sized according to:

$$t_{st} = t_w + 1.6 \text{ mm} \quad \left(1.6 \text{ mm} = \frac{1}{16} \text{ in.} \right) \quad (11)$$

Step 4: Design of web bolts

The elastic vector method was previously recommended for determination of bolt shear demands [24]. In this method, the slip resistance of each bolt is designed to exceed to the shear demand of the most heavily loaded bolt. This method makes simplifications to shear force distributions and conservative estimates of bolt force demands [56]; however conservatism is favored for this application particularly when stiffness of the web connection

is considered. Numerical studies reported herein have found the elastic vector method to be suitable for this application.

Details of the elastic vector method are presented in the AISC LRFD specification [34] and are not reproduced here.

Once the shear demand on the most heavily loaded bolt is determined, the bolts may be selected based on their minimum pretension loads and the choice of an appropriately prepared faying surface to resist applied shear forces through friction according to:

$$F_{max} < \phi R_n \quad (12)$$

Where F_{max} is the shear demand on the most heavily loaded bolt, and ϕR_n is the design slip resistance of each bolt according to the AISC LRFD specification [35]. Since bolt slippage is detrimental to the performance of this connection ϕ is taken to be 0.85 in accordance with the specification [35].

It is noted that the proposed connection does increase the number of bolts and possibly bolt size and strength requirements (A490 vs. A325). In addition, class B faying surfaces (unpainted blast-cleaned steel surfaces or surfaces with class B coatings on blast cleaned steel [35]) may be required to obtain larger friction forces to resist slip. For example in the case of specimen 6.1 which was previously analyzed (see section 3), the modified connection design results in the use of 12- 28.6 mm A490 bolts and a class B faying surface (this connection is analyzed in the subsequent section) as opposed to 8-25.4 mm A325 bolts and a class A faying surface. However, it is anticipated that despite these cost increases, the proposed connection will still offer better economy and faster erection, when compared to all welded connections especially in shallow beam sections ($\leq W30$).

4.2 Finite element analysis of enhanced WUF-B connection

4.2.1 Global responses of enhanced WUF-B connection

The improvements to connection performance realized by the incorporation of the two afore-mentioned performance enhancement techniques are evaluated through FE analysis. Monotonic simulations were conducted at first to facilitate direct comparison to previously studied connections. Cyclic simulations were then performed to evaluate the performance of the purposed connection under AISC seismic provision loading protocol [57]. The stress and strain data from cyclic sub model simulations were used as inputs to the CVGM to assess ductile fracture potential.

The monotonic moment vs. rotation response of connections with various web connection details all of which are enhanced with the HBS technique are plotted and compared in fig 12a. These include an all welded connection (HBS-W), the proposed modified bolted web connection (HBS-B) shown in Fig. 8a and the post Northridge WUF-B (WUF-B w/HBS). Yield moments and plastic moments for connections with HBS were calculated by extrapolating (to the column face) the cross-section yield and plastic moments from the heat-treated beam section nearest to the column face.

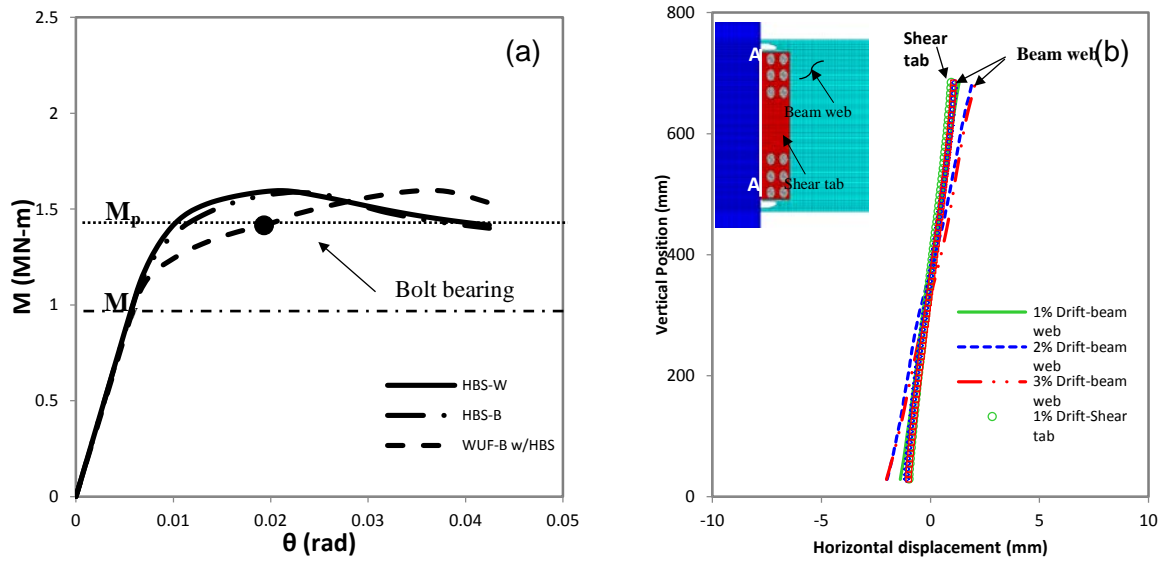


Fig. 12. Comparison of finite element monotonic response prediction for HBS-W, HBS-B and WUF-B w/HBS (a) moment-rotation responses (b) Horizontal nodal displacements on the vertical edge of the beam web adjacent to the column flange (along line A-A) and horizontal displacements of the adjacent nodes on the shear tab for WUF-B connection

All connections share the same member size, geometry and boundary conditions as those previously analyzed (see section 3). From fig. 12a, benefits obtained from both the HBS and the modified bolt detail are evident. Firstly, by reducing connection moment demands and promoting yielding in the HBS, connection strength appears to be less sensitive to the web connection detail i.e. all connections exhibit linear behavior to their calculated yield moments and all surpass their calculated plastic moment.

However, in a comparable (yet less pronounced) manner to the previously studied WUF-B, the WUF-B w/HBS connection exhibits low post yield stiffness as a result of substantial bolt slippage. The modified bolt design (HBS-B) significantly improves connection post yield stiffness although it displays slightly lower post yield stiffness than the all welded connection (HBS-W). This is as a result of very small amounts of bolt slippage

(less than 2mm) see fig. 12b, observed during this analysis. While the effect of this slippage is noticeable, as will be demonstrated later, it does not appear to have a considerable effect on the global or local connection behavior and connection resilience. This bolt slippage is plotted in the same manner (for the HBS-B connection) as was described previously for the WUF-B connection in Fig. 9b. This figure shows that between story drift angles of 0.01 radians and 0.02 radians there is small but noticeable slippage (approximately 1.9 mm at the top and bottom of the web), however, this slippage does not increase as loading progress from 0.02 to 0.03 radians. As a result, throughout the load history web moments and shear forces were transferred by friction as bolts were not observed to bear against the holes of the beam web and shear tab.

4.2.2 Local responses of enhanced WUF-B connection

As mentioned previously the modified bolt design provides a stiffener web connection and as a result, is capable of developing beam web bending moments leading to significant reduction of bending stress redistribution to the beam flanges. This is illustrated in Fig. 13a where the bending (longitudinal) stress acting on the beam flange at the access hole location (as shown in the figure inset) are plotted and compared for a connection with the traditional bolt design (i.e. post Northridge WUF-B, Fig.1a), the modified bolt design fig. 9a and the all welded design. In all connections, forces were applied at the beam tip to produce a moment equal to half the yield moment of the beam section at the column face. By doing this, all connections remained elastic and were subjected to the same shear forces and bending moments. As shown in the figure, the modified bolt design not only lowers the

flange stresses (when compared to the traditional bolt design) but also lowers the stress gradients across the flange width.

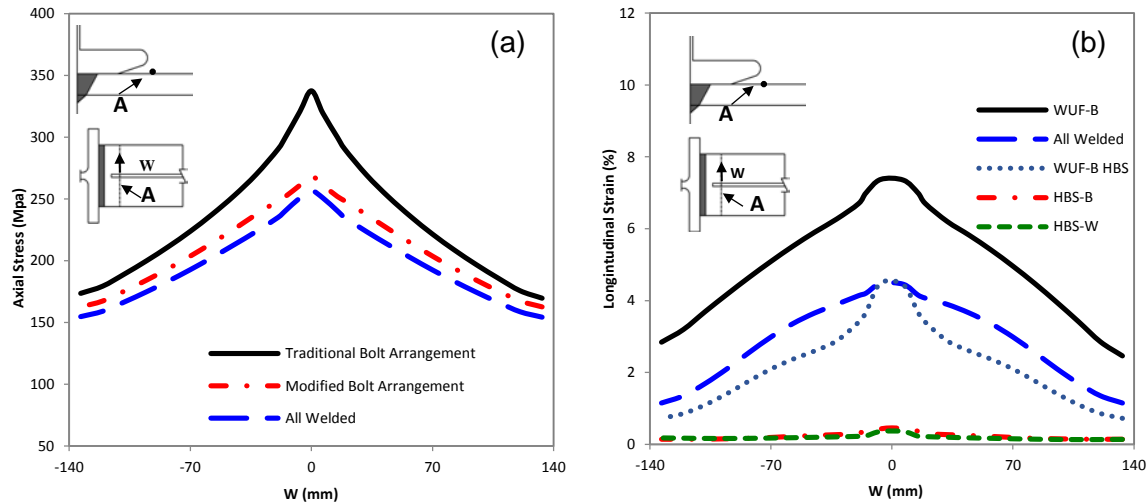


Fig. 13. Stress and strain acting on beam flange at the access hole location under monotonic loading (a) longitudinal stress acting on beam flange at access hole location. Beam tip forces applied to produce a bending moment equal to half M_y at the column face (b) Longitudinal strains across beam flange at 0.03 radians story drift

The combination of the improved bolt design with the HBS significantly reduces strain demands in the access hole region during loading at large rotations. This is illustrated in Fig. 13b where axial strains (at 0.03 rads story drift) along the width of the beam flange at the bottom flange access hole are plotted. Strains are plotted and compared for all the connections so far studied. This comparison highlights again the enhancements gained from the HBS and the modified bolt design.

The effect of the HBS can be seen by comparing the strain distribution of the WUF-B with that of the WUF-B w/HBS and by comparing the strain distribution of the all welded connection with the HBS-W. In these two cases the web connection detail is identical and the only parameter change is the HBS. In both cases the strain demands are reduced. The effect of the web connection detail can be seen in Fig. 13b by comparing the strain distribution of the WUF-B w/HBS with that of the HBS-B and by comparing the WUF-B to the all welded connection. In these two cases the only parameter change is the web attachment detail. In both cases it is observed that strain demands are reduced with an appropriately designed web connection that limits stress redistribution to the beam flanges.

From Fig. 13b it becomes clear that significant strain reductions are only obtained by utilizing an “overstress or overstrain” mitigation measure such as the HBS with a web connection detail capable of transferring web bending moments and shear forces. When these two techniques are combined, large strain concentrations in the access hole region are reduced and large deformations from yielding and buckling are shifted away from the connection region. The later of these two assertions is illustrated in Fig. 14 where the equivalent plastic strain contours are plotted and compared for the WUF-B (Fig. 14a) and the HBS-B (Fig. 14b) at a story drift angle of 0.04 radians. Note from the figure how the inelastic rotation demands are accommodated in both connections. In the case of the WUF-B, yielding and buckling is localized near to the connection joint while in the HBS-B, the majority of yielding and buckling is shifted away from the connection to the HBS region where widespread yielding is promoted. This leads to lower strain demands which are evident by comparing plastic strains magnitudes in Figs. 14a and 14b.

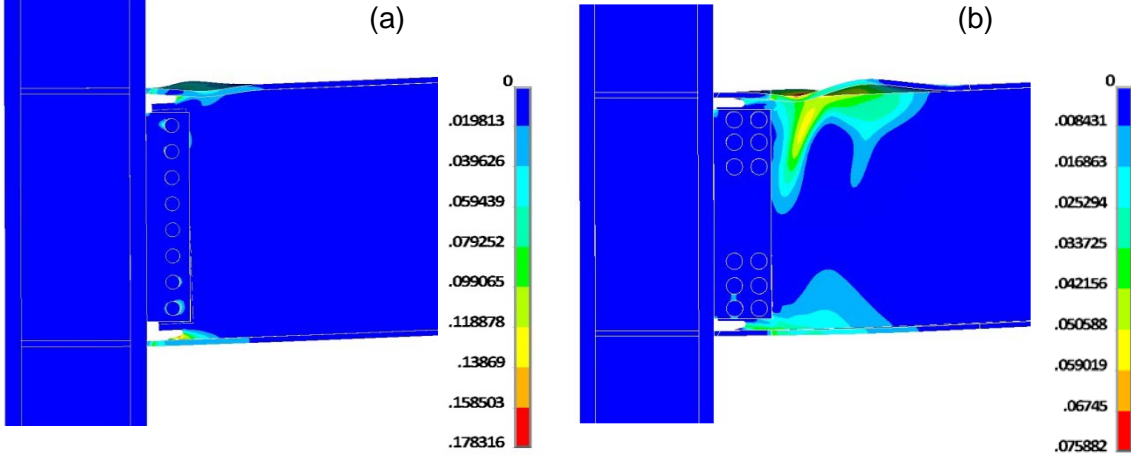


Fig. 14. Finite element analysis of WUF-B and HBS-B connections a) equivalent plastic strain solution of WUF-B at 0.04 radians story drift b) equivalent plastic strain solution of HBS-B at 0.04 radians story drift

4.2.3 Cyclic Analysis of enhanced WUF-B connection

Despite the promise shown by the enhanced HBS-B connection under monotonic loading FE simulations, the proposed connection was further evaluated under cyclic loading for ULCF failure potential. Cyclic loading was prescribed according to the AISC seismic provision loading protocol [57] and sub-modelling along with the CVGM used to assess the potential for ULCF failure in the weld access hole and weld toe region. The moment rotation response prediction is shown in Fig. 15a while the evolution of void growth indices (for the CVGM) which were calculated from stress and strain data extracted from the submodel is shown in Fig. 15b. The location at which the void growth indices are plotted was one of several locations evaluated. However this location found to have the largest “void growth” demands throughout the loading history.

The moment rotation response shows that connections exceeds the calculated plastic moment and display gradual strength degradation due to local buckling in the plastic hinge initiating during the second loading cycle at 2% drift. The void growth indices show that due to the large reduction in strain demands in the access hole region ULCF failure is not predicted. Based upon these results large scale experiments were performed to validate the proposed connection as described in the following.

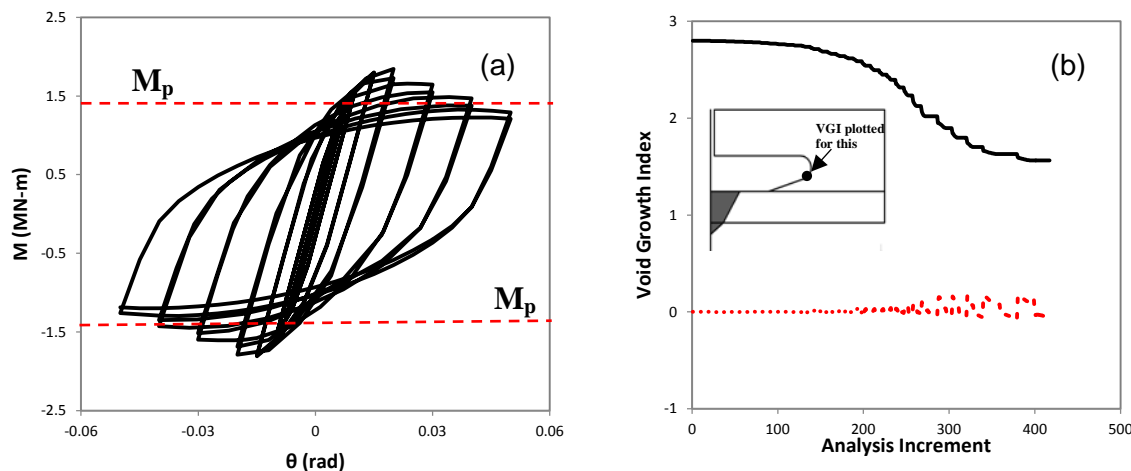


Fig. 15. Cyclic FE analysis of HBS-B (a) Moment rotation response prediction (b) Void growth indices for CVGM failure prediction

5. Experimental Validation

5.1. Connection Design and Experimental Setup

One large scale specimen (HBS 6) was tested to evaluate the proposed performance enhancing modifications. Upon completion of beam fabrication, heat-treatment was performed using electrical resistance ceramic mat heating pads as shown in Fig.16a. Heating

pads were sized according to the required dimensions of the HBS and were installed on the inner and outer surface of the beam flanges. The heating pads were connected to a power supply and type K thermocouples were used to monitor temperatures and provide continuous feed back to the power supply. Three (3) layers of 50 mm (2 inch) high density ceramic fiber insulation blankets were wrapped around the beam flanges as shown in fig. 16b to provide well controlled heating and cooling. More details about the heat-treatment setup and procedure are provided in Morrison et al. 2014 [25].

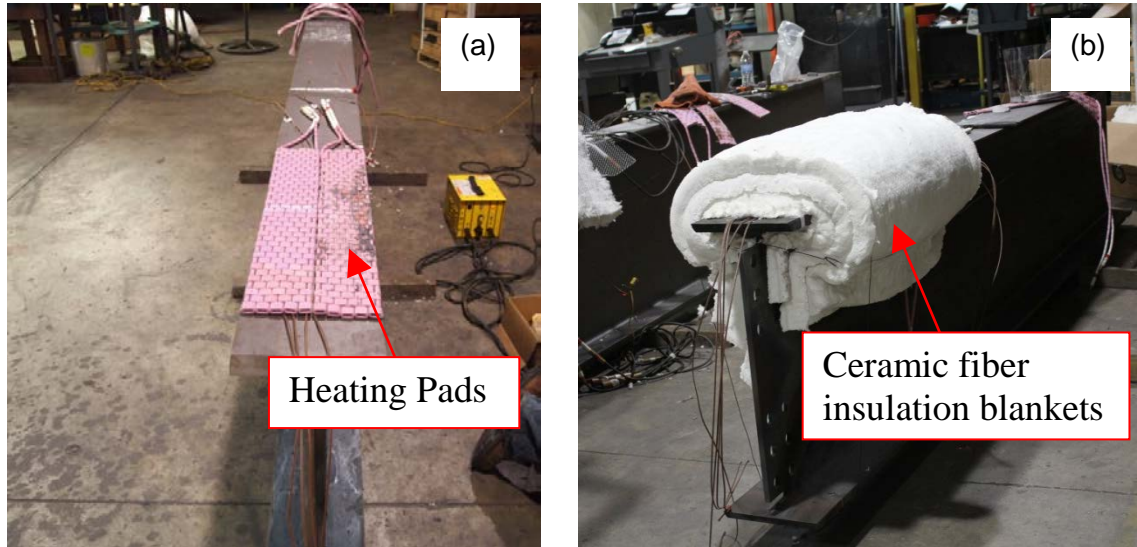


Fig. 16. Heat-treatment setup (a) photograph showing electric surface heating pads during installation on a beam flange, (b) photograph showing insulation of beam flange for well controlled heating and cooling

The test setup, instrumentation and details of the test specimen are shown in Figs. 17a and 17b and the photograph shown in fig 17c and 17d. The member lengths were chosen to be similar to those used in other experimental studies [12]. Connection welding was

performed outdoors with the column oriented vertically by a welder qualified in accordance with the requirements of AWS D1.1-10 and AWS D1.8-09. Bolts were installed and tightened to be “snug tight” prior to welding of the beam flanges. This was done to reduce restraint to thermally induced expansion and contraction during welding so as to minimize welding induced residual stresses. Welding was accomplished with self-shielded flux cored arc welding (FCAW) process. E70-T6 electrodes were used for beam flange welds, while E71-T8 electrodes were used for the bottom and top flange reinforcing welds. Both of these electrodes were specified by the manufacturer to deposit metal with a minimum Charpy V-notch toughness of 27 J (20 ft.-lbs.) at -28 °C (-20°F) .

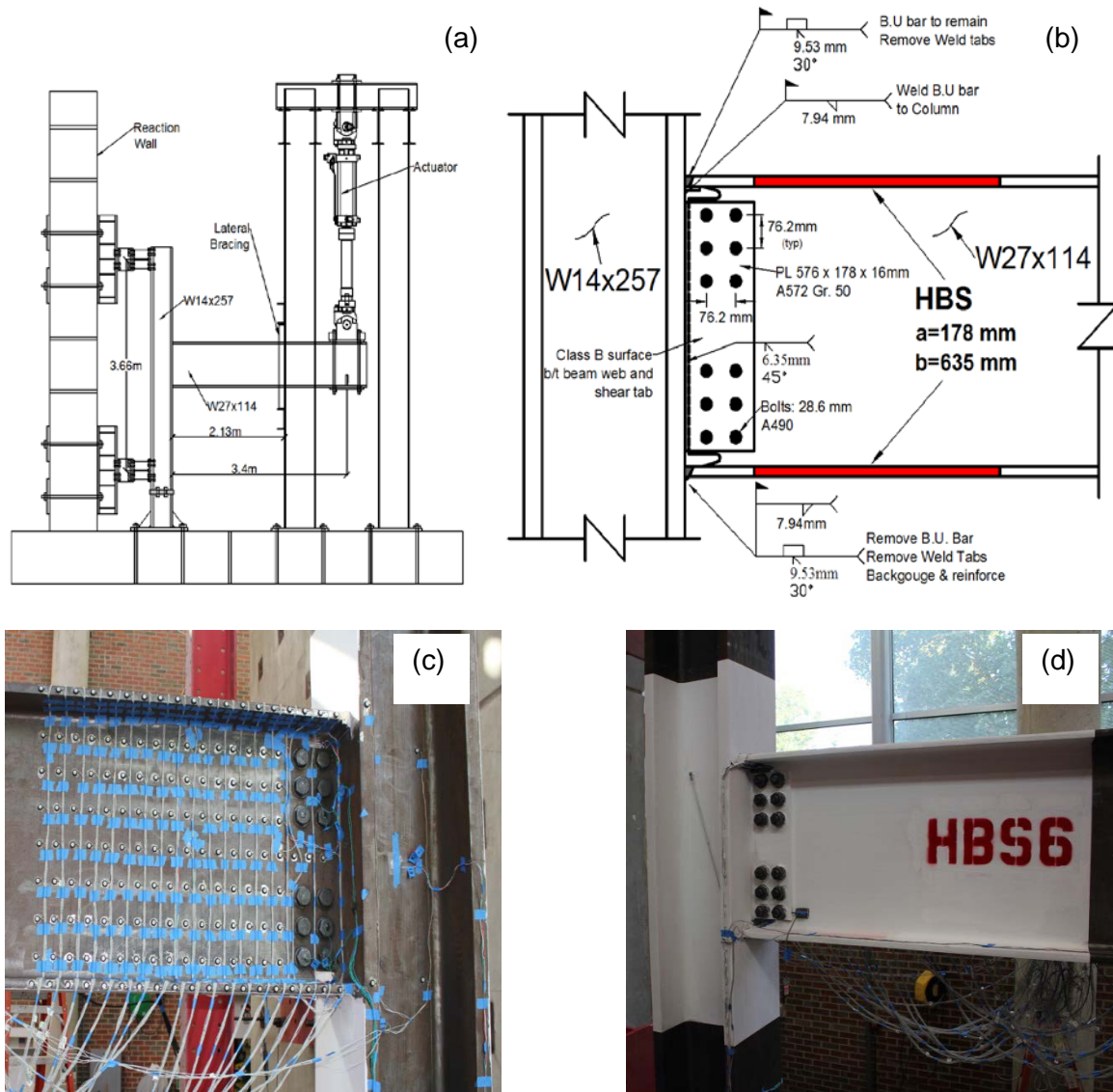


Fig. 17. HBS 6 test setup, connection details and instrumentation a) sketch of test setup, b) sketch of connection details, c) LED markers placed on beam web and the sides of beam top and bottom flanges and, d) photograph of HBS 6 connection prior to testing

After the flange CJP welds were completed, the bottom flange backing bar was removed and a reinforcing weld was placed at the root of the groove weld. The top flange backing bar was left in place, however a fillet weld was provided between the backing bar

and the column flange. The bottom flange backing bar as well as weld tabs from the top and bottom beam flange groove welds were removed by carbon air arc gouging.

After welding, bolts were ‘tightened’ using the turn-of-nut method. The turn-of-nut procedure was first verified by tightening bolts from the same batch of those used in the test specimen in a Skidmore Wilhelm bolt tension calibrator to the minimum pretension specified by the AISC LRFD Specification [35].

5.2 Instrumentation

The test specimen was equipped with strain gauges along the beam flanges to monitor longitudinal flange strains, at various locations including the weld toe and HBS region. String and linear potentiometers were used to monitor displacements and rotations in the column, beam and panel zone. A calibrated load cell in the hydraulic actuator provided readings of force response during the experiment.

Bolt response was of interest; as such, two of the 12 bolts were instrumented by installing a strain gauge in the center of the unthreaded portion of the bolt shank. The Optotak Certus HD three-dimensional (3D) position system was used to capture the positions of markers placed along the beam flanges and web as shown in fig. 17c. Two Optotak cameras were used which were able to capture the motion of markers placed on the top and sides of the beam top flange, the beam web and the side of the beam bottom flange. Position time history data obtained from this system was post processed to calculate displacements and strains in areas of interest. The Optotak system provides the advantage of being able to record large cyclic inelastic strains while electrical resistance strain gages may either exhibit gradual strain drift or fail to remain adhered

5.3. Test Results

Testing was conducted at the North Carolina State University Constructed Facilities Laboratory (CFL) on an exterior type sub-assemblage (single cantilever). Loads were applied at the beam tip in accordance with the 2010 ANSI/AISC 341 [57] seismic provisions appendix S loading protocol consisting of quasi-static increasing amplitude displacement cycles. Figure 15 shows the moment-rotation response of HBS 6 which displays wide hysteresis loops indicating good energy dissipation. The specimen exceeded the 2010 AISC Seismic Provisions (ANSI/AISC 341-10) [57] SMF qualifying 4% interstory drift angle without significant strength loss. Strength degradation due to local flange, web and lateral torsional buckling initiated during the 2nd cycle of loading at 4% drift (see Figs. 18 and 19b) and continued during later loading cycles. Loading of HBS 6 was terminated during the second cycle of loading at 5% drift due to a fracture in the location of significant flange buckling (see fig.19e and fig. 19f). This failure mechanism was similar to that observed in all welded connections and extended end plate connections enhanced with the HBS [25, 36]. In all three connection types, plastic hinge formation in the HBS was followed by local buckling, strength degradation and fracture in the location of most severe flange buckling.

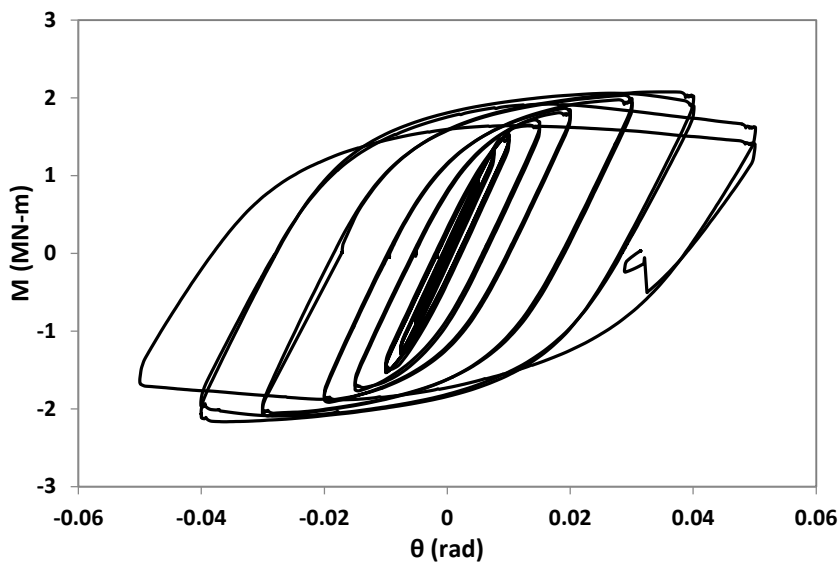


Fig. 18. Moment-rotation response of HBS 6

The response of the HBS 6 is further analyzed by plotting the moment-plastic rotation curves for each component of the connection assembly which were calculated using data measured by instrumentation during the test and equations proposed by Popov et al. [6]. These graphs are shown in Fig. 20. They indicate that inelastic action in the beam accounted for a majority of the total plastic rotation of connection assembly.

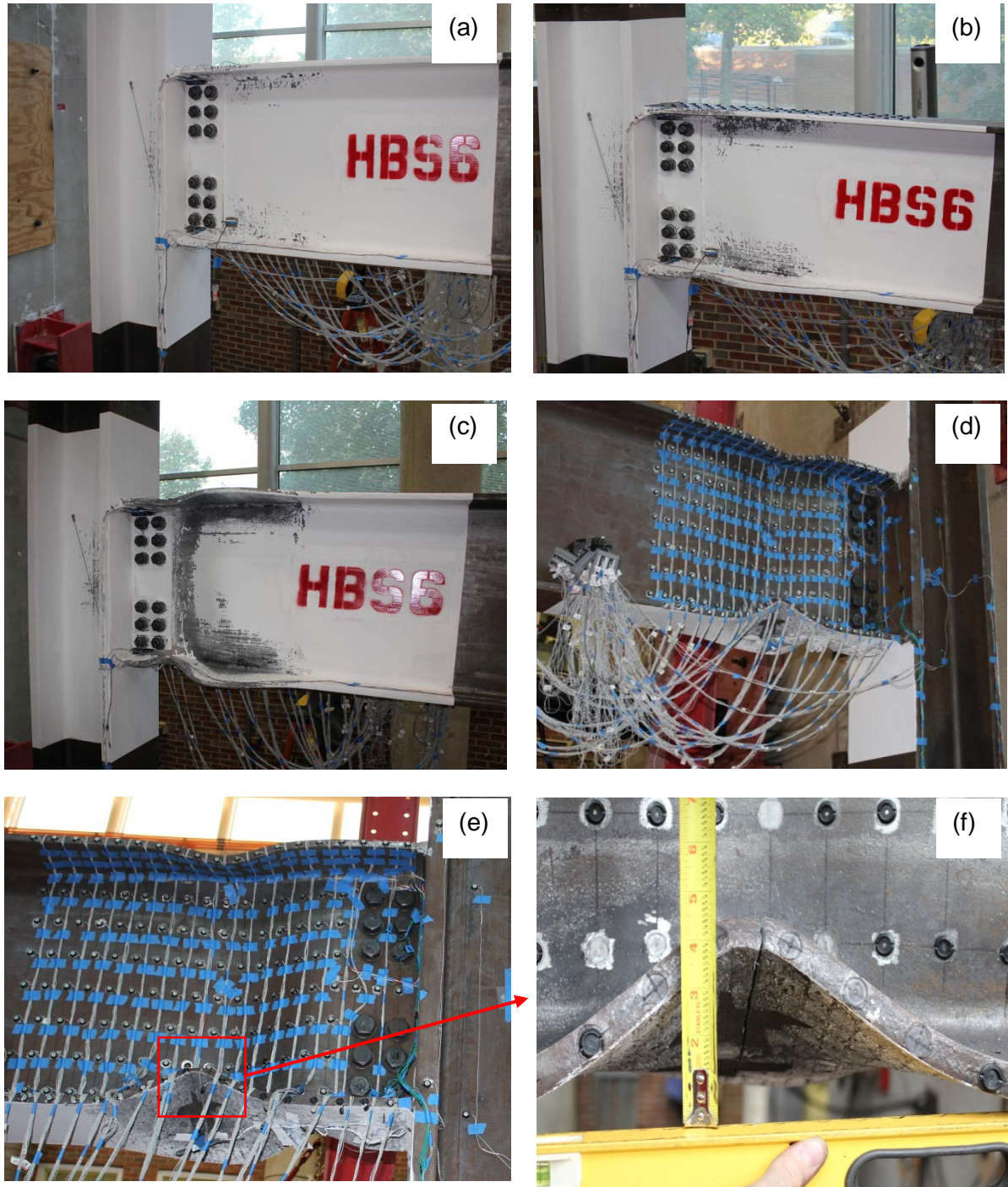


Fig. 19. Yielding, plastic hinge formation and fracture of HBS 6, (a) connection at 3 % drift, (b) connection at 4% drift, (c) connection at 5% drift and, (d) west view of connection at 5% drift showing beam flange buckling (e) fracture of beam flange at 5% drift and (f) close up view of beam flange at location of fracture

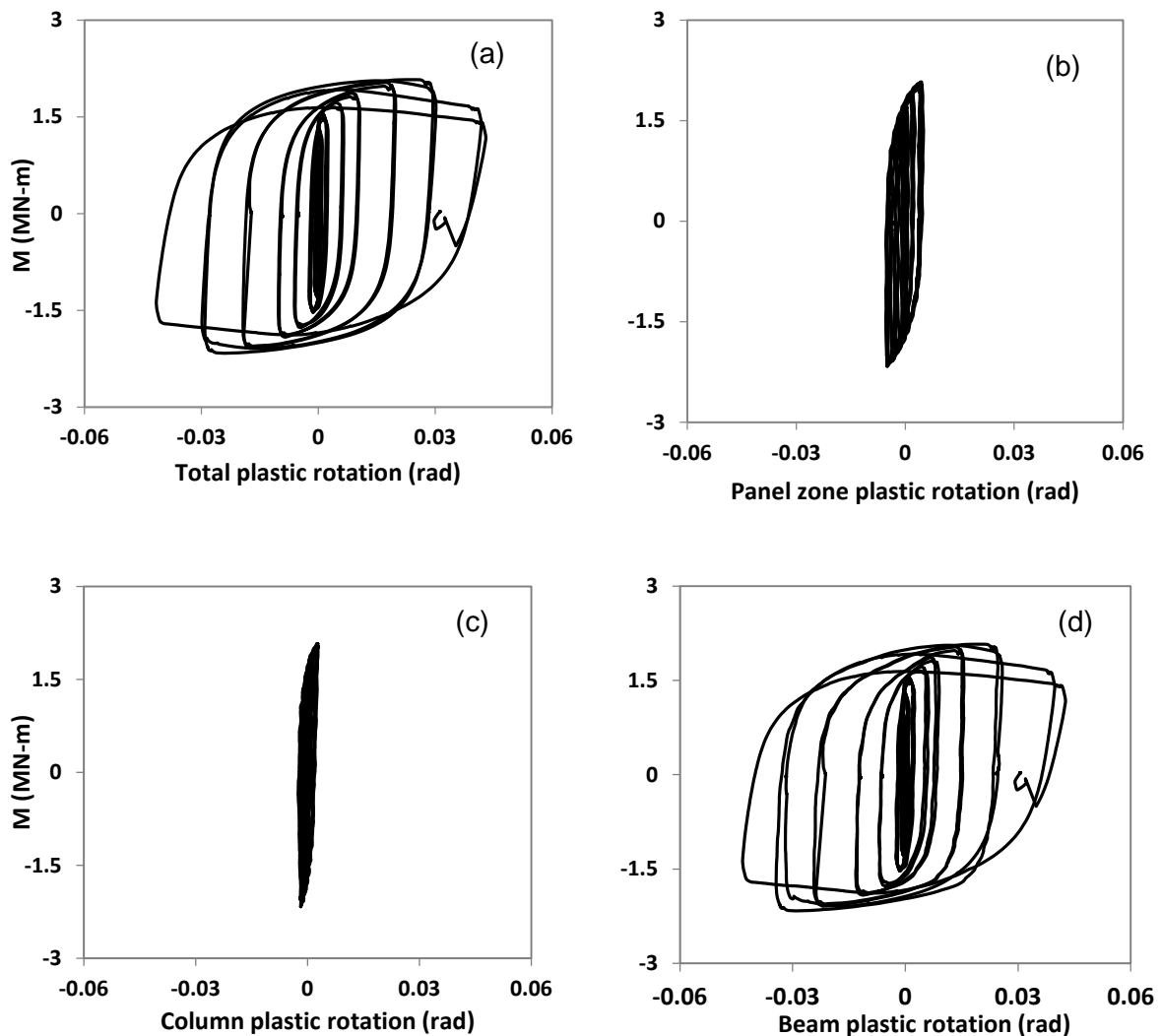


Fig. 20. Plastic rotation contributions by components of HBS 6, (a) total connection plastic rotation, (b) panel zone shear plastic rotation (c) column flexural plastic rotation and, (d) beam plastic rotation

5.4 Plastic hinge formation in the modified WUF-B connection

Figure 21 a-d illustrates the progression of inelastic action along the beam flange via bar graphs in which the distribution of longitudinal tensile strains (normalized by the yield

strain) along the centerline of the beam flange at various stages of the loading history are plotted. Bars highlighted in red represent the strains in the heat-treated (weakened) regions. Strains were calculated by post processing data obtained from 3D noncontact spatial displacement measurement sensors placed along the beam flange.

These plots illustrate the influence of the HBS in promoting majority of the inelastic action away from the beam flange to endplate connection. Similar observations have made in all welded connections modified with HBS [25]. The strain profiles indicate that flexural yielding initiates in the heat-treated areas between 1% and 1.5% story drift. As loading is continued, longitudinal strains increase more in the heat-treated areas than in the unheat-treated regions adjacent to the beam flange to column flange welds. It is important to note that the beam length of 3.4m (134in) used in this test corresponds to a moment frame with a clear span of 6.8m (22 feet). This relatively short span results in a large moment gradient which is reflected in the strain profiles. As drift angles increase from 3% to 4% (see Fig.21c, 21d, 19a and 19b) (longitudinal strain in the heat-treated regions increase significantly while strains outside of the heat-treated areas grow only slightly. This demonstrates that the large displacements imposed at the beam tip are mostly accommodated by flexural deformation in the HBS.

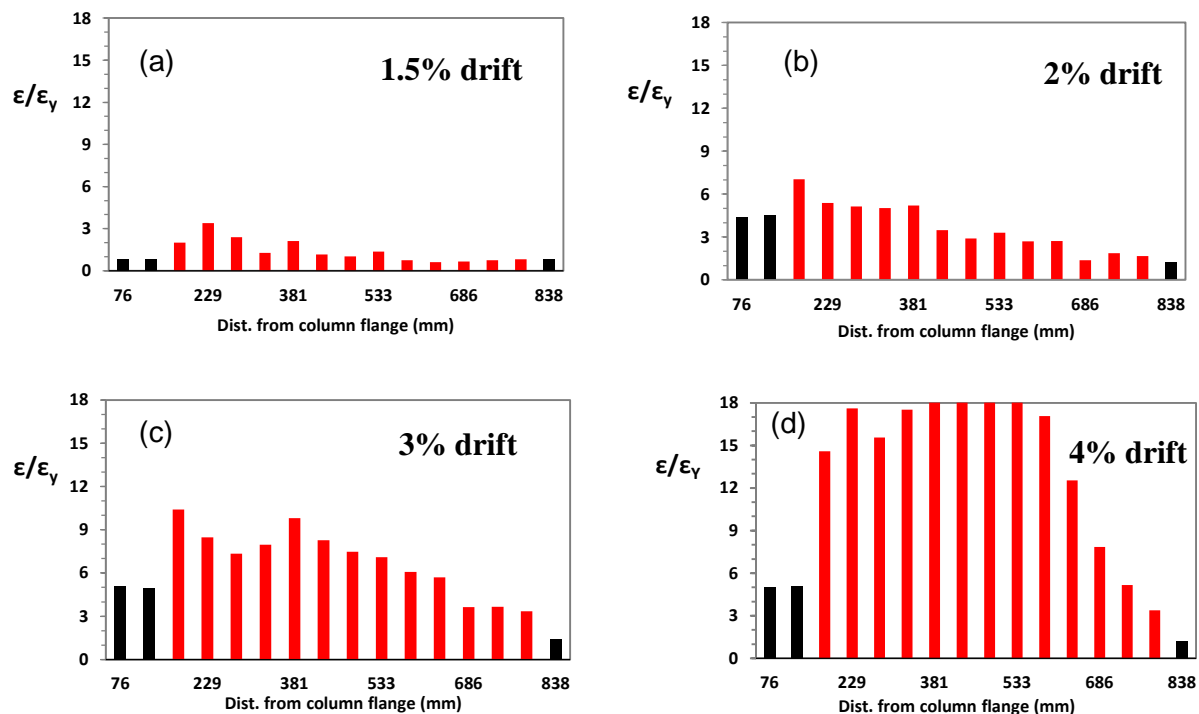


Fig. 21. Recorded longitudinal strains along the center of top flange of the beam from HBS 6.

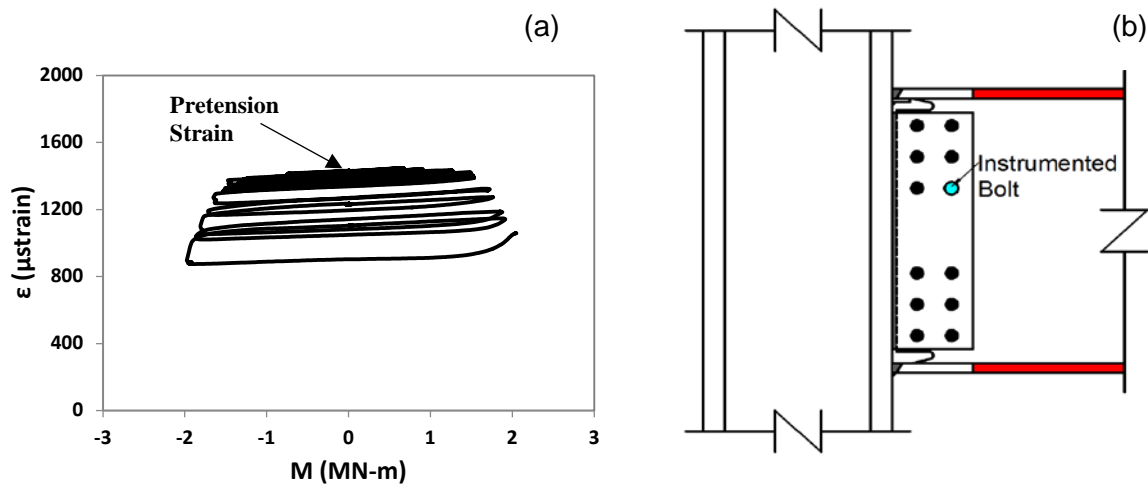


Fig. 22. (a) Recorded axial bolt strain vs column centerline moment (b) Sketch showing location of instrumented bolt

5.5 Bolt response in the modified WUF-B connection

The measured axial bolt strain vs. column centerline bending moment is shown in Fig. 22 for one of the 2 bolts which were instrumented with strain gages. In general bolt axial strain behavior is characterized by a slight increase in strain during positive bending (i.e. top flange in compression) followed by a slight reduction in strain when the loading is reversed. This behavior is a result of the Poisson effect which causes the clamped parts (beam web and shear tab) to expand and contract in the lateral direction. Gradual relaxation of the bolt strains was observed with progressive loading. At the end of testing bolt strains had reduced by approximately 25% of their initial values. This behavior was anticipated based on observations made during pre-test FE analysis and seemed not to be detrimental to connection performance. However, additional research is warranted to better understand and quantify bolt relaxation in slip critical bolt assemblies subjected to cyclic loading in the inelastic range.

6. Future work on modified WUF-B connections

Due to limited resources only one test specimen was evaluated in this study. Future work on the proposed connection needs to be conducted to determine the suitability of this connection over a range of beam and column sizes. More work is also needed to understand the extent to which connecting bolts relax during cyclic loading and large deformations. Given the high cost of full scale testing, detailed numerical analysis (such as those outlined earlier) may provide a good starting point for further evaluation.

7. Conclusion

This study has presented detailed FE analysis and experimental validation of an improved WUF-B moment connection. In addition, detailed FE analysis was used to study the behavior and failure mechanism of post-Northridge WUF-B connections. The following are concluded from the study:

1. FE analysis shows that the post Northridge WUF-B connection displays significant bolt slippage which begins at relatively low story drift angles.
2. This bolt slippage leads to a reduction in connection stiffness and bending stress redistribution near the connection. It is observed that bending stresses developed in the beam web are redistributed to the beam flanges near the connection leading to significantly higher flange stresses than those experienced by all welded connections.
3. Web bolt slippage also leads to increased flange shear, resulting in significant prying of the beam flanges adjacent to the weld access hole.
4. Upon yielding, stress concentrations at the access hole become strain concentrations which may lead to ductile fracture of the beam flanges initiating at the weld access hole.
5. A modified WUF-B connection which combines an improved bolted design originally proposed by Lee and Kim [24], and the recently validated HBS [25] shows significantly improved seismic performance when compared to the post-Northridge WUF-B. FE analysis showed that the combination of these performance enhancement techniques lead to significantly lowered strain demands at the weld access hole and weld toe when compared to the post Northridge WUF-B.

6. The modified WUF-B connection was experimentally validated through full scale testing. The connection displayed ductile response to simulated seismic loading exceeding the 2010 AISC Seismic Provisions (ANSI/AISC 341-10) SMF qualifying 4% interstory drift angle without significant strength loss. No weld or near weld cracks were observed. Instead, fracture occurred in the region of significant flange buckling (in the plastic hinge) during cycles at 5% interstory drift.

Rigorous numerical calculations are in many cases not performed with the notion that the outcomes may not justify the time and efforts. Detailed three dimensional numerical modelling of the WUF-B connection which accounted for bolt pre-stress and contact interactions in the web connection and included the implementation of an advanced constitutive model and CVGM provided important information in exploring failure mechanisms and developing effective yet simple design improvements. Such numerical schemes may reduce the scope on experiments needed in future design code development.

8. References

- [1] Hamburger RO, Krawinkler H, Malley JO, Adan SM. (2009) "Seismic Design of Steel Special Moment Frames: A Guide for Practicing Engineers" NEHRP Seismic Design Technical Briefs: National Institute of Standards and Technology, U.S. Department of Commerce.
- [2] Bruneau, M., Uang, C.M., and Whittaker, A. (1998). *Ductile design of steel structures*. New York: McGraw Hill Companies.
- [3] AISC/ANSI (1992) Seismic Provisions for structural steel buildings, Chicago.
- [4] Popov, E. P., and Stephen, R. M. (1972). "Cyclic loading of full size steel connections." *Bull. No.21* American Iron and Steel Institute (AISI), Washington, D.C.
- [5] Popov, E. P. , Amin, N. R. , Louie, J. , and Stephen, R. M. (1986). "Cyclic behavior of large beam-column assemblies." *Engrg. J. , 23 (1)*, 9–23.

- [6] Popov, Egor P., and K. C. Tsai. "Performance of large seismic steel moment connections under cyclic loads." *Engineering Journal* 26.2 (1989).
- [7] Engelhardt, M. and Husain, A.S., (1993) "Cyclic-Loading Performance of Welded Flange- Bolted Web Connections" *Journal of Structural Engineering*, 119(12), 3537-3550.
- [8] Kaufmann, E.J., Xue, M., Lu, L. and Fisher, J.W., (1996) "Achieving Ductile Behavior of Moment Connections " *Modern Steel Construction June 1996*.
- [9] Popov, E.P., Yang, T., and Chang, S., (1998) "Design of steel MRF connections before and after 1994 Northridge earthquake," *Engineering Structures*, 20(12), 1030-1038.
- [10] Sabol, T.A., Engelhardt, M.D., Aboutaha, R.S., Frank, K.H., "Overview of the AISC Northridge Moment Connection Test Program", in Proceeding of the World Conference on Earthquake Engineering (11WCEE), 1996.
- [11] Kim, T., Stojadinović, B., and Whittaker, A. (2008). "Seismic Performance of Pre-Northridge Welded Steel Moment Connections to Built-Up Box Columns." *J. Struct. Eng.*, 134(2), 289–299
- [12] SAC Joint Venture (2000) "Parametric Tests on Unreinforced Connections Volume 1-Final Report" *Rep. No. SAC/BD-00/01*.
- [13] SAC Joint Venture (2000) "Dynamic Tension Tests of Simulated Welded Beam Flange Connections" *Rep. No. SAC/BD-00/07*.
- [14] Stojadinovic, B., Subhash C.G., Lee, K-H, Margarian, A.G., and Choi, J-H (2000), "Parametric Tests on Unreinforced Steel Moment Connections," *Journal of Structural Engineering*, Vol. 126, pp. 40-49.
- [15] Chen, C.C., Chen S. W., Chung M. D. and Lin M. C. (2005) "Cyclic behaviour of unreinforced and rib-reinforced moment connections." *Journal of Constructional Steel Research* 61.1:1-21.
- [16] Han, S.W., Kwon, G.U., & Moon, K.H., (2007), "Cyclic Behavior of Post-Northridge WUF-B connections," *Journal of Constructional Steel Research*, 63, pp. 365-374.
- [17] Iwankiw, N. R. and Carter, C. J. "The Dogbone: A New Idea to Chew On." *Modern Steel Construction*. April 1996. pp. 18-23.
- [18] SAC Joint Venture (2000) "Behavior and Design of Radius Cut Reduced Beam Section Connections" *Rep. No. SAC/BD-00/17*.

- [19] Lee, C., Jeon, S., Kim, J., and Uang, C. (2005). "Effects of Panel Zone Strength and Beam Web Connection Method on Seismic Performance of Reduced Beam Section Steel Moment Connections." *J. Struct. Eng.*, 131(12), 1854–1865.
- [20] Krawinkler, Helmut, and Egor P. Popov. "Seismic behavior of moment connections and joints." *Journal of the Structural Division* 108.2 (1982): 373-391.
- [21] SAC Joint Venture (2000) "Development and Evaluation of Improved details for Ductile Welded Unreinforced Flange Connections" *Rep. No. SAC/BD-00/24*.
- [22] Engelhardt, M. D. and Sabol, T. A. (1997), Seismic-resistant steel moment connections: developments since the 1994 Northridge earthquake. *Prog. Struct. Engng Mater.*, 1: 68–77.
- [23] Kanvinde, A. M., and G. G. Deierlein. "Cyclic void growth model to assess ductile fracture initiation in structural steels due to ultra-low cycle fatigue." *Journal of engineering mechanics* 133.6 (2007): 701-712.
- [24] Lee, Cheol-Ho, and Jae-Hoon Kim. "Seismic design of reduced beam section steel moment connections with bolted web attachment." *Journal of Constructional Steel Research* 63.4 (2007): 522-531.
- [25] Morrison, M.L., Schweizer, D.Q., Hassan, T., (2014) "An Innovative Seismic Performance Enhancement Technique for Steel Building Moment Resisting Connections." *Submitted to Journal of Constructional Steel Research*
- [26] Mao, Changshi, et al. "Effect of local details on ductility of welded moment connections." *Journal of Structural engineering* 127.9 (2001): 1036-1044.
- [27] Richard, R.M., Partridge, J.E., Allen, J., "Finite Element Analyses and Tests of Beam-To- Column Connections", Modern Steel Construction, AISC, October 1995.
- [28] SAC Joint Venture (1998) "Strength and Ductility of FR Welded-Bolted Connections" *Rep. No. SAC/BD-98/01*
- [29] SAC Joint Venture (1997) "Finite Element Fracture Mechanics Investigation of Welded Beam-Column Connections" *Rep. No. SAC/BD-97/05*
- [30] Hajjar, Jerome F., et al. "Seismic response of composite moment-resisting connections. II: Behavior." *Journal of Structural Engineering* 124.8 (1998): 877-885.
- [31] ANSYS® Academic Research, Release 14.5, Help System, Structural Analysis Guide, ANSYS, Inc.

- [32] Kaufmann, E. J., Metrovich, B., & Pense, A. W. (2001). Characterization of Cyclic Inelastic Strain Behavior on Properties of A572 Gr. 50 and A913 Gr. 50 Rolled Sections: *Final Report to American Institute of Steel Construction*. Lehigh University.
- [33] RCSC. Specification for Structural Joints Using High-Strength Bolts,(2009). Chicago, IL.
- [34] Polyzois, D. and K.H. Frank, 1986, "Effect of Overspray and Incomplete Masking of Faying Surfaces on the Slip Resistance of Bolted Connections," *Engineering Journal*, Vol. 23, No. 2, (2nd Qtr), AISC, Chicago, IL.
- [35] AISC. Manual of steel construction load and resistance factor design. 13th ed. Chicago, IL, 2006.
- [36] Quayyum, S., " Advanced Finite Element Anlyses of Moment Resisting Connections for Improving Seismic Performance and Exploring Effects of Residual Stress and Fire Damage" Ph.D. Dissertation, North Carolina State University, Raleigh, NC 2014.
- [37] Kiamanesh R, Abolmaali A, Razavi M. Effect of circular bolt pattern on behavior of extended end-plate connection. *Journal of Structural Engineering* 2012; 139.11:1833-1841.
- [38] Swanson, J. A. , Kokan, D. S. , and Leon, R. T. (2002). "Advanced finite element modelling of bolted T-stub connection components." *J. Constr. Steel Res.* , **58** (5–8), 1015–1031
- [39] Rahman, A., Mahamid, M., Amro, A., & Ghorbanpoor, A. (2007). The analyses of extended shear tab steel connections-Part I: The unstiffened connections. *Engineering Journal*, 44(2), 117-132.
- [40] Chaboche, J. L. (1986) Time-independent constitutive theories for cyclic plasticity, *International Journal of Plasticity* Vol. 2, No. 2 pp. 149- 188.
- [41] ASTM A6 / A6M-14, Standard Specification for General Requirements for Rolled Structural Steel Bars, Plates, Shapes, and Sheet Piling, ASTM International, West Conshohocken, PA, 2014.
- [42] Castiglioni, C. (2005). "Effects of the Loading History on the Local Buckling Behavior and Failure Mode of Welded Beam-to-Column Joints in Moment-Resisting Steel Frames." *J. Eng. Mech.* 131, SPECIAL ISSUE: ADVANCES IN THE STABILITY OF FRAMED STRUCTURES, 568–585.
- [43] SAC Joint Venture (1999) "Local and Lateral-Torsion Buckling of Wide Flange Beams" Rep. No. SAC/BD-99/20

- [44] Ricles, J., Zhang, X., Lu, L.W., and J. Fisher, (2004). "Development of Seismic Guidelines for Deep-Column Steel Moment Connections," *ATLSS Report No. 04-13*, ATLSS Engineering Research Center, Lehigh University, Bethlehem, PA.
- [45] Myers A, "Testing and probabilistic simulation of ductile fracture initiation in structural steel components and weldments" Ph.D. Dissertation Stanford University; May 2009.
- [46] Kanvinde, A. and Deierlein, G. (2008). "Validation of Cyclic Void Growth Model for Fracture Initiation in Blunt Notch and Dogbone Steel Specimens." *J. Struct. Eng.*, 134(9), 1528–1537
- [47] Kanvinde, A. M. , and Deierlein, G. G. (2007b). "Finite-element simulation of ductile fracture in reduced section pull plates using micromechanics fracture models." *J. Struct. Eng.*, 133 (5), 656–664
- [48] Kanvinde, A. M. , and Deierlein, G. G. (2004). "Micromechanical simulation of earthquake induced fracture in steel structures." *Technical Rep. No. 145*, John A. Blume Earthquake Engineering Center, Stanford Univ., Stanford, Calif.
- [49] Myers, A., Kanvinde, A., Deierlein, G., and Baker, J. (2014). "Probabilistic Formulation of the Cyclic Void Growth Model to Predict Ultralow Cycle Fatigue in Structural Steel." *J. Eng. Mech.*, 140(6), 04014028
- [50] Amiri, H. R., et al. "Finite element simulation of ultra low cycle fatigue cracking in steel structures." *Journal of Constructional Steel Research* 89 (2013): 175-184.
- [51] Rice, J. R., and Tracey, D. M. _1969_. "On the ductile enlargement of voids in triaxial stress fields." *J. Mech. Phys. Solids*, 17_3_, 201–217.
- [52] Huang, Yong-hui, et al. "Finite element analysis and experimental study on high strength bolted friction grip connections in steel bridges." *Journal of Constructional Steel Research* 66.6 (2010): 803-815.
- [53] Goel, S. C., Stojadinovic, B., and Lee, H. K. (1997). "Truss analogy for steel moment connections." *Eng. J.*, Second Quarter, 43–53.
- [54] Richard, Ralph M., C. Jay Allen, and J. E. Partridge. "Proprietary slotted beam connection designs." *Modern Steel Construction* (1997): 28-33.
- [55] SAC Joint Venture (2000) "Parametric Tests on the Free Flange Connections" *Rep. No. SAC/BD-00/02*.

[56] Salmon, Charles G., John E. Johnson, and Faris Malhas. *Steel Structures Design and Behavior (5th Edition)*. Upper Saddle River: Prentice Hall, 2007. Print.

[57] AISC/ANSI 341-10 (2010) Seismic Provisions for structural steel buildings, Chicago.

CHAPTER 7: Resilient Welded Steel Moment Connections (WSMC) by Enhanced Beam Buckling Resistance

Abstract

This study develops a simple but effective technique for enhancing buckling resistance of welded steel moment connections (WSMCs). The ANSI/AISC 358-10 prequalified connections satisfy the 4% interstory drift requirement, however their strength degradation may *initiate* as early as 3% drift. In several laboratory tests, this strength degradation has been observed to be initiated by buckling of the beam web which is followed by buckling of the beam flange. Once the strength degradation initiates it propagates quickly with continued incremental cycles. By 4% interstory drift, the local beam web and flange buckling damages in the plastic hinge region become significant. Consequently, buildings with the prequalified connections may sustain significant buckling damages under severe earthquakes and it is questionable as to whether these connections are capable of resisting gravity loads or lateral loads from strong aftershocks following a severe earthquake. To improve upon these drawbacks, two performance enhancing techniques are proposed and investigated through finite element analysis (FEA). The more promising of the two is a novel technique called *web stiffener*. Finite element analysis demonstrated that web stiffener enhances the beam buckling resistance of WSMCs and thereby significantly reduces the beam buckling damages even at 5% interstory drift. The potential of the technique is analytically and experimentally demonstrated for the recently developed heat-treated beam section (HBS) WSMCs. Results and detailed analysis of experimental data from full scale experimental testing to validate the WS technique is presented. Test results confirm that the WS was effective in reducing local

buckling damage in the plastic hinge and the associated strength degradation, thereby improving the energy dissipation of WSMCs. Areas for application and future development of the technique are identified.

Keywords: Steel moment connection; seismic performance enhancement; beam plastic hinge; heat-treated beam section; web stiffener

1. Introduction

More than a decade of research activities after the Northridge and Kobe earthquakes has developed modified designs of welded steel moment connections (WSMCs) with improved ductility [1,2,3]. By eliminating premature weld or near weld failures the current moment connections prequalified for special and intermediate moment frames (SMF and IMF) by the ANSI/AISC 358-10 [4] have demonstrated, the ability to attain at least 4% interstory drift while sustaining 80% of the nominal flexural strength M_p . In the ANSI/AISC 314-10 [5], it is noted that while connection qualification emphasizes the level of plastic rotation attainable, the tendency for connections to experience strength degradation is of concern as this strength degradation can increase rotational demands from P-delta effects and adversely affect frame stability.

In reported studies [6-10], prequalified connections such as the welded unreinforced flange-welded web (WUF-W), reduced beam section (RBS), extended end plate (EEP), bolted flange plate (BFP) and Kaiser bolted bracket (KBB) experience severe strength loss due to beam buckling prior to the termination of loading. Due to this rapid strength loss, it is

questionable as to whether these connections are capable of resisting gravity loads or strong aftershocks following a severe earthquake. Figure 1 shows examples of this buckling damage occurring in RBS (with concrete slab), EEP and KBB connections.

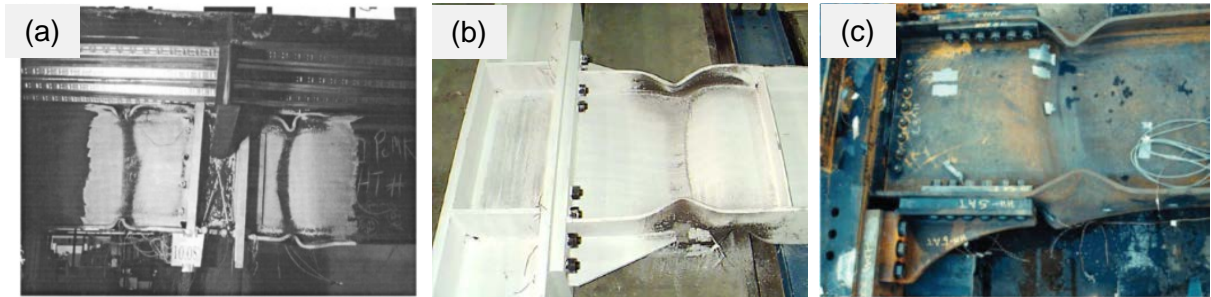


Fig. 1. Web and flange buckling in the plastic hinge region, a) RBS w/concrete floor slab [Jones et. al. [7]] b) eight bolted stiffened EEP [8], c) KBB [10].

Research efforts on the seismic performance of WSMCs have mainly been focused on circumventing weld or near weld failures which limit the attainable plastic rotation of these connections. However some research has been conducted on beam buckling failures and the associated strength loss. The following is a brief review of the findings of research studies conducted to either improve understanding of the local buckling failure modes of beam to column moment connections or to prescribe and evaluate techniques to improve the resistance of WSMCs to such failures.

Kwasniewski et al. [11] conducted nonlinear finite element analysis (FEA) to examine the effect of various geometric parameters on local and lateral torsional buckling of beams in moment resisting frames under monotonic loading. This study found that the effect

of beam web and flange slenderness on plastic rotation capacity was moderate. The effect of the number and location of lateral braces was also found to be small. Axial restraint of beam deformation from the columns in a frame system was found to be ineffective in delaying the onset of strength degradation but did reduce the rate of strength degradation. In connections with reduced beam sections (RBS) the onset of strength degradation was found to take place slightly earlier than unreduced sections.

Yu et al. [12] collected experimental data of the local buckling modes that result in strength loss in RBS connections. Results from their test of an all welded RBS connection with a W30x99 beam connected to a W14x176 column are shown in Fig. 2. It is noted here that although trimming of the beam flange improves the compactness of the beam flange in the reduced section, it increases the likelihood of web local and lateral torsional buckling (WLB and LTB) by reducing flange stiffness and consequently the lateral restraint provided to the ‘slender’ web. Accordingly, in Fig. 2 it can be observed that WLB and LTB initiate during cycles at 2% drift while FLB initiates during cycles at 4% drift. During cycles at 4% drift all three buckling modes increase rapidly leading to substantial strength loss shown in Fig. 2a and severe deformations in the beam plastic hinge shown in Fig. 2b.

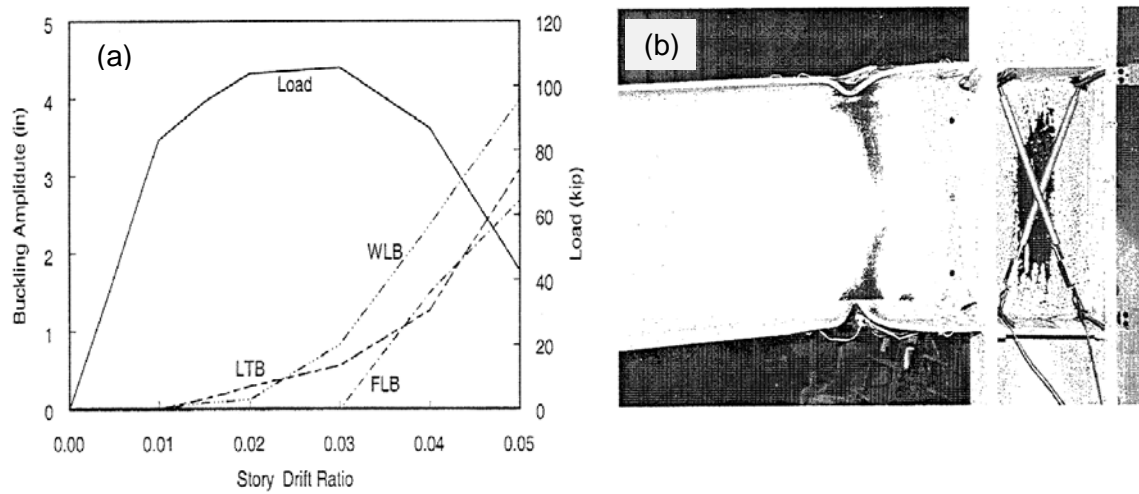


Fig. 2. Beam buckling of RBS connection, (a) Web local buckling (WLB), lateral torsional buckling (LTB) and flange local buckling (FLB), and strength degradation at 3% interstory drift, (b) buckling damage in the RBS at 0.03 radians plastic rotation [SAC/BD-99/19, Uang and Fan [14]].

Yu et al. [12] also evaluated the effect of near fault loading history and additional lateral bracing on the response of RBS moment connections through full scale experiments. Their results showed that specimens tested with near fault loading histories experienced smaller buckling amplitudes at comparable drift levels than those experienced by specimens tested with the standard loading protocol in the ANSI/AISC 341-10 Seismic provisions [5]. The study also showed that additional bracing near the RBS region did not delay the onset of strength degradation but did slow the rate of strength degradation. Finally, finite element analysis reported in this study showed that the axial restraining effects from the columns in a frame system can also reduce strength degradation rates for RBS moment connections confirming the earlier findings of Kwasniewski et al. [11].

Uang and Fan [13, 14] performed nonlinear regression based on the test results of 55 full-scale RBS moment connections. The study showed that despite the significant reduction in the torsional properties at the reduced section, the response quantities of interest (plastic rotation and strength degradation rate) were sensitive to the non-dimensional web slenderness parameter (λ_w) but not to the corresponding parameter for LTB (λ_L). As a result, a limiting web slenderness of $1100/\sqrt{F_y}$, (where F_y is the yield stress in MPa) was recommended for seismic design of RBS beams in moment frames. The study also showed that the concrete slab increases plastic rotation capacity under positive bending but not under negative bending.

Okazaki et al. [15] combined FEA with the nonlinear regression techniques used by Uang and Fan [13,14] to study lateral torsional and local buckling of beams subjected to cyclic loads. The results of the study showed there to be interaction between both flange and web slenderness parameters on the strength loss of moment connections due to buckling. The study also found that the stability requirements of the AISC 341-05 seismic provisions were adequate to maintain 80% of the nominal beam plastic moment (Mp) at a story drift of 0.04 rad.

Some attempts have also been made to delay the onset and slow the rate of strength degradation due to buckling by reinforcing the beam in the anticipated plastic hinge region with longitudinal web stiffeners. Kim et al. [16] identified web local buckling as a trigger for strength degradation in their cyclic tests of welded cover plate connections. As a result, they tested one welded cover plate specimen in which two pairs of horizontal stiffeners were

attached to the beam web approximately one quarter of the beam depth from the top and bottom flanges. These stiffeners were welded to the beam web in the expected plastic hinge region and were designed to delay the onset of strength degradation rather than increase the strength of the connection. Test results show that the stiffeners did not delay the onset of strength degradation but did slow the rate of strength loss with increasing plastic rotation. Reduction of web slenderness limits for beams designed for seismic use was recommended based on these observations.

Wang et al. [17] also used horizontal web stiffeners on welded flange-welded web built up non compact beams to delay the onset of strength degradation due to buckling. These stiffeners were welded to the beam web and column flange in the anticipated plastic hinge region. Improvement in delaying the onset of strength degradation was obtained when two pairs of stiffeners located one third of the beam depth from the top and bottom flanges were used in lieu of one stiffener attached at the beam centerline. However, in these specimens the beams were shop welded to the columns without bolted shear tabs and are as a result not representative of current WSMC design and construction practice in the United States.

The afore-described local and lateral torsional buckling failures observed in WUF-W, RBS, EEP, BFP and KBB connections described above have been also observed on recently developed connections involving a novel concept called heat-treated beam section (HBS). The study presented in this article will examine local buckling and the associated strength degradation which has been observed during full scale testing of welded connections modified with the HBS. From this analysis, two strategies to enhance the buckling resistance of this connection are studied numerically through finite element analysis (FEA) one of

which is experimentally validated through full scale simulated seismic testing. Details of the experimental study are presented and areas for future development and application of this technique to other types of moment connections are identified.

It is noted here that due to limitation of available data this study was conducted on rolled wide flange sections. As demonstrated in the above review of the literature, rolled wide flange beams do suffer from strength degradation due to buckling. However, most of these shapes satisfy the slenderness requirements of the 2010 ANSI/AISC seismic provisions [5] and as a result are able to meet target plastic rotations of these specifications [15]. Therefore, the strategies outlined in this article are anticipated to add greater value in enhancing the buckling resistance of non-compact built up beams used in welded moment connections. However, they can also be used for rolled wide flange sections in cases where superior performance is desired.

2. Buckling of Recently Developed Seismically Resilient WSMC

In *HBS* connections, specific locations of the top and bottom beam flanges are heated to a temperature in the range of 1050-1100°C for 15 minutes followed by slow cooling. The areas heat-treated are highlighted red in Fig. 3a which show the HBS applied to an all welded (welded flange welded web) connection. This heat-treatment reduces the strength of A992 steel as shown in Fig. 3b. As a consequence of this softening, plastic hinging of the beam takes place in the heat-treated beam section (HBS). In a similar manner to the RBS, this connection provides a ductile seismic fuse through weakening, but because the elastic modulus of the HBS is unchanged, a connection modified with such a technique does not sacrifice elastic stiffness as does the RBS.

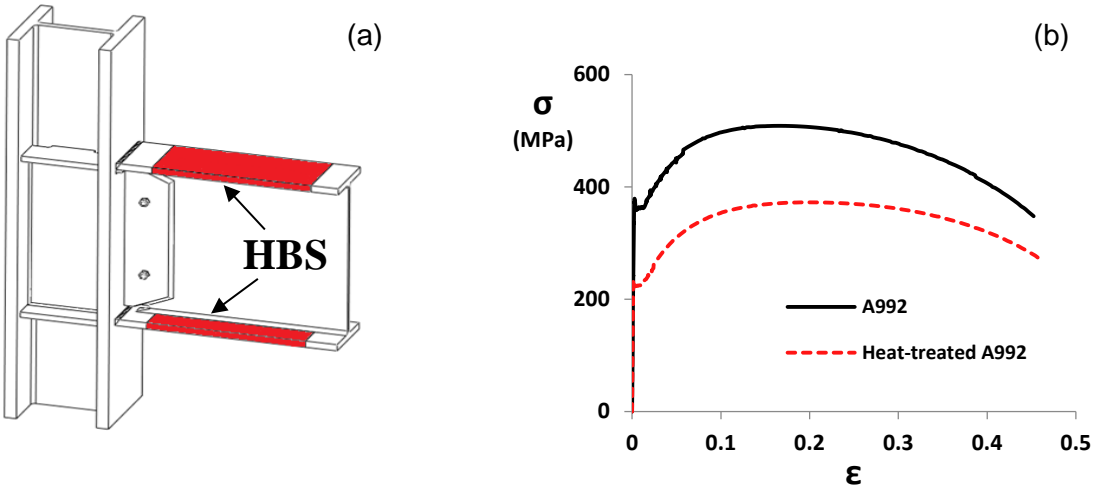


Fig. 3. (a) Sketch of Heat-treated Beam Section (HBS) connection (b) Engineering Stress-Strain response of A992 and heat-treated A992 steel

The moment-rotation response shown in Fig. 4a and peak envelope in Fig. 4b demonstrate the seismic performance of the HBS connection (HBS 5) which exceeds current AISC 341-10 seismic provision [12] requirements for use in SMFs. FE simulations are compared to the experimental responses and will be discussed in more detail later. These global responses of HBS 5 show wide hysteresis loops indicating good energy dissipation. Strength degradation due to local flange, web and lateral torsional buckling initiated during the 2nd cycle of loading at 4% drift (see Fig. 4c) and continued during later loading cycles. Loading of HBS 5 was terminated after sustaining 2 loading cycles at 5% drift due to a fracture in the location of significant flange buckling (see Fig. 4c and 4d).

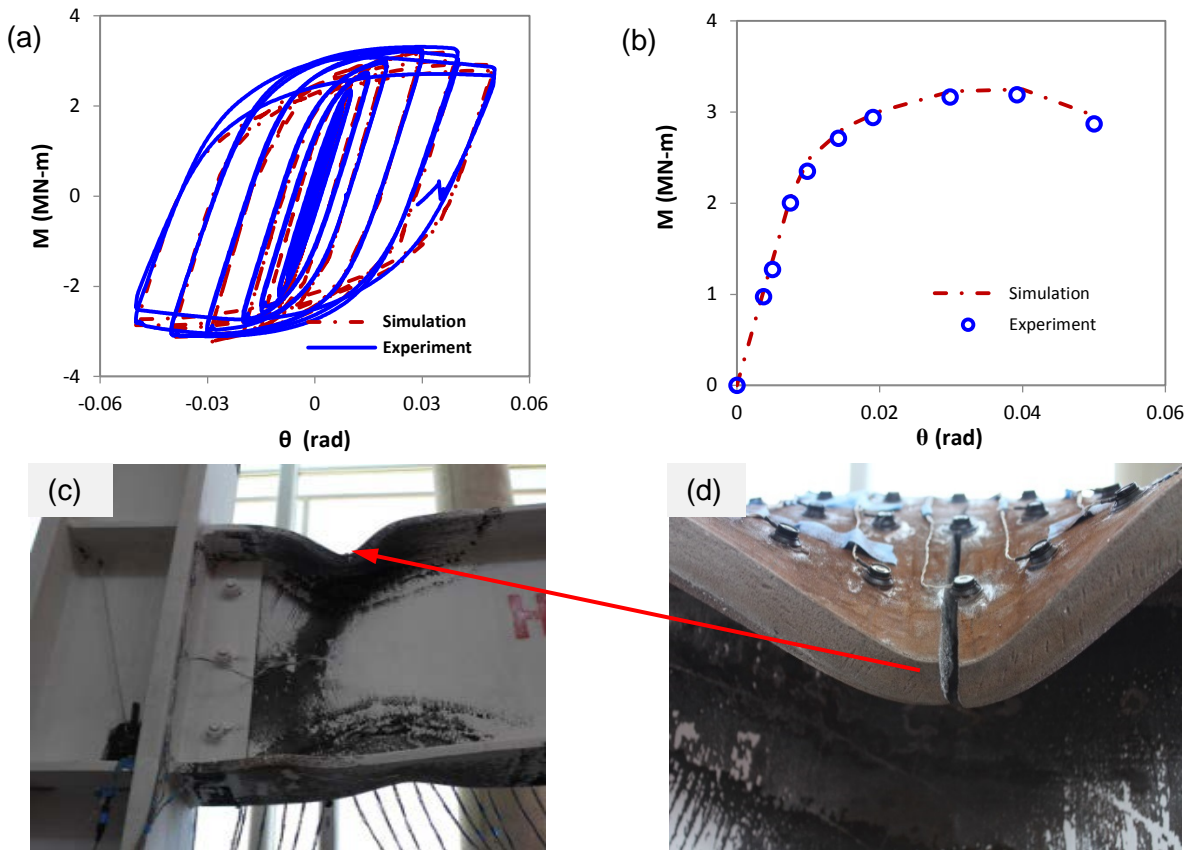


Fig. 4. Test results of HBS 5 connection, (a) moment-rotation experimental response and FE simulation (b) experimental backbone curve and FE simulation (c) photograph showing plastic hinge formation at 5% interstory drift (d) Photograph showing fracture of beam flange in the crest of flange buckle

To demonstrate the progressive strength degradation mechanism, 3-dimensional plots (Fig. 5) of displacement measurements from Optotrak LED sensors located on the beam web (see Fig. 7a and 7b) are presented. From these plots local buckling of the beam web within the HBS is clearly noticeable at 3% drift (Fig. 5c). Buckling amplitudes continued to increase with increased drift angles as shown in Fig. 5d and 5e. By 5 % drift, severe twisting of the web is noticeable as well as double curvature from buckling during loading in the opposite direction (negative bending).

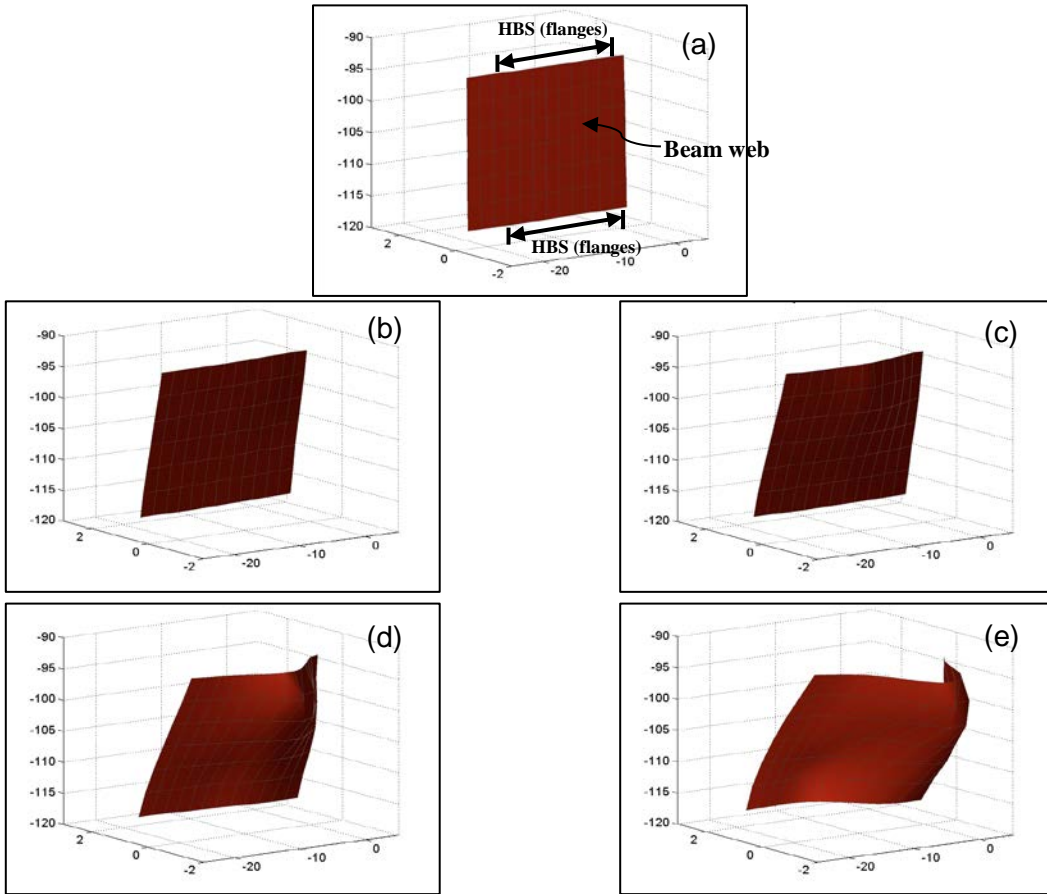


Fig. 5. Progression of buckling in beam web of HBS 5 at various stages of loading history
 (a) initial position (b) 2.0% drift (c) 3.0% drift (d) 4.0% drift (e) 5.0% drift (Beam is in positive bending i.e. top flange in compression)

The buckling mechanism is further analyzed by plotting planar displacements of the beam cross-section located 406 mm away from the column flange (within the HBS) using the recorded vertical and horizontal positions of Optotrak markers placed along the top flange (see Fig. 4d) and web of HBS 5. In this plot, FE simulations are compared to the experimental responses. Here again it is observed that the degradation mechanism is initiated by slight local buckling of the beam web in the plastic hinge during loading cycles at 3% interstory drift (Fig. 6a). This local web buckling was soon followed by local flange

buckling and twisting of the beam as the loading amplitude was increased (Figs. 6b and 6c). The amplitudes of flange and web buckling gradually increased with the rotation amplitude resulting in the observed strength degradation (Fig. 4a and 4b).

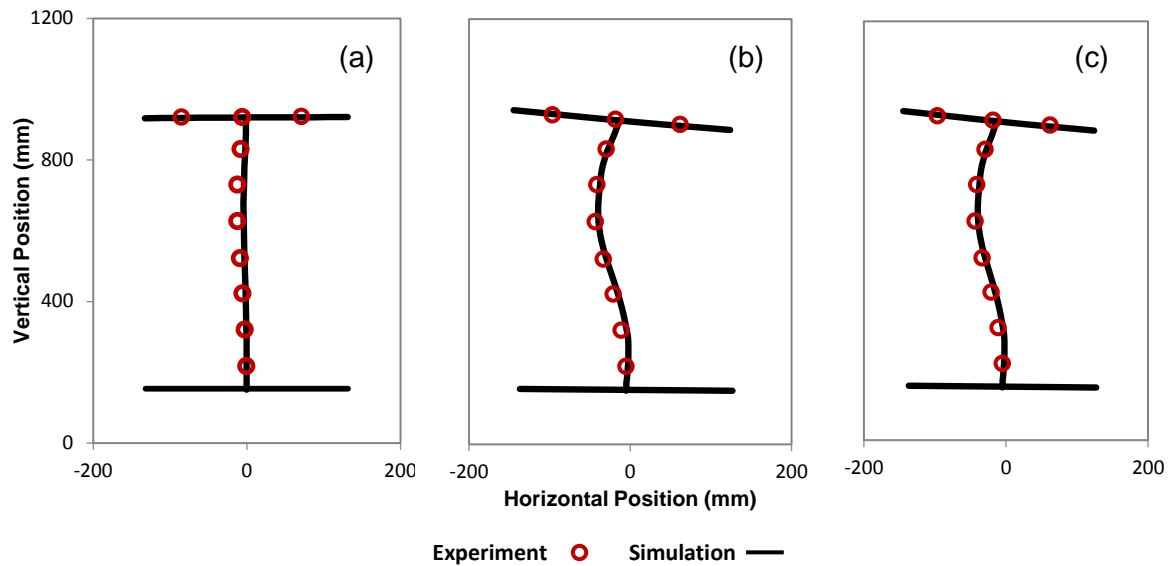


Fig. 6. Progression of HBS beam cross-section buckling at interstory drifts, (a) 3%, (b) 4%, and (c) 5%. Cross-section is located 406mm from the column face, FE simulation predictions are plotted against recorded data from test

The afore-described, buckling damage is similar to those observed in the prequalified connections shown in Figs. 1 and 2b and have also been observed in other connections modified with the HBS which are shown in Fig. 7. In other words, the buckling damage discussed above for HBS beams is not induced because of the softening of material from the heat-treatment or by the connection method, but it is a characteristic behavior of the W shape cross section.

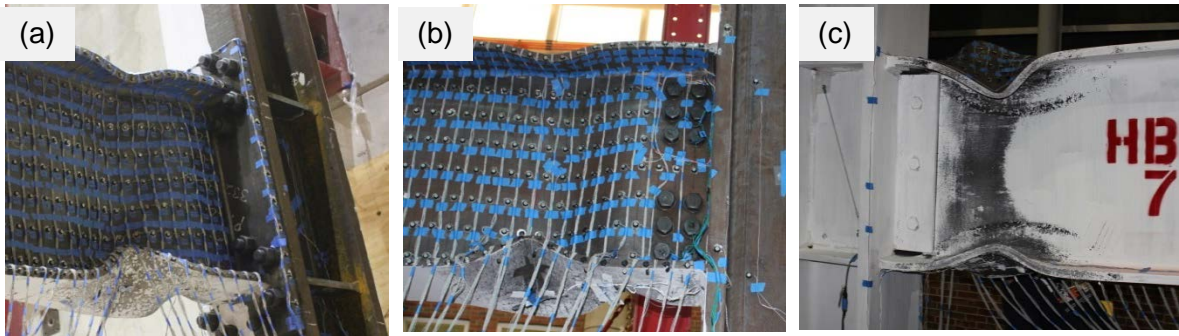


Fig. 7. Buckling failures in HBS connections (a) 8 bolt unreinforced EEP (HBS 4), (b) welded unreinforced flange bolted web (HBS 6) (c) HBS 7 (Repeat of HBS 5, all welded connection)

3. Proposed Techniques for enhancing beam buckling resistance of WSMC

Based on the afore-described local buckling mechanism and consequential strength degradation, two (2) techniques to enhance buckling resistance are proposed and evaluated through FE analysis. The first involves the attachment of a plate to the column flange and beam web in the anticipated plastic hinge region. This “web stiffener” (shown in Fig. 8a) is designed to reduce the slenderness of the beam web in the region of anticipated buckling and consequently provide greater resistance to flexural buckling and twisting. By combining the web stiffener with the HBS, plastic hinging of the beam still takes place away from the welded joint, however strength degradation is delayed and the rate of strength loss is reduced. The combination of these two features (HBS and web stiffener) creates a connection that is both fatigue resilient and buckling resilient. This connection is referred to as HBS-WS in the forthcoming discussion.

As an alternative to improving the compactness of the beam web in the plastic hinge region, reduction of the material strength of the beam web is proposed. This reduction of the

material strength simply involves extending the HBS to the beam web as shown in Fig 8b. As a consequence, flexural (and shear) stresses are reduced in the beam web. In addition, since heat-treatment does not reduce the plastic modulus of A992 steel (note the downward shift of the stress-strain curve shown in Fig. 4b² the buckling resistance of the beam is not reduced. Therefore with reduced bending stresses acting on the beam web and flange in the plastic hinge, and no deterioration of the inelastic buckling resistance of the beam section in the plastic hinge, less buckling damage and strength degradation is likely as a result. This connection is referred to as HBS-W in the forthcoming discussion.

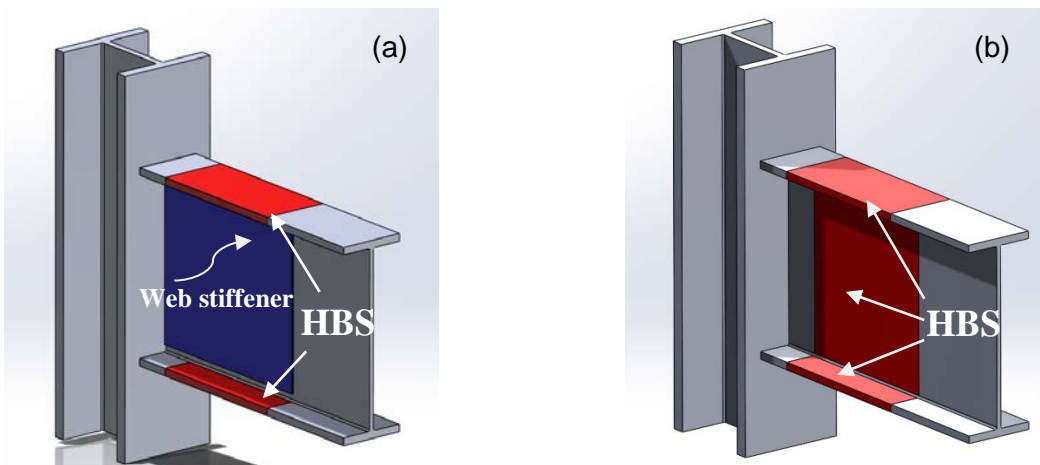


Fig. 8. Proposed enhanced Connections (a) HBS with web stiffener (HBS-WS) (b) HBS applied to both flanges and web (HBS-W)

² In fact the work hardening rate of A992 steel increases as a consequence of heat-treatment. The yield strength is reduced by 38%, but the tensile strength is reduced by 25%.

3.1 Finite Element Modeling of Enhanced Connections

Three dimensional nonlinear finite element models were developed for the proposed connections using the commercial finite element analysis software ANSYS Mechanical ADPL [18]. Geometric and material nonlinearities were incorporated in the finite element models. An example of the finite element mesh and boundary conditions is shown in Fig. 9a and Fig. 9b. The beam, column, web stiffener and continuity plates were modeled with 8 noded solid hexahedral elements (SOLID185) with selective reduced integration scheme. Welding attachment of the web stiffener to the beam web and column flange was simulated by prescribing multi-point displacement constraints between the nodes of the web stiffener, column flange and beam web as shown in Fig 9b. This method has been used in previous studies to simulate reinforcing fillet welds between the beam web and shear tab in WUF-W connections by Ricles et al. [19]. The weld pattern shown in Fig. 9b is intended to simulate attachment of the web stiffener through slot welds on the interior portion of the plate and fillet welds around the edges. The web stiffener plate is intended to be shop welded to the beam web and then field welded to the shear tab.

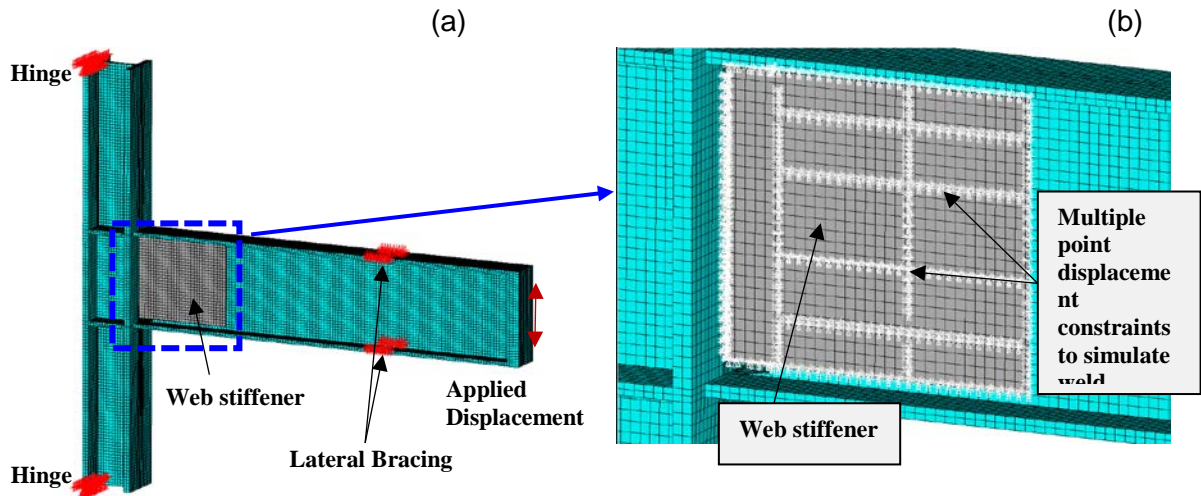


Fig. 9. Finite element mesh (a) Beam to column connection mesh and boundary conditions (b) Close up view of mesh showing multi point displacement constraints used to simulate welding attachment of web stiffener to beam web

Finite element models accounted for material nonlinearity through rate-independent metal plasticity theory based on the von Mises yield criterion, additive strain decomposition and associated flow rule. The Chaboche non-linear kinematic hardening model was used for A992 beam and column material while a multilinear kinematic hardening model was used for heat-treated A992 material.

Geometric nonlinearities were accounted for via a large displacement formulation. During the development of these finite element models it was found that with the large displacement cyclic loading history applied to the beam-column connections, local buckling of the beam is predicted without the introduction of any eccentricities either from initial geometric imperfections or small lateral loads. This observation has also been made by Myers [20]. Despite the symmetry of the mesh, boundary conditions and applied loads, small

eccentricities accumulate during cyclic loading due to numerical rounds off made during the nonlinear solution process. This eccentricity provides perturbation for buckling and in some cases produces results of reasonable accuracy. However, the same is not true of monotonic simulations; in fact, a monotonic FE simulation of a beam to column moment connection with symmetric geometry, boundary conditions and loads will highly over predict the connection capacity and fail to accurately predict local buckling.

In general, accurate numerical prediction of experimentally observed local buckling is challenging as geometric imperfections of the structure can be quite complex and as a result, difficult to measure and model. Cyclic simulations in which buckling is perturb by accumulated eccentricities arising from numerical round-offs can be viewed as an upper bound solution and may in some instances make un-conservative predictions. Therefore, in this study initial geometric imperfections were imposed by first conducting an eigenvalue analysis of the perfect structure and then prescribing a scaled value of the first eigenmode displacement field as the initial configuration of the structure. The scaling was chosen to represent realistic values of W-shape “out of squareness” based on ASTM A6 [21] tolerances. Similar approaches have been used in other studies [22-24].

3.2 Finite Element Analysis Results and Discussion

Proposed connections HBS-WS and HBS-W were subjected to cyclic loading prescribed according to the ANSI/AISC 341-10 [5] loading protocol for SMF connections. The moment rotation responses for both connections are shown in Fig. 10. The normalized moment-rotation envelops for both connections are compared to the earlier presented HBS 5 connection experimental and simulation responses in Fig. 11. Moments have been

normalized to the plastic moment of the unheat-treated beam cross-section. Both moments and rotations have been calculated at the column face. In addition, the accumulated equivalent plastic strain contour plots at 5% story drift for HBS, HBS-W and HBS-WS simulations are presented in Fig. 12. Analysis of Figs. 10, 11, and 12 have led to the observations discussed in the following.

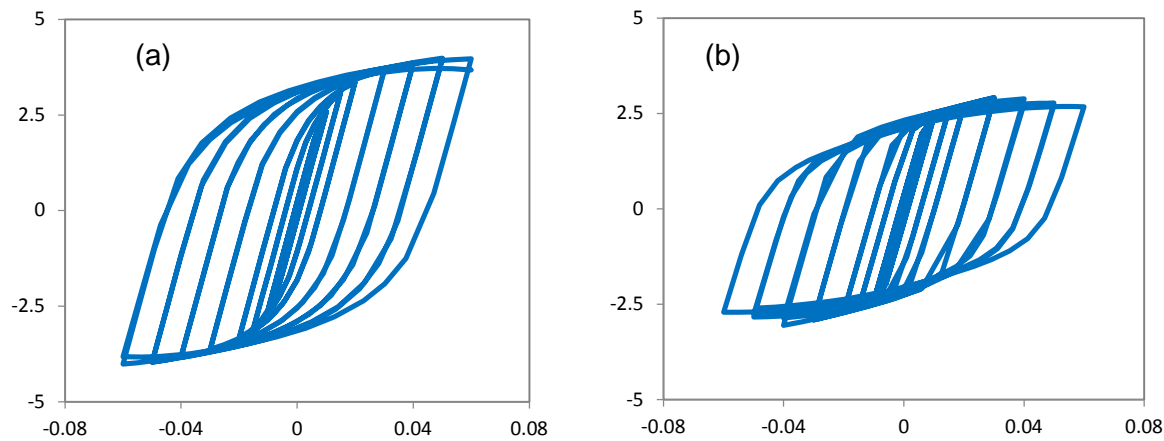


Fig. 10. Moment rotation response for proposed connections (a) HBS-WS (b) HBS-W

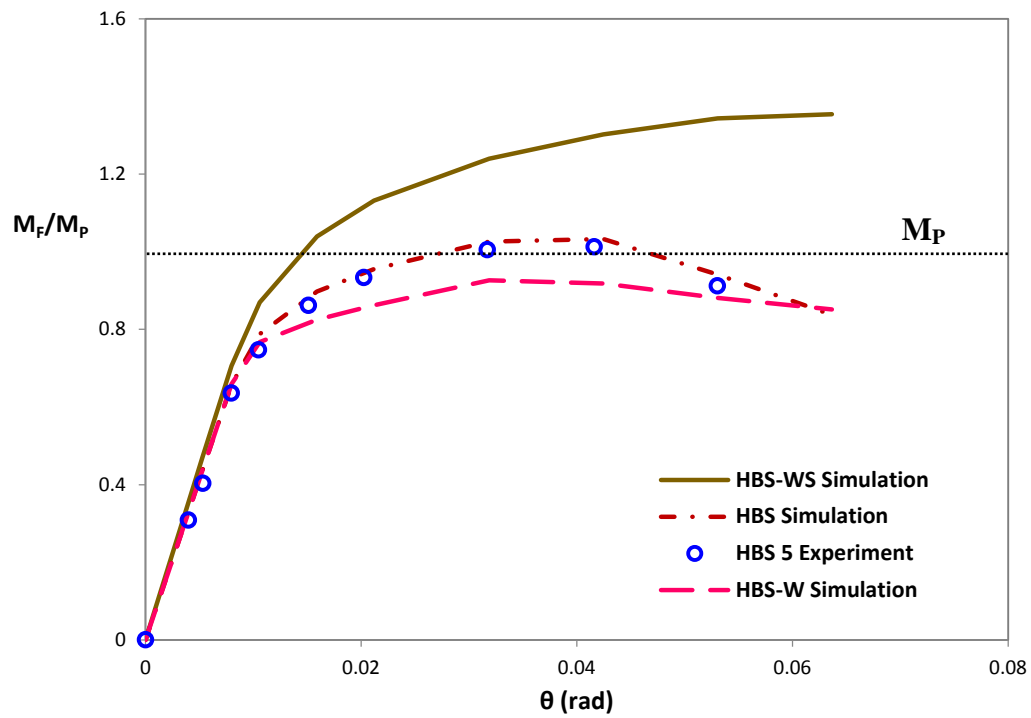


Fig. 11. Moment rotation backbone curves for HBS (experiment and simulation) , HBS-WS and HBS-W

The addition of the web stiffener increases connection stiffness (both elastic and post yield, see Fig. 11), strength and delays the onset of buckling from the second cycle of loading at 4% drift to the second cycle of loading at 6% drift (compare Fig 4a and Fig10a). As a result, energy dissipation is improved significantly and buckling damages are also reduced (Compare Figs. 12a and 12b with Figs. 12e and 12f). Drawbacks to this method of seismic enhancement are mainly economic. For example, extensive amounts of welding and fabrication are necessary to install the web stiffener plate. Also the approximately 30% increase in beam strength (Fig. 11) places higher demands on the column. As such, heavier

columns and/or added panel zone reinforcement may be required to prevent excessive panel zone distortions or soft story mechanisms.

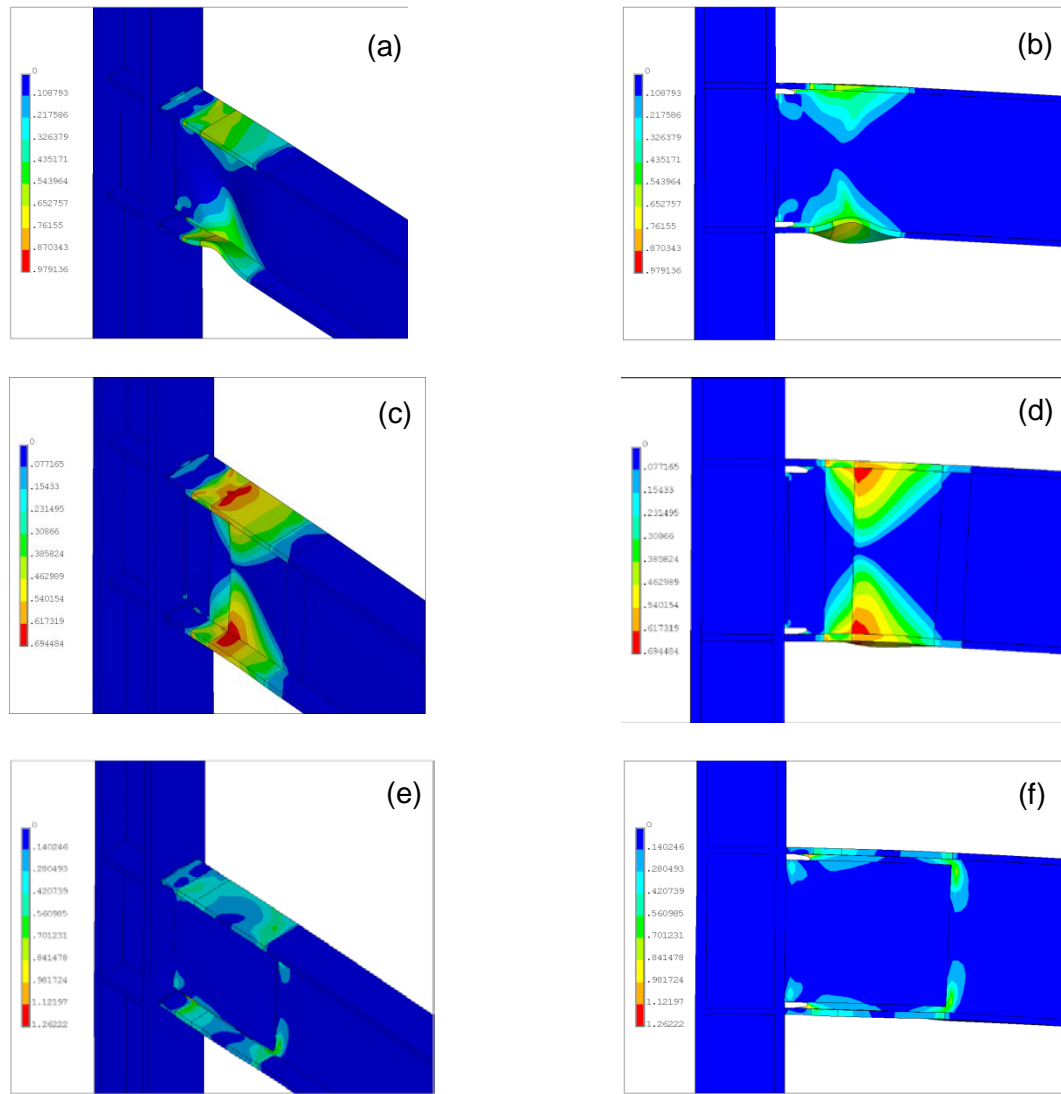


Fig. 12. Accumulated Equivalent Plastic strain contours at 5% story drift for moment connecitons (a) HBS (isometric) (b) HBS (elevation) (c) HBS-W (isometric) (d) HBS-W (elevation) (e) HBS-WS (isometric) (f) HBS-WS (elevation)

As an alternative, extending heat-treatment to the beam web (HBS-W) reduces connection strength (Fig. 11) and though it does not delay the onset of strength loss, it significantly reduces the rate of degradation (Fig. 11) and the associated local buckling damage in the plastic hinge (Compare Figs 12a and 12b with Figs 12 c and 12d). As a result the HBS-W connection is predicted to lose only 10% of its maximum moment strength at 6% drift as opposed to the HBS connection which loses 21% of its maximum moment strength during the second cycle of loading at 5% drift (Compare Fig. 4a and Fig. 10b). This method involves less fabrication and welding than the web stiffening method, and extension of heat-treatment to the beam web is expected to only marginally raise costs. However, this connection reduces the moment strength below the beam plastic moment (M_p) (Fig. 11). Consequently, larger beams may have to be used than otherwise necessary to compensate for this reduction in strength.

In summary, both strategies to enhance seismic performance appear to be fatigue resilient (plastic hinge forms away from welded joint) and show promise in delaying and/or slowing the rate of strength degradation and reducing local buckling deformations in the plastic hinge. The web-stiffening method is certainly more involved from a fabrication, welding and erection standpoint but does seem to provide greater improvements in seismic performance. Based on these promising results, full scale testing was conducted to validate the web stiffener concept as described in the following.

4. Experimental Validation

4.1 Connection Design and Experimental Setup

One large scale specimen (HBS 8) was tested to evaluate the performance enhancement provided by the web stiffener. The test setup and details of the test specimen are shown Fig 13. In order to closely study the effect of the web stiffener, beam and column sizes, beam to column CJP welding details, test setup, loading protocol, etc. were kept identical to other HBS connections (HBS 5 and HBS 7) tested during the experimental program. Therefore the only parameter varied was the addition of the web stiffener. The web stiffener plate was fabricated in the shop with horizontal and vertical slots as shown in Figs. 13b and 13d. Welding of the web stiffener to the beam web was accomplished using gas shielded metal arc welding (GMAW) with E71T-1C-H8 electrodes (Lincoln ultra core 71C) which is specified to meet all the requirements of AWS D1.8. Fillet welds were used to connect the perimeter of web stiffener to the beam web. In addition fillet welds were placed in the vertical and horizontal slots to provide added reinforcement to the beam web and to prevent premature local buckling of the web stiffener. The weld design was decided upon numerically through trial and error using the FE modeling presented earlier (see section 3). Fillet welds were used instead of full depth slot welds to minimize heat input from welding and consequential distortions to the beam. Therefore the slots were only partially filled with weld metal.

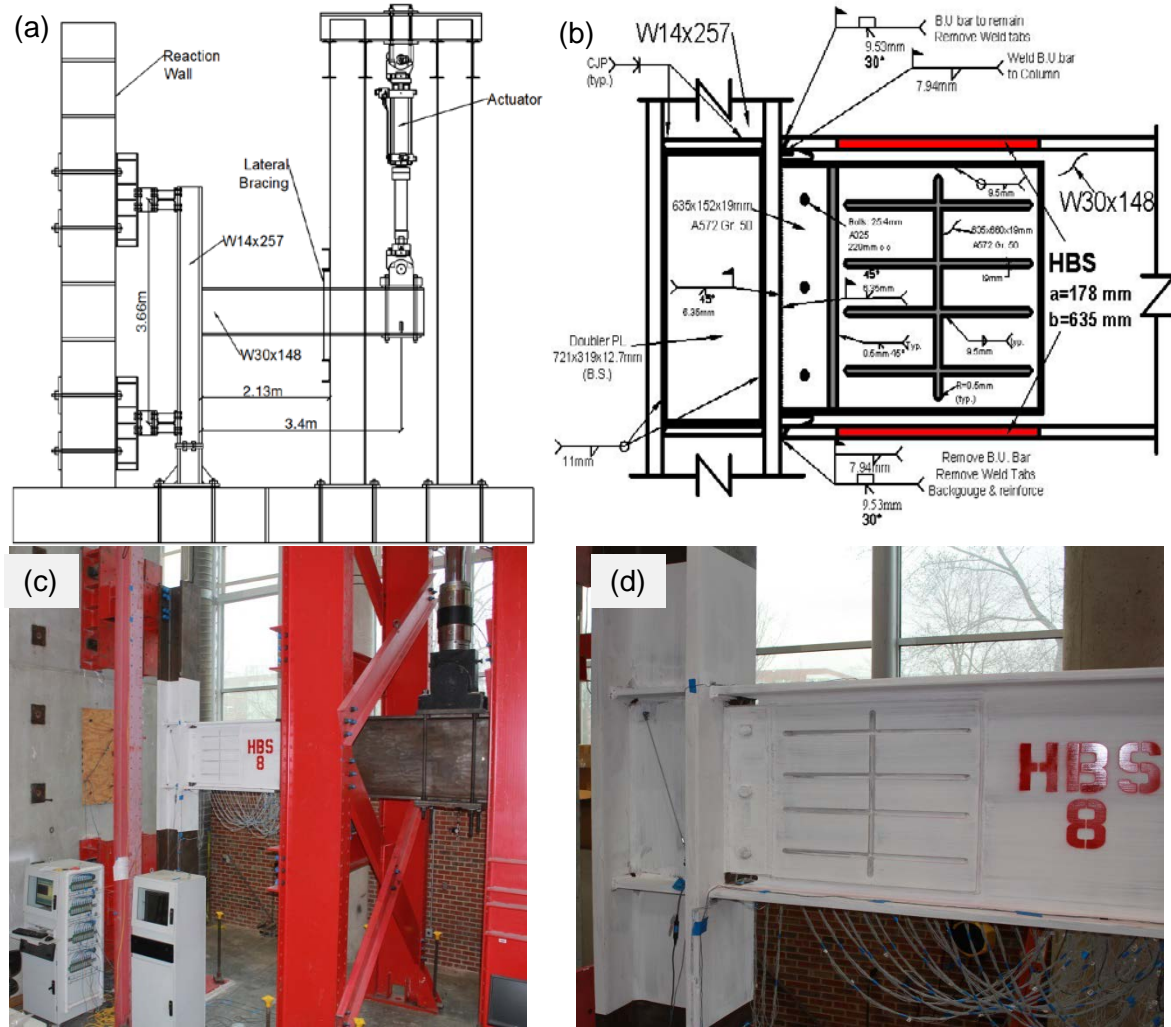


Fig. 12. HBS 8 test setup and connection details a) sketch of the test setup, b) sketch of the connection details, c) photograph showing test setup and, d) photograph of HBS 8 connection prior to testing

Upon completion of beam fabrication, heat-treatment was performed using electrical resistance ceramic mat heating pads as shown in Fig.14a. Heating pads were sized according to the required dimensions of the HBS and were installed on the inner and outer surface of the beam flanges. The heating pads were connected to a power supply and type K

thermocouples were used to monitor temperatures and provide continuous feed back to the power supply. Three (3) layers of 50 mm (2 in.) high density ceramic fiber insulation blankets were wrapped around the beam flanges as shown in Fig. 14b to provide well controlled heating and cooling. More details about the heat-treatment setup and procedure are provided in Morrison et al. [25].

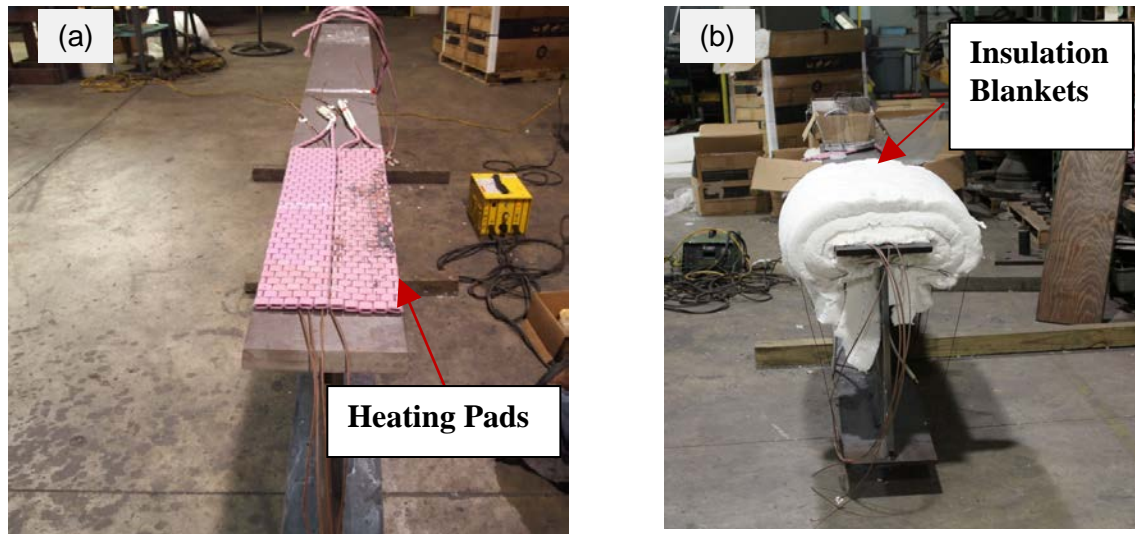


Fig. 13. Heat-treatment setup (a) photograph showing electric surface heating pads during installation on a beam flange, (b) photograph showing insulation of beam flange for well controlled heating and cooling

Connection welding was performed outdoors with the column oriented vertically by a welder qualified in accordance with the requirements of AWS D1.1-10 and AWS D1.8-09. Welding was accomplished with self-shielded flux cored arc welding (FCAW) process. E70-T6 electrodes were used for beam flange complete joint penetration (CJP) welds, while E71-T8 electrodes were used for the beam web weld. Both of these electrodes were specified by

the manufacturer to deposit metal with a minimum Charpy V-notch toughness of 27 J (20 ft.-lbs.) at -28 °C (-20°F) . The bottom flange backing bar was removed and a reinforcing weld was placed at the root of the groove weld.

The top flange backing bar was left in place, however a fillet weld was provided between the backing bar and the column flange. Weld tabs from the top and bottom beam flange CJP welds were removed by carbon air arc gouging. After the beam to column CJP welds were completed, a CJP weld was installed between the shear tab and the web stiffener as shown in Fig. 13b. Finally, all CJP welds were ultrasonically (UT) tested by a certified welding inspector (CWI) in conformance with AWS D1.1-10 and AWS D1.8-09.

4.2 Instrumentation

Each specimen was equipped with strain gauges along the beam flanges to monitor longitudinal flange strains, at various locations including the weld toe and HBS region. String and linear potentiometers were used to monitor displacements and rotations in the beam, column, and panel zone. A calibrated load cell in the hydraulic actuator provided readings of force response during the experiment. The specimen was also painted with hydrated lime prior to testing to visually indicate regions of yielding.

The Optotak Certus HD three-dimensional (3D) position system was used to capture the positions of markers placed along the beam flanges and web as shown in Fig. 7. Two Optotak cameras were used which were able to capture the motion of markers placed on the top and sides of the beam top flange, the beam web and the side of the beam bottom flange. Position time history data obtained from this system was post processed to calculate displacements and strains in areas of interest.

5. Test Results

5.1 Global response of HBS 8

Testing was conducted at the North Carolina State University Constructed Facilities Laboratory (CFL) on an exterior type sub-assemblage (single cantilever). Loads were applied at the beam tip in accordance with the 2010 ANSI/AISC 341-10 [5] loading protocol consisting of quasi-static increasing amplitude displacement cycles. Figure 15 shows the moment-rotation response of HBS 8. This global response shows wide and stable hysteresis loops indicating good energy dissipation. HBS 8 met the 2010 AISC Seismic Provisions (ANSI/AISC 341-10) SMF qualifying 4% interstory drift angle without strength loss. Slight strength degradation due to a fracture sustained in the fillet weld of the vertical slot in the center of the web stiffener, was observed during the 1st cycle of loading at 5% story drift. Photographs of this fracture are shown in Fig. 21 and will be discussed more later. Loading of HBS 8 was terminated after 1 cycle of loading at 5% story drift as a result of this failure.

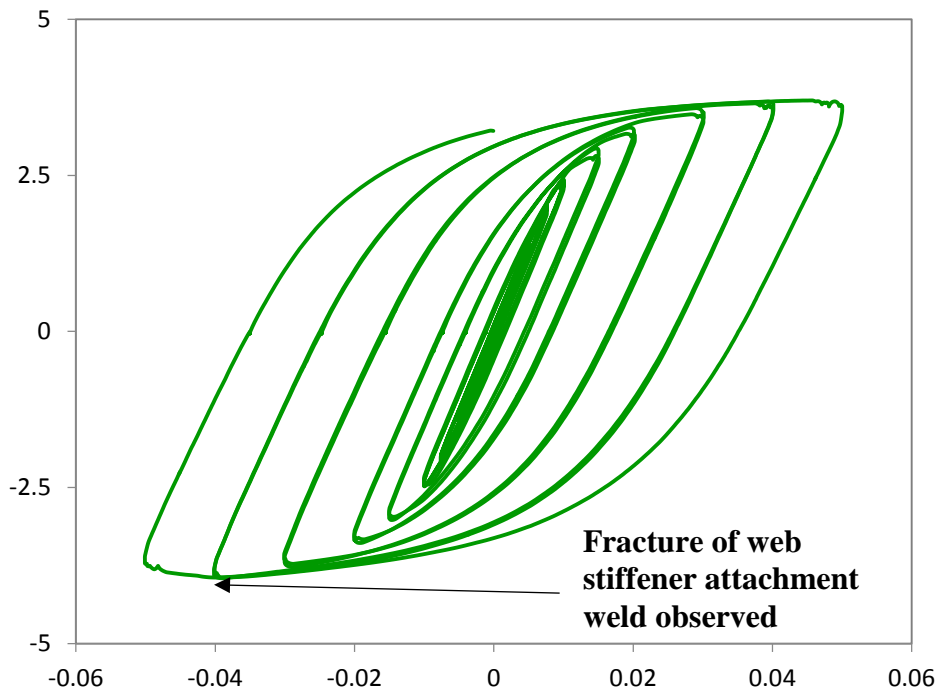


Fig. 14. Moment-rotation response of HBS 8

The response of HBS 8 is further analyzed by plotting the moment-plastic rotation curves for each component of the connection assembly which were calculated using data measured by instrumentation during the test and equations proposed by Popov et al. [26]. These graphs are shown in Fig. 16. They indicate that inelastic action in the beam accounted for a majority (93%) of the total plastic rotation of connection assembly.

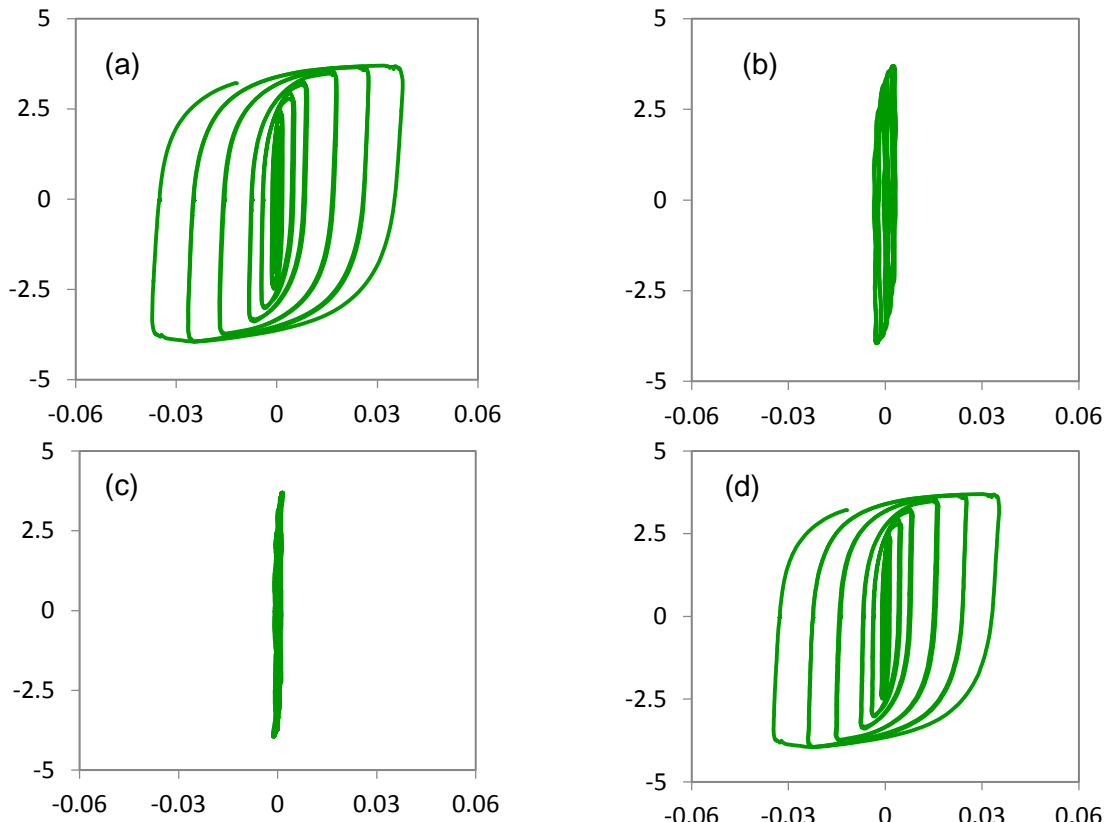


Fig. 15. Plastic rotation contributions by components of HBS 6, (a) total connection plastic rotation, (b) panel zone shear plastic rotation (c) column flexural plastic rotation and, (d) beam plastic rotation

5.2 Comparative Analysis of HBS 8

5.2.1 Global Response

The peak moment-rotation response of HBS 8 is compared to those of HBS 5 and HBS 7 in Fig. 17. It is noted here that HBS 7 was a repeat test of HBS 5 i.e. both specimens have the same geometry (beam and column sizes), connection method and both are heat-treated. As anticipated from pretest analysis HBS 8 displays increased strength and stiffness compared to HBS 5 and HBS 7. However, connection stiffness and strength are somewhat lower than pretest predictions. This is likely due to the partially filled (see Fig. 13b and Fig.

21) slots in the web stiffener which were not explicitly modeled in the FE analysis. The onset of strength degradation was also delayed in HBS 8 which validates the concept of improving buckling resistance of wide flange beam to column HBS moment connections through web reinforcement.

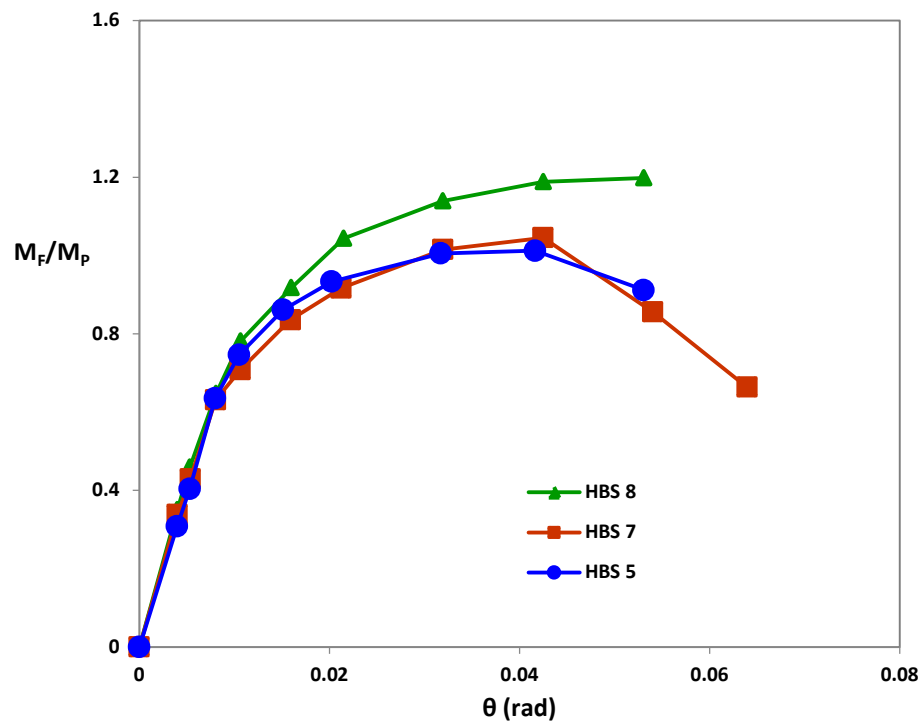


Fig. 16. Moment rotation backbone curves for HBS 5, HBS 7 and HBS 8

5.2.2 Plastic Hinge Formation

Figure 18 compares the progression of inelastic action along the beam flange for HBS 5 and HBS 8. These bar graphs show the distribution of longitudinal tensile strains (normalized by the yield strain) along the centerline of the beam flange at various stages of the loading history. Bars highlighted in red represent the strains in the heat-treated

(weakened) regions. Strains were calculated by post processing data obtained from 3D noncontact spatial displacement measurement sensors placed along the beam flange as shown in Fig. 4d.

Comparison of the strain responses show that the combination of the web stiffener and HBS leads to more uniformly distributed strain distributions along the beam flange. As a result, at

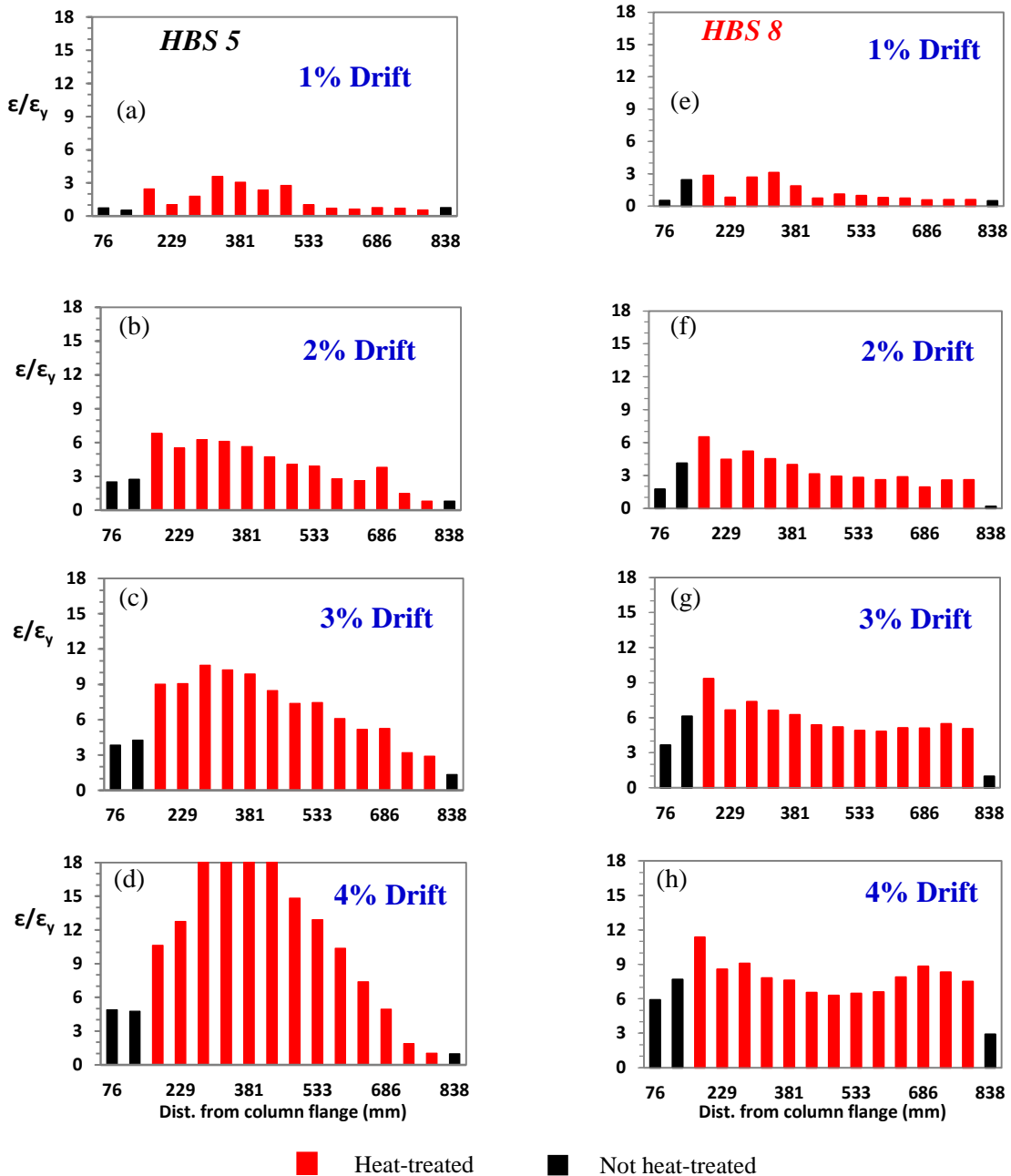


Fig. 18. Recorded longitudinal strains along the center of top flange of the beam (a-d) HBS 5 and (e-h) HBS 8

comparable drift angles strain demands are lowered in the heat-treated region in HBS 8. This effect leads to a favorable condition both in terms of fatigue resistance and delay of beam flange local buckling.

5.2.3 Local buckling

Figure 19 compares planar displacements of the beam cross-section located 406 mm away from the column flange of HBS 5 and HBS 8 at 3%, 4% and 5% interstory drift. Dotted lines have been traced between data points to make evident the progressive buckling of the beam. Figure 20 compares photographs of HBS 5, HBS 7 and HBS 8 at corresponding stages of the loading history. These two figures provide validation of the web stiffener technique in significantly reducing FLB, WLB and LTB for HBS beam to column moment connections. Note that even though no reinforcement of the flanges was provided, flange local buckling is significantly reduced by the presence of the web stiffener. This supports the findings of Uang and Fan [14] and Okazaki et al. [15] who both demonstrated the interaction between non dimensional web and flange slenderness parameters through nonlinear regression analysis. Evidence from the experimental results presented in this article suggests that WLB and FLB are at the least, weakly coupled. Reduced strain accumulation along the beam flanges as demonstrated in Fig.18 may have been a contributing factor to the reduced local flange buckling observed in HBS 8.

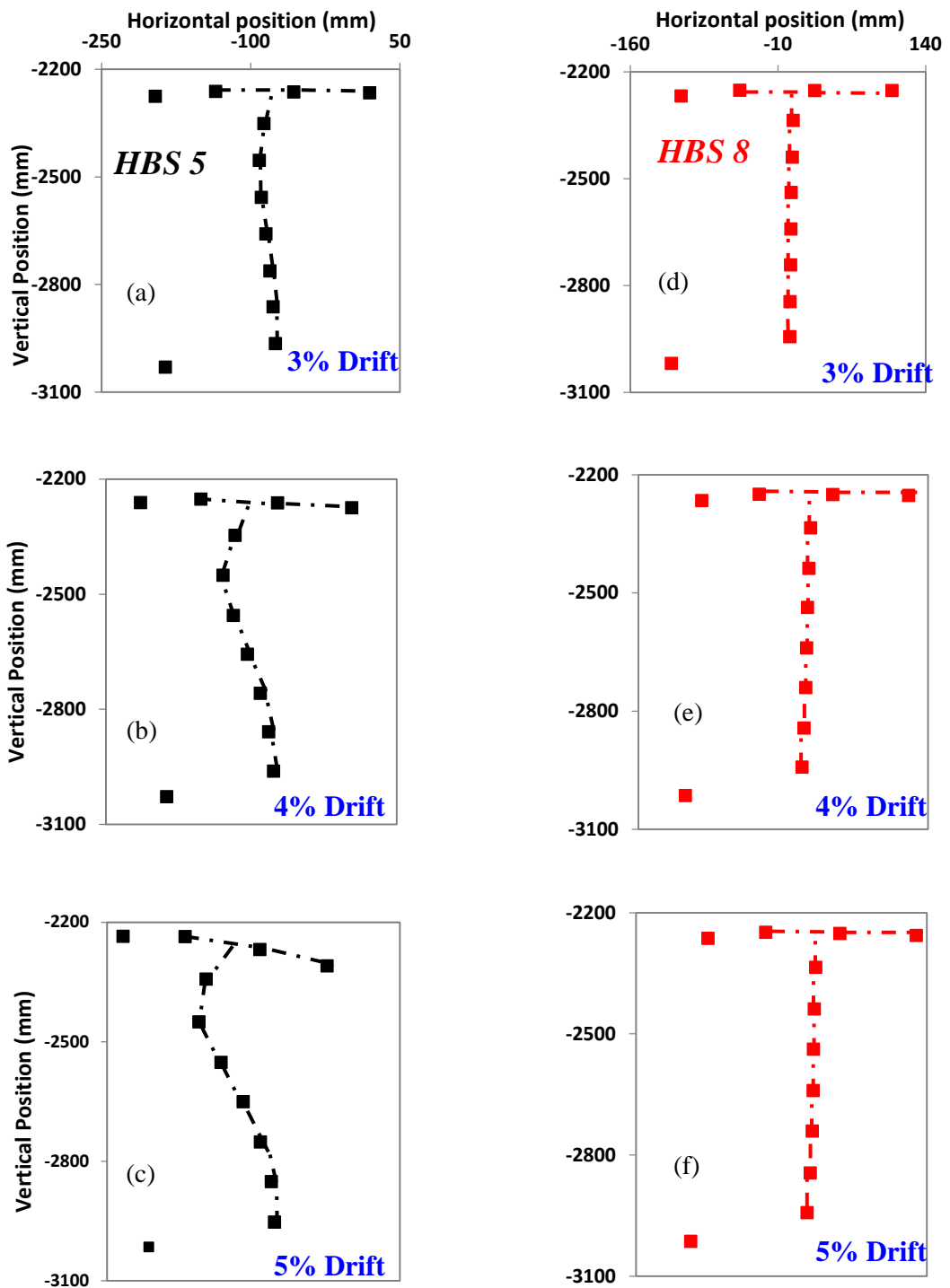


Fig. 19. Progression of beam web and flange buckling recorded 406mm away from the column flange (a-c) HBS 5 and (d-f) HBS 8 (Beam is in positive bending i.e. top flange in compression).

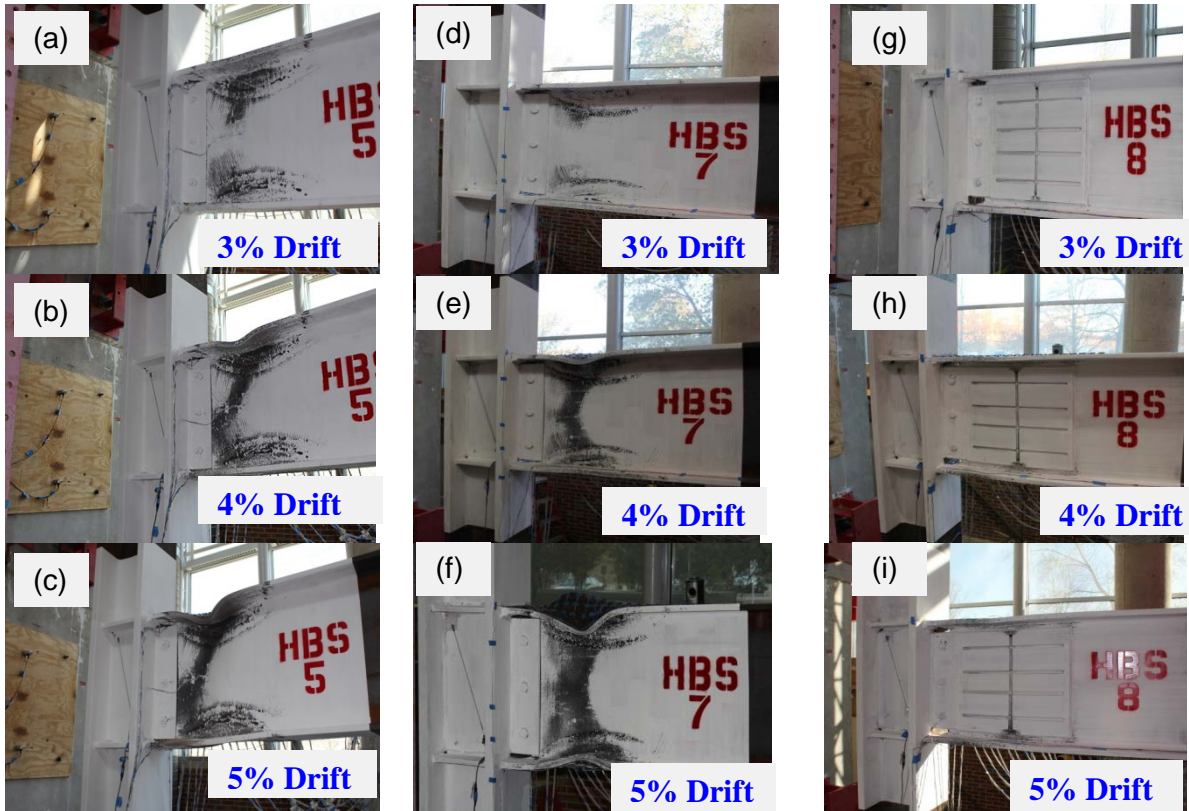


Fig. 20. Photographs comparing the yielding, plastic hinging and local buckling at various stages of the loading history for (a-c) HBS 5, (d-f) HBS7, and (g-i) HBS8

5.2.4 HBS 8 Web stiffener fillet weld failure

As previously stated loading of HBS 8 was terminated after one complete loading cycle at 5% story drift due to a crack in the bottom of the fillet weld in the vertical slot of the web stiffener. Photographs of the failure location and rupture are shown in Fig. 21. The crack which measured 127 mm (5in.) in length propagated through the beam web and extended vertically as shown in Fig. 21b, resulting in strength loss as shown in Fig. 15. This failure underscores the well-established understanding that fillet welds are less ductile when loaded perpendicular to their longitudinal axes. In addition the “v-shaped” topography of the fillet

welds in the web stiffener slots (Fig .21b and 21c) create an unfavorable stress concentration which may have also contributed to this failure.

6. Future Work on web stiffener

Despite the promising results of the web stiffener technique further research is necessary to continue to develop and improve this method. Future studies on this technique should incorporate more detailed FE studies to optimize the web stiffener weld attachment design to minimize stress and strain concentrations as well as welding induced distortions. It is recommended that vertical slots and fillet welds be avoided based on the results of the current study. In addition, numerical and experimental studies should focus on the application of this technique to non-compact built up sections. Emphasis should be placed on finding economic details to ensure that these sections satisfy the rotation capacities of current seismic design codes. This technique may also be used at column base in moment frames which employ deep columns (W27 and deeper sections). These deep members have reduced torsional properties and more slender elements when compared to W sections (W14 and shallower) traditionally used for columns in gravity frames. In addition, these members carry gravity loads and are expected to sustain large plastic rotations during the formation of a beam sway mechanism in a severe earthquake.

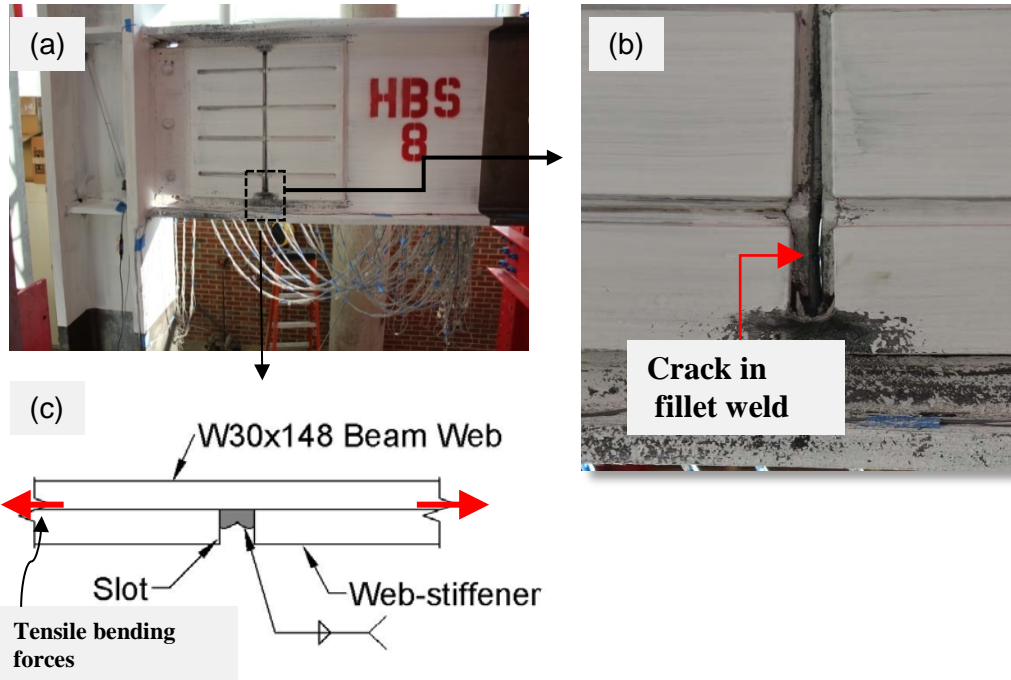


Fig. 21. (a) Posttest photograph showing fracture of web stiffener fillet weld and beam web
(b) Enlarged photograph at the fracture location (c) Sketch of web stiffener slot fillet weld detail

7. Conclusion

Strength degradation initiated by local buckling damages in WSMC's have been studied experimentally and through FE analysis. This strength degradation is observed to be initiated by buckling of the beam web which is followed by buckling of the beam flange. It is observed that once the strength degradation initiates it propagates quickly with continued incremental cycles. By 4% interstory drift test data show that local beam web and flange buckling damages in the plastic hinge region become large. To counter this, two techniques for improving the seismic performance of HBS WSMCs have been proposed and studied through finite element analysis. One technique called web stiffener involves welding a plate to beam web and column flange in the plastic hinge region, while the other technique

involves extending the HBS to the beam web. FE studies show both techniques to be fatigue resilient (i.e. plastic hinge forms away from welded joint) and to reduce buckling damage and associated strength degradation.

The web stiffener technique was validated through full scale simulated seismic testing. Test results show the web stiffener to be effective in improving strength, stiffness, reducing buckling damages and delaying the onset of strength degradation of HBS WSMCs. Results show that these benefits are obtained without changing the plastic hinge location. In fact it was observed that the webstiffener reduces and more uniformly distributes and strains in the plastic hinge. However, test results also show that careful detailing of the web stiffener welding attachment to the beam web is necessary to circumvent premature failures to these welds. Other areas for application of this technique include moment connection with non-compact built up section beams and the bases of deep wide flange section columns in special moment frames. Suffice it to say that future analytical and experimental studies are needed to further develop and eventually implement this technique in the field. In this regard, the experimental and analytical data and observations presented in this article should provide a valuable starting point for such efforts.

8. References

- [1] FEMA-350, 2000, *Recommended Seismic Design Criteria for New Steel Moment-FrameBuildings*, prepared by the SAC Joint Venture for the Federal Emergency Management Agency, Washington, DC.
- [2] FEMA-353, 2000, *Recommended Specifications and Quality Assurance Guidelines for Steel Moment-Frame Construction for Seismic Applications*, prepared by the SAC Joint Venture for the Federal Emergency Management Agency, Washington, DC.

- [3] FEMA-355D, 2000, *State of the Art Report on Connection Performance*, prepared by the SAC Joint Venture for the Federal Emergency Management Agency, Washington, DC.
- [4] AISC/ANSI 358-10 (2010) Prequalified Connections for special and intermediate steel moment frames for Seismic Applications, Chicago.
- [5] AISC/ANSI 341-10 (2010) Seismic Provisions for structural steel buildings, Chicago.
- [6] Ricles, J.M., Mao, C., Lu, L.W., & Fisher, J.W. (2002). “Inelastic Cyclic Testing of Welded Unreinforced Moment Connections”. *J. Struct. Eng*, Vol. 128, No. 4 pp. 40-49.
- [7] Jones, S.L., Fry, G.T., & Engelhardt, M.D., (2002), “Experimental Evaluation of Cyclically Loaded Reduced Beam Section Moment Connections.” *J. Struct. Eng*, Vol. 128, pp. 441-451.
- [8] Sumner, E.A., & Murray, T.M. (2002). “Behavior of extended end-plate moment connections subject to cyclic loading” *J. Struct. Eng*, Vol. 128, No. 4 pp.501-508.
- [9] Schneider, S.P. & Teeraprbwong, I. (2002) “Inelastic Behavior of Bolted Flange Plate Connections” *J. Struct. Eng*, Vol. 128, pp. 492-500.
- [10] Adan, S.M., & Gibb, W. (2009). “Experimental evaluation of Kaiser Bolted Bracket steel moment-resisting connections,” *Engineering Journal*, 181-195.
- [11] Kwasniewski L, Stojadinovic B, Goel SC. Local and lateral-torsion buckling of wide flange beams. SAC Joint Venture: Report SAC/BD-99/20; 1999.
- [12] Yu, Q. S. Yu, Gilton, C., Uang C.M. Cyclic Response of RBS Moment Connections: Loading Sequence and Lateral Bracing Effects, SAC Joint Venture: Report SAC BD-00/22; 2000.
- [13] Uang C.M. and Fan C.C. Cyclic instability of steel moment connections with reduced beam section. SAC Joint Venture: Report SAC BD-99/19; 1999.
- [14] Uang, C. and Fan, C. (2001). “Cyclic Stability Criteria for Steel Moment Connections with Reduced Beam Section.” *J. Struct. Eng.*, 127(9), 1021–1027.
- [15] Okazaki, T., Liu, D., Nakashima, M., & Engelhardt, M. D. (2006). “Stability requirements for beams in seismic steel moment frames” *J. Struct. Eng*, 132(9), 1334-1342.
- [16] Kim, T., Whittaker, A.S., Bertero, V.V., Gilani, A.S.J., and Takhirov, S.M. “Steel Moment Resisting Connections Reinforced with Cover and Flange Plates, SAC Joint Venture: Report SAC BD-00/27; 2000.

- [17] Wang, W., Zhang, Y., Chen, Y., & Lu, Z. (2013). Enhancement of ductility of steel moment connections with noncompact beam web. *Journal of Constructional Steel Research*, 81, 114-123.
- [18] ANSYS® Academic Research, Release 14.5, Help System, Structural Analysis Guide, ANSYS, Inc.
- [19] SAC Joint Venture (2000) “Development and Evaluation of Improved details for Ductile Welded Unreinforced Flange Connections” *Rep. No. SAC/BD-00/24*.
- [20] Myers A, “Testing and probabilistic simulation of ductile fracture initiation in structural steel components and weldments” Ph.D. Dissertation Stanford University; May 2009.
- [21] ASTM A6 / A6M-14, Standard Specification for General Requirements for Rolled Structural Steel Bars, Plates, Shapes, and Sheet Piling, ASTM International, West Conshohocken, PA, 2014.
- [22] Castiglioni, C. (2005). “Effects of the Loading History on the Local Buckling Behavior and Failure Mode of Welded Beam-to-Column Joints in Moment-Resisting Steel Frames.” *J. Eng. Mech.* 131, SPECIAL ISSUE: ADVANCES IN THE STABILITY OF FRAMED STRUCTURES, 568–585.
- [23] SAC Joint Venture (1999) “Local and Lateral-Torsion Buckling of Wide Flange Beams” *Rep. No. SAC/BD-99/20*.
- [24] Ricles, J., Zhang, X., Lu, L.W., and J. Fisher, (2004). “Development of Seismic Guidelines for Deep-Column Steel Moment Connections,” *ATLSS Report No. 04-13*, ATLSS Engineering Research Center, Lehigh University, Bethlehem, PA.
- [25] Morrison, M., Schweizer, D., and Hassan, T. "An innovative seismic performance enhancement technique for steel building moment resisting connections." *Journal of Constructional Steel Research* 109 (2015): 34-46.

CHAPTER 8: Conclusions and Recommendations

1. Conclusions

This dissertation has developed and validated seismic enhancement techniques for steel building beam to column moment resisting connections. The first and foremost of these techniques is the heat-treated beam section. This technique involves selectively reducing the strength of beam flanges by subjecting them to high temperatures followed by slow cooling. As a consequence of this material strength reduction, upon simulated seismic loading, yielding and plastic hinging of the beam takes place in the heat-treated beam section (HBS). In a similar manner to the RBS, this connection provides a ductile seismic fuse through weakening, but because the elastic modulus and beam moment of inertia of the heat-treated section remain unchanged, the HBS does not sacrifice elastic stiffness as does the RBS. Also, since the cross section of the beam is unaltered and the inelastic portion of the stress-strain curve is also not significantly changed, the buckling resistance of a beam modified with the HBS is similar to that of an un-weakened beam.

In chapters 2 and 3 the HBS concept was developed through extensive experimentation. This involved material testing to study the effect of peak temperature and cooling rate on the tensile properties of A992 steel. Material testing was followed by heat-treatment of full scale beams (W30x148) using induction heating (chapter 2) and electric resistance heating (chapter 3). Induction heating presented challenges in maintaining uniform temperatures and achieving prescribed cooling rates. As a result, fast rates of work hardening were observed during tensile testing of induction heat-treated A992 steel which resulted in higher bending moments than anticipated in connections modified with induction heat-

treatment. This setback was overcome in chapter 3 by using electrical resistance heating pads which produced uniform temperature and well controlled cooling. Two all welded connections enhanced with the HBS displayed ductile seismic response, which exceeded the 2010 AISC Seismic Provisions (ANSI/AISC 341-10) SMF qualifying 4% interstory drift angle without much strength loss. Test data also shows that the HBS was successful in shifting the majority of inelastic action and lateral deformation due to local flange and web buckling away from the welded joint.

Seismic performance enhancements to 8 bolt extended endplate (EEP) connections were developed through finite element (FE) analysis in chapter 4 and validated through full scale simulated seismic testing in chapter 5. The performance enhancements include removal of the endplate stiffener to eliminate the associated stress concentration, rearranging the bolts into a hexagonal pattern to distribute the flange forces evenly to the connecting bolts, heat-treating the beam flanges to ensure formation of plastic hinge away from the connection region, and adding stiffeners on both the sides of the beam web to delay the onset of strength degradation. In numerical simulations this connection showed significant improvements over the stiffened 8 bolt extended end plate connection in terms of fatigue failure resilience, buckling resistance, and energy dissipation.

Experimental validation of the 8 bolt extended endplate connection shows that the modified bolt arrangement performed well in distributing bolt forces uniformly amongst the bolt group while the HBS was successful in shifting the majority of inelastic action away from the beam flange to end plate welds. These observations were consistent with pre-test FE analysis predictions. However, the web stiffener did not perform as predicted. This

discrepancy was shown by post-test FE analysis to be attributable to the presence of welding induced distortions of the web stiffener plates.

The post-Northridge welded unreinforced flange-bolted web (WUF-B) connection was evaluated in detail using FE analysis in chapter 6. FE simulations were able to capture bolt slippage and the resulting redistribution of shear and bending stresses to the beam flanges. The cyclic void growth model (CVGM) was used to successfully predict the ductile fracture at the toe of the access hole commonly observed in laboratory testing of post Northridge WUF-B connections. This FE model was then used to evaluate a modified slip critical bolt design intended to transfer web developed shear forces and bending moments. In FE simulations, the modified bolt design combined with the HBS led to significantly lowered strain demands at the weld access hole and weld toe when compared to the post Northridge WUF-B. The modified WUF-B connection was experimentally validated through full scale testing. The connection displayed ductile response to simulated seismic loading exceeding the 2010 AISC Seismic Provisions (ANSI/AISC 341-10) SMF qualifying 4% interstory drift angle without significant strength loss. No weld or near weld cracks were observed. Instead, fracture occurred in the region of significant flange buckling (in the plastic hinge) during cycles at 5% interstory drift.

Strength degradation initiated by local buckling damages in all welded HBS connections was studied experimentally and through FE analysis in chapter 7. To counter this, two techniques for improving the seismic performance of all welded HBS connections were studied through FE analysis. One technique called ‘web stiffener’ involves welding a plate to the beam web and column flange in the plastic hinge region, while the other

technique involves extending the HBS to the beam web. The web stiffener was the technique which showed superior performance in FE simulations and as a result was experimentally validated. Test results show the web stiffener to be effective in improving stiffness, reducing buckling damages and delaying the onset of strength degradation of all welded HBS connections. However, test results also show that careful detailing of the web stiffener welding attachment to the beam web is necessary to circumvent premature failures to these welds.

2. Recommendations

The seismic performance enhancements presented in this dissertation show promise, but there are several areas where further study is needed. The following are some recommendations for future study.

2.1 Heat-treatment method and Thermal cycle

The induction heating method, which is more energy efficient and can provide faster heating rates than electrical resistance heating, should be further explored for HBS connections. This will require improved coil designs to ensure uniform temperature distributions and better insulation to prevent unwanted heat loss during the cooling down.

The thermal cycle for annealing heat treatment of A992 steel can be optimized to shorten cycle times. Some effort should be devoted to determining the upper critical and lower critical transformation temperatures for A992 steel. This will allow thermal cycles to be adjusted so that slow cooling rates needed to facilitate grain growth are only prescribed over the necessary temperature range.

2.2 All welded HBS connections

Experimental studies are needed to evaluate the suitability of all welded HBS connections for a range of beam and column sizes, especially larger and heavier sections which experience more severe strain concentrations during seismic loading. Numerical and analytical parametric studies may be paired with such experimental investigations to develop reliable design methods for accurately predicting strength and performance limit states of HBS moment connections.

2.3 Modified 8 bolt unreinforced extended end plate connection

Future numerical, analytical and experimental studies are needed to develop design procedures for this connection. In particular reliable design methods are needed for selecting end plate thickness. Experimental study of the modified 8 bolt unreinforced extended end plate connection without the HBS or web stiffeners may find this connection to be capable of exceeding AISC seismic provision performance requirements for use in special moment frames. This assertion is made based on the fact that EEP connections are shop welded in controlled environments and are made without access hole cuts which introduce stress concentrations near the connection.

2.4 Modified post Northridge WUF-B connection

Future studies are needed to explore the effect of beam size on the performance of this connection. The numerical analysis methods presented in this portion of the study provide a good starting point for such future study. In addition, relaxation of high strength bolts in slip critical connections subjected to cyclic loading should be explored to determine

whether current design methods are conservative in calculating slip resistance in the presence of large amplitude cyclic loading where components undergo widespread yielding.

2.5 Web stiffener

The web stiffener technique may add greatest value in non-compact built up beams in moment resisting connections. Therefore future work on developing the web stiffener should be focused in this area. The web stiffener also has the potential to be used at the base of deep column sections in moment resisting frames. However, for best results the web stiffener attachment method and details still needs improvement. Slot weld or plug weld designs need to be optimized for reducing residual stress and distortion from welding as well as reducing stress concentrations which may lead to premature fractures. Numerical and experimental studies should be paired towards meeting this goal.